The role of Wnt/β-catenin antagonists - sclerostin and DKK1 - in bone homeostasis and mechanotransduction

Alyson Ruth Morse

B Biotech (Hons)

A thesis submitted in fulfilment of the requirements for the degree of

Doctor of Philosophy

Supervisor: Prof David G Little

Co-supervisors: A/Prof Aaron Schindeler

Dr Michelle M McDonald

2017

The University of Sydney

Sydney Medical School

Statement of Originality

This is to certify that to the best of my knowledge, the content of this thesis is my own work. This thesis has not been submitted for any degree or other purposes.

I certify that the intellectual content of this thesis is the product of my own work and that all the assistance received in preparing this thesis and sources have been acknowledged.

Alyson Morse

Acknowledgments

It has been a long, long journey with many people to thank. My husband, James: he is my number one supporter and inspiration. He has a drive and desire for achievement that I see unmatched. My little girl, Lyndsey: who has been the motivating force every day over the past two years to get this thesis finished! My parents and family: they have always believed in my abilities and maintained interest in my achievements - thank you for all that you have given for me. My supervisor, David: he has shown more confidence in me than I ever did in myself. I'm sure he is unaware of the full influence and ambition that he has instilled. My associate supervisors, Michelle and Aaron: each have provided invaluable guidance, experience and knowledge during different stages of my candidature - thank you! The additional experts that have helped me along the way: Prof Marjolein van der Meulen, Dr Wendy Gold, and Dr Ciara Murphy - you have been invaluable.

Abstract

Promising avenues for improving bone mass and fracture resistance include loading-based exercise and agents modulating Wnt/β-catenin signalling. This thesis examines the intersection between these. Murine models of tibial loading and unloading, genetic knockout (KO) models of Wnt antagonists sclerostin and dickkopf-1/DKK1 (encoded by *Sost* and *Dkk1* genes), and neutralising antibodies for sclerostin (Scl-Ab) were applied.

Sost KO mice underwent unloading and compressive loading of the tibiae. Sclerostin was vital for the bone response to unloading yet not for loading. Rather, loading-induced anabolism was synergistically augmented in *Sost* KO mice. It was hypothesised that other Wnt antagonists, such as DKK1, may up-regulate following long-term sclerostin deficiency.

Similarly, *Dkk1* KO mice exhibited a synergistically augmented anabolic bone response to loading compared to wild type. However, compensation by sclerostin was doubtful as the primary cause for the augmented response with similar sclerostin expression seen in non-loaded tibiae of *Dkk1* KO and wild type mice, and similar down-regulation following loading.

Dkk1 KO mice treated with Scl-Ab resulted in additive increases in bone volume above either individual DKK1 or sclerostin deficiency. Prominent and synergistic effects were within cancellous bone. Immunohistochemical staining did not support the hypothesis that sclerostin up-regulates to compensate for long-term DKK1 deficiency.

Finally, Scl-Ab was co-administered to mice undergoing tibial compressive loading, with additional anabolic increases seen above either monotherapy. RNA sequencing provided insight into mechanisms involved in the augmented response to loading with Scl-Ab use.

This thesis supports future clinical use of antibodies targeting Wnt antagonists, whereby load/resistance exercise or dual-agents may increase the efficacy of Scl-Ab or DKK1-Ab therapy. This may have a critical impact for treatment of osteoporosis and other conditions of bone-loss.

Original Publications

Over the course of this candidature, several studies have been published as articles within peer-reviewed scientific journals.

Publications related to this thesis

Original published articles related to the submission of this thesis:

Morse A, McDonald MM, Kelly NH, Melville KM, Schindeler A, Kramer I, Kneissel M, van der Meulen MC, Little DG. Mechanical load increases in bone formation via a sclerostin-independent pathway. J Bone Miner Res, 2014;29(11):2456-67. **Chapter 2 p68.**

Morse A, Cheng TL, Schindeler A, McDonald MM, Mohanty S, Kneissel M, Kramer I, Little DG. Dkk1 KO mice treated with sclerostin antibody have additional increases in bone volume. Calcif Tissue Int. 2018 May 29; [Epub ahead of print]. **Chapter 4 p113.**

Morse A, Schindeler A, McDonald MM, Kneissel M, Kramer I, Little DG. Sclerostin antibody augments the anabolic bone formation response in a mouse model of mechanical tibial loading. J Bone Miner Res. 2017 Nov 1; [Epub ahead of print]. **Chapter 5 p146.**

Publications not related to this thesis

Original articles published not related to the submission of this thesis:

Liu R, Birke O, **Morse A**, Peacock L, Mikulec K, Little DG, Schindeler A. Myogenic progenitors contribute to open but not closed fracture repair. BMC Musculoskelet Disord, 2011;22(12):288.

Yang N, Schindeler A, McDonald MM, Seto JT, Houweling PJ, Lek M, Hogarth M, **Morse AR**, Raftery JM, Balasuriya D, MacArthur DG, Berman Y, Quinlan KG, Eisman JA, Nguyen TV, Center JR, Prince RL, Wilson SG, Zhu K, Little DG, North KN (2011). α-Actinin-3 deficiency is associated with reduced bone mass in human and mouse. Bone. 2011;49(4):790-8.

McDonald MM, **Morse A**, Peacock L, Mikulec K, Schindeler A, Little DG. Characterization of the bone phenotype and fracture repair in osteopetrotic incisors absent rats. J Orthop Res. 2011;29(5):726-33.

McDonald MM, **Morse A**, Mikulec K, Peacock L, Yu N, Baldock PA, Birke O, Liu M, Ke HZ, Little DG. Inhibition of sclerostin by systemic treatment with sclerostin antibody enhances healing of proximal tibial defects in ovariectomized rats. J Orthop Res. 2012;30(10):1541-8.

McDonald MM, **Morse A**, Mikulec K, Peacock L, Baldock PA, Kostenuik PJ, Little DG. Matrix metalloproteinase-driven endochondral fracture union proceeds independently of osteoclast activity. J Bone Miner Res. 2013;28(7):1550-60.

Morse A, Yu NY, Peacock L, Mikulec K, Kramer I, Kneissel M, McDonald MM, Little DG. Endochondral fracture healing with external fixation in the *Sost* knockout mouse results in earlier fibrocartilage callus removal and increased bone volume fraction and strength. Bone. 2015;71:155-63.

Morse A, Cheng TL, Peacock L, Mikulec K, Little DG, Schindeler A. RAP-011 augments callus formation in closed fractures in rats. J Orthop Res. 2016;34(2):320-30

McDonald MM, Reagan MR, Youlten SE, Mohanty ST, Seckinger A, Terry RL, Pettitt JA, Simic MK, Cheng TL, **Morse A**, Le LMT, Abi-Hanna D, Kramer I, Falank C, Fairfield H, Ghobrial IM, Baldock PA, Little DG, Kneissel M, Vanderkerken K, Bassett JHD, Williams GR, Oyajobi BO, Hose D, Phan TG, Croucher PI. Inhibiting the osteocyte specific protein sclerostin increases bone mass and fracture resistance in multiple myeloma. Blood. 2017;129(26):3452-3464

Morse A, McDonald MM, Schindeler A, Peacock L, Mikulec K, Cheng TL, Liu M, Ke HZ, Little DG. Sclerostin Antibody Increases Callus Size and Strength but does not Improve Fracture Union in a Challenged Open Rat Fracture Model. Calcif Tissue Int. 2017;101(2):217-228

McDonald MM, **Morse A***, Birke O, Yu NYC, Mikulec K, Peacock L, Schindeler A, Liu M, Ke HZ, Little DG. Sclerostin antibody enhances bone formation in a rat model of distraction osteogenesis. J Orthop Res. 2017; [Epub ahead of print]

***equal first author**

McDonald MM, **Morse A**, Schindeler A, Mikulec K, Peacock L, Liu M, Ke HZ, Little DG. Homozygous *Dkk1* knockout mice exhibit high bone mass phenotype due to increased bone formation. Calcif Tissue Int. 2017; [Epub ahead of print]

Authorship attribution statement

The work presented in this thesis was conducted during my full time candidature to fulfil the requirements of Doctor of Philosophy through the Sydney Medical School, The University of Sydney. Unless otherwise stated, all experiments were conducted, and data collected and analysed, by myself at the Orthopaedic Research and Biotechnology Unit at The Children's Hospital at Westmead. Animal ethics was approved by the South Western Area Health Service (SWAHS) Animal Ethics Committee and/or CMRI/CHW animal ethics. Experimental conception, and manuscript and thesis editing, was conducted in conjunction with my supervisors Prof David G Little, A/Prof Aaron Schindeler and Dr Michelle M McDonald.

Chapter 2 of this thesis is published as:

Morse A, McDonald MM, Kelly NH, Melville KM, Schindeler A, Kramer I, Kneissel M, van der Meulen MC, Little DG. Mechanical load increases in bone formation via a sclerostin-independent pathway. J Bone Miner Res. 2014;29(11):2456-67.

KNH and KMM performed strain gauging experiments. IK, MK and MCVDM were involved with experimental design and the review of the manuscript and data. Guy Smith assisted with some DXA data collection.

Chapter 3 of this thesis is drafted for submission for review with Bone.

Morse A, Ko F, McDonald MM, Schindeler A, van der Meulen MC, Lee L, Little DG. A *Dkk1* KO mouse shows an increased anabolic bone response following compressive tibial loading.

FK assisted in strain gauging experiments. MCVDM was involved in experimental design and review of manuscript and data. LL, Kathy Mikulec-Langton and Matthew Summers assisted with some specimen collection/homogenisation and/or RNA extractions. Kathy Mikulec-Langton and Lauren Peacock assisted with some mechanical loading and DXA scans.

Chapter 4 of this thesis is published as:

Morse A, Cheng TL, Schindeler A, McDonald MM, Mohanty S, Kneissel M, Kramer I, Little DG. Dkk1 KO mice treated with sclerostin antibody have additional increases in bone volume. Calcif Tissue Int. 2018 May 29 [Epub ahead of print].

With my assistance, TLC performed and analysed mechanical testing experiments. SM performed immunohistochemistry. IK and MK were involved with experimental design and the review of the manuscript and data. Confocal imaging was conducted with assistance of, and methods developed with, Dr Ciara Murphy. Kathy Mikulec-Langton and Lauren Peacock performed animal drug dosing.

Chapter 5 of this thesis is published as:

Morse A, Schindeler A, McDonald MM, Kneissel M, Kramer I, Little DG. Sclerostin antibody augments the anabolic bone formation response in a mouse model of mechanical tibial loading. J Bone Miner Res. 2017 Nov 1 [Epub ahead of print].

IK and MK were involved with experimental design and the review of the manuscript and data. The Australian Genome Research Facility (AGRF) undertook RNASequencing and analysis. Kathy Mikulec-Langton and Lauren Peacock performed animal drug dosing and assisted with some DXA scans. Kathy Mikulec-Langton assisted with some RNA extractions and/or specimen collection/homogenisation.

Attest to the authorship attribution statement

As supervisor for the candidature upon which this thesis is based, I can confirm that the authorship attribution statements above are correct.

Prof. David G Little

30 November, 2017

Table of Contents

List of Figures

Chapter 1

Chapter 2

Chapter 3

Chapter 4

Chapter 5

List of Tables

Chapter 2

Chapter 3

Chapter 4

Chapter 5

Chapter 6

Nomenclature and Abbreviations

3D	three-dimensional
ALP	alkaline phosphatase
APC	adenomatous polyosis coli
ATP	adenosine triphosphate
BFR/BS	bone formation rate/bone surface
BMC	bone mineral content
BMD	bone mineral density
BMP	bone morphogenetic protein
BTX	botulinum toxin
BV	bone volume
BV/TV	bone volume/total volume
CK1	casein kinase 1
COX	cyclooxygenase
Ct.Th	cortical thickness
CTx	C-terminal telopeptide
DEGs	differentially expressed genes
DKK/Dkk	dickkopf
DMP1	dentin matrix protein 1
DXA	dual-energy X-ray absorptiometry
Dvl	dishevelled
E2	estradiol
Ec	endocortical surface
ER	estrogen receptor

EVS	Exercise Vital Sign questionnaire
FDR	false discovery rate
FRAT	frequently arranged in advanced T-cell
Fzd	frizzled
GSK-3	glycogen synthase kinase-3
GTP	guanine nucleotide
HBM	high bone mass
*I*ap	moment of inertia about the anteroposterior axis
IGF-1	insulin-like growth factor 1
IHC	immunohistochemistry
KO	knockout
Krm	kremen protein
J	polar moment of inertia (also denoted as "MMI(polar)")
JNK	c-Jun N-terminal Kinase
LBM	low bone mass
LDLR	low density lipoprotein receptor
LRP	lowdensity-lipoprotein receptor-related protein
MAPK	mitogen-activated protein kinase
MAR	mineral apposition rate
microCT	micro-computed tomography
MMI(polar)	polar moment of inertia (also denoted as "*J*")
MS/BS	mineralizing surface/bone surface
MSC	mesenchymal stem/stromal cell
M-CSF	monocyte colony-stimulating factor

NLK	NEMO-like kinase
N.Oc	number of osteoclasts
N.Oc/BS	number of osteoclasts/bone surface
Oc.S	osteoclast surface
Oc.S/BS	osteoclast surface/bone surface
Oc.S/N.Oc	osteoclast surface/number of osteoclasts
OPG	osteoprotegrin
OPN	osteopontin
OPPG	osteoporosis pseudoglioma
OVX	ovariectomised
PAVS	Physical Activity Vital Sign questionnaire
PCP	planer cell polarity
PGE	prostaglandin
PKA	protein kinase A
PGE_2	prostaglandin E2
Ps	periosteal surface
PTH	parathyroid hormone
RABT	reference based assembly option
RANK	receptor activator nuclear factor-kappaβ
RANKL	receptor activator nuclear factor kappaβ ligand
RNASeq	RNA sequencing
ROI	region of interest
Scl-Ab	anti-sclerostin antibody/neutralizing antibodies to sclerostin
SERM	selective estrogen-receptor modulators

sFRP	secreted Fzd-related-proteins
Tb.N	trabecular number
Tb.Sp	trabecular separation
Tb.Th	trabecular thickness
TMD	tissue mineral density
TRAP	tartrate-resistant acid phosphatase
TV	total volume
VOI	volume of interest
WIF	Wnt inhibitory protein
WISE	Wnt1 induced secreted protein
WT	wild type

Chapter 1. Introduction

1. Overview of the Skeletal System

The skeletal system is vital to the human physique, providing a framework and structure for the body, whilst allowing movement, absorbing daily applied forces and protecting vital organs. The musculoskeletal system is comprised of bone and associated connective tissues. These connective tissues include muscles, ligaments, tendons, and cartilage, which join bones, dictate and constrain their movement, and provide comfort and cushioning between the bones.

However, it is bone, with its unique hardness, rigidity, and shape that is the major component of the skeleton. Along with the physical mechanical function of bone, the mineral content and marrow cavity of bones also provide metabolic functionality to the body, storing essential ions such as calcium, and also housing the majority of the body's pool of hematopoietic cells (1). Bone is primarily composed of mineral, organic matrix, cells and water (1). The mineral, which makes up 65% of bone and is formed into crystals, is mainly impure calcium hydroxyapatite [$Ca_{10}(PO_4)_6(OH)_2$], with carbonate, magnesium, fluoride, citrate and strontium incorporated (1, 3). The organic matrix, also known as the osteoid, makes up 35% of bone and consists primarily of collagen, with some non-collagenous proteins incorporated, such as osteocalcin, osteopontin, osteonectin, bone sialoprotein, and TGF-β family members including bone morphogenetic proteins (BMPs) (1, 3).

1.1. Anatomy and physiology

An adult skeleton has 213 bones (or 206 when the fused vertebrae within the sacrum and the coccyx are considered as one bone each) (4). Though there are four groups of bones classified by their basic structure: short, flat, long and irregular (4), the majority of this research will investigate the long bones and so the anatomy of these bones will follow.

The long bones include the fibulae, tibiae, femora, ulnae, radii, humeri, metacarpals, metatarsals, phalanges, and clavicles (4). Under gross morphologic inspection, adult long bones are long in shape (Figure 1.1). The main central shaft of the bone, the

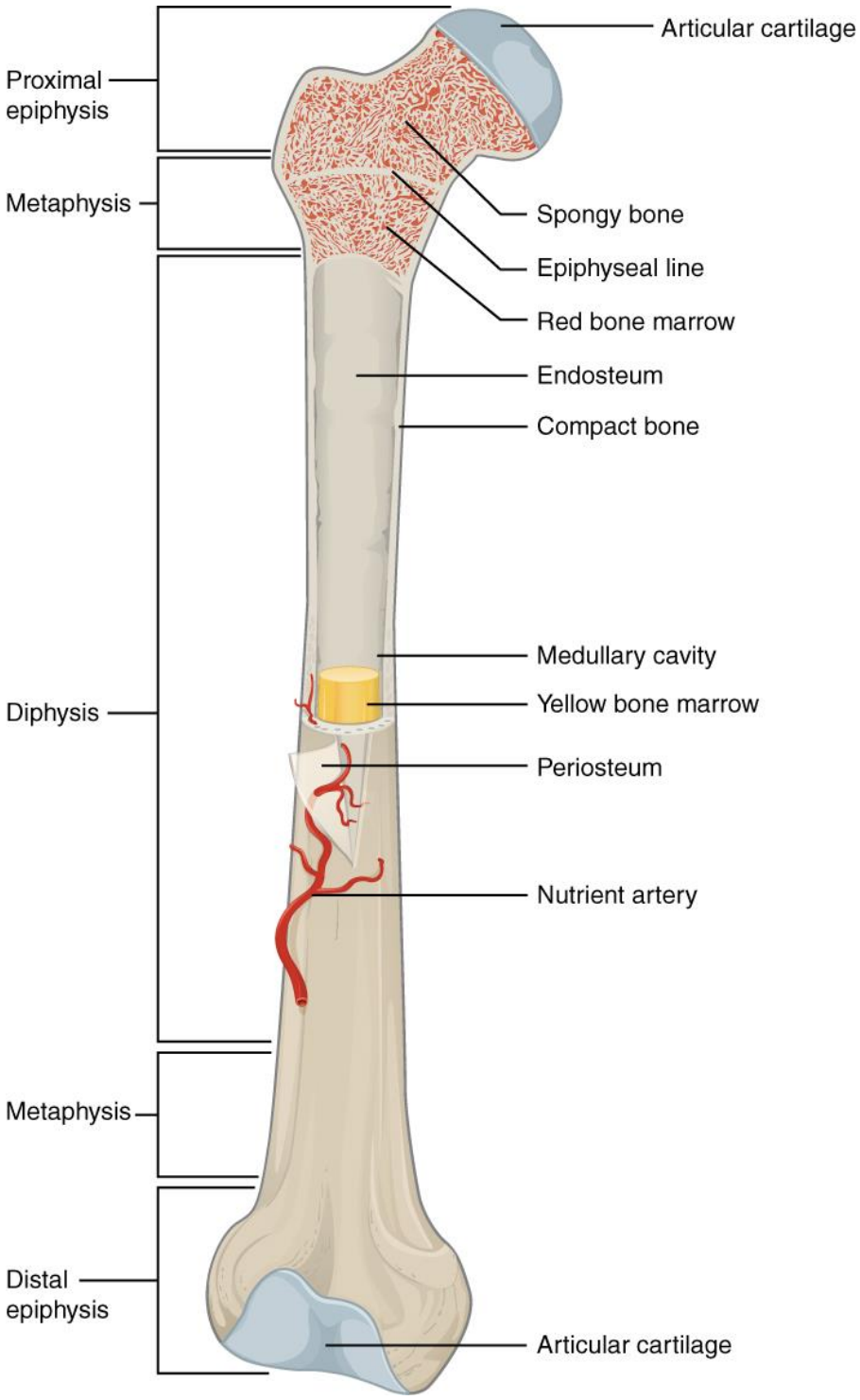

Figure 1.1: Diagram depicting the gross anatomical features of the long bone. Image from OpenStax College, 2013 (5).

diaphysis, is tubular in form (6). It is within this region that the medullary cavity is enclosed, which contains hematopoietic marrow and blood forming cells (6). At either end of the long bone are regions entitled the epiphysis. These ends meet other bones at the joint and so are covered by a thin layer of articular cartilage to aid cushioning and allow motion (1). The epiphysis and the diaphysis at either end of the bone are separated by an expanded region called the metaphysis. This region is broader than the tubular shaft of the diaphysis. Separating the metaphysis and the epiphysis in the immature skeleton is a cartilaginous region called the growth plate, or the physis, an essential region in the growth of long bones (1). The periosteum, a layer of vascularised connective tissue membrane, covers the majority of the bone. Excluded regions are where tendons and ligaments join the bone or where articular cartilage covers the bone at joints (1). A similar, but mostly cellular, membrane called the endosteum exists on the inner bone surface inside the medullary cavity.

Bone tissue is categorised into two macroscopic structural types: *cortical* (or compact) bone and *trabecular* (or cancellous) bone (Figure 1.2). These comprise approximately 80% and 20% of the adult skeleton respectively (6). The structure, composition and material properties of the matrix is the same for cortical and trabecular bone, but cortical bone is more dense, and its compressive strength greater than that of trabecular bone (6). Trabecular bone is a framework of interconnected plates and rods and thus has approximately twenty times more surface area than cortical bone (1). In long bones, trabecular bone is found filling the broader epiphyses and metaphyses, which are surrounded by only a thin layer of cortical bone. This cortical bone thickens and decreases in diameter as it forms the tubular diaphysis. The distribution of these bone structures is an important aspect mechanically for long bones. The broader structure of trabecular bone, surrounded by a thin cortex at the metaphyses and epiphyses provides pliancy and absorbency in load bearing in compression, while the thick, dense cortical bone of the diaphysis resists torsion and bending to load (6).

There are two microscopic structural types of bone existing in the skeleton; *woven* and *lamellar* bone. These relate to the organisation of collagen fibres. Woven bone is made up from coarse random interwoven collagen fibres with a random distribution of osteocytes, formed in early or ongoing repair scenarios (3). Lamellar bone, however, is highly organised and regular. It is built up of layers (lamellae), 3-7μm thick and comprised of a cross-hatching of fine fibres that run on the same plane (1). During embryonic bone growth it is the woven bone that is formed to make

the skeleton. This is then resorbed and replaced with the more mature lamellar bone so that, apart from a few exceptions, woven bone rarely exists in the human skeleton past 4 years of age outside of a repair setting or disease setting (e.g. Paget's disease) (6).

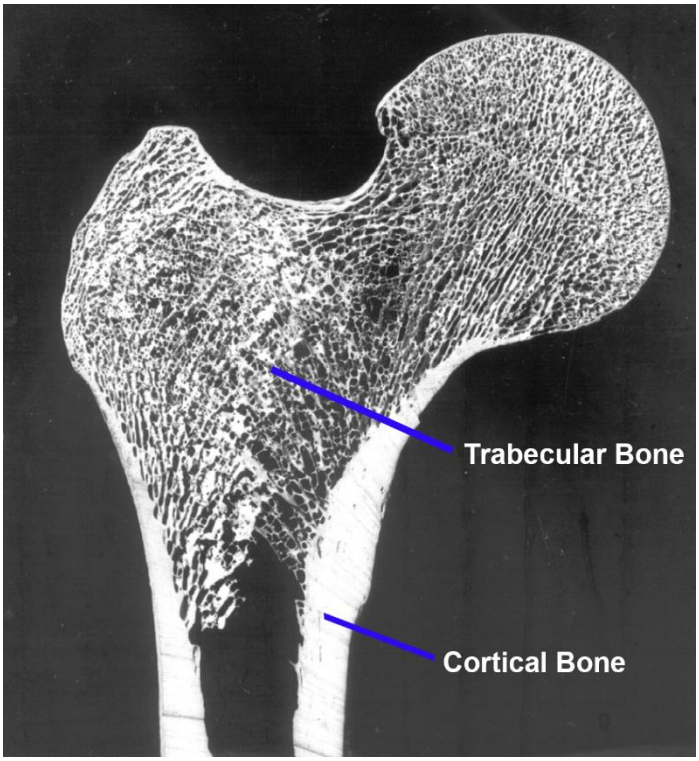

Figure 1.2: Image depicting the structural differences and the general distribution of trabecular and cortical bone within the long bone. Image modified from Glimcher, 2006 (7).

1.2. Bone cell biology

There are four major cells types involved in bone formation and remodelling. These are the bone-forming *osteoblasts*, *osteocytes* and *bone-lining cells*, and the bone-resorbing *osteoclasts*. Bone cells are characterised based on function, location and morphology and derive from two lineages. Osteoblasts, osteocytes and bone-lining cells share a single lineage, but are at varying stages. They derive from local osteoprogenitor cells, which are pluripotent precursors that stem from mesenchymal stem cells (MSCs) (8). These MSCs are also responsible for cells involved in

cartilage, muscle, fat and fibrosis (8). Osteoclasts originate from the hematopoietic stem-cell line and are at the end-stage of the monocyte lineage (8, 9). Osteoclast precursors differentiate and circulate in the marrow or blood (6). These osteoclast precursors can multiply and fuse to develop into the large, multinucleated osteoclasts (9).

1.2.1. Osteoblasts

Osteoblasts are essential in the process of bone formation. Active osteoblasts are found lining the bone surface, tightly packed in a row. They are distinct in their polyhedral, rounded-oblong shape (3, 6). Osteoblasts also have cytoplasmic processes which can extend through the osteoid to reach osteocytes (6). Initially, osteoblasts synthesise an organic matrix, the osteoid, to form the major structural element of bone (8). They are also involved in the organisation of the osteoid and aid in its mineralisation. Osteoblasts may reduce their activity whilst on the surface of the bone and become bone-lining cells. Alternatively they may become enveloped in bone matrix and differentiate into osteocytes (6). Thus the osteoblast, osteocytes and bone lining cells share a common lineage. The third fate for the osteoblast is to undergo apoptosis, which occurs in approximately 50-70% of osteoblasts (10).

1.2.2. Bone-lining cells

Bone-lining cells are found flattened and elongated upon resting bone surfaces (6). They have cytoplasmic processes that meet adjoining bone-lining cells, and also extend through the bone matrix to meet osteocytes (1). Bone-lining cells are able to become either osteoblasts or osteocytes, but are also thought to have their own regulatory function in this bone-lining state. They are known to be important in bone resorption and remodelling, with evidence that they can mediate enzymatic-driven removal of the osteoid lining on bone (6). The bone-lining cell enters a lacuna following the departure of the osteoclast, cleans the pit of remaining bone matrix, and deposits a protein cement line, including osteopontin, at the base of the pit followed by the deposition of collagen fibrils (11). This appears to be a requirement before osteoid deposition and bone formation by the osteoblast (11).

1.2.3. Osteocytes

Osteocytes represent the most abundant bone cell type. They form from mature osteoblasts that are gradually embedded within type I collagen-rich osteoid during bone formation (12). They transition to pre-osteocytes or osteoid osteocytes, and later osteocytes as the osteoid mineralises (13). They sit within the bone matrix inside lacunae and are elliptical in shape (6). They characteristically have a system of long cytoplasmic processes which connect to other osteocytes, blood vessels and other cells at the bone surface, such as osteoblasts and bone lining cells (9). The processes sit within canaliculi, which are small canals that cut through the bone matrix (14). This composition forms the lacuna-canalicular network. At the connection points between osteocyte processes there are gap junctions, a specialised matrix with channels allowing direct movement of ions and small molecules between cells (8). This connection allows functional communication through the bone matrix.

1.2.4. Osteoclasts

Osteoclasts, are large, multinucleated cells responsible for bone resorption (9). Active osteoclasts are found on bone surfaces at sites of bone resorption. This can include the periosteal and endosteal surfaces, trabecular bone surfaces, and even Haversian canals (6). The active osteoclast has two plasma membrane sites important to the process of bone resorption. First, complex folding of the cytoplasmic membrane to form a ruffled border occurs at the site of bone resorption (6). Second, a microfilament-rich region of the membrane, the clear zone, surrounds the ruffled border to seal the bone for resorption (9). Resorption involves two processes: the dissolution of inorganic bone mineral and the enzymatic digestion of organic macromolecules (8). At the region of the ruffled border, proton-pumps within the osteoclast move to the membrane surface and pump H^+ ions and proteolytic enzymes, including cathepsin K and matrix metalloproteinases (MMPs), into the sealed space at the bone surface. This creates an acidic environment and results in bone mineral degradation (6). Further to this, the osteoclast secretes acid and glycosidases to break down the organic matrix and is also able to phagocytise matrix fragments (6, 8).

Osteoclasts are derived from the hematopoietic monocyte lineage. Osteoclastic differentiation is dependent on the presence of the receptor activator nuclear factor kappaβ ligand (RANKL) system and monocyte colony-stimulating factor (M-CSF, also known as CSF-1) (15-17). RANKL binding

to receptor activator nuclear factor-kappaβ (RANK) expressed by osteoclast precursors stimulates osteoclastogenesis (18, 19). A regulator of RANKL, OPG, is expressed by osteoblasts (20). It acts as a decoy RANK receptor and blocks RANK/RANKL interaction and subsequently prevents osteoclast differentiation. The movement of osteoclast precursors are controlled by chemoattractants (osteocalcin and collagen-1) deposited within the bone matrix (10).

There is contention over the source of RANKL controlling osteoclast differentiation. Osteoblasts express RANKL and have traditionally believed to have a role in the differentiation of osteoclasts and osteoclast precursor recruitment to the cell surface (10). However it is osteocyte- and chondrocyte-derived RANKL which are essential for resorption matrix surrounding these cells (21). Both membrane-bound and soluble RANKL are produced and both may have roles in osteoclastogenesis (21).

1.3. Bone formation and development

Bone formation occurs not only during embryonic development, but also during skeletal growth, and furthermore throughout life to achieve maintenance and repair. Bone formation occurs through three distinct processes: *endochondral ossification, intramembranous and appositional*.

(i) Endochondral ossification

Endochondral ossification is the process of bone formation that requires cartilage as a template that is progressively replaced with ossified bone. Undifferentiated mesenchymal cells condense as a blastema and differentiate into chondrocytes, the cartilage forming cells. These cells, which secrete cartilaginous matrix, hypertrophy and mineralise, forming calcified matrix and the basis of the cartilage template (22, 23). Blood vessels are able to invade following some resorption of the cartilage matrix. This brings in new osteoprogenitors that are able to differentiate into osteoblasts and synthesize bone matrix on unresorbed mineralised cartilage surfaces (22, 24). This forms the *primary spongiosa*. This primitive bone is resorbed and replaced with *secondary spongiosa*, which has a mature lamellar structure.

Endochondral ossification is involved in the embryonic development of the axial and appendicular skeleton, including the base of the skull, the pelvis and vertebral column, along with the long bones

(1, 24). Endochondral ossification continues until skeletal maturity in the growing bones at the physes and epiphyses at regions called the growth plate. It is also seen in fracture repair, particularly in the long bones (22).

(ii) Intramembranous bone formation

Intramembranous bone formation occurs without the need for cartilage, but rather through ossification of an osteoid or embryonic connective tissue. Bone forms instead through the recruitment of undifferentiated mesenchymal cells to a future site of bone formation. These cells form spicules and islands of organic matrix, containing osteoprogenitors, blood vessels and fibroblastic cells, which are able to mineralise (22). The osteoprogenitors also differentiate into osteoblasts which further create osteoid which is then mineralised (22). The woven bone which forms appears trabecular in nature due to the spicules of organic matrix originally formed. These undergo remodelling to define cortical and trabecular regions of lamellar bone.

Intramembranous formation occurs embryonically in flat bones, such as the bones of the face, the vault of the skull, and parts of the mandible and clavicle. It is also seen in the adult in some fractures and in appositional sites (1, 22).

(iii) Appositional bone formation

Appositional bone formation involves osteoblasts lining up on existing bone to build up the bone layer by layer, through osteoid formation which is then mineralised (22). This process is involved alongside both intramembranous and endochondral ossification, where both form a primary spongiosa. Bone is covered with a cellular layer, the periosteum. Cells of the periosteum secrete osteoid, building up the bone with subsequent mineralisation (22). Appositional bone formation can also be seen within the adult bone in instances of bone widening and bone remodelling (22).

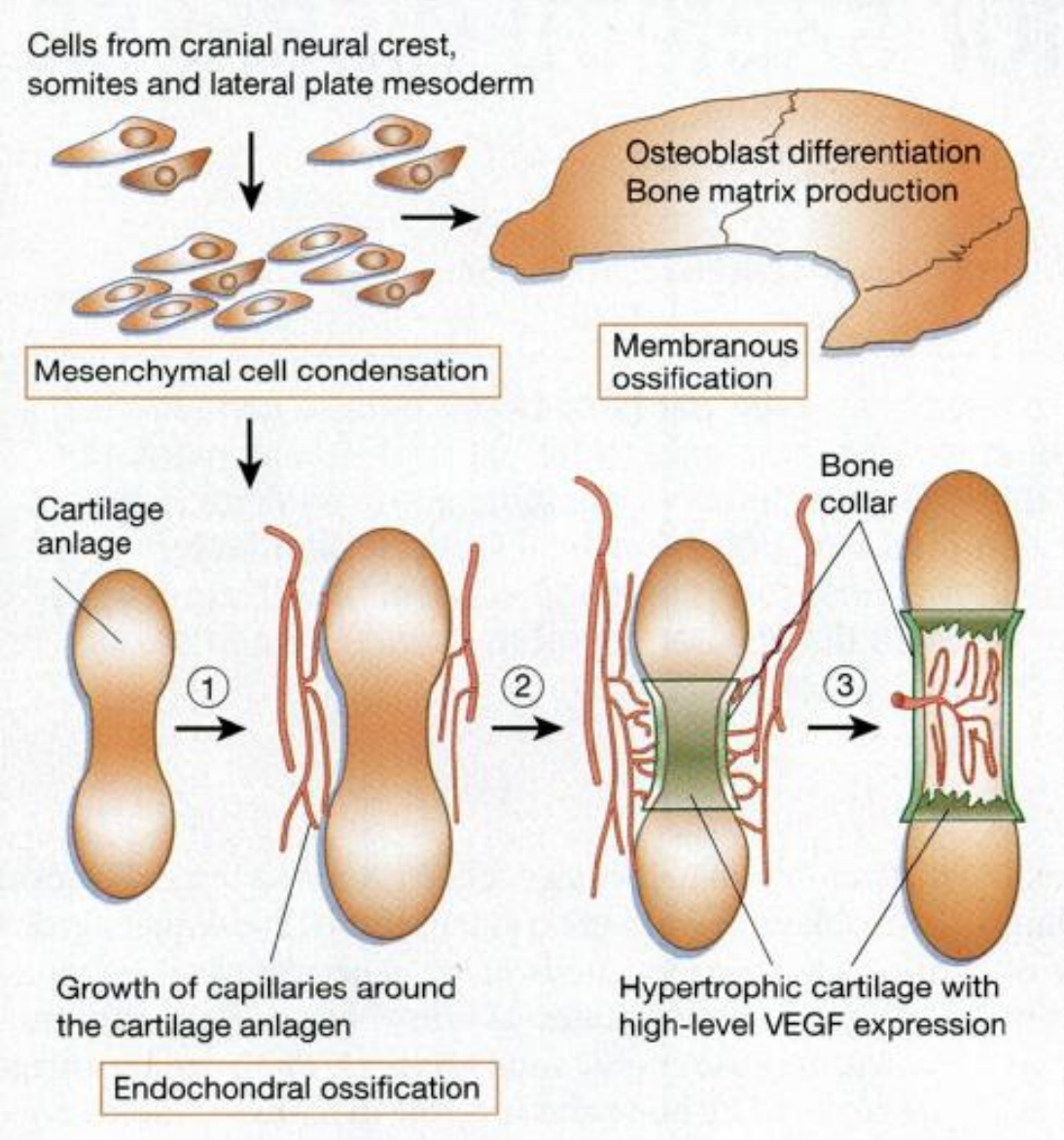

Figure 1.3. Embryonic long bone formation. Mesenchymal cells assemble and synthesise a cartilage template. Cells differentiate into chondrocytes at the diaphysis and a process of hypertrophy and apoptosis follows, along with cartilage matrix mineralisation. Blood vessels invade and osteogenic precursors arrive, differentiate to osteoblasts, and create bone at the diaphysis, the primary ossification centre. The growth plates are established at the ends of the bone and continual chondrocyte differentiation and cartilage conversion to bone allows for bone growth. The secondary ossification centres occur later in the epiphyses. Image from Zelzer and Olsen, 2003 (25).

1.3.1. Embryonic bone formation

During embryonic growth the axial and appendicular skeleton arise from different progenitor pools. The axial skeleton includes the formation of the skull, spine, sternum and ribs, whilst the appendicular component incorporates the extremities, including the long bones (24). Both intramembranous and endochondral ossification bone formation requires first the recruitment of a mesenchymal blastema during the foetal stage (1). Cells originate from either the neural crest, somites or lateral plate mesoderm (25), however most of the axial skeleton comes from the somites, with the neural crest mainly used for craniofacial development.

In contrast, the appendicular skeleton, which includes all of the long bones, is formed from the cells of the lateral plate mesoderm. In brief, the cells assemble and this leads to the synthesis of a cartilage template; endochondral bone formation (Figure 1.3). Blood vessels invade the perichondrium around the site of the future diaphysis and it becomes the periosteum. Further at the central diaphysis, just below the bone collar, cells differentiate into chondrocytes. This leads to the process of chondrocyte hypertrophy, and apoptosis, along with cartilage matrix mineralisation.

Osteogenic precursors arrive via the invading blood vessels, differentiate to osteoblasts, and create bone at this site of the diaphysis, the primary ossification centre. This establishes the growth plates at the ends of the bone and continual chondrocyte differentiation and cartilage conversion to bone allows for bone growth (24). Later in foetal development and early childhood secondary ossification sites appear at the cartilaginous epiphyses in a similar manner as the diaphysis. Cartilage remains at the growth plate until post-puberty and at the joint as hyaline articular cartilage throughout adulthood (24).

1.3.2. Growth of the long bones

Long bones continue to grow via the growth plate up to the end of puberty, when the growth plate is replaced by bone. The growth plate consists of four distinct zones, which are designed as a merging continuum (24). The *reserve zone* consists of randomly placed, spherical chondrocytes separated by a collagen II and proteoglycan rich matrix. Cells eventually become regularly

arranged into columns to form the *proliferative zone*, and appear flattened in shape. The appearance of flattened cells in columns is a result of the method of chondrocyte proliferation. Mitosis occurs perpendicular to the long bone axis, and daughter cells are flattened in shape and separated by cartilage matrix. Cells eventually begin enlarging at the *prehypertrophic zone*, and they further mature, hypertrophy (enlarge), and secrete a collagen X rich matrix at the *hypertrophic zone*. Eventually the glycogen stores of the chondrocytes deplete so much that the cells undergo apoptotic cell death. This results in empty lacunae separated by septae of cartilaginous matrix which become mineralised. Transverse septae remain unmineralized and are invaded by blood vessels, which bring along chondroclasts that remove the calcified cartilage. The mineralised longitudinal septae extend into the diaphysis, and osteoblasts use these as templates for bone formation to form the primary spongiosa (24).

1.4. Bone remodelling and homeostasis

Following the initial formation of the skeleton, bones begin undergoing a process of modelling and remodelling to achieve optimal size, shape and design. During bone development, *bone modelling* occurs to alter the size, shape, architecture and strength of the bone by patterning and laying down new bone (22). This process is largely controlled by genetics and the mechanical environment. Once a bone has developed *bone remodelling* occurs, where osteoblasts work in tandem with osteoclasts (22). This process of bone resorption and bone formation, also termed as *bone turnover*, are achieved by different cells yet are tightly *coupled* (see section 1.2). Remodelling is important in the adult skeleton as it enables repair of microdamage and is important in mineral metabolism (26). Further, it allows bone mass, size and shape to adapt to metabolic changes, as well as to changes to the mechanical loading of the skeleton (3, 22, 27).

1.5. Response of bone to the mechanical environment

Julius Wolff, in 1892, was the first to suggest that the skeleton was designed to distribute applied loads and furthermore was able to adapt to such loads (28). A century later, Harold Frost proposed the mechanostat hypothesis (29). It was suggested that, based on the everyday activities upon the skeleton, there is a window of normal strain levels on bone. Bone homeostasis occurs at this strain

set-point. Any alteration to this strain set-point will result in changes to bone mass and architecture. This effect is through a process known as *mechanotransduction*, whereby physical forces elicit biochemical signals which induce cellular responses.

Mechanical loading results in an increase in bone mass. This has been displayed in both clinical and experimental scenarios. Bed rest studies and long-term space flight have shown an absence of weight-bearing activity or disuse on the skeleton leads to a significant reduction in bone mass throughout the body (30-33). Localised bone loss has also been shown in a number of animal loss of function experiments following immobilisation of hind-limbs, a single limb, bone or even a part of a bone (34-36).

A reduced loading state results in increased bone resorption. Studies looking at consistently active sporting players versus non-active controls have shown increases in bone mineral content and bone mineral density in the consistently used limbs (37-40). Furthermore, assessment of dominant versus non-dominant arms in tennis players has shown increases in bone volume and bone mineral content in the dominant (loaded) arm (41, 42). Animal models of limb loading have also shown the direct effects on bone volume, density and content (43-45).

The osteoclast, the osteoblast, the osteocyte and the MSC are all mechanosensitive cells capable of interacting to regulate osteoclast and osteoblast recruitment, proliferation and differentiation (46). However, as osteocytes are located within the bone's lacuna-canalicular network, the network connecting osteocytes, bone-lining cells, osteoblasts and hematopoietic stem cells, it seems that they are ideally placed to both receive the strain from the mechanical environment and transduce signal (47, 48). For this reason, it has long been assumed that osteocytes mediate the osteoblast/osteoclast response due to changes in physical activity or load. It is known that osteoclasts resorb in regions of osteocyte underloading, while osteoblasts are recruited in regions of osteocyte overloading (14, 49). Critically, osteocytes are required for signalling during bone unloading, with a mouse model with targeted osteocyte ablation preventing bone loss associated with unloading (50). Further, these mice did result in low bone mass and fragility during normal load conditions, suggesting the importance of osteocytes in maintaining bone mass.

There are numerous mechanosensors capable of detecting the physical forces and mechanical alterations. These constructs and cellular products include the cytoskeleton, focal adhesions, primary cilia, integrins, extracellular matrix proteins, tethering elements, plasma membrane

structures, cadherins, ephrins, gap-junctions and ion channels (46, 51). These mechanisms are not likely to work alone in any given situation. However, within the osteocyte one of the major mechanisms in which load changes are sensed is thought to be through the changes in fluid flow through the canalicular network (14). The bone matrix may compress or relax with the changes in loading and affect the flow of the canalicular fluid. As the osteocytes are surrounded by a sheath of unmineralised matrix, which is permeable to macromolecules like albumin and peroxidases, a flow of fluid over the sheath and diffusion of macromolecules may be driven by loading (52, 53). Furthermore, osteocytes themselves are sensitive to shear stress (54-56). This may be a result of the composition of the osteocyte cytoskeleton and also the composition of the matrix sheath surrounding the osteocyte. There is evidence of interaction between receptors on the osteocyte and macromolecules in the matrix sheath (14).

Within the mechanotransduction process, there are many pathways utilised to transduce signals intracellularly for consequent cellular responses. These include prostaglandins, calcium signalling, kinase signalling, G-protein mediated signalling, nitric oxide, estrogens, nucleotide signalling, and the Wnt/β-catenin pathway (46, 51). Early responders include adenosine triphosphate (ATP) release and intracellular calcium signalling, followed by prostaglandins, nitric oxide, and mitogen-activated protein kinase (MAPK) signalling (57). Notably, there is increasing evidence of cross-interaction between these pathways during mechanotransduction (58-64).

The osteocyte responds metabolically to the mechanical environment with subsequent paracrine signalling that can directly promote osteoblastogenesis and inhibit osteoclastogenesis (14, 65-67). It is likely that this mechanism allows signals from the osteocyte to be transferred to osteoblasts and osteoclasts to initiate/inhibit differentiation, and bone formation or resorption. In experiments where media from mechanically stimulated osteocytes was added to osteoblast precursor cells there was upregulation of osteopontin (OPN) and cyclooxygenase (COX) -2 within these precursor cells, indicating osteoblast differentiation (65). In experiments investigating osteoclast differentiation in the presence of mechanically stimulated osteocytes, RANKL and OPG was released by the osteocytes, inhibiting osteoclastogenesis (66). The expression levels of RANKL and OPG correlated with the mechanical stimulation (66).

2. Wnt signalling

Wnt signalling is an evolutionary conserved cell signalling pathway, which is involved in many processes of embryonic development, including limb polarity, sex determination, and organogenesis (2, 68, 69). Post-developmentally it is also important in driving cellular differentiation and proliferation in many tissues (70). Wnt signalling is categorized into *canonical* and *non-canonical Wnt pathways*. The canonical Wnt pathway is often also referred to as the *Wnt/β-catenin pathway*, and will be referred as this within this thesis.

2.1. Wnt/β-catenin signalling

Wnt/β-catenin signalling is triggered by the binding of a protein from the Wnt family to a co-receptor complex on the surface of the cell (Figure 1.4A). This complex includes frizzled (Fzd) and low density lipoprotein receptor-related protein -5 or -6 (LRP5/6), and some evidence that they also bind to LRP4 (71-73). Activated Fzd, following Wnt activation on the cell surface, is able to bind dishevelled (Dvl) within the cytoplasm (74). Additionally, LRP5/6 binds with axin within the cytoplasm through their serine and proline rich cytoplasmic tail (75). Dvl and axin are both part of an intracellular complex with glycogen synthase kinase-3 (GSK-3) (76), which also includes adenomatous polyosis coli (APC) and β-catenin (77), and Casein kinase 1 (CK1) family members (78). The binding of the GSK-3 complex to the cell surface results in GSK-3 inhibition and disruption of the complex leading to dephosphorylation and a release of β-catenin. Unbound β-catenin accumulates in the cytoplasm and subsequently translocates into the nucleus where it stimulates TCF/LEF dependent transcription.

When Wnt protein binding to the cell surface is prevented, possible by a variety of inhibitors, β-catenin is bound within the GSK-3 complex, resulting in its phosphorylation and subsequent degradation by proteasomal machinery (Figure 1.4B). Inhibition of Wnt protein binding thus prevents downstream gene transcription. β-catenin activated gene transcription may also be inhibited within the canonical Wnt pathway by antagonists within the cytoplasm and the nucleus. These are covered in more detail within section 2.3.3.

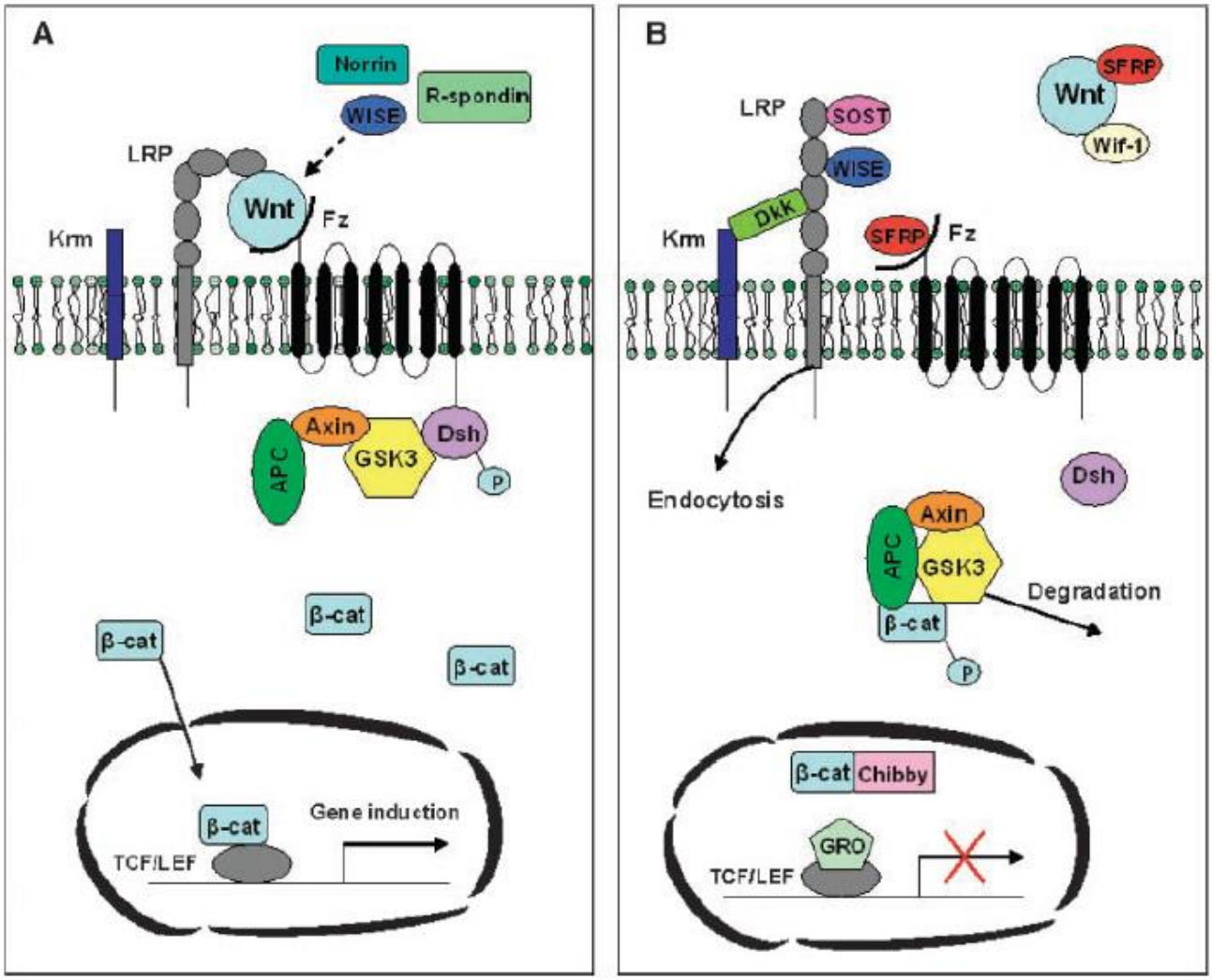

Figure 1.4. Diagram of the canonical Wnt pathway. A) Wnt binding to co-receptors LRP5/6 and Fzd initiates an intracellular cascade resulting in unphosphorylated β-catenin accumulating in the cytoplasm, then translocating into the nucleus and initiating TCF/LEF dependent gene transcription. B) Canonical Wnt binding is inhibited by a variety of inhibitors extracellularly, intracellularly, and within the nucleus. The resultant effect of such pathway inhibition is reduced downstream TCF/LEF dependent gene transcription. Diagram from Macsai *et al*., 2008 (2).

2.2. Non-canonical Wnt signalling

The non-canonical Wnt pathways broadly encompass a range of Wnt activated pathways that do not involve β-catenin (79). The primary two are the Wnt/calcium (Wnt-Ca^{2+}) pathway and the JNK/planer cell polarity (PCP) pathway (2, 80, 81). The Wnt/calcium and PCP pathways both utilise Fzd as the cell surface receptor and Dvl within the cell, but they do not involve the LRP co-receptors and result in intracellular cascades that differ to that of the Wnt/β-catenin pathway (70, 82, 83). Recently, another β-catenin independent Wnt pathway was identified in tumour cells (84). This pathway is mediated by FYN tyrosine kinase and STST3 transcriptional regulator.

Though it is the Wnt/β-catenin pathway in which this research will focus, it must be noted that there is potential competition between non-canonical and Wnt/β-catenin pathways for Wnt binding to Fzd, and for the intracellular action of Dvl. Further, a number of studies have shown suppression of Wnt/β-catenin signalling by non-canonical Wnt signalling (85-88).

2.3. Wnt/β-catenin pathway proteins, receptors, inhibitors and activators

Canonical Wnt signalling involves a large range of Wnt proteins, Wnt receptors, activators and antagonists, which all act to regulate β-catenin activity.

2.3.1. Wnt/β-catenin pathway activators

Wnt proteins are cysteine-rich glycoproteins of about 350-400 amino acids containing an N-terminal signal peptide for secretion (2, 71). Wnt proteins are hydrophobic due to post-translational modification (89). This occurs at a conserved cysteine region and is important for signalling. There are 19 known Wnt proteins in humans and mice (Wnt-1, -2, -2b, -3, -3a, -4, -5a, -5b, -6, -7a, -7b, -8a, -8b, -9a, -9b, -10a, -10b, -11 and -16) (90). Some of these Wnts are known to activate the Wnt/β-catenin pathway, some the non-canonical Wnt pathways, and others have evidence of activation of either (91). It is still not completely elucidated the involvement of these 19 Wnts have, and it remains a complexity within bone biology.

There are also other known activators of Wnt/β-catenin signalling. These are unrelated to Wnt proteins and include Norrin, R-spondin and WISE (Wnt1 induced secreted protein). Norrin binds

Fzd-4 and LRP-5, and R-spondin binds to Fzd-8 and LRP-6, initiating Wnt/β-catenin signalling (71, 92, 93). WISE, typically known to be an antagonist of the canonical Wnt pathway, can also behave as an activator at times (94).

2.3.2. Wnt/β-catenin pathway receptors

Within the Wnt/β-catenin pathway Wnt proteins bind in a receptor trimeric complex with the co-receptors Fzd and LRP5/6 (95). There are 10 Fzd genes in the mammalian genome, though they have variable binding capacities and some may possibly be redundant (71, 89). Fzds pass the transmembrane seven times and contain a cysteine-rich domain on the N-terminus that is implicated in the binding to Wnt proteins (89, 96). LRP5/6 belong to the low density lipoprotein receptor (LDLR) family of proteins, which are able to bind and internalise ligands (75). LRP5/6 however cannot perform endocytosis due to the absence of the internalisation sequence common in LDLR receptors. Also distinguishing LRP5/6 from the other LDLRs is their proline and serine rich cytoplasmic tail which, as mentioned, recruits axin. Another LRP, LRP4, shares similar binding domains to LRP5 and LRP6 (72), however it may actually be a negative regulator of Wnt signalling by augmenting the binding of sclerostin with LRP5/6 (97).

LRP5 and LRP6 have 71% homology and may have some redundancy within the gastrulation stage of embryonic development (98). However, their roles beyond this may differ. LRP5 is dispensable in embryonic development, with the survival of LRP5 deficient mice, yet vital in adult bone homeostasis (71). Mice completely deficient of LRP6 however exhibit developmental defects indicating the necessity of this receptor during embryogenesis (99).

2.3.3. Wnt/β-catenin pathway antagonists

There are a range of antagonists of the canonical Wnt pathway at the extracellular, intracellular and nuclear levels, and this review will only cover a number of these.

Within the nucleus the inhibitor Chibby is able to bind β-catenin, preventing activation of the TCF-LEF transcription factors, and further may possibly translocate β-catenin out from the nucleus (100). Further, the proteins Groucho, ICAT and NEMO-like kinase (NLK) are all able to dissolve

the binding of β-catenin to transcriptional factors and thus repress transcription activity (75, 101, 102).

The number of factors involved within the GSK-3 complex provide a multitude of mechanisms for the regulation of Wnt/β-catenin signalling within the cytoplasm. Axin can be dephosphorylated by Protein Phosphatases -1 and -2C preventing the formation of the GSK-3 complex (103, 104). The GSK-3 kinase activity can be mitigated by a number of kinases including protein kinases A, B (Akt) and C, and also MAPK-activating protein (105). The interaction of GSK-3 to Axin is inhibited by FRAT (frequently arranged in advanced T-cell) -1 and -2 (106-108).

The extracellular inhibitors include those which bind to and neutralise the Wnt proteins, and those that bind to the LRP5/6 or Fzd co-receptors. Wnt inhibitory protein (WIF) and secreted Fzd-related-proteins (sFRP) can both bind directly to Wnt proteins inhibiting their receptor binding capabilities (2). sFRP can also form non-functional complexes to Fzd and so prevent Wnt protein binding (2). There are also antagonists which bind directly to LRP5/6 co-receptors preventing Wnt activation. These include Dickkopf (DKK), sclerostin, WISE (which can also behave as an agonist), and also the LRP5/6 β-propeller maturation chaperone Mesd (71, 109).

There are four DKK family members, DKK1-4, and also a DKK3 related protein called Soggy (2). Along with affinity to LRPs, DKK proteins also are able to bind Kremen proteins (Krm) (110). In doing so, when binding LRP5/6 they can cause the receptor to undergo endocytosis (2, 71). Thus, though DKK proteins can inhibit Wnt signalling alone, it is thought that with Krm the inhibition is sustained due to the subsequent reduction in LRP receptors on the membrane surface (75). DKK1 is the most potent of the DKK proteins and has a high affinity to LRP6 (111). DKK1 is widely expressed developmentally, including in the posterior mesoderm, gut endoderm, and the neural plate, limb morphogenesis and is important in regulating Wnt3 for normal head morphogenesis (112, 113). In adults, DKK1 is highly expressed in and largely restricted to bone (75, 114), however DKK1 expression has also been seen in cartilage (115, 116) and evidence of weak expression in thymus, lung, duodenum and brown adipose tissue (114).

Sclerostin and WISE share homology and are both members of the CCN family – proteins known for cell adhesion and signalling, extracellular matrix regulation and roles in skeletal development, chondrogenesis and angiogenesis (75, 117). As mentioned, WISE is able to both activate and inhibit canonical Wnt signalling, depending on the circumstances in which it is secreted (94).

Sclerostin is a potent and specific canonical Wnt pathway inhibitor, but is restricted in expression to the bone compartment. Sclerostin is expressed mainly by osteocytes and mineralising osteoblasts, though some expression has also been seen in cementocytes (similar to an osteocytes within the lacunae of tooth cement) and mineralized hypertrophic chondrocytes (118-120).

Mesd is vital as a chaperone in the maturation of the LRP5/6 β-propeller modules (121, 122). However, as Mesd has such an affinity to these modules it functions within the extracellular space to inhibit Wnt binding to LRP5/6 and thus antagonises Wnt signalling (123).

3. Role of the Wnt/β-catenin pathway in bone

Wnt/β-catenin signalling is active in many tissues, and the modulation of this pathway has important effects on cellular proliferation and differentiation. In bone, Wnt/β-catenin signalling helps regulate cells of the osteoblast lineage, but has also been implicated in both chondrogenesis and osteoclastogenesis. The Wnt/β-catenin pathway is therefore a critical regulator of skeletal development, homeostasis and even repair.

3.1. Osteogenesis and the Wnt/β-catenin pathway

Wnt/β-catenin pathway primarily impacts on bone and bone anabolism via its regulation of osteoblasts, through their cell commitment, cell proliferation, apoptosis, and cell functioning (75, 124). Increased Wnt/β-catenin signalling results in increased osteoblast proliferation, differentiation and function, and reduced apoptosis (125-128). Modulation occurs through the number of Wnt proteins, inhibitors, and receptors involved in the Wnt/β-catenin pathway. Much of the understanding of Wnt/β-catenin signalling and osteoblastogenesis has been gained from clinical and pre-clinical studies involving mutations of these factors. Some of these studies are discussed in section 3.4, however below is a brief overview of the role of the Wnt/β-catenin pathway in osteoblast differentiation and terminal cell fate.

Osteoblasts and chondrocytes are derived from the same mesenchymal precursors and Wnt/β-catenin signalling positively pushes these precursors towards osteoblastogenesis and away from chondrogenesis. Wnt/β-catenin regulates osteoblast differentiation from mesenchymal stem cells and inhibition of the Wnt pathway, and thus inhibition of β-catenin initiated transcription, in mesenchymal cells prevents osteoblastic differentiation, instead promoting chondrogenesis (129-131). *In vivo*, mice with β-catenin knocked-out show an overall decrease in mature osteoblasts, and a reduction in expressed collagen I, osterix, and osteocalcin, usually expressed by the mature osteoblast (130, 132). *In vitro*, early osteoblastic progenitors with β-catenin knocked out converted to the chondrogenic lineage rather than differentiating into osteoblasts (133).

Wnt/β-catenin also regulates the later terminal stages of osteoblastogenesis, requiring a reduction in β-catenin signalling. Osteoblast precursor cells expressing stabilised β-catenin had increased proliferation and differentiation, but reduction in later stage cell differentiation shown by the lack

of osteocalcin expression (133). Further, when β-catenin was knocked-out *in vitro* from differentiated osteoblasts already expressing osteocalcin, the cells failed to terminally mature (131). The importance of β-catenin signalling is highlighted by upregulation of Wnt inhibitors in osteoblasts at the terminal stages of differentiation, such as DKK1, WIF1, Sfrp2, and FzdB (75).

3.2. Chondrogenesis and the Wnt/β-catenin pathway

Along with the role of Wnt/β-catenin signalling within mesenchymal progenitor cell fate determination of chondrocytes/osteoblasts, the pathway also is critically important for chondrocyte differentiation and maturation. These chondrocyte differentiation/maturation roles are seen both embryonically and postnatally and affects processes such as limb formation, bone formation and growth (2).

Developmentally, Wnt/β-catenin signalling, such as that driven by Wnt7a and Wnt3a, inhibits mesenchymal differentiation into chondrocytes (134, 135). This likely occurs through regulation of Sox9, a chondrogenic transcription factor, as well as other cell cycle regulators. Furthermore, β-catenin can also block the maturation of nascent chondrocytes (136). Chick limb bud formation experiments have further demonstrated roles for Wnt6, Wnt5a, and Wnt7a in achieving normal pattern formation through control of chondrogenic differentiation (137-139).

A more intricate process for Wnt signalling in chondrogenesis has arisen, where it seems that sequential modulation of Wnt proteins either in a stage-dependent manner, or through a number of Wnts, is likely to be an important factor in chondrocyte differentiation. For example, at the embryonic growth plate Wnt5b promotes chondrocyte proliferation and prevent differentiation, while Wnt5a actually stimulates differentiation of proliferative chondrocytes into prehypertrophic chondrocytes (140, 141). Further, cells extracted from embryonic limb buds and treated with Wnt5a were again stimulated to chondrogenic differentiation, while Wnt5a treatment of already hypertrophic chondrocytes inhibited further maturation (142). It is still to be disproved that inhibition of Wnt/β-catenin is required for complete maturation of the chondrocyte, but it appears that the Wnt signalling requirement is stage-dependent during chondrogenesis.

The likely temporal and spatial Wnt requirement for chondrogenesis is further indicated by region specific Wnt presence in the developing limb bud (143). Further it is indicated in the postnatal

growth plate, where expression of at least eight of the 19 Wnts has been demonstrated in some, or all of the four zones of the growth plate, and at different levels (2, 141). They have specific roles within each of these zones, and are modulated through the large number of Wnt activators, receptors and inhibitors of this pathway (143). A figure by Macsai et al., 2008 illustrates the spatial Wnt expression within the postnatal growth plate, along with the before mentioned action of Wnt5a and Wnt5b on the proliferative and prehypertropic chondrocytes (Figure 1.5).

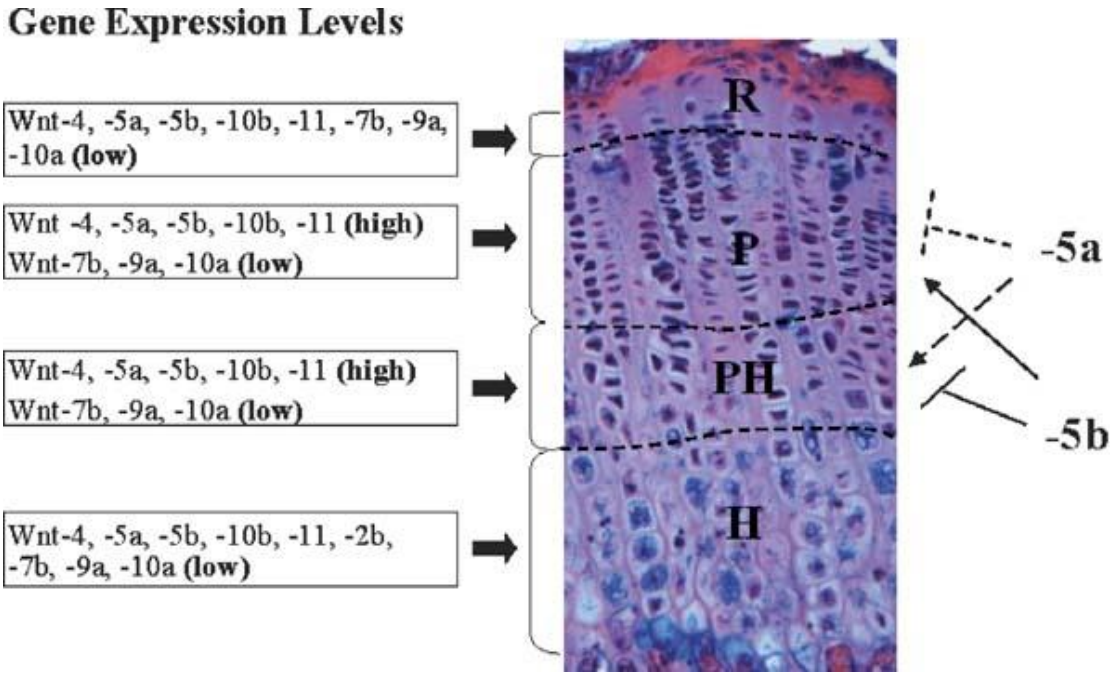

Figure 1.5. Wnt ligand expression and function within the zones of the postnatal growth plate. R: resting zone; P: proliferative zone; PH: prehypertrophic zone; H: hypertrophic zone. Image modified from Macsai et al., 2008 (2).

3.3. Osteoclastogenesis and the Wnt/β-catenin pathway

Osteoclastogenesis and bone resorption is inhibited following Wnt/β-catenin signalling in osteoblasts and osteocytes. This modulation is through OPG and RANKL expression induced by Wnt/β-catenin signalling (144-147). Interestingly, there is some evidence that osteoclast precursors may express the Wnt antagonist sclerostin, and that mature osteoclasts may express Wnt ligands (148). This indicates a likely canonical Wnt pathway mediated feedback loop.

3.4. Bone homeostasis and mechanotransduction, and the Wnt/β-catenin pathway

Bone homeostasis requires a balance between bone formation and bone resorption, both of which are affected by the Wnt/β-catenin pathway. Osteoblasts and osteoclasts work in a coupled manner to repair microdamage, release and store essential minerals, and further to maintain the size, shape or mass of the bone. Changes to size, shape and mass of the bone can occur when bone anabolism and catabolism becomes uncoupled or when everyday activities upon the skeleton are altered. The canonical Wnt pathway is modulated in these instances of changes to bone homeostasis and mechanotransduction, as detailed below.

3.4.1. Bone homeostasis and the Wnt/β-catenin pathway

The appreciation of the Wnt/β-catenin pathway as a prominent regulator of bone homeostasis developed through genetic analysis of rare human diseases of low or high bone mass, which have been further investigated in pre-clinical experimental studies.

3.4.1.1. LRP5 and LRP6 mutations

Osteoporosis pseudoglioma syndrome (OPPG) results in low bone density, bone deformation and fractures, and is caused by a loss-of-function mutation in the *Lrp5* gene, thus reduced Wnt/β-catenin signalling (149). Conversely, gain-of-function mutations in the *Lrp5* gene, which prevent binding of Wnt antagonists and thus increases Wnt/β-catenin signalling, is associated with high bone mass and density in humans (150-154).

These effects on bone mass have been confirmed in *Lrp5* gene mutation animal studies. Mice with mutations causing ubiquitous inactivation of LRP5 have been created (155-157). Complete disruption of LRP5 function results in abnormal osteoblast proliferation, leading to decreased bone formation and osteopenia. The level of severity is greater in mice with mutations within both alleles, however $Lrp5^{+/-}$ mice also have significantly lower bone volume (155). Conditional deletion of *Lrp5* within DMP1 (dentin matrix protein 1) expressing bone cells similarly resulted in a lower bone mass, confirming the critical role of LRP5 in osteocytes and/or late-stage osteoblasts (158). DMP1 is expressed in osteoblasts, osteocytes and some tooth cells (159), and is commonly utilised for selective cre recombinase deletion of genes within osteocytes and late osteoblasts (160).

A LRP5-related high bone mass (HBM) phenotype has also been created using mouse models (126, 158, 161). These involve missense mutations within the extracellular domain: either Gly171-to-Val substitution mutation (G171V) or an Ala214-to-Val substitution mutation (A214V), though the former has been more extensively investigated. The G171V mutation has been reported in humans who have an autosomal dominant HBM trait (151, 154). This single amino acid substitution within the extracellular domain of LRP5 results in a decrease in sclerostin/LRP5 and DKK1/LRP5 interaction causing a reduction in Wnt inhibition and effectively an increase in Wnt signalling (162, 163). There is also evidence that the G171V mutation disrupts the interaction of Mesd with LRP5 leading to a reduction in LRP5 on the cell surface due to decrease in the maturation of these receptors (164). These LRP5 HBM mice have increased bone mass regardless of whether the HBM mutation is ubiquitous or within DMP1 expressing bone cells only (158). This confirms the action of LRP5 to be within osteocytes and possibly late-stage osteoblasts. The HBM effect seen in these mice is a result of increased bone formation, rather than an effect on bone resorption (126).

$Lrp6^{-/-}$ homozygous deletion is neonatal lethal in mice (99). Developmental abnormalities, including truncated axial skeleton, limb defects and microphtalmia, are similar to defect reported in mice with Wnt gene mutations, such as Wnt-3a, Wnt-1 and Wnt-7a. These defects are however less severe and are likely due to the presence of the LRP5 receptor may have an overlapping function. Holmen et al. (157) showed that haploinsufficiency of LRP6 results in decreased bone mass and further decreased the osteopenia seen in $Lrp5^{-/-}$ mice. Similar low bone mass effects were

also seen in reduced function LRP6 mice, where bone mass is decreased and there is delayed ossification (165).

3.4.1.2. Sclerostin and DKK1 mutations

Other human high bone mass diseases are a result of reduced expression of the Wnt antagonist sclerostin, leading to increased Wnt/β-catenin signalling. Sclerosteosis is characterised by progressive bone overproduction, with either no effect or a small decrease in bone resorption, which results in tall stature, facial deformation, and more critically potential cranial nerve entrapment and high intracranial pressure (166-168). Sclerosteosis is caused by a mutation in the *Sost* gene resulting in a loss of the gene product sclerostin (169, 170). A similar high bone mass condition van Buchem disease, is also a result of a reduction in active sclerostin. A deletion downstream of the *Sost* gene likely has a negative outcome on sclerostin expression (171, 172). As the action of sclerostin is to prevent Wnt binding to the LRP co-receptors, like the LRP5/6 mutations, there is again a distinct increase in Wnt signalling in Sclerosteosis and van Buchem disease.

Animal studies investigating the modulation of sclerostin, and the similar Wnt antagonist DKK1, confirm the prominent effect that these antagonists have on bone mass. Mice overexpressing sclerostin or DKK1 ubiquitously, or within osteoblasts only, have a reduced number of osteoblasts and a resultant low bone mass (114, 173-175). Conversely, *Sost*$^{-/-}$ mice and *Dkk1*$^{+/-}$ mice both show a high bone mass phenotype due to increases in bone formation (112, 176-179). Complete loss of *Dkk1* is embryonically lethal, due to the requirement of DKK1 to down-regulate *Wnt3* signalling for head morphogenesis (112). Reducing *Wnt3* expression through a heterozygous allele rescued the mouse, however with a halved birth rate (112). I have been part of a recent assessment of the bone phenotype of this mouse and we have confirmed it to have high bone mass, most predominately within cancellous bone (180).

3.4.2. Bone mechanotransduction and the Wnt/β-catenin pathway

3.4.2.1. Wnt/β-catenin pathway modulation is important within bone mechanotransduction

Wnt/β-catenin signalling has been implicated as an important circuit for transducing mechanotransduction signals in bone. Historically, LRP5/6 has been envisaged as a mechanoreceptor that regulates bone mass. The anabolic response to mechanical loading is inhibited within *Lrp5*$^{-/-}$ mice, suggesting the requirement of this receptor, and Wnt/β-catenin signalling, for new bone formation (181, 182). Conversely, LRP5 gain-of-function mutations increase the response to mechanical stimulation, confirming LRP5 as a mechanosensor (182-184).

The Wnt antagonist, sclerostin, is emerging as a powerful modulator of Wnt/β-catenin signalling within bone mechanotransduction. Notably, the osteocyte, which is vital for bone mechanotransduction, is the principal source of sclerostin (118, 185). Recently, increased osteocyte expression of sclerostin has been associated with decreased loading (disuse) in rodent models, suggesting a decrease in Wnt/β-catenin signalling within this unloading model (186, 187). Further, a decline in sclerostin expression was seen with the return of loading. Notably, mice deficient in sclerostin, through genetic knock-out or short-term treatment of neutralising antibodies to sclerostin, displayed abrogated response to disuse (188, 189). This suggests the secretion of sclerostin, and the blockade of Wnt/β-catenin signalling, as a requirement to bone resorption following unloading. In addition, down-regulation of sclerostin expression was associated with mechanical loading, with the change in sclerostin expression proportional to the strain energy (186, 187). Further, within a transgenic mouse that constitutively expressed elevated sclerostin levels, the anabolic response to mechanical loading was abrogated, suggesting the necessity for sclerostin down-regulation, and for an intact Wnt/β-catenin pathway, for the anabolic response to mechanical loading to occur (190).

3.4.2.2. β-catenin signalling is a requirement for bone mechanotransduction

The downstream target for Wnt/β-catenin signalling is β-catenin and TCF/LEF related transcription. Both β-catenin levels and TCF/LEF activity are increased following *in vitro* mechanical stimulation (191, 192). However most notably, a critical threshold of β-catenin appears to be a requirement for the anabolic response of bone to mechanical loading (193). The loss of a

single β-catenin allele within DMP1 expressing cells in mice abolished the response of bone to mechanical loading.

Most of our knowledge of β-catenin and mechanotransduction is in relation to increased loading, however an i*n vitro* osteoblast study suggests that β-catenin is required for a response to unloading with β-catenin mediating RhoA GTPase down-regulation (194). It is therefore likely that β-catenin regulation is the crucial factor within bone mechanotransduction, and is the core regulatory component of the bone resorption and formation responses (195).

3.4.2.3. Regulation of β-catenin signalling via multiple pathways and paracrine factors

The regulation of β-catenin levels and activity is likely to be not solely reliant upon Wnt/LRP5/6 signalling, and may occur through a number of LRP5/6-independent pathways that interact with the Wnt/β-catenin pathway downstream of Wnt/LRP5/6 signalling. Within MSC *in vitro* shear stress studies, focal-adhesion based connections and mTORC2 activation has downstream effects on β-catenin activity through direct modulation of GSK3β (196, 197). β-catenin activity was also shown to be modulated by the Akt-signalling pathway through a mechanism involving nitric oxide and focal adhesion kinase within an *in vitro* study of MLO-Y4 osteocytes undergoing pulsating fluid flow (198). Akt is known to phosphorylate β-catenin and increase its transcriptional activity (199, 200). These results were confirmed within an *in vitro* strain study of osteoblasts whereby the nitric oxide pathway was vital for β-catenin activation and TCF/LEF transcription and the Wnt/β-catenin pathway was activated at the stage of Akt phosphorylation (201). The cytoplasmic levels of β-catenin also increased within *in vitro* MSCs following shear stress (202). This was due to a direct release of β-catenin from the transmembrane protein N-cadherin, which is a known mechanotransducer (203). These *in vitro* data suggest that mechanical stimulation of bone cells can lead to modulation of β-catenin levels and activity via LRP5/6-independent systems.

The paracrine factors prostaglandins also have implications within bone mechanotransduction and the regulation of β-catenin activity. The anabolic response to bone loading has previously been shown within both *in vivo* and *in vitro* studies to be dependent on COX-2, a protein that facilitates prostaglandin formation (204-206). And prostaglandin E2 (PGE_2) is able to induce β-catenin nuclear translocation within *in vitro* osteoblasts and osteocytes (207). Further, PGE_2 is also known to down-regulate sclerostin expression, and in turn increase Wnt/β-catenin signalling (208). PGE_2

release has also been shown to occur following mechanical loading of *Lrp5*$^{-/-}$ mice, despite the absence of an anabolic bone response (181). These data combined intimate that PGE_2 release occurs independent of LRP5 activation and Wnt/β-catenin signalling, and that the regulation of Wnt antagonists by these early responses may provide a mechanism for subsequent Wnt/β-catenin modulation.

PTH regulates levels of some Wnt antagonists, likely through modulation of β-catenin signalling and TCF/LEF transcription of these Wnt factors. Animal models of PTH administration results in decreases in sclerostin, DKK1 and WIFI (174, 209-211), and clinical studies of elevated endogenous PTH or administered PTH show decreased serum sclerostin levels (212-214). Alternatively, in a mouse study whereby PTH/PTHrP receptors were ablated in osteocytes, mice had greater sclerostin expression and were mildly osteopenic (215). PTH, binding its receptor PTH1R, can directly associate with LRP6 *in vitro*, activating signalling, axin recruitment and β-catenin phosphorylation/stabilisation, in the absence of Wnt ligands (174, 216). *In vivo* rodent studies of PTH administration corroborated LRP6 phosphorylation and β-catenin increases within osteoblasts alongside increased bone formation (216). This phosphorylation of LRP6 by PTH-PTH1R binding likely occurs through activation of protein kinase A (PKA) (216). Notably, PKA can by a downstream target of non-canonical Wnt signalling (217).

There is also some evidence of the cross-talk between estrogen receptor (ER) and Wnt/β-catenin signalling pathways during mechanotransduction and bone anabolism. In particular, downstream events of the Wnt/β-catenin signalling pathway are dependent upon ERα. Within *in vitro* mechanical strain studies on established and primary osteoblastic cells, increased nuclear β-catenin accumulation and TCF/LEF activity were blocked by selective estrogen-receptor modulators (SERM) ICI 182, 780 and tamoxifen (192). Further, β-catenin accumulation and TCF/LEF activity following *in* vitro mechanical stimulation was abrogated within primary osteoblastic cells lacking ERα. Furthermore, within primary mesenchymal progenitor cells the activation of ER signalling by estradiol (E2), or exogenously expressed ERα, synergistically enhanced Wnt3A-induced osteogenic markers and matrix mineralisation (218). E2 induces GSK3β phosphorylation leading to activation and nuclear accumulation of β-catenin within preosteoblastic cells (219). Notably, TCF1 and TCF4 directly bind ER and modulate its transcriptional activity, with the TCF4 interaction being antagonistic and the TCF1 interaction being synergistic (220).

In the consideration of the above data, is likely that β-catenin is the critical target within bone mechanotransduction, and though the LRP5/6 receptors are mechanosensitive the Wnt/β-catenin pathway is not the sole regulator of β-catenin dependent transcription. The Wnt/β-catenin pathway appears to be vital as a "switch-on" mechanism in bone mechanotransduction to ensure β-catenin signalling. This is a requirement for the downstream modulation of β-catenin in response to changes in load upon bone, both by the Wnt/β-catenin pathway itself and other interconnected pathways.

Notably, much of the literature and current knowledge relates to Wnt/β-catenin pathway mechanotransduction involvement due to increased mechanical stimulation. It is not completely clear whether the same processes are involved in the transduction of signals following reduced load. Reduced loading may see a reduction in the signalling seen in normal load or high load situations, or in contrast it may involve novel processes. It has previously been shown within a murine microarray study that the genes and pathways altered with decreased loading/disuse were different to those altered with increased loading (63). Further, the bone of mice with ablated osteocytes did not respond to disuse, however did respond to returned loading activity (50). These studies suggest that distinct processes may be involved in the response of bone to increased and decreased load.

4. Orthopaedic clinical potential for Wnt/β-catenin pathway manipulation

Due to the direct effect that the Wnt/β-catenin pathway has on bone anabolism, and the indirect effect on bone catabolism, manipulation of this pathway has great potential in orthopaedic conditions. There is the potential for improvements in diseases of inferior bone quality (such as osteogenesis imperfecta), the improvement of fracture repair, and even the treatment of multiple myeloma. Several recent pre-clinical manuscripts that I have published exemplify some of the possible uses of Wnt/β-catenin modulation. Activation of the Wnt pathway, through sclerostin deficiency, improved callus bone volume and strength in rodent closed and open fracture models (221, 222), and improved bone formation in a rat model of distraction osteogenesis (223). Further, inhibition of sclerostin through a neutralising antibody also improved the bone mass and strength in a mouse model of multiple myeloma, a plasma cell cancer that develops in the skeleton causing bone destruction and reduced strength (224).

One of the most promising possibilities for Wnt/β-catenin pathway manipulation however is in diseases of low bone quantity, particularly osteoporosis. Osteoporosis is a prevalent and potentially debilitating disease. Bone becomes of such low mass that it is more susceptible to fracture. It affects over 75 million within the USA, Europe and Japan (225), and results in 8.9 million fractures worldwide each year (226). Though due to hormonal imbalances it is prevalent in the aged, osteoporosis is not restricted to the elderly. Premature generalized osteoporosis is also seen in OPPG, interestingly as a result of a loss-of-function mutation in the LRP5 receptor (73). Also not age discriminatory is secondary osteoporosis, which can result from primary diseases or through the treatment of primary diseases, such as thyroid conditions or following corticosteroid use (227). Bone loss is also prevalent in cases of skeletal disuse. This can be due to bed or chair confinement or in diseases of skeletal restriction, such as Duchene Muscular dystrophy.

Osteoporosis develops following an imbalance of bone anabolism and catabolism, resulting in an overall loss of bone. Regulation of Wnt/β-catenin signalling may allow an increase in net bone formation, and perhaps an adjacent decrease in bone resorption, and thus could prevent or improve such low bone mass conditions.

As there are a multitude of stages of regulation, both extracellular and intracellular, within the Wnt/β-catenin pathway (see section 2.2) there are a number of potential strategies for therapeutic manipulation to improve low bone mass diseases.

4.1. Targeting GSK-3β

Already in long-term clinical use as a mood stabiliser is lithium, in the form of lithium salts. These are able to inhibit GSK-3β and thus drive downstream β-catenin signalling, resulting in an increase in osteogenesis. Pre-clinical investigations have shown that lithium improves bone mass due to increased bone formation in both wild type and low bone mass (LBM) *Lrp5*$^{-/-}$ mice (228), and also in tail suspended (unloaded/disuse) wild type mice (229). And there some contested evidence of reduced fracture risk in humans treated with lithium (230, 231). Similarly, a synthesised dual inhibitor of GSK-3α and GSK-3β also prevented bone loss in a pre-clinical rat model of osteopenia due to increased bone formation and a mild reduction in bone resorption, and also improved bone mass in wildtype (balb/c) mice due to mesenchymal progenitor proliferation and subsequent osteogenesis (232, 233). A rodent model of fracture healing was also improved with a GSK-3 inhibitor (234). Such small molecule therapeutics inhibiting GSK-3β may be of use in protecting against further bone loss in osteoporosis and even potentially improving bone mass.

The use of these drugs are however likely to be limited due to the potential of serious side-effects. Lithium is involved in other signalling pathways and lithium salts are widely known to have a narrow window of use due to potential toxicity. Some of the side effects of lithium treatment include impacts on kidney function, thyroid and parathyroid gland function, teratogenicity, tremor and weight gain (235). And though the GSK-3α/β dual inhibitor is specific to GSK-3 more than just β-catenin phosphorylation is affected. GSK-3 is known to be involved in the regulation of glycol and other glucose homeostasis steps, in inflammation and in the regulation of immune and migratory processes (105, 236-240). Dysregulation of GSK-3 is known to be involved in muscle hypertrophy, diabetes and insulin resistance, cancer and mental health disorders including bipolar mood disorder, schizophrenia, and Alzheimer's disease (241).

4.2. Targeting exogenous Wnt proteins

Upstream of the canonical Wnt pathway are other potential targets to modulate Wnt/β-catenin signalling in bone. With LRP5 loss or gain of function studies (see section 3.4.1) we understand that bone mass can be effectively regulated at this extracellular step of the pathway. Avenues for

modulation at this extracellular level include increasing the level of Wnt/β-catenin pathway agonists or inhibiting endogenous canonical Wnt pathway antagonists. Preclinical studies of endogenously up-regulated Wnt10b have shown improvement in bone mass, providing some support for treatment with Wnt proteins (242, 243). However, there is a limitation to exogenous Wnt treatment due to the low solubility of Wnt molecules which impact on clinical administration. Local delivery of Wnt3a to skeletal defects within murine pre-clinical tests has been successful though by packaging Wnt3a within liposomal vesicles (244). The local Wnt3a administration resulted in proliferation of skeletal progenitors, accelerated osteoblastogenesis and accelerated bone formation within the mice. However, the ability to treat the entire skeleton with Wnts, such as would be required in osteoporosis, seems to be limited unless further work is undertaken to improve administration.

4.3. Inhibition of Wnt antagonists

Another avenue for upstream modulation of Wnt/β-catenin signalling is the regulation of Wnt antagonists. At the time of this review, there were a number of prospective Wnt antagonist targets, most of which had begun to be utilised within pre-clinical investigations and some within clinical trials.

4.3.1. Utilising small molecules that bind SFRP-1

SFRP-1 prevents Frizzled interaction with Wnts, and an elevated bone mass phenotype is seen in mice with deleted SFRP-1 (127). Some work has commenced into screening for small molecules that bind SFRP-1. *Ex vivo* calvarial culture studies have shown some evidence of some small molecules antagonising SFRP-1 resulting in increased osteoblast numbers and even increased bone area (245-247). These small molecules include iminooxothiazolidines, diarylsulfone sulphonamide and piperidinyl diphenylsulfonyl sulphonamides. However, again the modulation of SFRP-1 would not be specific to the bone compartment with the possibility of deleterious effects seen elsewhere in the body. For example, progressive abnormal cardiac structure and dysfunction is seen in the *Sfrp-1*$^{-/-}$ mice (248) and intense SFRP-1 inhibition may cause similar outcomes.

4.3.2. DKK1 neutralizing antibodies

DKK1 is not specific to bone but it is largely limited to it with high expression seen in osteoblasts and maturing osteocytes (114). DKK1 therefore plays an important role in bone. As mentioned in section 3.4.1, down-regulation of DKK1 results in high bone mass, and the converse is also true. Pre-clinical investigations have been undertaken within rodents assessing the effect that neutralizing DKK1 antibodies have on bone (249, 250). Positive effects on bone formation and increased bone mass were seen in studies on gonad-intact growing mice and rats, however anti-DKK1 antibody (DKK1-Ab) was not able to impact on the low bone mass in ovariectomized (OVX) rats. Neutralizing DKK1 antibodies have also shown improvement in healing rodent fracture models (249, 251).

Further investigation into dosing regimens may allow us to see an action of DKK1-Ab in improving low bone mass conditions, however there is a high risk of adverse effects with DKK1-Ab use. DKK1 is expressed elsewhere in the body, beyond the bone compartment, including within platelets, skin and cells of the joint (252-255). Despite the complicated adverse effects in DKK1 modulation, continuing development and investigation into the potential of DKK1-Ab is likely due to promising outcomes that have also been observed in pre-clinical models of multiple myeloma (256-258), rheumatoid arthritis (254) and ankylosing spondylitis (259).

4.3.3. Sclerostin neutralizing antibodies

Of greater prospective for clinical Wnt modulation of bone is targeting sclerostin. As mentioned in section 3.4.1 a lack, or repression, of sclerostin results in an increased bone mass phenotype in both humans and mice, with increased bone density and content primarily as a result of increased bone formation. Anti-sclerostin antibody (Scl-Ab) treatment has been investigated in pre-clinical animal models, with resultant increases in bone formation, bone mass and bone strength (260-264). These studies involved healthy non-human primates, aged rats, and OVX rats, which is a model for osteoporosis. Importantly, the anabolic effects were seen on both remodelling and previously resting bone surfaces within these studies suggesting anti-sclerostin antibody may be a viable treatment in low bone mass diseases. These studies all involved neutralizing antibodies to sclerostin developed by Amgen Inc. These were murine Scl-AbII, ratized Scl-AbII, ratized Scl-AbIII and humanized Scl-AbV.

There have been two humanised Scl-Ab, romosumab (Amgen Inc. and UBC Inc.) and blosozumab (Eli Lilly), which have undergone clinical trials aimed for the treatment of osteoporosis and other low bone mass conditions. Romosumab has reached Phase III (265-267) and blosozumab Phase II (268-270).

In a brief summary, all clinical trials have involved postmenopausal women (and also healthy males in Phase I romosumab). Treatment dose and length has varied from single doses (Phase I) (265, 268) to one year of treatment [monthly/quarterly (266, 267) or every 2 or 4 weeks (269)]. Increases in bone formation markers (such as P1NP, alkaline phosphatase or osteocalcin) and bone mineral density (with significant measurements recorded in the lumbar spine and/or total hip) were seen in all studies, along with decreases in CTx (C-terminal telopeptide, a bone resorption marker). Results overall confirm that Scl-Ab is an effective anabolic agent and may aid in returning uncoupled bone remodelling to a normalised state.

The levels of bone formation markers however have shown to be transient, returning to or below baseline before the end of the trial and within the period of Scl-Ab dosing within Phase II and III trials (266, 267, 269). CTx levels however remained below baseline in these studies. Similar effects have been shown within pre-clinical data: OVX rats treated weekly with Scl-Ab for 26 weeks had rapid increases in bone formation, however these anabolic effects were also transient (271). Notably, the anti-catabolic effects remained throughout the anti-sclerostin antibody treatment period. Similar cessation of strong anabolic effects have been seen in patients with Sclerosteosis (272).

It is therefore likely that longer administration of Scl-Ab, or more potentially subsequent therapy with an anti-catabolic, may be required for Scl-Ab to be effective long-term in maintaining improved bone mass. An additional Phase II romosozumab trial involved an additional year extension of Scl-Ab (romosozumab) treatment, followed by 6-monthly treatment with denosumab (which targets RANKL and is used as an anti-catabolic therapy) (273). Results, though only in abstract form, suggest that subjects shifted to denosumab maintained BMD increases, whilst subjects shifted to a placebo in the third year had BMD levels that returned to pre-treatment levels. The Phase III romosozumab trial also included a second year of 6-monthly denosumab treatment for all subjects (267). Subjects from the original romosozumab group had reduced vertebral fracture after 12 months denosumab therapy compared to the control group. These data suggest

that the subsequent therapy of an anti-catabolic following a Scl-Ab regimen may allow for a more sustained outcome of improved bone mass.

The mechanism behind the loss of prolonged bone anabolism with Scl-Ab therapy is not elucidated, however increased expression of the similar Wnt antagonist, DKK1, is noted when sclerostin is deficient (274-276). This has been seen within human and mouse conditions of *Sost* knock-out and also with the use of neutralizing antibodies to sclerostin. This may be negative feed-back response due to the absence of sclerostin and activated Wnt/β-catenin signalling. It is unknown whether DKK1, or other Wnt factors, are modulated to compensate.

There is some evidence that sclerostin is also expressed within articular cartilage (277, 278), and weak expression has been seen in adult kidney (169) and aorta (279). The risk to these tissues appears to be low however and evidence indicates that sclerostin inhibition does not seem to impact on the ability of cartilage to remodel following injury or during aging in rodents (278), though there is some contention over this (277).

Only mild adverse side-effects, which were not deemed serious, were seen within Phase I and II clinical trials of Scl-Ab therapy. However, a recent news release from Amgen has indicated a safety concern with an imbalance of cardiovascular events within the Phase III romosozumab (branded as EVENITY) trial (280). The occurrence of positively adjudicated cardiovascular serious adverse events at 12 months was 2.5% with Scl-Ab treatment, but only 1.9% within the control alendronate group. This serious outcome may delay the soon to be expected release of romosozumab/EVENITY on to the market.

5. Aims and Hypotheses

The Wnt/β-catenin pathway has an essential role in bone development, however its precise roles in bone homeostasis and mechanotransduction of bone loading requires further investigation. The Wnt/β-catenin pathway can be modulated with profound effects on bone formation/resorption and ultimately bone mass using neutralising antibodies to Wnt antagonists. Sclerostin antibodies provide effective bone anabolic and anti-catabolic actions, while producing minimal adverse effects. The transience of sclerostin antibody activity on bone anabolism has been speculated to be due to compensatory upregulation of DKK1, but has yet to be definitively shown. Sclerostin and DKK1 are also responsive to mechanical load, leading to supposition that these factors are important for bone mechanotransduction.

Based on this background, the objective of this thesis was to investigate the effects of modulating the Wnt/β-catenin pathway on bone homeostasis and mechanotransduction. This was based on several key hypotheses:

1) That exercise is redundant with therapies antagonizing the Wnt/β-catenin pathway

Following mechanical loading there is a decrease in the expression of Wnt antagonists, sclerostin and DKK1. Furthermore, deficiency in these antagonists or other factors influencing Wnt/β-catenin signalling (e.g. LRP5 gain-of-function mutations, increased levels of Wnt agonists) increases bone formation and mass. It was hypothesized that the decreases in sclerostin and DKK1 expression following bone loading would be redundant with neutralising antibodies to sclerostin.

2) That combined Wnt/β-catenin activating therapies have synergistic effects

Neutralising antibodies to DKK1 and sclerostin show promising anabolic effects on bone. Based on emerging data that Wnt antagonists could be up-regulated in response to deficiency in other family members, it is possible that combining Wnt/β-catenin activating treatments could have synergistic effects by preventing any negative feedback. I hypothesise that having

combined deficiency in DKK1 and sclerostin will provide a synergistic anabolic response within bone.

3) **That any lack of redundancy between exercise and neutralising antibodies to sclerostin would be the result of compensation by other Wnt antagonists, such as DKK1**

While it was hypothesized that exercise and sclerostin antibodies would be redundant, however if this is proven incorrect this could be due to the result of a negative feedback loop within the Wnt/β-catenin pathway. As DKK1 levels are increased with *Sost* inactivation or with anti-sclerostin antibody therapy, I hypothesise that DKK1 is a primary candidate for any lack of redundancy.

Experimental Models

Knock-out mouse models featuring gene inactivation for sclerostin (*Sost* KO) and DKK1 (*Dkk1* KO) were available to me. I also had access to a murine neutralising antibody to sclerostin, which was developed by Novartis Pharma AG and gifted by them and Mereo BioPharma.

The mechanotransduction responses were assessed using tibial model of mechanical loading in both knockout and control mice. This loading model was developed by the Biomedical Engineering group at Cornell University, (Ithaca, NY, USA), and is widely used as an *in vivo* mechanical loading model (43, 45, 281-283). This model involves compressive axial cyclic loading of the mid-diaphysis of the tibiae, with the contralateral limb as non-loaded control. Of note, bilateral tibiae are symmetrical within growing rodents, with contralateral limbs suitable for use as controls (284).

Due to the increased bone volume and strength of *Sost* KO and *Dkk1* KO mice, it was hypothesized that there may be differences between animals matched for load versus those matched for strain, and thus both cohorts were examined. Sclerostin knockout mice were also assessed using a model of tibial disuse (unloading). While other groups have reported using an unloading hind-limb suspension model (188, 189), we utilised a unilateral tibial disuse model where muscle paralysis

is induced by intramuscular botulinum toxin (BTX) injection. Mice were strain, sex, and age matched with loading studies, allowing the two treatments to be directly compared.

In terms of outcome measures, this work was analysed by dual-energy X-ray absorptiometry (DXA; GE Lunar PIXImus; Lunar Piximus Corp, Madison, WI, USA) and microcomputed tomography (microCT; Skyscan 1174 2; Skyscan NV, Kontich, Belgium), mechanical testing (Instron 5944; Massachusetts, USA), and histomorphometric analysis. Critical outcome measures included bone volume, bone density, bone strength, dynamic bone formation and osteoclast activity. Quantitative polymerase chain reaction (qPCR) for the *Sost* gene or immunohistochemical staining for sclerostin were also undertaken within studies involving *Dkk1* KO mice. RNA sequencing was also performed (outsourced) for one study from mRNA collected from tibial mid-diaphyses following two sessions of loading. This technology provided some mechanistic insight into the genes and pathways altered within loading treatment, sclerostin antibody treatment, and with combination therapy. These techniques are standard for high-quality bone analysis and important in the arena of bone mechanotransduction – microCT provides three-dimensional (3D) density, volume and architecture information, whereas histology of samples double-labelled with the fluorochrome calcein provides rate of bone apposition, and qPCR and RNASeq provide changes in gene transcription (43, 45, 190, 281, 283, 285, 286). End-points were chosen to allow comparison to other studies of bone mechanotransduction (43, 45, 186, 283).

In conclusion, the aim of this project was to examine the juxtaposition between Wnt/β-catenin activation, biomechanical loading, and bone quantity/quality. In particular, the effects of short term and chronic inhibition of Wnt antagonists were trialled in a variety of preclinical models.

References

1. Jee WSS. Integrated Bone Tissue Physiology: Anatomy and Physiology. In: Cowin SC, editor. Bone Mechanics Handbook 2nd Edition. Florida: Boca Raton; 2001.

2. Macsai CE, Foster BK, Xian CJ. Roles of Wnt signalling in bone growth, remodelling, skeletal disorders and fracture repair. J Cell Physiol. 2008;215(3):578-87.

3. Sommerfeldt DW, Rubin CT. Biology of bone and how it orchestrates the form and function of the skeleton. European Spine Journal. 2001(10):S86-S95.

4. Clarke B. Normal bone anatomy and physiology. Clinical journal of the American Society of Nephrology : CJASN. 2008;3 Suppl 3:S131-9.

5. Browne D. Skeletal System Module 4: Bone Structure.: OpenStax CNX.; 2013. Available from: http://cnx.org/contents/e4e7ed87-dca1-4c48-be92-9eb45065b8f0@2.

6. Buckwalter JA, Glimcher MJ, Cooper RR, Recker R. Bone biology. I: Structure, blood supply, cells, matrix, and mineralization. Instr Course Lect. 1996;45:371-86.

7. Glimcher MJ. Bone: Nature of the Calcium Phosphate Crystals and Cellular, Structural, and Physical Chemical Mechanisms in Their Formation. Reviews in Mineralogy and Geochemistry. 2006;64(1):223-82.

8. Majeska RJ. Cell Biology of Bone. In: Cowin SC, editor. Bone Mechanics Handbook 2nd Edition. Florida: Boca Raton; 2001.

9. Marks SC, Odgren PR. Structure and Development of the Skeleton. In: Bilezikian JP, Raisz LG, Rodan GA, editors. Principles of Bone Biology. 1. 2 ed. San Diego: Academic Press; 2002. p. 3-15.

10. Kular J, Tickner J, Chim SM, Xu J. An overview of the regulation of bone remodelling at the cellular level. Clinical biochemistry. 2012;45(12):863-73.

11. Everts V, Delaisse JM, Korper W, Jansen DC, Tigchelaar-Gutter W, Saftig P, et al. The bone lining cell: its role in cleaning Howship's lacunae and initiating bone formation. J Bone Miner Res. 2002;17(1):77-90.

12. Aubin JE, Turksen K. Monoclonal antibodies as tools for studying the osteoblast lineage. Microscopy research and technique. 1996;33(2):128-40.

13. Capulli M, Paone R, Rucci N. Osteoblast and osteocyte: games without frontiers. Archives of biochemistry and biophysics. 2014;561:3-12.

14. Nijeweide PJ, Burger EH, Klein-Nulend J. The Osteocyte. In: Bilezikian JP, Raisz LG, Rodan GA, editors. Principles of Bone Biology. 1. 2 ed. San Diego: Academic Press; 2002. p. 93-107.

15. Blair JM, Zheng Y, Dunstan CR. RANK ligand. The international journal of biochemistry & cell biology. 2007;39(6):1077-81.

16. Yasuda H, Shima N, Nakagawa N, Yamaguchi K, Kinosaki M, Mochizuki S, et al. Osteoclast differentiation factor is a ligand for osteoprotegerin/osteoclastogenesis-inhibitory factor and is identical to TRANCE/RANKL. Proc Natl Acad Sci U S A. 1998;95(7):3597-602.

17. Lacey DL, Timms E, Tan HL, Kelley MJ, Dunstan CR, Burgess T, et al. Osteoprotegerin ligand is a cytokine that regulates osteoclast differentiation and activation. Cell. 1998;93(2):165-76.

18. Hsu H, Lacey DL, Dunstan CR, Solovyev I, Colombero A, Timms E, et al. Tumor necrosis factor receptor family member RANK mediates osteoclast differentiation and activation induced by osteoprotegerin ligand. Proc Natl Acad Sci U S A. 1999;96(7):3540-5.

19. Burgess TL, Qian Y, Kaufman S, Ring BD, Van G, Capparelli C, et al. The ligand for osteoprotegerin (OPGL) directly activates mature osteoclasts. The Journal of cell biology. 1999;145(3):527-38.

20. Yasuda H, Shima N, Nakagawa N, Mochizuki SI, Yano K, Fujise N, et al. Identity of osteoclastogenesis inhibitory factor (OCIF) and osteoprotegerin (OPG): a mechanism by which OPG/OCIF inhibits osteoclastogenesis in vitro. Endocrinology. 1998;139(3):1329-37.

21. Xiong J, Onal M, Jilka RL, Weinstein RS, Manolagas SC, O'Brien CA. Matrix-embedded cells control osteoclast formation. Nature Medicine. 2011;17:1235.

22. Buckwalter JA, Glimcher MJ, Cooper RR, Recker R. Bone biology. II: Formation, form, modeling, remodeling, and regulation of cell function. Instr Course Lect. 1996;45:387-99.

23. Provot S, Schipani E. Molecular mechanisms of endochondral bone development. Biochem Biophys Res Commun. 2005;328(3):658-65.

24. Karaplis AC. Embryonic Development of Bone and the Molecular Regulation of Intramembranous and Endochondral Bone Formation. In: Bilezikian JP, Raisz LG, Rodan GA, editors. Principles of Bone Biology. 1. 2 ed. San Diego: Academic Press; 2002. p. 33-58.

25. Zelzer E, Olsen BR. The genetic basis for skeletal diseases. Nature. 2003;423(6937):343-8.

26. Ott SM. Histomorphometric analysis of bone remodelling. Principles of bone biology. 2 ed. New York: Academic Press; 2002. p. 303-19.

27. Goodship AE, Cunningham JL. Functional Adaptation of Bone in Remodeling and Repair in Vivo. In: Cowin SC, editor. Bone Mechanics Handbook 2nd Edition. Florida: Boca Raton; 2001.

28. Wolff J. The Classic: On the Significance of the Architecture of the Spongy Substance for the Question of Bone Growth: A preliminary publication. Clinical Orthopaedics and Related Research. 2011;469(11):3077-8.

29. Frost HM. The mechanostat: a proposed pathogenic mechanism of osteoporoses and the bone mass effects of mechanical and nonmechanical agents. Bone and mineral. 1987;2(2):73-85.

30. Burkhart JM, Jowsey J. Parathyroid and thyroid hormones in the development of immobilization osteoporosis. Endocrinology. 1967;81(5):1053-62.

31. Vogel JM, Whittle MW. Bone mineral changes: the second manned Skylab mission. Aviation, space, and environmental medicine. 1976;47(4):396-400.

32. Leblanc AD, Schneider VS, Evans HJ, Engelbretson DA, Krebs JM. Bone mineral loss and recovery after 17 weeks of bed rest. J Bone Miner Res. 1990;5(8):843-50.

33. Collet P, Uebelhart D, Vico L, Moro L, Hartmann D, Roth M, et al. Effects of 1- and 6-month spaceflight on bone mass and biochemistry in two humans. Bone. 1997;20(6):547-51.

34. Uhthoff HK, Jaworski ZF. Bone loss in response to long-term immobilisation. The Journal of bone and joint surgery British volume. 1978;60-b(3):420-9.

35. Skerry TM, Lanyon LE. Interruption of disuse by short duration walking exercise does not prevent bone loss in the sheep calcaneus. Bone. 1995;16(2):269-74.

36. Globus RK, Bikle DD, Morey-Holton E. The temporal response of bone to unloading. Endocrinology. 1986;118(2):733-42.

37. Alfredson H, Nordstrom P, Pietila T, Lorentzon R. Long-term loading and regional bone mass of the arm in female volleyball players. Calcif Tissue Int. 1998;62(4):303-8.

38. Kontulainen S, Sievanen H, Kannus P, Pasanen M, Vuori I. Effect of long-term impact-loading on mass, size, and estimated strength of humerus and radius of female racquet-sports players: a peripheral quantitative computed tomography study between young and old starters and controls. J Bone Miner Res. 2003;18(2):352-9.

39. Cheng S, Suominen H, Rantanen T, Parkatti T, Heikkinen E. Bone mineral density and physical activity in 50-60-year-old women. Bone and mineral. 1991;12(2):123-32.

40. Kirk S, Sharp CF, Elbaum N, Endres DB, Simons SM, Mohler JG, et al. Effect of long-distance running on bone mass in women. J Bone Miner Res. 1989;4(4):515-22.

41. Ducher G, Jaffre C, Arlettaz A, Benhamou CL, Courteix D. Effects of long-term tennis playing on the muscle-bone relationship in the dominant and nondominant forearms. Canadian journal of applied physiology = Revue canadienne de physiologie appliquee. 2005;30(1):3-17.

42. Haapasalo H, Sievanen H, Kannus P, Heinonen A, Oja P, Vuori I. Dimensions and estimated mechanical characteristics of the humerus after long-term tennis loading. J Bone Miner Res. 1996;11(6):864-72.

43. Lynch ME, Main RP, Xu Q, Walsh DJ, Schaffler MB, Wright TM, et al. Cancellous bone adaptation to tibial compression is not sex dependent in growing mice. J Appl Physiol. 2010;109(3):685-91.

44. De Souza RL, Matsuura M, Eckstein F, Rawlinson SC, Lanyon LE, Pitsillides AA. Non-invasive axial loading of mouse tibiae increases cortical bone formation and modifies trabecular organization: a new model to study cortical and cancellous compartments in a single loaded element. Bone. 2005;37(6):810-8.

45. Fritton JC, Myers ER, Wright TM, van der Meulen MC. Loading induces site-specific increases in mineral content assessed by microcomputed tomography of the mouse tibia. Bone. 2005;36(6):1030-8.

46. Thompson WR, Rubin CT, Rubin J. Mechanical regulation of signaling pathways in bone. Gene. 2012;503(2):179-93.

47. Burger EH, Klein-Nulend J. Mechanotransduction in bone--role of the lacuno-canalicular network. FASEB journal : official publication of the Federation of American Societies for Experimental Biology. 1999;13 Suppl:S101-12.

48. Asada N, Katayama Y, Sato M, Minagawa K, Wakahashi K, Kawano H, et al. Matrix-embedded osteocytes regulate mobilization of hematopoietic stem/progenitor cells. Cell Stem Cell. 2013;12(6):737-47.

49. Smit TH, Burger EH. Is BMU-coupling a strain-regulated phenomenon? A finite element analysis. J Bone Miner Res. 2000;15(2):301-7.

50. Tatsumi S, Ishii K, Amizuka N, Li M, Kobayashi T, Kohno K, et al. Targeted ablation of osteocytes induces osteoporosis with defective mechanotransduction. Cell Metab. 2007;5(6):464-75.

51. Yavropoulou MP, Yovos JG. The molecular basis of bone mechanotransduction. J Musculoskelet Neuronal Interact. 2016;16(3):221-36.

52. Knothe Tate ML, Niederer P, Knothe U. In vivo tracer transport through the lacunocanalicular system of rat bone in an environment devoid of mechanical loading. Bone. 1998;22(2):107-17.

53. Knothe Tate ML, Steck R, Forwood MR, Niederer P. In vivo demonstration of load-induced fluid flow in the rat tibia and its potential implications for processes associated with functional adaptation. The Journal of experimental biology. 2000;203(Pt 18):2737-45.

54. Mikuni-Takagaki Y, Suzuki Y, Kawase T, Saito S. Distinct responses of different populations of bone cells to mechanical stress. Endocrinology. 1996;137(5):2028-35.

55. Kawata A, Mikuni-Takagaki Y. Mechanotransduction in stretched osteocytes--temporal expression of immediate early and other genes. Biochem Biophys Res Commun. 1998;246(2):404-8.

56. Miyauchi A, Notoya K, Mikuni-Takagaki Y, Takagi Y, Goto M, Miki Y, et al. Parathyroid hormone-activated volume-sensitive calcium influx pathways in mechanically loaded osteocytes. J Biol Chem. 2000;275(5):3335-42.

57. Turner CH, Warden SJ, Bellido T, Plotkin LI, Kumar N, Jasiuk I, et al. Mechanobiology of the skeleton. Science signaling. 2009;2(68):pt3.

58. Liedert A, Wagner L, Seefried L, Ebert R, Jakob F, Ignatius A. Estrogen receptor and Wnt signaling interact to regulate early gene expression in response to mechanical strain in osteoblastic cells. Biochem Biophys Res Commun. 2010;394(3):755-9.

59. Lara-Castillo N, Kim-Weroha NA, Kamel MA, Javaheri B, Ellies DL, Krumlauf RE, et al. In vivo mechanical loading rapidly activates beta-catenin signaling in osteocytes through a prostaglandin mediated mechanism. Bone. 2015;76:58-66.

60. Sun C, Yuan H, Wang L, Wei X, Williams L, Krebsbach PH, et al. FAK Promotes Osteoblast Progenitor Cell Proliferation and Differentiation by Enhancing Wnt Signaling. J Bone Miner Res. 2016;31(12):2227-38.

61. Ryder KD, Duncan RL. Parathyroid hormone enhances fluid shear-induced [Ca2+]i signaling in osteoblastic cells through activation of mechanosensitive and voltage-sensitive Ca2+ channels. J Bone Miner Res. 2001;16(2):240-8.

62. McAllister TN, Frangos JA. Steady and transient fluid shear stress stimulate NO release in osteoblasts through distinct biochemical pathways. J Bone Miner Res. 1999;14(6):930-6.

63. Zaman G, Saxon LK, Sunters A, Hilton H, Underhill P, Williams D, et al. Loading-related regulation of gene expression in bone in the contexts of estrogen deficiency, lack of estrogen receptor alpha and disuse. Bone. 2010;46(3):628-42.

64. Bonewald LF, Johnson ML. Osteocytes, mechanosensing and Wnt signaling. Bone. 2008;42(4):606-15.

65. Hoey DA, Kelly DJ, Jacobs CR. A role for the primary cilium in paracrine signaling between mechanically stimulated osteocytes and mesenchymal stem cells. Biochemical and Biophysical Research Communications. 2011;412(1):182-7.

66. You L, Temiyasathit S, Lee P, Kim CH, Tummala P, Yao W, et al. Osteocytes as mechanosensors in the inhibition of bone resorption due to mechanical loading. Bone. 2008;42(1):172-9.

67. Skerry TM, Bitensky L, Chayen J, Lanyon LE. Early strain-related changes in enzyme activity in osteocytes following bone loading in vivo. J Bone Miner Res. 1989;4(5):783-8.

68. Swarup S, Verheyen EM. Wnt/Wingless signaling in Drosophila. Cold Spring Harbor perspectives in biology. 2012;4(6).

69. Clevers H. Wnt/beta-catenin signaling in development and disease. Cell. 2006;127(3):469-80.

70. Angers S, Moon RT. Proximal events in Wnt signal transduction. Nature reviews Molecular cell biology. 2009;10(7):468-77.

71. MacDonald BT, Tamai K, He X. Wnt/beta-catenin signaling: components, mechanisms, and diseases. Dev Cell. 2009;17(1):9-26.

72. Choi HY, Dieckmann M, Herz J, Niemeier A. Lrp4, a novel receptor for Dickkopf 1 and sclerostin, is expressed by osteoblasts and regulates bone growth and turnover in vivo. PLoS One. 2009;4(11):e7930.

73. Williams BO, Insogna KL. Where Wnts went: the exploding field of Lrp5 and Lrp6 signaling in bone. J Bone Miner Res. 2009;24(2):171-8.

74. Chen W, ten Berge D, Brown J, Ahn S, Hu LA, Miller WE, et al. Dishevelled 2 recruits beta-arrestin 2 to mediate Wnt5A-stimulated endocytosis of Frizzled 4. Science. 2003;301(5638):1391-4.

75. Baron R, Rawadi G. Targeting the Wnt/beta-catenin pathway to regulate bone formation in the adult skeleton. Endocrinology. 2007;148(6):2635-43.

76. Hart MJ, de los Santos R, Albert IN, Rubinfeld B, Polakis P. Downregulation of beta-catenin by human Axin and its association with the APC tumor suppressor, beta-catenin and GSK3 beta. Current biology : CB. 1998;8(10):573-81.

77. Rubinfeld B, Albert I, Porfiri E, Fiol C, Munemitsu S, Polakis P. Binding of GSK3beta to the APC-beta-catenin complex and regulation of complex assembly. Science. 1996;272(5264):1023-6.

78. Del Valle-Perez B, Arques O, Vinyoles M, de Herreros AG, Dunach M. Coordinated action of CK1 isoforms in canonical Wnt signaling. Molecular and cellular biology. 2011;31(14):2877-88.

79. Semenov MV, Habas R, Macdonald BT, He X. SnapShot: Noncanonical Wnt Signaling Pathways. Cell. 2007;131(7):1378.

80. Jenny A. Planar cell polarity signaling in the Drosophila eye. Curr Top Dev Biol. 2010;93:189-227.

81. Kohn AD, Moon RT. Wnt and calcium signaling: beta-catenin-independent pathways. Cell calcium. 2005;38(3-4):439-46.

82. Grumolato L, Liu G, Mong P, Mudbhary R, Biswas R, Arroyave R, et al. Canonical and noncanonical Wnts use a common mechanism to activate completely unrelated coreceptors. Genes Dev. 2010;24(22):2517-30.

83. Green JL, Kuntz SG, Sternberg PW. Ror receptor tyrosine kinases: orphans no more. Trends in cell biology. 2008;18(11):536-44.

84. Gujral TS, Chan M, Peshkin L, Sorger PK, Kirschner MW, MacBeath G. A noncanonical Frizzled2 pathway regulates epithelial-mesenchymal transition and metastasis. Cell. 2014;159(4):844-56.

85. Saneyoshi T, Kume S, Amasaki Y, Mikoshiba K. The Wnt/calcium pathway activates NF-AT and promotes ventral cell fate in Xenopus embryos. Nature. 2002;417(6886):295-9.

86. Topol L, Jiang X, Choi H, Garrett-Beal L, Carolan PJ, Yang Y. Wnt-5a inhibits the canonical Wnt pathway by promoting GSK-3-independent beta-catenin degradation. The Journal of cell biology. 2003;162(5):899-908.

87. Ishitani T, Kishida S, Hyodo-Miura J, Ueno N, Yasuda J, Waterman M, et al. The TAK1-NLK mitogen-activated protein kinase cascade functions in the Wnt-5a/Ca(2+) pathway to antagonize Wnt/beta-catenin signaling. Molecular and cellular biology. 2003;23(1):131-9.

88. Lee JM, Kim IS, Kim H, Lee JS, Kim K, Yim HY, et al. RORalpha attenuates Wnt/beta-catenin signaling by PKCalpha-dependent phosphorylation in colon cancer. Molecular cell. 2010;37(2):183-95.

89. Logan CY, Nusse R. The Wnt signaling pathway in development and disease. Annu Rev Cell Dev Biol. 2004;20:781-810.

90. Nusse R. The Wnt homepage CA, USA [updated June 2017. Available from: http://web.stanford.edu/group/nusselab/cgi-bin/wnt/.

91. Habas R, Dawid IB. Dishevelled and Wnt signaling: is the nucleus the final frontier? Journal of biology. 2005;4(1):2.

92. Xu Q, Wang Y, Dabdoub A, Smallwood PM, Williams J, Woods C, et al. Vascular development in the retina and inner ear: control by Norrin and Frizzled-4, a high-affinity ligand-receptor pair. Cell. 2004;116(6):883-95.

93. Nam JS, Turcotte TJ, Smith PF, Choi S, Yoon JK. Mouse cristin/R-spondin family proteins are novel ligands for the Frizzled 8 and LRP6 receptors and activate beta-catenin-dependent gene expression. J Biol Chem. 2006;281(19):13247-57.

94. Itasaki N, Jones CM, Mercurio S, Rowe A, Domingos PM, Smith JC, et al. Wise, a context-dependent activator and inhibitor of Wnt signalling. Development. 2003;130(18):4295-305.

95. Wu CH, Nusse R. Ligand receptor interactions in the Wnt signaling pathway in Drosophila. J Biol Chem. 2002;277(44):41762-9.

96. Dann CE, Hsieh JC, Rattner A, Sharma D, Nathans J, Leahy DJ. Insights into Wnt binding and signalling from the structures of two Frizzled cysteine-rich domains. Nature. 2001;412(6842):86-90.

97. Leupin O, Piters E, Halleux C, Hu S, Kramer I, Morvan F, et al. Bone overgrowth-associated mutations in the LRP4 gene impair sclerostin facilitator function. J Biol Chem. 2011;286(22):19489-500.

98. He X, Semenov M, Tamai K, Zeng X. LDL receptor-related proteins 5 and 6 in Wnt/beta-catenin signaling: arrows point the way. Development. 2004;131(8):1663-77.

99. Pinson KI, Brennan J, Monkley S, Avery BJ, Skarnes WC. An LDL-receptor-related protein mediates Wnt signalling in mice. Nature. 2000;407(6803):535-8.

100. Takemaru K, Yamaguchi S, Lee YS, Zhang Y, Carthew RW, Moon RT. Chibby, a nuclear beta-catenin-associated antagonist of the Wnt/Wingless pathway. Nature. 2003;422(6934):905-9.

101. Daniels DL, Weis WI. ICAT inhibits beta-catenin binding to Tcf/Lef-family transcription factors and the general coactivator p300 using independent structural modules. Molecular cell. 2002;10(3):573-84.

102. Ishitani T, Ninomiya-Tsuji J, Nagai S, Nishita M, Meneghini M, Barker N, et al. The TAK1-NLK-MAPK-related pathway antagonizes signalling between beta-catenin and transcription factor TCF. Nature. 1999;399(6738):798-802.

103. Luo W, Peterson A, Garcia BA, Coombs G, Kofahl B, Heinrich R, et al. Protein phosphatase 1 regulates assembly and function of the beta-catenin degradation complex. The EMBO journal. 2007;26(6):1511-21.

104. Strovel ET, Wu D, Sussman DJ. Protein phosphatase 2Calpha dephosphorylates axin and activates LEF-1-dependent transcription. J Biol Chem. 2000;275(4):2399-403.

105. Rayasam GV, Tulasi VK, Sodhi R, Davis JA, Ray A. Glycogen synthase kinase 3: more than a namesake. British journal of pharmacology. 2009;156(6):885-98.

106. Yost C, Farr GH, 3rd, Pierce SB, Ferkey DM, Chen MM, Kimelman D. GBP, an inhibitor of GSK-3, is implicated in Xenopus development and oncogenesis. Cell. 1998;93(6):1031-41.

107. Li L, Yuan H, Weaver CD, Mao J, Farr GH, 3rd, Sussman DJ, et al. Axin and Frat1 interact with dvl and GSK, bridging Dvl to GSK in Wnt-mediated regulation of LEF-1. The EMBO journal. 1999;18(15):4233-40.

108. Freemantle SJ, Portland HB, Ewings K, Dmitrovsky F, DiPetrillo K, Spinella MJ, et al. Characterization and tissue-specific expression of human GSK-3-binding proteins FRAT1 and FRAT2. Gene. 2002;291(1-2):17-27.

109. Lu W, Liu CC, Thottassery JV, Bu G, Li Y. Mesd is a universal inhibitor of Wnt coreceptors LRP5 and LRP6 and blocks Wnt/beta-catenin signaling in cancer cells. Biochemistry. 2010;49(22):4635-43.

110. Mao B, Wu W, Davidson G, Marhold J, Li M, Mechler BM, et al. Kremen proteins are Dickkopf receptors that regulate Wnt/beta-catenin signalling. Nature. 2002;417(6889):664-7.

111. Semenov MV, Tamai K, Brott BK, Kuhl M, Sokol S, He X. Head inducer Dickkopf-1 is a ligand for Wnt coreceptor LRP6. Current biology : CB. 2001;11(12):951-61.

112. Lewis SL, Khoo PL, De Young RA, Steiner K, Wilcock C, Mukhopadhyay M, et al. Dkk1 and Wnt3 interact to control head morphogenesis in the mouse. Development. 2008;135(10):1791-801.

113. Mukhopadhyay M, Shtrom S, Rodriguez-Esteban C, Chen L, Tsukui T, Gomer L, et al. Dickkopf1 is required for embryonic head induction and limb morphogenesis in the mouse. Dev Cell. 2001;1(3):423-34.

114. Li J, Sarosi I, Cattley RC, Pretorius J, Asuncion F, Grisanti M, et al. Dkk1-mediated inhibition of Wnt signaling in bone results in osteopenia. Bone. 2006;39(4):754-66.

115. Oh H, Chun CH, Chun JS. Dkk-1 expression in chondrocytes inhibits experimental osteoarthritic cartilage destruction in mice. Arthritis and rheumatism. 2012;64(8):2568-78.

116. Duesterdieck-Zellmer K, Semevolos S, Kinsley M, Riddick T. Age-related differential gene and protein expression in postnatal cartilage canal and osteochondral junction chondrocytes. Gene expression patterns : GEP. 2015;17(1):1-10.

117. Holbourn KP, Acharya KR, Perbal B. The CCN family of proteins: structure-function relationships. Trends in biochemical sciences. 2008;33(10):461-73.

118. Poole KE, van Bezooijen RL, Loveridge N, Hamersma H, Papapoulos SE, Lowik CW, et al. Sclerostin is a delayed secreted product of osteocytes that inhibits bone formation. FASEB journal : official publication of the Federation of American Societies for Experimental Biology. 2005;19(13):1842-4.

119. Jager A, Gotz W, Lossdorfer S, Rath-Deschner B. Localization of SOST/sclerostin in cementocytes in vivo and in mineralizing periodontal ligament cells in vitro. Journal of periodontal research. 2010;45(2):246-54.

120. van Bezooijen RL, Bronckers AL, Gortzak RA, Hogendoorn PC, van der Wee-Pals L, Balemans W, et al. Sclerostin in mineralized matrices and van Buchem disease. Journal of dental research. 2009;88(6):569-74.

121. Culi J, Mann RS. Boca, an endoplasmic reticulum protein required for wingless signaling and trafficking of LDL receptor family members in Drosophila. Cell. 2003;112(3):343-54.

122. Hsieh JC, Lee L, Zhang L, Wefer S, Brown K, DeRossi C, et al. Mesd encodes an LRP5/6 chaperone essential for specification of mouse embryonic polarity. Cell. 2003;112(3):355-67.

123. Lin C, Lu W, Zhai L, Bethea T, Berry K, Qu Z, et al. Mesd is a general inhibitor of different Wnt ligands in Wnt/LRP signaling and inhibits PC-3 tumor growth in vivo. FEBS letters. 2011;585(19):3120-5.

124. Baron R, Rawadi G, Roman-Roman S. Wnt signaling: a key regulator of bone mass. Curr Top Dev Biol. 2006;76:103-27.

125. Yu HM, Jerchow B, Sheu TJ, Liu B, Costantini F, Puzas JE, et al. The role of Axin2 in calvarial morphogenesis and craniosynostosis. Development. 2005;132(8):1995-2005.

126. Babij P, Zhao W, Small C, Kharode Y, Yaworsky PJ, Bouxsein ML, et al. High bone mass in mice expressing a mutant LRP5 gene. J Bone Miner Res. 2003;18(6):960-74.

127. Bodine PV, Zhao W, Kharode YP, Bex FJ, Lambert AJ, Goad MB, et al. The Wnt antagonist secreted frizzled-related protein-1 is a negative regulator of trabecular bone formation in adult mice. Mol Endocrinol. 2004;18(5):1222-37.

128. Almeida M, Han L, Bellido T, Manolagas SC, Kousteni S. Wnt proteins prevent apoptosis of both uncommitted osteoblast progenitors and differentiated osteoblasts by beta-catenin-dependent and -independent signaling cascades involving Src/ERK and phosphatidylinositol 3-kinase/AKT. J Biol Chem. 2005;280(50):41342-51.

129. Baksh D, Boland GM, Tuan RS. Cross-talk between Wnt signaling pathways in human mesenchymal stem cells leads to functional antagonism during osteogenic differentiation. J Cell Biochem. 2007;101(5):1109-24.

130. Day TF, Guo X, Garrett-Beal L, Yang Y. Wnt/beta-catenin signaling in mesenchymal progenitors controls osteoblast and chondrocyte differentiation during vertebrate skeletogenesis. Dev Cell. 2005;8(5):739-50.

131. Hill TP, Spater D, Taketo MM, Birchmeier W, Hartmann C. Canonical Wnt/beta-catenin signaling prevents osteoblasts from differentiating into chondrocytes. Dev Cell. 2005;8(5):727-38.

132. Hu H, Hilton MJ, Tu X, Yu K, Ornitz DM, Long F. Sequential roles of Hedgehog and Wnt signaling in osteoblast development. Development. 2005;132(1):49-60.

133. Rodda SJ, McMahon AP. Distinct roles for Hedgehog and canonical Wnt signaling in specification, differentiation and maintenance of osteoblast progenitors. Development. 2006;133(16):3231-44.

134. Tufan AC, Tuan RS. Wnt regulation of limb mesenchymal chondrogenesis is accompanied by altered N-cadherin-related functions. FASEB journal : official publication of the Federation of American Societies for Experimental Biology. 2001;15(8):1436-8.

135. Hwang SG, Yu SS, Lee SW, Chun JS. Wnt-3a regulates chondrocyte differentiation via c-Jun/AP-1 pathway. FEBS letters. 2005;579(21):4837-42.

136. Tamamura Y, Otani T, Kanatani N, Koyama E, Kitagaki J, Komori T, et al. Developmental regulation of Wnt/beta-catenin signals is required for growth plate assembly, cartilage integrity, and endochondral ossification. J Biol Chem. 2005;280(19):19185-95.

137. Geetha-Loganathan P, Nimmagadda S, Christ B, Huang R, Scaal M. Ectodermal Wnt6 is an early negative regulator of limb chondrogenesis in the chicken embryo. BMC developmental biology. 2010;10:32.

138. Kawakami Y, Wada N, Nishimatsu SI, Ishikawa T, Noji S, Nohno T. Involvement of Wnt-5a in chondrogenic pattern formation in the chick limb bud. Development, growth & differentiation. 1999;41(1):29-40.

139. Dealy CN, Roth A, Ferrari D, Brown AM, Kosher RA. Wnt-5a and Wnt-7a are expressed in the developing chick limb bud in a manner suggesting roles in pattern formation along the proximodistal and dorsoventral axes. Mechanisms of development. 1993;43(2-3):175-86.

140. Yang Y, Topol L, Lee H, Wu J. Wnt5a and Wnt5b exhibit distinct activities in coordinating chondrocyte proliferation and differentiation. Development. 2003;130(5):1003-15.

141. Andrade AC, Nilsson O, Barnes KM, Baron J. Wnt gene expression in the post-natal growth plate: regulation with chondrocyte differentiation. Bone. 2007;40(5):1361-9.

142. Bradley EW, Drissi MH. WNT5A regulates chondrocyte differentiation through differential use of the CaN/NFAT and IKK/NF-kappaB pathways. Mol Endocrinol. 2010;24(8):1581-93.

143. Witte F, Dokas J, Neuendorf F, Mundlos S, Stricker S. Comprehensive expression analysis of all Wnt genes and their major secreted antagonists during mouse limb development and cartilage differentiation. Gene expression patterns : GEP. 2009;9(4):215-23.

144. Glass DA, 2nd, Bialek P, Ahn JD, Starbuck M, Patel MS, Clevers H, et al. Canonical Wnt signaling in differentiated osteoblasts controls osteoclast differentiation. Dev Cell. 2005;8(5):751-64.

145. Spencer GJ, Utting JC, Etheridge SL, Arnett TR, Genever PG. Wnt signalling in osteoblasts regulates expression of the receptor activator of NFkappaB ligand and inhibits osteoclastogenesis in vitro. Journal of cell science. 2006;119(Pt 7):1283-96.

146. Kramer I, Halleux C, Keller H, Pegurri M, Gooi JH, Weber PB, et al. Osteocyte Wnt/beta-catenin signaling is required for normal bone homeostasis. Molecular and cellular biology. 2010;30(12):3071-85.

147. Holmen SL, Zylstra CR, Mukherjee A, Sigler RE, Faugere MC, Bouxsein ML, et al. Essential role of beta-catenin in postnatal bone acquisition. J Biol Chem. 2005;280(22):21162-8.

148. Pederson L, Ruan M, Westendorf JJ, Khosla S, Oursler MJ. Regulation of bone formation by osteoclasts involves Wnt/BMP signaling and the chemokine sphingosine-1-phosphate. Proc Natl Acad Sci U S A. 2008;105(52):20764-9.

149. Gong Y, Slee RB, Fukai N, Rawadi G, Roman-Roman S, Reginato AM, et al. LDL receptor-related protein 5 (LRP5) affects bone accrual and eye development. Cell. 2001;107(4):513-23.

150. Boyden LM, Mao J, Belsky J, Mitzner L, Farhi A, Mitnick MA, et al. High bone density due to a mutation in LDL-receptor-related protein 5. The New England journal of medicine. 2002;346(20):1513-21.

151. Little RD, Carulli JP, Del Mastro RG, Dupuis J, Osborne M, Folz C, et al. A mutation in the LDL receptor-related protein 5 gene results in the autosomal dominant high-bone-mass trait. American journal of human genetics. 2002;70(1):11-9.

152. Pangrazio A, Boudin E, Piters E, Damante G, Lo Iacono N, D'Elia AV, et al. Identification of the first deletion in the LRP5 gene in a patient with autosomal dominant osteopetrosis type I. Bone. 2011;49(3):568-71.

153. Van Wesenbeeck L, Cleiren E, Gram J, Beals RK, Benichou O, Scopelliti D, et al. Six novel missense mutations in the LDL receptor-related protein 5 (LRP5) gene in different conditions with an increased bone density. American journal of human genetics. 2003;72(3):763-71.

154. Johnson ML, Gong G, Kimberling W, Reckér SM, Kimmel DB, Recker RB. Linkage of a gene causing high bone mass to human chromosome 11 (11q12-13). American journal of human genetics. 1997;60(6):1326-32.

155. Kato M, Patel MS, Levasseur R, Lobov I, Chang BH, Glass DA, 2nd, et al. Cbfa1-independent decrease in osteoblast proliferation, osteopenia, and persistent embryonic eye vascularization in mice deficient in Lrp5, a Wnt coreceptor. The Journal of cell biology. 2002;157(2):303-14.

156. Iwaniec UT, Wronski TJ, Liu J, Rivera MF, Arzaga RR, Hansen G, et al. PTH stimulates bone formation in mice deficient in Lrp5. J Bone Miner Res. 2007;22(3):394-402.

157. Holmen SL, Giambernardi TA, Zylstra CR, Buckner-Berghuis BD, Resau JH, Hess JF, et al. Decreased BMD and limb deformities in mice carrying mutations in both Lrp5 and Lrp6. J Bone Miner Res. 2004;19(12):2033-40.

158. Cui Y, Niziolek PJ, MacDonald BT, Zylstra CR, Alenina N, Robinson DR, et al. Lrp5 functions in bone to regulate bone mass. Nat Med. 2011;17(6):684-91.

159. Terasawa M, Shimokawa R, Terashima T, Ohya K, Takagi Y, Shimokawa H. Expression of dentin matrix protein 1 (DMP1) in nonmineralized tissues. Journal of bone and mineral metabolism. 2004;22(5):430-8.

160. Kalajzic I, Matthews BG, Torreggiani E, Harris MA, Divieti Pajevic P, Harris SE. In vitro and in vivo approaches to study osteocyte biology. Bone. 2013;54(2):296-306.

161. Akhter MP, Wells DJ, Short SJ, Cullen DM, Johnson ML, Haynatzki GR, et al. Bone biomechanical properties in LRP5 mutant mice. Bone. 2004;35(1):162-9.

162. Semenov MV, He X. LRP5 mutations linked to high bone mass diseases cause reduced LRP5 binding and inhibition by SOST. J Biol Chem. 2006;281(50):38276-84.

163. Bhat BM, Allen KM, Liu W, Graham J, Morales A, Anisowicz A, et al. Structure-based mutation analysis shows the importance of LRP5 beta-propeller 1 in modulating Dkk1-mediated inhibition of Wnt signaling. Gene. 2007;391(1-2):103-12.

164. Zhang Y, Wang Y, Li X, Zhang J, Mao J, Li Z, et al. The LRP5 high-bone-mass G171V mutation disrupts LRP5 interaction with Mesd. Molecular and cellular biology. 2004;24(11):4677-84.

165. Li C, Williams BO, Cao X, Wan M. LRP6 in mesenchymal stem cells is required for bone formation during bone growth and bone remodeling. Bone research. 2014;2:14006.

166. Stein SA, Witkop C, Hill S, Fallon MD, Viernstein L, Gucer G, et al. Sclerosteosis: neurogenetic and pathophysiologic analysis of an American kinship. Neurology. 1983;33(3):267-77.

167. Hill SC, Stein SA, Dwyer A, Altman J, Dorwart R, Doppman J. Cranial CT findings in sclerosteosis. AJNR American journal of neuroradiology. 1986;7(3):505-11.

168. Beighton P. Sclerosteosis. J Med Genet. 1988;25(3):200-3.

169. Balemans W, Ebeling M, Patel N, Van Hul E, Olson P, Dioszegi M, et al. Increased bone density in sclerosteosis is due to the deficiency of a novel secreted protein (SOST). Human molecular genetics. 2001;10(5):537-43.

170. Brunkow ME, Gardner JC, Van Ness J, Paeper BW, Kovacevich BR, Proll S, et al. Bone dysplasia sclerosteosis results from loss of the SOST gene product, a novel cystine knot-containing protein. American journal of human genetics. 2001;68(3):577-89.

171. Balemans W, Patel N, Ebeling M, Van Hul E, Wuyts W, Lacza C, et al. Identification of a 52 kb deletion downstream of the SOST gene in patients with van Buchem disease. J Med Genet. 2002;39(2):91-7.

172. Loots GG, Kneissel M, Keller H, Baptist M, Chang J, Collette NM, et al. Genomic deletion of a long-range bone enhancer misregulates sclerostin in Van Buchem disease. Genome Res. 2005;15(7):928-35.

173. Winkler DG, Sutherland MK, Geoghegan JC, Yu C, Hayes T, Skonier JE, et al. Osteocyte control of bone formation via sclerostin, a novel BMP antagonist. The EMBO journal. 2003;22(23):6267-76.

174. Guo J, Liu M, Yang D, Bouxsein ML, Saito H, Galvin RJ, et al. Suppression of Wnt signaling by Dkk1 attenuates PTH-mediated stromal cell response and new bone formation. Cell Metab. 2010;11(2):161-71.

175. Yao GQ, Wu JJ, Troiano N, Insogna K. Targeted overexpression of Dkk1 in osteoblasts reduces bone mass but does not impair the anabolic response to intermittent PTH treatment in mice. Journal of bone and mineral metabolism. 2011;29(2):141-8.

176. Li X, Ominsky MS, Niu QT, Sun N, Daugherty B, D'Agostin D, et al. Targeted deletion of the sclerostin gene in mice results in increased bone formation and bone strength. J Bone Miner Res. 2008;23(6):860-9.

177. Kramer I, Loots GG, Studer A, Keller H, Kneissel M. Parathyroid hormone (PTH)-induced bone gain is blunted in SOST overexpressing and deficient mice. J Bone Miner Res. 2010;25(2):178-89.

178. Morvan F, Boulukos K, Clement-Lacroix P, Roman Roman S, Suc-Royer I, Vayssiere B, et al. Deletion of a single allele of the Dkk1 gene leads to an increase in bone formation and bone mass. J Bone Miner Res. 2006;21(6):934-45.

179. MacDonald BT, Joiner DM, Oyserman SM, Sharma P, Goldstein SA, He X, et al. Bone mass is inversely proportional to Dkk1 levels in mice. Bone. 2007;41(3):331-9.

180. McDonald MM, Morse A, Schindeler A, Mikulec K, Peacock L, Cheng T, et al. Homozygous Dkk1 Knockout Mice Exhibit High Bone Mass Phenotype Due to Increased Bone Formation. Calcif Tissue Int. 2017.

181. Sawakami K, Robling AG, Ai M, Pitner ND, Liu D, Warden SJ, et al. The Wnt co-receptor LRP5 is essential for skeletal mechanotransduction but not for the anabolic bone response to parathyroid hormone treatment. J Biol Chem. 2006;281(33):23698-711.

182. Saxon LK, Jackson BF, Sugiyama T, Lanyon LE, Price JS. Analysis of multiple bone responses to graded strains above functional levels, and to disuse, in mice in vivo show that the human Lrp5 G171V High Bone Mass mutation increases the osteogenic response to loading but that lack of Lrp5 activity reduces it. Bone. 2011;49(2):184-93.

183. Robinson JA, Chatterjee-Kishore M, Yaworsky PJ, Cullen DM, Zhao W, Li C, et al. Wnt/beta-catenin signaling is a normal physiological response to mechanical loading in bone. J Biol Chem. 2006;281(42):31720-8.

184. Niziolek PJ, Warman ML, Robling AG. Mechanotransduction in bone tissue: The A214V and G171V mutations in Lrp5 enhance load-induced osteogenesis in a surface-selective manner. Bone. 2012;51(3):459-65.

185. van Bezooijen RL, Roelen BA, Visser A, van der Wee-Pals L, de Wilt E, Karperien M, et al. Sclerostin is an osteocyte-expressed negative regulator of bone formation, but not a classical BMP antagonist. The Journal of experimental medicine. 2004;199(6):805-14.

186. Moustafa A, Sugiyama T, Prasad J, Zaman G, Gross T, Lanyon L, et al. Mechanical loading-related changes in osteocyte sclerostin expression in mice are more closely associated with the subsequent osteogenic response than the peak strains engendered. Osteoporosis International. 2011:1-10.

187. Robling AG, Niziolek PJ, Baldridge LA, Condon KW, Allen MR, Alam I, et al. Mechanical stimulation of bone in vivo reduces osteocyte expression of Sost/sclerostin. J Biol Chem. 2008;283(9):5866-75.

188. Lin C, Jiang X, Dai Z, Guo X, Weng T, Wang J, et al. Sclerostin mediates bone response to mechanical unloading through antagonizing Wnt/beta-catenin signaling. J Bone Miner Res. 2009;24(10):1651-61.

189. Spatz JM, Ellman R, Cloutier AM, Louis L, van Vliet M, Suva LJ, et al. Sclerostin antibody inhibits skeletal deterioration due to reduced mechanical loading. J Bone Miner Res. 2013;28(4):865-74.

190. Tu X, Rhee Y, Condon KW, Bivi N, Allen MR, Dwyer D, et al. Sost downregulation and local Wnt signaling are required for the osteogenic response to mechanical loading. Bone. 2012;50(1):209-17.

191. Case N, Ma M, Sen B, Xie Z, Gross TS, Rubin J. Beta-catenin levels influence rapid mechanical responses in osteoblasts. J Biol Chem. 2008;283(43):29196-205.

192. Armstrong VJ, Muzylak M, Sunters A, Zaman G, Saxon LK, Price JS, et al. Wnt/beta-catenin signaling is a component of osteoblastic bone cell early responses to load-bearing and requires estrogen receptor alpha. J Biol Chem. 2007;282(28):20715-27.

193. Javaheri B, Stern AR, Lara N, Dallas M, Zhao H, Liu Y, et al. Deletion of a single beta-catenin allele in osteocytes abolishes the bone anabolic response to loading. J Bone Miner Res. 2014;29(3):705-15.

194. Wan Q, Cho E, Yokota H, Na S. RhoA GTPase interacts with beta-catenin signaling in clinorotated osteoblasts. Journal of bone and mineral metabolism. 2013;31(5):520-32.

195. Cui L, Cheng H, Song C, Li C, Simonet WS, Ke HZ, et al. Time-dependent effects of sclerostin antibody on a mouse fracture healing model. J Musculoskelet Neuronal Interact. 2013;13(2):178-84.

196. Sen B, Styner M, Xie Z, Case N, Rubin CT, Rubin J. Mechanical loading regulates NFATc1 and beta-catenin signaling through a GSK3beta control node. J Biol Chem. 2009;284(50):34607-17.

197. Case N, Thomas J, Sen B, Styner M, Xie Z, Galior K, et al. Mechanical regulation of glycogen synthase kinase 3beta (GSK3beta) in mesenchymal stem cells is dependent on Akt protein serine 473 phosphorylation via mTORC2 protein. J Biol Chem. 2011;286(45):39450-6.

198. Santos A, Bakker AD, Zandieh-Doulabi B, de Blieck-Hogervorst JM, Klein-Nulend J. Early activation of the beta-catenin pathway in osteocytes is mediated by nitric oxide, phosphatidyl inositol-3 kinase/Akt, and focal adhesion kinase. Biochem Biophys Res Commun. 2010;391(1):364-9.

199. Fang D, Hawke D, Zheng Y, Xia Y, Meisenhelder J, Nika H, et al. Phosphorylation of beta-catenin by AKT promotes beta-catenin transcriptional activity. J Biol Chem. 2007;282(15):11221-9.

200. Ponce DP, Maturana JL, Cabello P, Yefi R, Niechi I, Silva E, et al. Phosphorylation of AKT/PKB by CK2 is necessary for the AKT-dependent up-regulation of beta-catenin transcriptional activity. J Cell Physiol. 2011;226(7):1953-9.

201. Sunters A, Armstrong VJ, Zaman G, Kypta RM, Kawano Y, Lanyon LE, et al. Mechano-transduction in osteoblastic cells involves strain-regulated estrogen receptor alpha-mediated control of insulin-like growth factor (IGF) I receptor sensitivity to Ambient IGF, leading to phosphatidylinositol 3-kinase/AKT-dependent Wnt/LRP5 receptor-independent activation of beta-catenin signaling. J Biol Chem. 2010;285(12):8743-58.

202. Norvell SM, Alvarez M, Bidwell JP, Pavalko FM. Fluid shear stress induces beta-catenin signaling in osteoblasts. Calcif Tissue Int. 2004;75(5):396-404.

203. Schwartz MA, DeSimone DW. Cell adhesion receptors in mechanotransduction. Current opinion in cell biology. 2008;20(5):551-6.

204. Forwood MR. Inducible cyclo-oxygenase (COX-2) mediates the induction of bone formation by mechanical loading in vivo. J Bone Miner Res. 1996;11(11):1688-93.

205. Li J, Burr DB, Turner CH. Suppression of prostaglandin synthesis with NS-398 has different effects on endocortical and periosteal bone formation induced by mechanical loading. Calcif Tissue Int. 2002;70(4):320-9.

206. Kunnel JG, Igarashi K, Gilbert JL, Stern PH. Bone anabolic responses to mechanical load in vitro involve COX-2 and constitutive NOS. Connective tissue research. 2004;45(1):40-9.

207. Kamel MA, Picconi JL, Lara-Castillo N, Johnson ML. Activation of beta-catenin signaling in MLO-Y4 osteocytic cells versus 2T3 osteoblastic cells by fluid flow shear stress and PGE2: Implications for the study of mechanosensation in bone. Bone. 2010;47(5):872-81.

208. Genetos DC, Yellowley CE, Loots GG. Prostaglandin E2 signals through PTGER2 to regulate sclerostin expression. PLoS One. 2011;6(3):e17772.

209. Keller H, Kneissel M. SOST is a target gene for PTH in bone. Bone. 2005;37(2):148-58.

210. Bellido T, Ali AA, Gubrij I, Plotkin LI, Fu Q, O'Brien CA, et al. Chronic elevation of parathyroid hormone in mice reduces expression of sclerostin by osteocytes: a novel mechanism for hormonal control of osteoblastogenesis. Endocrinology. 2005;146(11):4577-83.

211. Li X, Liu H, Qin L, Tamasi J, Bergenstock M, Shapses S, et al. Determination of dual effects of parathyroid hormone on skeletal gene expression in vivo by microarray and network analysis. J Biol Chem. 2007;282(45):33086-97.

212. Kaji H, Imanishi Y, Sugimoto T, Seino S. Comparisons of serum sclerostin levels among patients with postmenopausal osteoporosis, primary hyperparathyroidism and osteomalacia. Experimental and clinical endocrinology & diabetes : official journal, German Society of Endocrinology [and] German Diabetes Association. 2011;119(7):440-4.

213. van Lierop AH, Witteveen JE, Hamdy NA, Papapoulos SE. Patients with primary hyperparathyroidism have lower circulating sclerostin levels than euparathyroid controls. European journal of endocrinology. 2010;163(5):833-7.

214. Drake MT, Srinivasan B, Modder UI, Peterson JM, McCready LK, Riggs BL, et al. Effects of parathyroid hormone treatment on circulating sclerostin levels in postmenopausal women. J Clin Endocrinol Metab. 2010;95(11):5056-62.

215. Powell WF, Jr., Barry KJ, Tulum I, Kobayashi T, Harris SE, Bringhurst FR, et al. Targeted ablation of the PTH/PTHrP receptor in osteocytes impairs bone structure and homeostatic calcemic responses. The Journal of endocrinology. 2011;209(1):21-32.

216. Wan M, Yang C, Li J, Wu X, Yuan H, Ma H, et al. Parathyroid hormone signaling through low-density lipoprotein-related protein 6. Genes Dev. 2008;22(21):2968-79.

217. Chen AE, Ginty DD, Fan CM. Protein kinase A signalling via CREB controls myogenesis induced by Wnt proteins. Nature. 2005;433(7023):317-22.

218. Gao Y, Huang E, Zhang H, Wang J, Wu N, Chen X, et al. Crosstalk between Wnt/β-Catenin and Estrogen Receptor Signaling Synergistically Promotes Osteogenic Differentiation of Mesenchymal Progenitor Cells. PLoS ONE. 2013;8(12):e82436.

219. Yin X, Wang X, Hu X, Chen Y, Zeng K, Zhang H. ERbeta induces the differentiation of cultured osteoblasts by both Wnt/beta-catenin signaling pathway and estrogen signaling pathways. Experimental cell research. 2015;335(1):107-14.

220. El-Tanani M, Fernig DG, Barraclough R, Green C, Rudland P. Differential modulation of transcriptional activity of estrogen receptors by direct protein-protein interactions with the T cell factor family of transcription factors. J Biol Chem. 2001;276(45):41675-82.

221. Morse A, Yu NY, Peacock L, Mikulec K, Kramer I, Kneissel M, et al. Endochondral fracture healing with external fixation in the Sost knockout mouse results in earlier fibrocartilage callus removal and increased bone volume fraction and strength. Bone. 2015;71:155-63.

222. Morse A, McDonald MM, Schindeler A, Peacock L, Mikulec K, Cheng TL, et al. Sclerostin Antibody Increases Callus Size and Strength but does not Improve Fracture Union in a Challenged Open Rat Fracture Model. Calcif Tissue Int. 2017;101(2):217-28.

223. McDonald MM, Morse A, Birke O, Yu NY, Mikulec K, Peacock L, et al. Sclerostin antibody enhances bone formation in a rat model of distraction osteogenesis. J Orthop Res. 2017.

224. McDonald MM, Reagan MR, Youlten SE, Mohanty ST, Seckinger A, Terry RL, et al. Inhibiting the osteocyte-specific protein sclerostin increases bone mass and fracture resistance in multiple myeloma. Blood. 2017;129(26):3452-64.

225. Who are candidates for prevention and treatment for osteoporosis? Osteoporosis international : a journal established as result of cooperation between the European Foundation for Osteoporosis and the National Osteoporosis Foundation of the USA. 1997;7(1):1-6.

226. Johnell O, Kanis JA. An estimate of the worldwide prevalence and disability associated with osteoporotic fractures. Osteoporosis international : a journal established as result of cooperation between the European Foundation for Osteoporosis and the National Osteoporosis Foundation of the USA. 2006;17(12):1726-33.

227. Sheu A, Diamond T. Secondary osteoporosis. Australian prescriber. 2016;39(3):85-7.

228. Clement-Lacroix P, Ai M, Morvan F, Roman-Roman S, Vayssiere B, Belleville C, et al. Lrp5-independent activation of Wnt signaling by lithium chloride increases bone formation and bone mass in mice. Proc Natl Acad Sci U S A. 2005;102(48):17406-11.

229. Warden SJ, Hassett SM, Bond JL, Rydberg J, Grogg JD, Hilles EL, et al. Psychotropic drugs have contrasting skeletal effects that are independent of their effects on physical activity levels. Bone. 2010;46(4):985-92.

230. Vestergaard P, Rejnmark L, Mosekilde L. Reduced relative risk of fractures among users of lithium. Calcif Tissue Int. 2005;77(1):1-8.

231. Wilting I, de Vries F, Thio BM, Cooper C, Heerdink ER, Leufkens HG, et al. Lithium use and the risk of fractures. Bone. 2007;40(5):1252-8.

232. Kulkarni NH, Onyia JE, Zeng Q, Tian X, Liu M, Halladay DL, et al. Orally bioavailable GSK-3alpha/beta dual inhibitor increases markers of cellular differentiation in vitro and bone mass in vivo. J Bone Miner Res. 2006;21(6):910-20.

233. Gambardella A, Nagaraju CK, O'Shea PJ, Mohanty ST, Kottam L, Pilling J, et al. Glycogen synthase kinase-3alpha/beta inhibition promotes in vivo amplification of endogenous mesenchymal progenitors with osteogenic and adipogenic potential and their differentiation to the osteogenic lineage. J Bone Miner Res. 2011;26(4):811-21.

234. Sisask G, Marsell R, Sundgren-Andersson A, Larsson S, Nilsson O, Ljunggren O, et al. Rats treated with AZD2858, a GSK3 inhibitor, heal fractures rapidly without endochondral bone formation. Bone. 2013;54(1):126-32.

235. Plotnikov EY, Silachev DN, Zorova LD, Pevzner IB, Jankauskas SS, Zorov SD, et al. Lithium salts -- simple but magic. Biochemistry Biokhimiia. 2014;79(8):740-9.

236. Liberman Z, Eldar-Finkelman H. Serine 332 phosphorylation of insulin receptor substrate-1 by glycogen synthase kinase-3 attenuates insulin signaling. J Biol Chem. 2005;280(6):4422-8.

237. Finlay D, Patel S, Dickson LM, Shpiro N, Marquez R, Rhodes CJ, et al. Glycogen synthase kinase-3 regulates IGFBP-1 gene transcription through the thymine-rich insulin response element. BMC molecular biology. 2004;5:15.

238. Lochhead PA, Coghlan M, Rice SQ, Sutherland C. Inhibition of GSK-3 selectively reduces glucose-6-phosphatase and phosphatase and phosphoenolypyruvate carboxykinase gene expression. Diabetes. 2001;50(5):937-46.

239. Jope RS, Yuskaitis CJ, Beurel E. Glycogen synthase kinase-3 (GSK3): inflammation, diseases, and therapeutics. Neurochemical research. 2007;32(4-5):577-95.

240. Wang H, Brown J, Martin M. Glycogen synthase kinase 3: a point of convergence for the host inflammatory response. Cytokine. 2011;53(2):130-40.

241. Jope RS, Johnson GV. The glamour and gloom of glycogen synthase kinase-3. Trends in biochemical sciences. 2004;29(2):95-102.

242. Bennett CN, Longo KA, Wright WS, Suva LJ, Lane TF, Hankenson KD, et al. Regulation of osteoblastogenesis and bone mass by Wnt10b. Proc Natl Acad Sci U S A. 2005;102(9):3324-9.

243. Bennett CN, Ouyang H, Ma YL, Zeng Q, Gerin I, Sousa KM, et al. Wnt10b increases postnatal bone formation by enhancing osteoblast differentiation. J Bone Miner Res. 2007;22(12):1924-32.

244. Minear S, Leucht P, Jiang J, Liu B, Zeng A, Fuerer C, et al. Wnt proteins promote bone regeneration. Science translational medicine. 2010;2(29):29ra30.

245. Bodine PV, Stauffer B, Ponce-de-Leon H, Bhat RA, Mangine A, Seestaller-Wehr LM, et al. A small molecule inhibitor of the Wnt antagonist secreted frizzled-related protein-1 stimulates bone formation. Bone. 2009;44(6):1063-8.

246. Moore WJ, Kern JC, Bhat R, Bodine PV, Fukyama S, Krishnamurthy G, et al. Modulation of Wnt signaling through inhibition of secreted frizzled-related protein I (sFRP-1) with N-substituted piperidinyl diphenylsulfonyl sulfonamides: part II. Bioorganic & medicinal chemistry. 2010;18(1):190-201.

247. Shi M, Stauffer B, Bhat R, Billiard J, Ponce-de-Leon H, Seestaller-Wehr L, et al. Identification of iminooxothiazolidines as secreted frizzled related protein-1 inhibitors. Bioorganic & medicinal chemistry letters. 2009;19(22):6337-9.

248. Sklepkiewicz P, Shiomi T, Kaur R, Sun J, Kwon S, Mercer B, et al. Loss of secreted frizzled-related protein-1 leads to deterioration of cardiac function in mice and plays a role in human cardiomyopathy. Circulation Heart failure. 2015;8(2):362-72.

249. Li X, Grisanti M, Fan W, Asuncion FJ, Tan HL, Dwyer D, et al. Dickkopf-1 regulates bone formation in young growing rodents and upon traumatic injury. J Bone Miner Res. 2011;26(11):2610-21.

250. Glantschnig H, Hampton RA, Lu P, Zhao JZ, Vitelli S, Huang L, et al. Generation and selection of novel fully human monoclonal antibodies that neutralize Dickkopf-1 (DKK1) inhibitory function in vitro and increase bone mass in vivo. J Biol Chem. 2010;285(51):40135-47.

251. Jin H, Wang B, Li J, Xie W, Mao Q, Li S, et al. Anti-DKK1 antibody promotes bone fracture healing through activation of beta-catenin signaling. Bone. 2015;71:63-75.

252. Ueland T, Otterdal K, Lekva T, Halvorsen B, Gabrielsen A, Sandberg WJ, et al. Dickkopf-1 enhances inflammatory interaction between platelets and endothelial cells and shows increased expression in atherosclerosis. Arteriosclerosis, thrombosis, and vascular biology. 2009;29(8):1228-34.

253. Yamaguchi Y, Passeron T, Hoashi T, Watabe H, Rouzaud F, Yasumoto K, et al. Dickkopf 1 (DKK1) regulates skin pigmentation and thickness by affecting Wnt/beta-catenin signaling in keratinocytes. FASEB journal : official publication of the Federation of American Societies for Experimental Biology. 2008;22(4):1009-20.

254. Diarra D, Stolina M, Polzer K, Zwerina J, Ominsky MS, Dwyer D, et al. Dickkopf-1 is a master regulator of joint remodeling. Nat Med. 2007;13(2):156-63.

255. Weng LH, Wang CJ, Ko JY, Sun YC, Su YS, Wang FS. Inflammation induction of Dickkopf-1 mediates chondrocyte apoptosis in osteoarthritic joint. Osteoarthritis and cartilage / OARS, Osteoarthritis Research Society. 2009;17(7):933-43.

256. Yaccoby S, Ling W, Zhan F, Walker R, Barlogie B, Shaughnessy JD, Jr. Antibody-based inhibition of DKK1 suppresses tumor-induced bone resorption and multiple myeloma growth in vivo. Blood. 2007;109(5):2106-11.

257. Fulciniti M, Tassone P, Hideshima T, Vallet S, Nanjappa P, Ettenberg SA, et al. Anti-DKK1 mAb (BHQ880) as a potential therapeutic agent for multiple myeloma. Blood. 2009;114(2):371-9.

258. Heath DJ, Chantry AD, Buckle CH, Coulton L, Shaughnessy JD, Jr., Evans HR, et al. Inhibiting Dickkopf-1 (Dkk1) removes suppression of bone formation and prevents the development of osteolytic bone disease in multiple myeloma. J Bone Miner Res. 2009;24(3):425-36.

259. Uderhardt S, Diarra D, Katzenbeisser J, David JP, Zwerina J, Richards W, et al. Blockade of Dickkopf (DKK)-1 induces fusion of sacroiliac joints. Ann Rheum Dis. 2010;69(3):592-7.

260. Li X, Ominsky MS, Warmington KS, Morony S, Gong J, Cao J, et al. Sclerostin antibody treatment increases bone formation, bone mass, and bone strength in a rat model of postmenopausal osteoporosis. J Bone Miner Res. 2009;24(4):578-88.

261. Ominsky MS, Vlasseros F, Jolette J, Smith SY, Stouch B, Doellgast G, et al. Two doses of sclerostin antibody in cynomolgus monkeys increases bone formation, bone mineral density, and bone strength. J Bone Miner Res. 2010;25(5):948-59.

262. Li X, Warmington KS, Niu QT, Asuncion FJ, Barrero M, Grisanti M, et al. Inhibition of sclerostin by monoclonal antibody increases bone formation, bone mass, and bone strength in aged male rats. J Bone Miner Res. 2010;25(12):2371-80.

263. Agholme F, Li X, Isaksson H, Ke HZ, Aspenberg P. Sclerostin antibody treatment enhances metaphyseal bone healing in rats. Journal of Bone and Mineral Research. 2010;25(11):2412-8.

264. Li X, Ominsky MS, Warmington KS, Niu QT, Asuncion FJ, Barrero M, et al. Increased bone formation and bone mass induced by sclerostin antibody is not affected by pretreatment or cotreatment with alendronate in osteopenic, ovariectomized rats. Endocrinology. 2011;152(9):3312-22.

265. Padhi D, Jang G, Stouch B, Fang L, Posvar E. Single-dose, placebo-controlled, randomized study of AMG 785, a sclerostin monoclonal antibody. J Bone Miner Res. 2011;26(1):19-26.

266. McClung MR, Grauer A, Boonen S, Bolognese MA, Brown JP, Diez-Perez A, et al. Romosozumab in Postmenopausal Women with Low Bone Mineral Density. The New England journal of medicine. 2014;370(5):412-20.

267. Cosman F, Crittenden DB, Adachi JD, Binkley N, Czerwinski E, Ferrari S, et al. Romosozumab Treatment in Postmenopausal Women with Osteoporosis. The New England journal of medicine. 2016;375(16):1532-43.

268. McColm J, Hu L, Womack T, Tang CC, Chiang AY. Single- and multiple-dose randomized studies of blosozumab, a monoclonal antibody against sclerostin, in healthy postmenopausal women. J Bone Miner Res. 2014;29(4):935-43.

269. Recker RR, Benson CT, Matsumoto T, Bolognese MA, Robins DA, Alam J, et al. A randomized, double-blind phase 2 clinical trial of blosozumab, a sclerostin antibody, in postmenopausal women with low bone mineral density. J Bone Miner Res. 2015;30(2):216-24.

270. Recknor CP, Recker RR, Benson CT, Robins DA, Chiang AY, Alam J, et al. The Effect of Discontinuing Treatment With Blosozumab: Follow-up Results of a Phase 2 Randomized Clinical Trial in Postmenopausal Women With Low Bone Mineral Density. J Bone Miner Res. 2015;30(9):1717-25.

271. Ominsky M SR, Jolette J, et. al. . Long-term Sclerostin Antibody Treatment in Cynomolgus Monkeys: Sustained Improvements in Vertebral Microarchitecture and Bone Strength Following a Temporal Increase in Cancellous Bone Formation. Journal of Bone and Mineral Research. 2012;27(S1):S1-S.

272. van Lierop AH, Hamdy NA, Hamersma H, van Bezooijen RL, Power J, Loveridge N, et al. Patients with sclerosteosis and disease carriers: human models of the effect of sclerostin on bone turnover. J Bone Miner Res. 2011;26(12):2804-11.

273. McClung MR CA, Brown JP, Diez-Perez A, Resch H, Caminis J, Bolognese MA, Goemaere S, Bone HG, Zanchetta JR, Maddox J, Rosen O, Bray S, Grauer A, . OP0251 Effects of 2 Years of Treatment with Romosozumab Followed by 1 Year of Denosumab or Placebo in Postmenopausal Women with Low Bone Mineral Density. Annals of the Rheumatic Diseases. 2015;74(Suppl 2):166-7.

274. van Lierop A, Moester M, Hamdy N, Papapoulos S. Serum Dickkopf 1 Levels in Sclerostin Deficiency. J Clin Endocrinol Metab. 2014;99(2):E252-6.

275. Chang MK, Kramer I, Keller H, Gooi JH, Collett C, Jenkins D, et al. Reversing LRP5-dependent osteoporosis and SOST-deficiency induced sclerosing bone disorders by altering WNT signaling activity. J Bone Miner Res. 2014;29(1):29-42.

276. Florio M, Gunasekaran K, Stolina M, Li X, Liu L, Tipton B, et al. A bispecific antibody targeting sclerostin and DKK-1 promotes bone mass accrual and fracture repair. Nature communications. 2016;7:11505.

277. Chan BY, Fuller ES, Russell AK, Smith SM, Smith MM, Jackson MT, et al. Increased chondrocyte sclerostin may protect against cartilage degradation in osteoarthritis. Osteoarthritis and cartilage / OARS, Osteoarthritis Research Society. 2011;19(7):874-85.

278. Roudier M, Li X, Niu QT, Pacheco E, Pretorius JK, Graham K, et al. Sclerostin is expressed in articular cartilage but loss or inhibition does not affect cartilage remodeling during aging or following mechanical injury. Arthritis and rheumatism. 2013;65(3):721-31.

279. Didangelos A, Yin X, Mandal K, Baumert M, Jahangiri M, Mayr M. Proteomics characterization of extracellular space components in the human aorta. Molecular & cellular proteomics : MCP. 2010;9(9):2048-62.

280. Amgen And UCB Announce Top-Line Phase 3 Data From Active-Comparator Study Of EVENITY™ (Romosozumab) In Postmenopausal Women With Osteoporosis [press release]. 21 May 2017.

281. Fritton JC, Myers ER, Wright TM, van der Meulen MC. Bone mass is preserved and cancellous architecture altered due to cyclic loading of the mouse tibia after orchidectomy. J Bone Miner Res. 2008;23(5):663-71.

282. Melville KM, Robling AG, van der Meulen MC. In vivo axial loading of the mouse tibia. Methods in molecular biology (Clifton, NJ). 2015;1226:99-115.

283. Lynch ME, Main RP, Xu Q, Schmicker TL, Schaffler MB, Wright TM, et al. Tibial compression is anabolic in the adult mouse skeleton despite reduced responsiveness with aging. Bone. 2011;49(3):439-46.

284. Mustafy T, Londono I, Villemure I. Can the contralateral limb be used as a control during the growing period in a rodent model? Medical engineering & physics. 2018.

285. Gaalen S, Kruyt M, Geuze R, de Bruijn J, Alblas J, Dhert W. Use of Fluorochrome Labels in In Vivo Bone Tissue Engineering Research2009. 209-17 p.

286. Kelly NH, Schimenti JC, Ross FP, van der Meulen MC. Transcriptional profiling of cortical versus cancellous bone from mechanically-loaded murine tibiae reveals differential gene expression. Bone. 2016;86:22-9.

Chapter 2. Mechanical load increases in bone formation via a sclerostin-independent pathway

This chapter has been published as:

Morse A, McDonald MM, Kelly NH, Melville KM, Schindeler A, Kramer I, Kneissel M, van der Meulen MC, Little DG. Mechanical load increases in bone formation via a sclerostin-independent pathway. J Bone Miner Res, 2014;29(11):2456-67.

ORIGINAL ARTICLE

JBMR®

Mechanical Load Increases in Bone Formation via a Sclerostin-Independent Pathway

Alyson Morse,[1,2] Michelle Maree McDonald,[3] Natalie H Kelly,[4,5] Katherine M Melville,[4,5] Aaron Schindeler,[1,2] Ina Kramer,[6] Michaela Kneissel,[6] Marjolein CH van der Meulen,[4,7] and David Graham Little[1,2]

[1]Orthopaedic Research and Biotechnology Unit, The Children's Hospital at Westmead, Sydney, Australia
[2]Discipline of Paediatrics and Child Health, Sydney Medical School, University of Sydney, Sydney, Australia
[3]Bone Biology Program, The Garvan Institute of Medical Research, Sydney, Australia
[4]Sibley School of Mechanical and Aerospace Engineering, Cornell University, Ithaca, NY, USA
[5]Biomedical Engineering, Cornell University, Ithaca, NY, USA
[6]Novartis Pharma, Basel, Switzerland
[7]Hospital for Special Surgery, New York, USA

ABSTRACT

Sclerostin, encoded by the *Sost* gene, is an important negative regulator of bone formation that has been proposed to have a key role in regulating the response to mechanical loading. To investigate the effect of long-term Sclerostin deficiency on mechanotransduction in bone, we performed experiments on unloaded or loaded tibiae of 10 week old female *Sost*−/− and wild type mice. Unloading was induced via 0.5U botulinum toxin (BTX) injections into the right quadriceps and calf muscles, causing muscle paralysis and limb disuse. On a separate group of mice, increased loading was performed on the left tibiae through unilateral cyclic axial compression of equivalent strains (+1200 με) at 1200 cycles/day, 5 days/week. Another cohort of mice receiving equivalent loads (−9.0 N) also were assessed. Contralateral tibiae served as normal load controls. Loaded/unloaded and normal load tibiae were assessed at day 14 for bone volume (BV) and formation changes. Loss of BV was seen in the unloaded tibiae of wild type mice, but BV was not different between normal load and unloaded *Sost*−/− tibiae. An increase in BV was seen in the loaded tibiae of wild type and *Sost*−/− mice over their normal load controls. The increased BV was associated with significantly increased mid-shaft periosteal mineralizing surface/bone surface (MS/BS), mineral apposition rate (MAR), and bone formation rate/bone surface (BFR/BS), and endosteal MAR and BFR/BS. Notably, loading induced a greater increase in periosteal MAR and BFR/BS in *Sost*−/− mice than in wild type controls. Thus, long-term Sclerostin deficiency inhibits the bone loss normally induced with decreased mechanical load, but it can augment the increase in bone formation with increased load. © 2014 American Society for Bone and Mineral Research.

KEY WORDS: MECHANOTRANSDUCTION; LOADING; BONE; UNLOADING; SCLEROSTIN; WNT

Introduction

Sclerostin, a secreted glycoprotein encoded by the *Sost* gene, is an important negative regulator of bone accumulation.[1,2] Sclerostin inhibits canonical Wnt signaling via blockade of low-density-lipoprotein receptor-related protein (LRP) receptors, including LRP5 and LRP6.[3] Sclerostin expression is specific to terminally differentiated cells embedded within mineralized matrix, including osteocytes, cementocytes, and hypertrophic chondrocytes, but not osteoblasts or bone lining cells.[1,4–6] The major downstream effect of Sclerostin expression is the inhibition of osteoblastogenesis,[6] although Sclerostin has also been shown to promote osteoclastogenesis,[7,8] via modulation of receptor activator of nuclear factor kappa-B ligand (RANKL) and osteoprotegerin (OPG), synthesis in osteocytes.[9,10]

The key role of Sclerostin in regulating bone homeostasis was identified via the human conditions van Buchem's disease and Sclerosteosis.[11–14] Both result from mutations in the *Sost* gene, leading to increased bone formation and high bone mass. A comparable high bone mass and increased bone formation phenotype has been described in mouse models in which *Sost* is knocked-out.[15,16] This role of Sclerostin has led to inhibitory strategies for the prevention and treatment of bone loss in osteoporosis and metabolic bone disease. Animal and human trials of anti-Sclerostin antibodies have demonstrated increased bone formation and mass with treatment.[17–22] Importantly, the effect on bone formation has been seen in models of osteoporosis and on resting bone surfaces along with remodeling surfaces.

Sclerostin has further been proposed to be a key regulator of mechanotransduction in bone. Increases in Sclerostin have been

Received in original form February 23, 2014; revised form April 22, 2014; accepted May 6, 2014. Accepted manuscript online May 12, 2014.
Address correspondence to: Alyson Morse, Orthopaedic Research and Biotechnology, The Children's Hospital at Westmead, Locked Bag 4001, Westmead, NSW, 2145, Australia. Email: alyson.morse@sydney.edu.au
Additional Supporting Information may be found in the online version of this article.
Journal of Bone and Mineral Research, Vol. 29, No. 11, November 2014, pp 2456–2467
DOI: 10.1002/jbmr.2278

implicated in the bone loss associated with reduced loading. *Sost* mRNA expression was reported to increase in rodent models of limb disuse and decline upon subsequent loading.[23,24] Mice deficient in Sclerostin, through genetic knock-out or short-term anti-Sclerostin antibody treatment, did not display the same extent of bone volume loss following hind limb unloading through tail suspension.[25,26] This result suggests that Sclerostin expression may mediate the response of bone to unloading. Discrepancies remain whether this bone loss inhibition is due to reduced bone anabolism, or rather decreased resorption. Conversely, *Sost* mRNA and Sclerostin protein expression were decreased following mechanical loading, and this reduction correlated with regions showing increased bone formation.[23,24] Importantly, in a transgenic mouse that constitutively expressed elevated Sclerostin levels, bone formation and bone volume gain associated with mechanical loading was inhibited.[27] However, limited research has been undertaken to understand the effect that Sclerostin deficiency has on bone's ability to respond to increased mechanical load. This investigation is important with the potential use of anti-Sclerostin antibodies.

The canonical Wnt/β-catenin pathway has many inhibitors and regulators aside from Sclerostin. Other Wnt inhibitors, such as secreted Fzd-related-proteins (sFRPs) and Dickkopfs may have a role in Wnt inhibition within the bone compartment, or may be compensatory in the absence of Sclerostin. Interestingly, Dickkopf-1 (Dkk1) is up-regulated when Sclerostin is absent.[28,29] Further, Dkk1 might have a Wnt3a-independent effect on cyclooxygenase-2 (Cox-2) expression, an early mechanical loading induced transcript.[30]

In this study, we aimed to investigate the effects of long-term Sclerostin deficiency on mechanotransduction. Increased and decreased loading studies were performed on the *Sost*−/− mouse and age-matched wild type controls. Bone volume and formation changes in loaded/unloaded and contralateral tibiae were examined using a combination of micro-computed tomography (microCT) and histomorphometry outcome measures.

Materials and Methods

Sost knockout mice

Sost−/− mice, previously described,[14,31] were backcrossed to C57BL/6J genetic background using founders with above 99.09% isogenicity/identity to the C57BL/6J strain. Age-matched *Sost*+/+ (wild type/WT) C57BL/6J control mice were obtained (Charles River Laboratories, Sulzfeld, Germany). All animal experiments were approved by the Western Sydney LHD Animal Ethics Committee, protocol 4174.

Botulinum toxin-induced tibial unloading

10 week old female *Sost*−/− and wild type mice ($N = 10$/strain) were anesthetized (70 mg/kg ketamine, 10 mg/kg xylazine) and then injected with 0.5U botulinum toxin (BTX, Allergen) into both the right quadriceps and the right calf muscles. This treatment caused tibial unloading by muscle paralysis and limb disuse. After 24 hours mice were unable to use their right hind limb. Left tibiae served as normal load controls. Mice were monitored throughout the study to ensure limb disuse was maintained; including assessing ability to grip, walk, and stretch out the right hind limb. Weekly body weights were recorded (Fig. S1). Mice were injected with calcein (10 mg/kg, Sigma Aldrich) 8 and 1 days before euthanasia, and euthanized at day 14. Post-harvest, hind limbs (tibia, fibular, femur and muscle) were weighed excluding skin and feet, and fixed 24 hours, 10% formalin and stored in 70% ethanol.

Tibial mid-diaphyseal strain gauging

As *Sost*−/− mice possessed denser bones than wild type, strain gauging was performed to calibrate the applied loading to reflect any stiffness differences present between the two genotypes. Strain (bone tissue deformation) levels at the midshaft of right and left tibiae were measured in 10 week old female *Sost*−/− and wild type mice ($N = 5$/strain) as previously described.[32] Briefly, mice were anesthetized (isoflurane inhalation) and a small incision was made in the skin at the anterior tibia, half way down the bone. Muscle and periosteum were scraped away to expose the diaphysis, and the bone cleaned/dried with methyl ethyl ketone. A miniature single element strain gauge (EA-06-015LA-120, Vishay Micromeasurements, NC, USA) was attached to the medial midshaft aligned with the bone's longitudinal axis.

The left hind limb was placed into a custom made loading apparatus so that the heel and knee were cupped and held securely. A range of cyclic axial compressive loads, ranging −4 to −24N, were applied using a 4 Hz haversine waveform. No tibial failures occurred with the load range. The strain at each load increment was recorded (National Instruments, Labview v8.2). The relationship between the axial force applied and the strain on the tibial midshaft was determined for each genotype and was used to calculate the load required to achieve +1200με at the tibial mid-shaft for both the *Sost*−/− and wild type mice.

Cyclic tibial loading

10 week old female *Sost*−/− and wild type mice ($N = 10$/strain) underwent unilateral cyclic axial compression of the left tibia. 1200 cycles were applied 5 days/week for 2 weeks, with rest on days 6, 7, 12, and 13. Equivalent loads for *Sost*−/− and wild type mice were applied to achieve +1200με on the mid-shaft. A separate cohort of wild type and *Sost*−/− mice all received −9.0N force to directly compare load-matched responses between the genotypes. Weekly body weights were recorded (Fig. S1).

Mice were injected with calcein (10 mg/kg, Sigma) 10 and 3 days before euthanasia, and euthanized at day 14. Tibiae were fixed 24 hours in 10% formalin and stored in 70% ethanol.

Dual-energy X-ray absorptiometry

Dual-energy X-ray absorptiometry (DXA) (GE Lunar PIXImus; Lunar Piximus Corp, Madison, WI, USA) was performed at days 0, 7, and 14 for unloading and loading studies, either under isoflurane anesthesia or post-euthanasia. For unloading studies a region of interest of 20 pixels long by 13 pixels wide was positioned below the growth plate within the metaphysis, which is the region most responsive to unloading-induced bone loss. For loading studies a region of interest of 30 pixels long by 13 pixels wide was analyzed in the diaphysis, centered half-way along the tibia, to correlate with the region where the known strain was produced. Bone mineral density (BMD) and bone mineral content (BMC) were obtained.

MicroCT

Right and left tibiae from unloading/loading studies were microCT scanned (Skyscan 1174 2; Skyscan NV, Kontich, Belgium)

using 12 μm isotropic voxel resolution, 0.5 mm aluminium filter, 50 kV X-ray tube voltage, 800 μA tube electric current, and 4500 ms exposure time. Images were reconstructed using a 0–0.1 greyscale (NRecon v1.6.1.7; Skyscan NV) and analysed with CTAnalyser (Skyscan NV). The minimum threshold for bone was 0.4 g/cm^3, determined through correlation to phantoms of known density.

All microCT analysis excluded the fibula. A volume of interest (VOI) denoted "7.8 mm VOI" was selected, commencing 0.5 mm below the growth plate and finishing 7.8 mm distally, proximal to the tibia-fibula joint (Fig. 1). Consecutive VOIs of height 0.06 mm were assessed along the 7.8 mm VOI to visualize bone volume change, between treated and control, along the loaded/unloaded tibiae. Sub-regional analysis was performed within the metaphysis and diaphysis (Fig. 1). A metaphyseal VOI height of a 1.2 mm, commencing 0.5 mm below the growth plate, was denoted the metaphyseal "Canc + Cort" VOI as it assessed both the cancellous and cortical metaphyseal bone together. Within this region, a "Cancellous" only VOI was analyzed by excluding the cortical sheath. The "Cortical" bone was also analyzed separately, excluding cancellous bone. Two diaphyseal VOIs of 0.5 mm height were assessed, 37% and 50% down the tibia from the proximal end. These VOIs correspond with other published studies that examine the response to increased load in the tibia.[23,32–34]

Bone parameters assessed within cancellous VOIs were trabecular bone volume (BV), trabecular bone volume/total volume (BV/TV), tissue volume (TV), and tissue mineral density (TMD), as well as microarchitecture parameters of trabecular thickness (Tb.Th), number (Tb.N), and separation (Tb.Sp). Within cortical VOIs cortical BV, cortical thickness (Ct.Th) and TMD were assessed, as well as periosteal (Ps) and endosteal (Ec) surface and polar moment of inertia [MMI(polar)], a geometric predictor of whole bone strength. When the metaphyseal VOI contained cancellous and cortical bone then BV and TV were assessed.

Bone histomorphometry

Mineralized diaphyseal samples were embedded in methyl methacrylate and 5 μm transverse sections cut at two regions of interest in each tibia: 37% and 50% from the proximal end of the tibiae. Images were captured using a Leica DMLA CTRMC microscope (Leica Microsystems, Heerbrugg, Switzerland) and a QICAM Fast 1394 color 12 bit camera with QCapture software version 2.6.8.2 (Quantitative Imaging Corporation, British Columbia, Canada). The diaphyseal cortical bone was analyzed for daily mineral apposition rate (MAR), mineralizing surface/bone surface (MS/BS), and bone formation rate/bone surface (BFR/BS).

Coronal sections of the proximal tibiae were cut for metaphyseal cancellous bone assessment. Mineralized metaphyseal samples were cryosectioned (5 μm) using Cryofilm type IIC[10] (Section-Lab Co., Hiroshima, Japan) and images captured using Aperio Scanscope FL, Scanscope CS2 and Aperio Imagescope v11.2.0.780 (Aperio, Vista, CA, USA). Samples were analyzed for MAR, MS/BS, and BFR/BS. Sections were also stained for tartrate-resistant acid phosphatase (TRAP) and analysis performed for osteoclast number (N.Oc), osteoclast surface (Oc.S), and bone surface (BS), with the size of the osteoclast (Oc.S/BS) and the fraction of bone surface with osteoclasts adhered (Oc.S/BS) examined. All histomorphometry was performed with BIOQUANT measure 32 Nova Prime (Nashville, TN, USA).

Statistical analysis

Statistical analysis of strain gauge data between mouse genotypes was performed using non-parametric Mann-Whitney U test. Remaining statistical assessment between genotypes was performed using parametric independent sample *t*-test with a 95% confidence interval. Analysis of contralateral tibiae was performed using parametric paired samples test with a 95% confidence interval. Comparison of the effect of loading/unloading treatment between genotypes was analyzed via

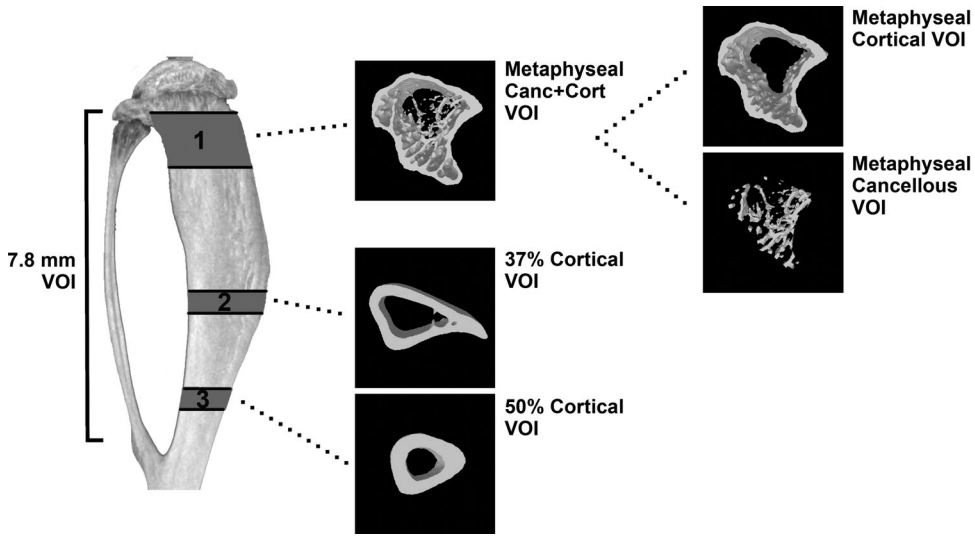

Fig. 1. A 7.8 mm VOI of the tibia starting 0.5 mm below the proximal growth plate was assessed. Sub-regional analysis was performed in 3 VOIs. VOI 1 (Metaphyseal Canc + Cort) represents metaphyseal bone with 1.2 mm height starting 0.5 mm below the growth plate. The Cortical and Cancellous bone compartments of this VOI were analysed separately and together. VOI 2 (37% Cortical) and VOI 3 (50% Cortical) represents diaphyseal cortical bone in two 0.5 mm height VOIs situated 37% and 50% down from the proximal tibia.

general linear analysis using univariate analysis of variance. For all testing a value of $p < 0.05$ was considered significant. All analysis was performed using IBM SPSS Statistics 20 (SPSS Inc., Chicago, IL, USA).

Results

Sclerostin deficiency prevents bone loss caused by unloading

Localized muscle wastage was evident following BTX treatment, with 26% decreases in weight of wild type and *Sost*−/− BTX-treated hind limbs versus their contralateral controls ($p < 0.01$, Fig. 2*A*). There were no differences in hind limb weight between genotypes when comparing treated hind-limbs only, or control hind limbs only.

Prior to BTX treatment the tibiae intended for unloading (right tibiae) of the wild type mice had significantly greater BMD within the metaphysis than contralateral control (left) tibiae, as measured by DXA (Fig. 2*B*); likely due to manual positioning of ROIs for analysis. However, the response with unloading in wild type mice was such that metaphyseal BMD was significantly reduced (−8%) by day 14, compared to control tibiae ($p < 0.01$). In contrast, longitudinal assessment by DXA in *Sost*−/− mice showed no significant change between the unloaded and control limbs in metaphyseal BMD at any time point. Percent change in BMD from day 0 was not related to body weight changes for the unloaded tibiae (Fig. S1). Metaphyseal BMC by DXA trended in response to unloading in a similar manner as BMD for wild type and *Sost*−/− mice (data not shown). MicroCT confirmed decreased bone volume with unloading in the wild type mice (−5%, $p < 0.01$, Fig. 2*C*), but there was no significant difference between the *Sost*−/− unloaded and contralateral tibiae. The BV change along the tibiae of wild type and *Sost*−/− mice was demonstrated in a histogram (Fig. 2*D*).

Sub-regional microCT analyses were performed (Tables 1 and 2). In unloaded wild type tibiae, metaphyseal bone volume decreased 9% compared to the control limb ($p < 0.01$). This decreased metaphyseal BV was within both cortical (−7%, $p < 0.05$) and cancellous (−20%, $p < 0.01$) bone. Cortical thickness (−10%, $p < 0.01$) and cortical TMD (−3%, $p < 0.05$) were also significantly decreased with unloading. This cortical bone loss in response to unloading appeared to be primarily on the endosteal surface with an increase in the endosteal perimeter (4%, $p < 0.01$) and also an increase in TV of the cancellous region (9%, $p < 0.01$). Cancellous BV/TV (−25%), Tb.N (−17%), and TMD (−8%) were all significantly decreased ($p < 0.01$). The mid-diaphysis showed similarly a loss of bone in response to unloading. The two mid-diaphyseal VOIs showed significant decreases (between −5% and −8%) in BV and cortical

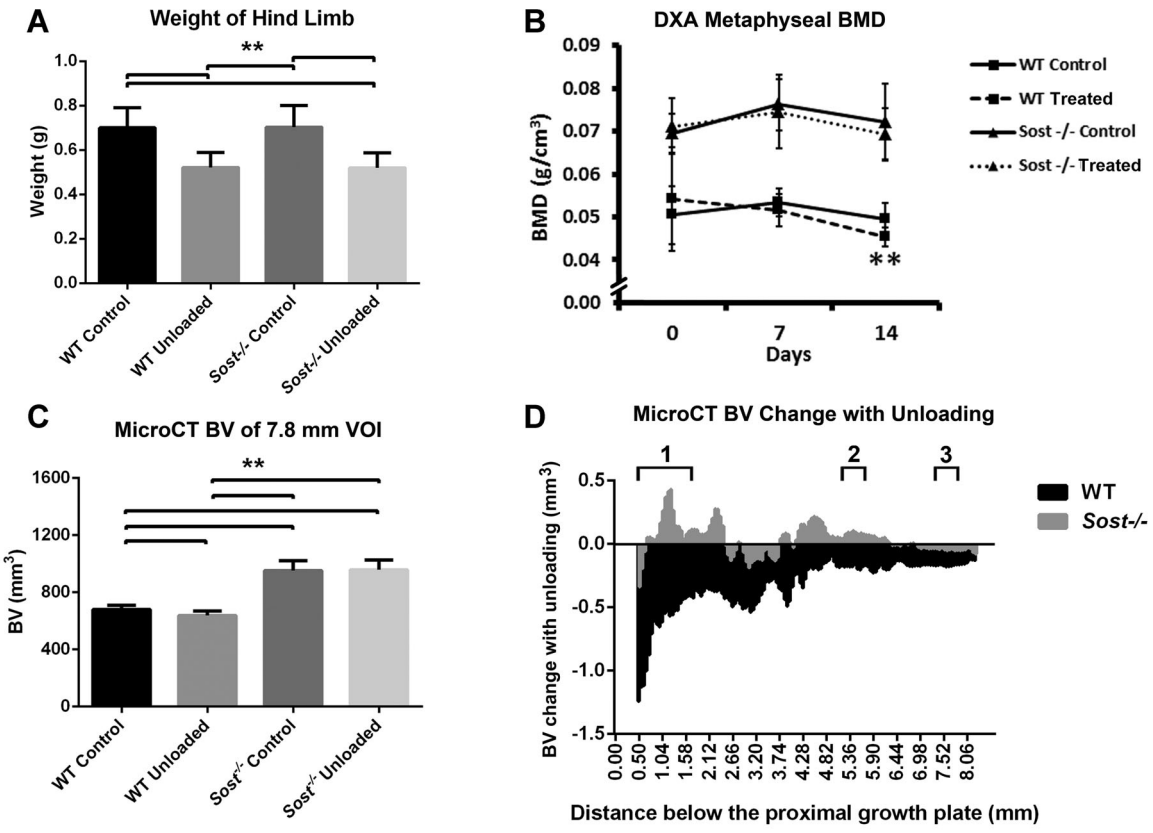

Fig. 2. Control and unloaded tibiae of WT (wild type) and *Sost*−/− mice: (*A*) End point weight of control and BTX-treated hind limbs: tibia, fibula, femur and muscle, excluding skin and feet; (*B*) DXA measured mean bone mineral (BMD) of the tibial metaphysis at days 0, 7, and 14. Bars represent ± SD; (*C*) MicroCT measured mean bone volume, within the 7.8 mm VOI of the tibiae. Bars represent + SD; (*D*) Bone volume change between unloaded and control tibiae along the 7.8 mm VOI. 1–3. Localities of sub-regional VOIs: 1. Metaphyseal VOI, 2. 37% Cortical VOI, 3. 50% Cortical VOI. $^{**}p < 0.01$.

Table 1. Metaphyseal Bone Parameters Measured by MicroCT for Strain-Matched (1200με) Loading and Unloading Studies

		Loading Study				Unloading Study			
		WT		*Sost*−/−		WT		*Sost*−/−	
Metaphyseal VOI	Parameters	Control	Loaded	Control	Loaded	Control	Unloaded	Control	Unloaded
Canc+Cort	TV (mm^3)	3.03 ± 0.15	3.31 ± 0.18[a]	3.30 ± 0.20	3.78 ± 0.25[a]	3.05 ± 0.14	3.09 ± 0.16	3.34 ± 0.19	3.44 ± 0.24[b]
	BV (mm^3)	1.74 ± 0.12	1.94 ± 0.11[a]	2.35 ± 0.17	2.85 ± 0.21[a]	1.63 ± 0.10	1.49 ± 0.08[a]	2.32 ± 0.18	2.34 ± 0.19
Cancellous	TV (mm^3)	1.36 ± 0.08	1.42 ± 0.13	1.28 ± 0.09	1.21 ± 0.10[a]	1.49 ± 0.06	1.62 ± 0.10[a]	1.44 ± 0.09	1.51 ± 0.12
	BV (mm^3)	0.23 ± 0.04	0.23 ± 0.07	0.48 ± 0.09	0.42 ± 0.10[b]	0.25 ± 0.05	0.20 ± 0.03[a]	0.56 ± 0.06	0.60 ± 0.11
	BV/TV (%)	16.91 ± 2.96	16.25 ± 4.16	37.10 ± 4.93	34.54 ± 6.15[b]	16.50 ± 3.33	12.45 ± 1.44[a]	38.53 ± 3.26	39.48 ± 5.77
	Tb.Th (mm)	0.09 ± 0.00	0.10 ± 0.00[a]	0.14 ± 0.04	0.13 ± 0.01	0.08 ± 0.00	0.08 ± 0.00[a]	0.12 ± 0.00	0.12 ± 0.01
	Tb.Sp (mm)	0.27 ± 0.03	0.28 ± 0.03	0.22 ± 0.06	0.22 ± 0.03	0.25 ± 0.02	0.25 ± 0.01	0.17 ± 0.01	0.17 ± 0.02
	Tb.N (mm^{-1})	1.90 ± 0.28	1.61 ± 0.35[b]	2.81 ± 0.56	2.63 ± 0.38	1.98 ± 0.32	1.65 ± 0.17[a]	3.17 ± 0.20	3.32 ± 0.42
	TMD (g/cm^3)	0.64 ± 0.03	0.68 ± 0.03[a]	0.80 ± 0.04	0.82 ± 0.04	0.64 ± 0.03	0.59 ± 0.02[a]	0.89 ± 0.18	0.83 ± 0.05
Cortical	BV (mm^3)	1.51 ± 0.09	1.70 ± 0.08[a]	1.87 ± 0.12	2.42 ± 0.20[a]	1.38 ± 0.08	1.29 ± 0.09[b]	1.75 ± 0.16	1.75 ± 0.16
	Ct.Th (mm)	0.24 ± 0.01	0.26 ± 0.01[a]	0.30 ± 0.1	0.37 ± 0.02[a]	0.21 ± 0.01	0.19 ± 0.01[a]	0.26 ± 0.02	0.26 ± 0.02
	Ps (mm)	7.10 ± 0.28	7.33 ± 0.22[a]	7.22 ± 0.25	7.56 ± 0.29[a]	7.31 ± 0.26	7.22 ± 0.24	7.47 ± 0.24	7.46 ± 0.16
	Ec (mm)	5.61 ± 0.24	5.73 ± 0.29	5.45 ± 0.32	5.41 ± 0.40	5.97 ± 0.22	6.18 ± 0.20[a]	5.94 ± 0.28	6.20 ± 0.32
	TMD (g/cm^3)	1.31 ± 0.04	1.35 ± 0.05	1.46 ± 0.02	1.49 ± 0.03[a]	1.27 ± 0.04	1.23 ± 0.04[b]	1.43 ± 0.04	1.43 ± 0.06
n		10	10	10	10	10	10	10	10

[a] $p < 0.01$.
[b] $p < 0.05$ compared to contralateral control.

thickness with unloading in the wild type tibiae ($p < 0.01$). In the 37% cortical VOI, the endosteal perimeter was significantly increased (7%, $p < 0.05$), suggesting localized widening of the marrow cavity at this region.

In the *Sost*−/− unloaded tibiae a statistically significant but small (−3%) decrease in cortical thickness was seen in the 50% cortical VOI ($p < 0.05$). This decrease did not translate into changes on any other bone parameters, for either the 50% or 37% cortical VOIs.

Dynamic histomorphometry of control wild type and *Sost*−/− tibiae indicated that bone formation in the metaphysis of *Sost*−/− mice approached that of wild type mice by 12 weeks of (Fig. 3). Further, unloading did not alter any of these bone formation parameters in wild type or *Sost*−/− mice, suggesting bone formation was not the major responder to decreased loading. However, no changes were seen in N.Oc, Oc.S/N.Oc, or Oc.S/BS with unloading compared to control tibiae for wild type and *Sost*−/− mice, suggesting no unloading-related changes in osteoclast size or the fraction of bone surface with osteoclasts adhered. Wild type control and unloaded tibiae did have significantly greater Oc.S/BS compared to *Sost*−/− control and unloaded tibiae ($p < 0.01$). This difference is likely due to a greater bone surface in the *Sost*−/− mice as N.Oc was not changed between the mouse strains or treatment.

Table 2. Diaphyseal Bone Parameters Measured by MicroCT for Strain-Matched (1200με) Loading and Unloading Studies

		Loading Study				Unloading Study			
		WT		*Sost*−/−		WT		*Sost*−/−	
Diaphyseal VOI	Parameters	Control	Loaded	Control	Loaded	Control	Unloaded	Control	Unloaded
37% Cortical	BV (mm^3)	0.55 ± 0.03	0.64 ± 0.03[a]	0.74 ± 0.05	0.88 ± 0.05[a]	0.50 ± 0.02	0.47 ± 0.02[a]	0.68 ± 0.06	0.68 ± 0.06
	Ct.Th (mm)	0.26 ± 0.01	0.30 ± 0.01[a]	0.34 ± 0.00	0.39 ± 0.01[a]	0.24 ± 0.01	0.22 ± 0.00[a]	0.31 ± 0.01	0.31 ± 0.02
	Ps (mm)	5.84 ± 0.26	6.14 ± 0.25[a]	6.06 ± 0.29	6.34 ± 0.29[a]	5.75 ± 0.19	5.68 ± 0.27	5.94 ± 0.33	5.95 ± 0.26
	Ec (mm)	3.66 ± 0.14	3.74 ± 0.22	3.51 ± 0.26	3.69 ± 0.45	3.85 ± 0.23	4.11 ± 0.27[b]	3.95 ± 0.42	3.96 ± 0.30
	MMI(polar) (mm^4)	0.48 ± 0.06	0.60 ± 0.07[a]	0.67 ± 0.10	0.87 ± 0.11[a]	0.42 ± 0.03	0.41 ± 0.06	0.61 ± 0.10	0.62 ± 0.09
	TMD (g/cm^3)	1.47 ± 0.03	1.48 ± 0.04	1.56 ± 0.03	1.59 ± 0.02[a]	1.39 ± 0.04	1.39 ± 0.07	1.52 ± 0.03	1.52 ± 0.04
50% Cortical	BV (mm^3)	0.41 ± 0.02	0.49 ± 0.03[a]	0.60 ± 0.04	0.68 ± 0.05[a]	0.38 ± 0.01	0.36 ± 0.02[a]	0.56 ± 0.03	0.55 ± 0.03
	Ct.Th (mm)	0.28 ± 0.00	0.32 ± 0.02[a]	0.37 ± 0.00	0.41 ± 0.01[a]	0.26 ± 0.00	0.24 ± 0.00[a]	0.36 ± 0.01	0.35 ± 0.01[b]
	Ps (mm)	4.10 ± 0.16	4.42 ± 0.17[a]	4.66 ± 0.25	4.85 ± 0.22[b]	4.13 ± 0.14	4.05 ± 0.17	4.48 ± 0.23	4.51 ± 0.24
	Ec (mm)	2.23 ± 0.12	2.31 ± 0.23	2.31 ± 0.36	2.29 ± 0.45	2.48 ± 0.19	2.50 ± 0.15	2.45 ± 0.33	2.35 ± 0.20
	MMI(polar) (mm^4)	0.19 ± 0.03	0.25 ± 0.03[a]	0.31 ± 0.05	0.37 ± 0.06[a]	0.17 ± 0.02	0.17 ± 0.02	0.28 ± 0.04	0.28 ± 0.03
	TMD (g/cm^3)	1.65 ± 0.03	1.64 ± 0.05	1.73 ± 0.04	1.74 ± 0.02	1.52 ± 0.05	1.53 ± 0.06	1.66 ± 0.04	1.67 ± 0.04
n		10	10	10	10	10	10	10	10

[a] $p < 0.01$.
[b] $p < 0.05$ compared to contralateral control.

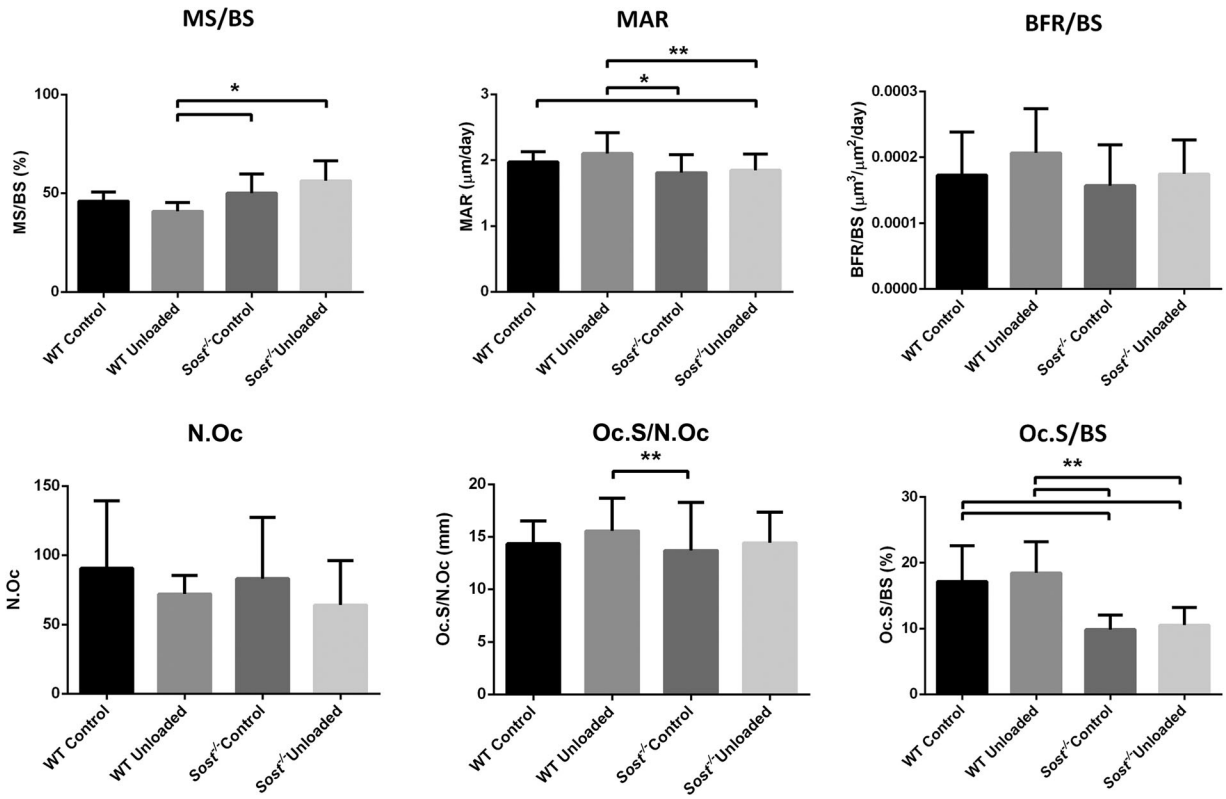

Fig. 3. Histomorphometric analysis of unloaded and control wild type (WT) and *Sost*−/− tibiae within metaphyseal cancellous bone. MS/BS, mineralizing surface/bone surface; MAR, mineral apposition rate/day; BFR/BS, bone formation rate/bone surface; N.Oc, osteoclast number; Oc.S/N.Oc, osteoclast surface/osteoclast number; Oc.S/BS, osteoclast surface/bone surface. Bars represent + SD, $n = 8$–10 per group. $^{**}p < 0.01$, $^{*}p < 0.05$.

Variation of bone strain in Sclerostin deficient mice

The *Sost*−/− tibiae showed a trend toward increased stiffness under the same compressive cyclic loading force compared to wild type control mice. While this difference did not reach significance ($p = 0.09$, Fig. 4), a post hoc power analysis indicated based on the effect size (Cohen *d* value = 1.24) that the observed power (β) was 0.32. Based on the high effect size both strain matched and force matched experiments were carried out. For strain-matched experiments, the *Sost*−/− and wild type mice received −12.5 N and −9.0 N force, respectively, to induce equivalent strains of 1200 με on the mid-diaphysis of the tibiae. For force matched experiments, separate groups of *Sost*−/− and wild type mice received −9.0 N loading.

Sclerostin deficiency results in increased load-induced bone formation

Prior to loading (day 0) the relative BMD of wild type tibial mid-diaphyses intended for loading (left tibiae) was less than that of the contralateral controls (right tibiae) ($p < 0.05$) as measured by DXA (Fig. 5*A*); likely due to manual positioning of ROIs for analysis. However, the response of strain-matched loading by day 14 was a significant increase in diaphyseal BMD over controls (16%, $p < 0.01$). No difference in BMD was seen at day 0 between the loaded/contralateral *Sost*−/− tibiae by DXA (Fig. 5*A*). Notably, diaphyseal BMD was significantly increased in the strain-matched *Sost*−/− mice following loading (11% at day 7, 23% at day 14; $p < 0.01$). Change in BMD over the study period was not related to body weight changes (Fig. S1). Diaphyseal BMC trended similarly to BMD in wild type and *Sost*−/− mice by DXA (data not shown).

Loading-induced increases in BV was confirmed by MicroCT in wild type and *Sost*−/− mice at day 14 ($p < 0.01$, Fig. 5*B*). The 20% BV increase in strain-matched *Sost*−/− tibiae was significantly greater than the 15% BV increase in wild type tibiae ($p < 0.01$).

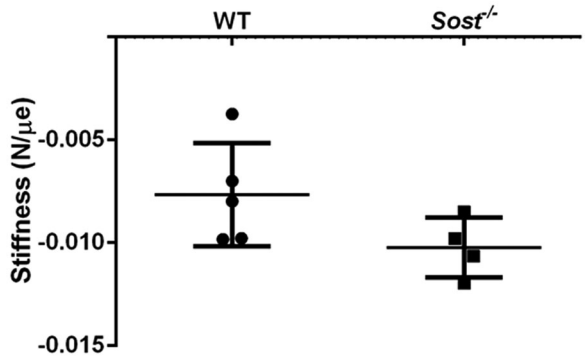

Fig. 4. Mean stiffness of wild type (WT) and *Sost*−/− tibiae measured by strain gauging of the mid-diaphysis. *Sost*−/− tibiae trended toward being stiffer than WT controls ($p = 0.09$). Bars represent ± SD, $n = 4$–5 per group.

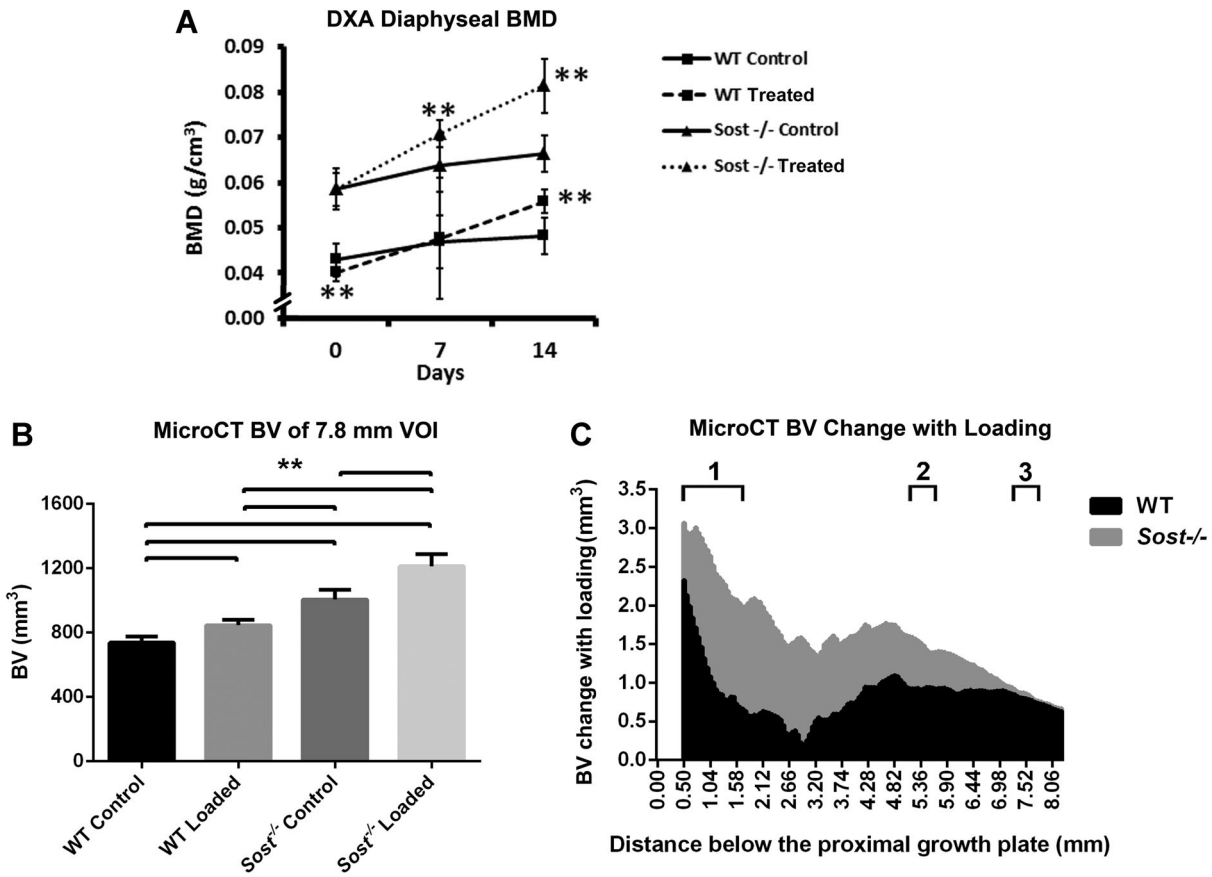

Fig. 5. Control and strain-matched (1200με) loaded tibiae of WT (wild type) and *Sost*−/− mice: (*A*) DXA measured mean bone mineral (BMD) of the tibial diaphysis at days 0, 7, and 14. Bars represent ± SD; (*B*) MicroCT measured mean bone volume, within the 7.8 mm VOI of the tibiae. Bars represent + SD; (*C*) Bone volume change between loaded and control tibiae along the 7.8 mm VOI. 1–3. Localities of sub-regional VOIs: 1. Metaphyseal VOI, 2. 37% Cortical VOI, 3. 50% Cortical VOI. $^{**}p < 0.01$

These BV increases were constant along the 7.8 mm diaphyseal region that was analyzed (Fig. 5*C*). Similar BMD and bone volume responses to loading were also seen in the load-matched study for the *Sost*−/− mice (Fig. 6). This confirmed that the response to loading in the *Sost*−/− mice was not only a result of the increased load applied in the strain-matched study.

As strain engendered on the bone, rather than an external load, correlates with mechanotransduction responses,[35–38] further microCT sub-regional analysis was performed for the strain-matched loading cohort of mice. Within the metaphysis effects with loading were similar in the wild type and *Sost*−/− mice (Table 1). BV was increased in the loaded tibiae compared to their contralateral controls, but only within the cortical bone compartment ($p < 0.01$). The 29% increase in *Sost*−/− cortical BV was significantly greater than the 13% increase in WT tibiae ($p < 0.01$). The cortical thickness of this metaphyseal sheath was increased for both wild type and *Sost*−/− loaded tibiae, due to increases in their periosteal perimeters ($p < 0.01$). A small 2% TMD increase was seen in the *Sost*−/− loaded metaphyseal cortex only ($p < 0.01$). No change in BV or BV/TV was seen in the cancellous metaphyseal bone of the wild type mice, while *Sost*−/− mice had a significant decrease in cancellous BV and BV/TV with loading (−13% and −7%, $p < 0.05$). However, TV of the cancellous compartment was also 5% decreased in the *Sost*−/− loaded mice ($p < 0.01$), suggesting a shift toward cortical bone within the metaphyseal VOI of the *Sost*−/− tibiae.

The cortical bone within the two mid-diaphyseal VOIs (37%, 50% along the tibiae, respectively) showed similar results to the metaphyseal cortical bone (Table 2). There were significant increases seen in BV (17%, 19% wild type; 19%, 13% *Sost*−/−), Ct.Th (16%, 17% wild type; 16%, 10% *Sost*−/−), and periosteal perimeter (5%, 8% wild type; 5%, 4% *Sost*−/−) ($p < 0.01$), suggesting periosteal expansion. These resulted in increased MMI(polar) in both wild type (26%, 30%) and *Sost*−/− (30%, 20%) loaded tibiae compared to their contralateral controls ($p < 0.01$). A small 2% increase in TMD was seen within the 37% VOI for *Sost*−/− loaded tibiae only ($p < 0.01$).

Dynamic histomorphometry of non-loaded control tibiae of the wild type and *Sost*−/− mice indicated that bone formation in the mid-diaphysis of *Sost*−/− mice approached that of wild type mice by 12 weeks of age (Fig. 7). Within the metaphyseal cancellous bone MS/BS, MAR and BFR/BS were not different between the genotypes. Within the mid-diaphysis (37% cortical ROI) MS/BS was significantly increased in the *Sost*−/− control tibiae compared to wild type control ($p < 0.01$), but MAR and BFR/BS were not different between the genotypes on either the periosteal or endosteal surfaces. Comparable findings were noted at the mid-diaphyseal 50% cortical ROI (data not shown).

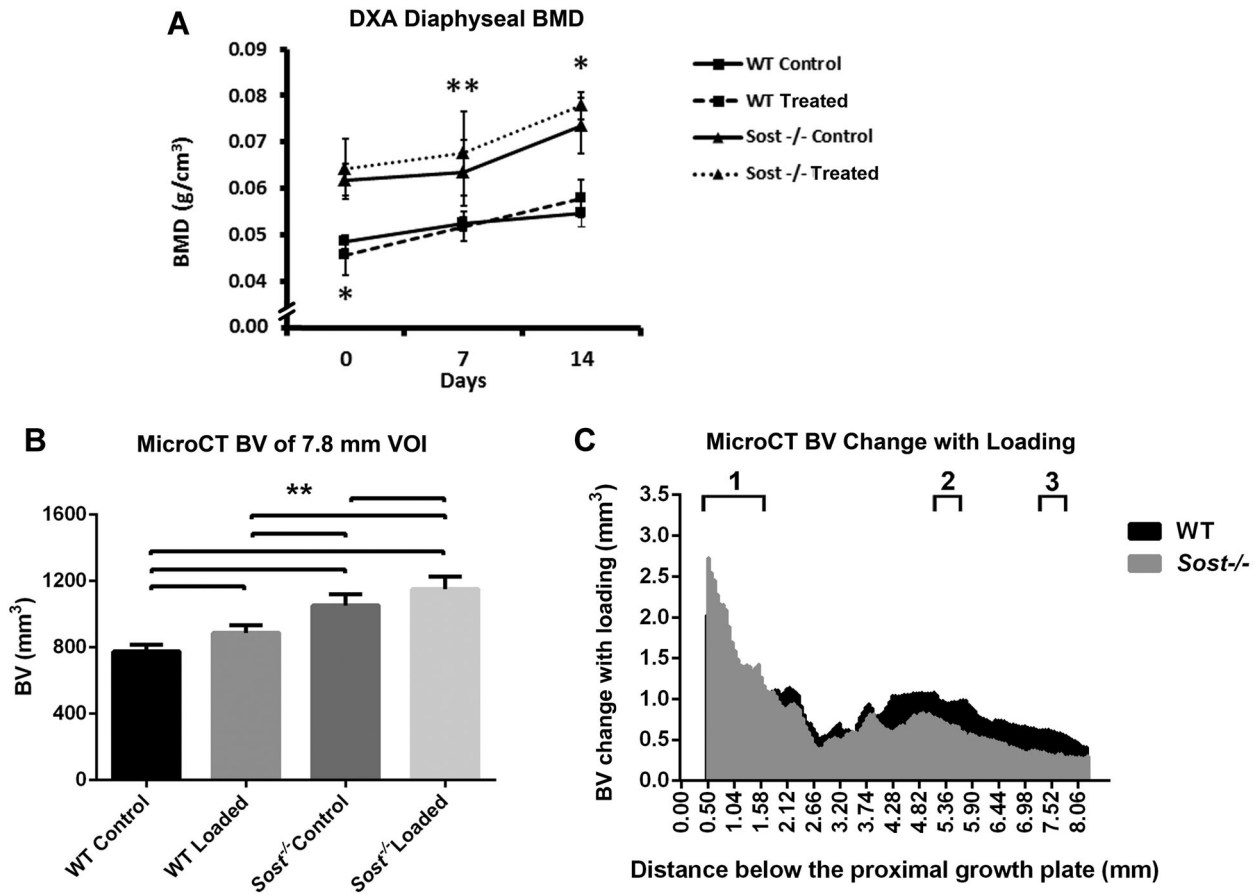

Fig. 6. Control and load-matched (−9.0N) loaded tibiae of WT (wild type) and *Sost*−/− mice: (*A*) DXA measured mean bone mineral (BMD) of the tibial diaphysis at days 0, 7, and 14. Bars represent ± SD; (*B*) MicroCT measured mean bone volume, within the 7.8 mm VOI of the tibiae. Bars represent + SD; (*C*) Bone volume change between loaded and control tibiae along the 7.8 mm VOI. 1–3. Localities of sub-regional VOIs: 1. Metaphyseal VOI, 2. 37% Cortical VOI, 3. 50% Cortical VOI. $^{**}p < 0.01$, $^{*}p < 0.05$.

Periosteal and endosteal responses were both seen with loading of wild type and *Sost*−/− mice. On the periosteal surface, MS/BS, MAR, and BFR/BS were all significantly increased compared to the contralateral control tibiae ($p < 0.01$). The MAR and BFR/BS response was greater in *Sost*−/− mice than wild type ($p < 0.01$). Endosteal MAR ($p < 0.01$) and BFR ($p < 0.05$) were also significantly increased for wild type and *Sost*−/− mice. However, MS/BS was decreased on this surface for both wild type ($p < 0.01$) and *Sost*−/− loaded tibiae ($p < 0.05$).

Discussion

This study comprehensively investigates the response of the *Sost*−/− mouse line to increased cyclic loading and Botox-induced unloading. Sclerostin plays a major role in mechanotransduction in bone. Acute and chronic Sclerostin deficiency can prevent bone loss associated with reduced loading[25,26] and upregulation of Sclerostin can prevent increases in bone volume associated with increased loading.[27] We hypothesized that the response of bone to mechanical loading and unloading would be significantly impaired in the absence of Sclerostin, in comparison to C57Bl/6J wild type controls.

Contrary to our initial hypothesis, *Sost*−/− mice responded positively to a cyclic load protocol; cortical bone volume increased significantly in both *Sost*−/− and control mice and correlated with increased bone formation. While Sclerostin has been identified as a key factor in the anabolic response of bone to load, our results indicate an alternative Sclerostin-independent mechanism. While prior findings indicate that Sclerostin down-regulation within osteocytes is necessary for bone response to loading,[27] our data suggest that *Sost* deficiency is not sufficient to induce maximal bone anabolism, and that anabolism can be further increased with mechanical load. Further, an enhanced bone formation response to increased load was seen in the *Sost*−/− tibiae. MAR and BFR/BS responses on the periosteal mid-diaphyseal surfaces of the *Sost*−/− tibiae were increased compared to the wild type responses. These data indicate an increased response to strain-matched loading with *Sost* deficiency.

While the anabolic response to load is not dependent on Sclerostin, unloading-induced bone loss was attenuated in *Sost*−/− mice. This is consistent with the prior literature showing Sclerostin to be a key modulator of unloading induced bone loss.[25,26,39] Direct resorption assessment would provide clearer information of this effect on catabolism, as the osteoclast

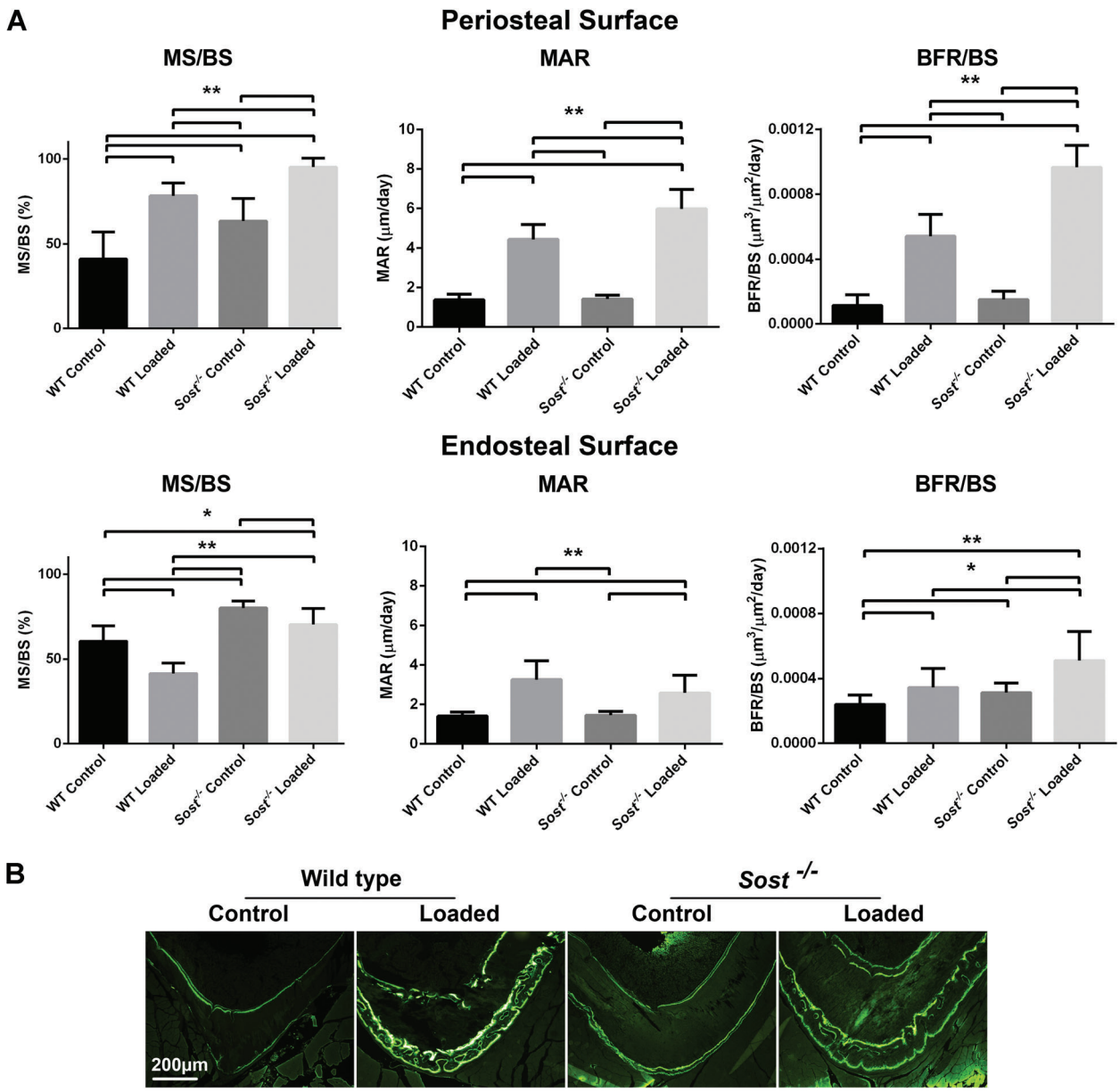

Fig. 7. Histomorphometric analysis of strain-matched (1200 με) loaded and control wild type (WT) and *Sost*−/− tibiae within the diaphyseal 37% Cortical VOI. (*A*) Periosteal and endosteal surfaces were analysed for: MS/BS, mineralizing surface/bone surface; MAR mineral apposition rate/day; BFR/BS, bone formation rate/bone surface. Bars represent + SD, $n = 8$–10 per group. $^{**}p < 0.01$, $^{*}p < 0.05$. (*B*) Representative images of Calcein bone labeling.

parameters measured only reflect their resorption activity. However, as bone formation was not effected by unloading this appears to disregard bone anabolism changes as the primary response of decrease bone volume with unloading.

These results of loading and unloading regimes in a situation of long-term Sclerostin deficiency provide clinically relevant findings. Human studies of bed-rest have reported elevated Sclerostin levels, suggesting that anti-Sclerostin treatment may target the mechanism of bone loss.[40,41] These data support the clinical utility of anti-Sclerostin therapies for treating boss loss associated with unloading, such as disuse osteopenia. Further, the benefit of encouraging exercise/bone loading for individuals with osteoporosis receiving anti-Sclerostin therapy is unknown. These data raise the possibility that exercise may provide an additive anabolic effect on bone even in the presence of Sclerostin blockade. However, this hypothesis will need to be validated via controlled clinical studies.

The Sclerostin-independent bone response to increased load indicates the involvement of other factors in bone mechanotransduction. Other inhibitors of the canonical Wnt/β-catenin signaling pathway may have a role in mechanotransduction, acting along-side Sclerostin or taking up such a role where Sclerostin is deficient. Such compensation may be the cause of the comparable metaphyseal and diaphyseal bone formation parameters between *Sost*−/− and wild type control tibiae at 12 weeks age. A key candidate is Dkk1 which is up-regulated in

the Sclerostin knock-out mouse and within van Buchem and Sclerosteosis patients.[28,29] Elevated Dkk1 levels within the bone compartment could down-regulate in response to increased load, leading to increased Wnt/β-catenin signaling and bone formation. Further, a more intricate system independent of, or in synergy with, the Wnt/β-catenin pathway may be involved in bone modulation. Factors of interest include estrogen receptor α (ERα), insulin-like growth factor 1 (IGF-1), parathyroid hormone (PTH), leptin, prostanoids, PGE2, connexin 43, interleukin-11, and bone morphogenetic proteins (BMPs).[30,42–47]

Future work investigating other potential mechanotransduction modulators is required. Such prospective modulators may be highlighted by gene and protein expression analysis following loading/unloading and also studies of longer loading/unloading periods. In particular, prolonged unloading in a Sclerostin deficient system has not been studied in detail and compensatory responses may emerge with longer unloading. Moreover, investigation of models that feature deficiency in multiple Wnt pathway regulators may reveal compensation or synergy with Sclerostin, or suggest modulators outside the Wnt pathway.

Bone volume was increased in diaphyseal and metaphyseal cortical bone of wild type and *Sost*−/− mice. The metaphyseal bone response was greater in the *Sost*−/− tibiae than the wild type tibiae, and could reflect site-specific differences in mechanical strain induced on the two genotypes. The strains induced when loading the *Sost*−/− and wild type bones were measured and calibrated, but only the diaphyseal strains could be concluded as equivalent. Differences in bone volume, stiffness, and geometry between the genotypes may affect the strain engendered within the metaphysis. However, bone compartment specific responses to changes in Wnt/β-catenin signaling are known and may support the site-specific responses seen in the *Sost*−/− tibiae as true effects.[28,39]

An anabolic bone response to loading was not seen within metaphyseal cancellous bone of either *Sost*−/− or wild type mice. Further, the overall tissue volume of the metaphyseal cancellous region was reduced in the *Sost*−/− mice. These data suggest a generalized corticalization of the *Sost*−/− metaphysis in response to increased loading.

The lack of an anabolic cancellous response is in contrast to other similar loading regimes within the literature,[32–34,48] likely due to the age of the mice used, the mechanical strain engendered, or the VOIs selected. An age-dependent response of cancellous bone to loading has been shown, particularly when comparing growing mice versus adult mice.[48] Further, studies with a cancellous bone response in C57Bl/6 mice, of comparable age and loading regimes as our investigation, were either loaded to induce a higher tibial mid-shaft strain, or were measured with more rudimentary VOIs.[32–34] These VOIs were cylinder volumes positioned within the marrow space of the metaphysis, providing only a representative examination of the cancellous bone. Our study provided a more expansive investigation. This does highlight the challenge of comparing results of published loading/unloading studies, with no commonly accepted standards for analysis. Other variables such as sex, loading period/regime, and mouse strain may also be responsible for inconsistencies in wild type responses within the literature. Of particular note, with emerging evidence of ERα involvement in mechanotransduction, there may be gender specific effects confounding comparisons.[30,44]

Some limitations existing within this study are worth note. Littermate controls, unavailable to us, would have provided optimal controls. Back-crossing of founder *Sost*−/− mice, of 99.09% isogenicity/identity to the C57BL/6J strain, supports minimum strain differences; however, genetic drift between the two colonies cannot be completely discounted. Further, age-matched non-treated mice would provide rigorous baseline controls, confirming contralateral tibiae as suitable controls. There is the potential for compensation by control limbs following treatment of the contralateral limbs, particularly in the BTX model. Previous murine unloading studies utilising BTX to induce hind-limb disuse have shown moderate systemic effects resulting in a lowering of bone mass in the contralateral (non-treated) tibiae compared to baseline controls, likely a result of reduced activity.[49,50] However, this does not discount the comparative effect of unloaded tibia.

Despite these limitations, this study presents a direct comparison of increased and decreased load responses in Sclerostin deficient bone and provides novel information about the role of Sclerostin in mechanotransduction. Although Sclerostin loss-of-function offers protection from unloading induced bone loss, it does not prevent bone gain in response to increased load but rather results in an increased bone formation response. Thus, while Sclerostin may be involved in bone mechanotransduction, it is not the sole modulator of the loading response. Future work is required to elucidate other factors that are essential for sensing and transducing mechanotransduction signals in response to bone load.

Disclosures

The authors received materials support for this study from Novartis Pharma. The authors have received additional funding and materials support from Novartis Pharma for research separate to this submission. Prof. Little has received funding support from Amgen and Celgene and Dr. Schindeler has received funding support from Celgene and N8 Medical for studies unrelated to this submission.

Acknowledgments

This project received funding from the Elizabeth Rosenthal Bone Research Bequest and Departmental funds. Travel funding was awarded through the Burroughs Wellcome Travel grant and the University of Sydney Postgraduate Research Scholarship Scheme. Novartis Pharma provided materials support (mice). The project received funding support for equipment costs from National Institutes of Health grant R01-AG028664. Dr. Schindeler received salary support from NHMRC Project Grant 1003478.

Authors' roles: Study design: DGL, MCHM, MMM, MK, and AM. Study conduct: AM, NHK, and KMM. Data collection: AM. Data interpretation: AM, MMM, DGL, MCHM, MK, and IK. Drafting manuscript: AM. Revising manuscript content: AS, MCHM, MMM, DGL, and IK. Approving final version of manuscript: all authors. AM takes responsibility for the integrity of the data analysis.

References

1. Poole KE, van Bezooijen RL, Loveridge N, et al. Sclerostin is a delayed secreted product of osteocytes that inhibits bone formation. FASEB J. 2005;19(13):1842–4.
2. van Bezooijen RL, ten Dijke P, Papapoulos SE, Lowik CW. SOST/sclerostin, an osteocyte-derived negative regulator of bone formation. Cytokine Growth Factor Rev. 2005;16(3):319–27.
3. Semenov M, Tamai K, He X. SOST is a ligand for LRP5/LRP6 and a Wnt signaling inhibitor. J Biol Chem. 2005;280(29):26770–5.

4. van Bezooijen RL, Bronckers AL, Gortzak RA, et al. Sclerostin in mineralized matrices and van Buchem disease. J Dental Res. 2009; 88(6):569–74.
5. Jager A, Gotz W, Lossdorfer S, Rath-Deschner B. Localization of SOST/sclerostin in cementocytes in vivo and in mineralizing periodontal ligament cells in vitro. J Periodontal Res. 2010;45(2):246–54.
6. van Bezooijen RL, Roelen BA, Visser A, et al. Sclerostin is an osteocyte-expressed negative regulator of bone formation, but not a classical BMP antagonist. The Journal of experimental medicine. 2004;199(6): 805–14.
7. Glass DA 2nd, Bialek P, Ahn JD, et al. Canonical Wnt signaling in differentiated osteoblasts controls osteoclast differentiation. Dev Cell. 2005;8(5):751–64.
8. Spencer GJ, Utting JC, Etheridge SL, Arnett TR, Genever PG. Wnt signalling in osteoblasts regulates expression of the receptor activator of NFkappaB ligand and inhibits osteoclastogenesis in vitro. Journal of cell science. 2006;119(Pt 7):1283–96.
9. Wijenayaka AR, Kogawa M, Lim HP, Bonewald LF, Findlay DM, Atkins GJ. Sclerostin stimulates osteocyte support of osteoclast activity by a RANKL-dependent pathway. PLoS One. 2011;6(10):e25900.
10. Kramer I, Halleux C, Keller H, et al. Osteocyte Wnt/beta-catenin signaling is required for normal bone homeostasis. Molecular and cellular biology. 2010;30(12):3071–85.
11. Staehling-Hampton K, Proll S, Paeper BW, et al. A 52-kb deletion in the SOST-MEOX1 intergenic region on 17q12-q21 is associated with van Buchem disease in the Dutch population. American journal of medical genetics. 2002;110(2):144–52.
12. Balemans W, Ebeling M, Patel N, et al. Increased bone density in sclerosteosis is due to the deficiency of a novel secreted protein (SOST). Human molecular genetics. 2001;10(5):537–43.
13. Gardner JC, van Bezooijen RL, Mervis B, et al. Bone mineral density in sclerosteosis; affected individuals and gene carriers. J Clin Endocrinol Metab. 2005;90(12):6392–5.
14. Loots GG, Kneissel M, Keller H, et al. Genomic deletion of a long-range bone enhancer misregulates sclerostin in Van Buchem disease. Genome Res. 2005;15(7):928–35.
15. Kramer I, Kneissel M. The high bone mass phenotype of Sost deficient mice is characterized by progressive increase in bone thickness, mineralization and predicted cortical bone strength in a gene dosage unrelated manner. Bone. 2008;42(Suppl 1):S57.
16. Li X, Ominsky MS, Niu QT, et al. Targeted deletion of the sclerostin gene in mice results in increased bone formation and bone strength. J Bone Miner Res. 2008;23(6):860–9.
17. Li X, Warmington KS, Niu QT, et al. Inhibition of sclerostin by monoclonal antibody increases bone formation, bone mass, and bone strength in aged male rats. J Bone Miner Res. 2010;25(12):2371–80.
18. Li X, Ominsky MS, Warmington KS, et al. Sclerostin antibody treatment increases bone formation, bone mass, and bone strength in a rat model of postmenopausal osteoporosis. J Bone Miner Res. 2009;24(4):578–88.
19. Li X, Warmington KS, Niu QT, et al. Inhibition of sclerostin by monoclonal antibody increases bone formation, bone mass, and bone strength in aged male rats. J Bone Miner Res. 2010;25(12):2647–56.
20. Ominsky MS, Vlasseros F, Jolette J, et al. Two doses of sclerostin antibody in cynomolgus monkeys increases bone formation, bone mineral density, and bone strength. J Bone Miner Res. 2010;25(5): 948–59.
21. Padhi D, Jang G, Stouch B, Fang L, Posvar E. Single-dose, placebo-controlled, randomized study of AMG 785, a sclerostin monoclonal antibody. J Bone Miner Res. 2011;26(1):19–26.
22. McClung MR, Grauer A, Boonen S, et al. Romosozumab in postmenopausal women with low bone mineral density. The New England journal of medicine. 2014;370:412–20.
23. Moustafa A, Sugiyama T, Prasad J, et al. Mechanical loading-related changes in osteocyte sclerostin expression in mice are more closely associated with the subsequent osteogenic response than the peak strains engendered. Osteoporosis Int. 2011;1–10.
24. Robling AG, Niziolek PJ, Baldridge LA, et al. Mechanical stimulation of bone in vivo reduces osteocyte expression of Sost/sclerostin. J Biol Chem. 2008;283(9):5866–75.
25. Lin C, Jiang X, Dai Z, et al. Sclerostin mediates bone response to mechanical unloading through antagonizing Wnt/beta-catenin signaling. J Bone Miner Res. 2009;24(10):1651–61.
26. Spatz JM, Ellman R, Cloutier AM, et al. Sclerostin antibody inhibits skeletal deterioration due to reduced mechanical loading. J Bone Miner Res. 2013;28(4):865–74.
27. Tu X, Rhee Y, Condon KW, et al. Sost downregulation and local Wnt signaling are required for the osteogenic response to mechanical loading. Bone. 2012;50(1):209–17.
28. Chang MK, Kramer I, Keller H, et al. Reversing LRP5-dependent osteoporosis and SOST-deficiency induced sclerosing bone disorders by altering WNT signaling activity. J Bone Miner Res. 2013.
29. van Lierop A, Moester M, Hamdy N, Papapoulos S. Serum Dickkopf 1 Levels in Sclerostin Deficiency. J Clin Endocrinol Metab. 2013;99: 252–6.
30. Liedert A, Wagner L, Seefried L, Ebert R, Jakob F, Ignatius A. Estrogen receptor and Wnt signaling interact to regulate early gene expression in response to mechanical strain in osteoblastic cells. Biochem Biophys Res Commun. 2010;394(3):755–9.
31. Kramer I, Loots GG, Studer A, Keller H, Kneissel M. Parathyroid hormone (PTH)-induced bone gain is blunted in SOST overexpressing and deficient mice. J Bone Miner Res. 2010;25(2):178–89.
32. Lynch ME, Main RP, Xu Q, et al. Cancellous bone adaptation to tibial compression is not sex dependent in growing mice. J Appl Physiol. 2010;109(3):685–91.
33. Fritton JC, Myers ER, Wright TM, van der Meulen MC. Bone mass is preserved and cancellous architecture altered due to cyclic loading of the mouse tibia after orchidectomy. J Bone Miner Res. 2008; 23(5):663–71.
34. Fritton JC, Myers ER, Wright TM, van der Meulen MC. Loading induces site-specific increases in mineral content assessed by microcomputed tomography of the mouse tibia. Bone. 2005;36(6):1030–8.
35. Gross TS, Edwards JL, McLeod KJ, Rubin CT. Strain gradients correlate with sites of periosteal bone formation. J Bone Miner Res. 1997; 12(6):982–8.
36. Mosley JR, Lanyon LE. Strain rate as a controlling influence on adaptive modeling in response to dynamic loading of the ulna in growing male rats. Bone. 1998;23(4):313–8.
37. Torrance AG, Mosley JR, Suswillo RF, Lanyon LE. Noninvasive loading of the rat ulna in vivo induces a strain-related modeling response uncomplicated by trauma or periostal pressure. Calcif Tissue Int. 1994;54(3):241–7.
38. Mosley JR, March BM, Lynch J, Lanyon LE. Strain magnitude related changes in whole bone architecture in growing rats. Bone. 1997;20(3):191–8.
39. Macias BR, Aspenberg P, Agholme F. Paradoxical Sost gene expression response to mechanical unloading in metaphyseal bone. Bone. 2013;53(2):515–9.
40. Gaudio A, Pennisi P, Bratengeier C, et al. Increased sclerostin serum levels associated with bone formation and resorption markers in patients with immobilization-induced bone loss. J Clin Endocrinol Metab. 2010;95(5):2248–53.
41. Spatz JM, Fields EE, Yu EW, et al. Serum sclerostin increases in healthy adult men during bed rest. J Clin Endocrinol Metab. 2012;97(9): E1736–40.
42. Price JS, Sugiyama T, Galea GL, Meakin LB, Sunters A, Lanyon LE. Role of Endocrine and Paracrine Factors in the Adaptation of Bone to Mechanical Loading. Curr Osteoporos Rep. 2011;9:76–82.
43. Bonewald LF, Johnson ML. Osteocytes, mechanosensing and Wnt signaling. Bone. 2008;42(4):606–15.
44. Zaman G, Saxon LK, Sunters A, et al. Loading-related regulation of gene expression in bone in the contexts of estrogen deficiency, lack of estrogen receptor alpha and disuse. Bone. 2010;46(3): 628–42.
45. Sunters A, Armstrong VJ, Zaman G, et al. Mechano-transduction in osteoblastic cells involves strain-regulated estrogen receptor alpha-mediated control of insulin-like growth factor (IGF) I receptor sensitivity to Ambient IGF, leading to phosphatidylinositol 3-kinase/AKT-dependent Wnt/LRP5 receptor-independent activation of beta-catenin signaling. J Biol Chem. 2010;285(12):8743–58.

46. Gross TS, Srinivasan S, Liu CC, Clemens TL, Bain SD. Noninvasive loading of the murine tibia: an in vivo model for the study of mechanotransduction. J Bone Miner Res. 2002;17(3):493–501.
47. Kesavan C, Wergedal JE, Lau KH, Mohan S. Conditional disruption of IGF-I gene in type 1alpha collagen-expressing cells shows an essential role of IGF-I in skeletal anabolic response to loading. American journal of physiology Endocrinology and metabolism. 2011;301(6):E1191–7.
48. De Souza RL, Matsuura M, Eckstein F, Rawlinson SC, Lanyon LE, Pitsillides AA. Non-invasive axial loading of mouse tibiae increases cortical bone formation and modifies trabecular organization: a new model to study cortical and cancellous compartments in a single loaded element. Bone. 2005;37(6):810–8.
49. Warner SE, Sanford DA, Becker BA, Bain SD, Srinivasan S, Gross TS. Botox induced muscle paralysis rapidly degrades bone. Bone. 2006; 38(2):257–64.
50. Marchand-Libouban H, Le Drevo MA, Chappard D. Disuse induced by Botulinum toxin affects the bone marrow expression profile of bone genes leading to a rapid bone loss. J Musculoskelet Neuronal Interact. 2013;13(1):27–36.

Chapter 3. A *Dkk1* KO mouse shows an increased anabolic bone response following compressive tibial loading

This chapter is to be submitted for review with Bone.

Morse A, Ko F, McDonald MM, Schindeler A, van der Meulen MC, Lee L, Little DG. A *Dkk1* KO mouse shows an increased anabolic bone response following compressive tibial loading.

Title: The *Dkk1* KO mouse shows an increased anabolic bone response following compressive tibial loading

Running Title: Bone mechanotransduction with DKK1 deficiency

Authors: Alyson Morse[1,2], Frank Ko[3], Aaron Schindeler[1,2], Michelle M McDonald[5], Marjolein CH van der Meulen[3,4,6], Lucinda Lee[1,2], and David G Little[1,2]*.

Affiliations:

1 Orthopaedic Research & Biotechnology Unit, The Children's Hospital at Westmead, Sydney, Australia

2 Discipline of Paediatrics and Child Health, Sydney Medical School, University of Sydney, Sydney, Australia

3 Sibley School of Mechanical and Aerospace Engineering, Cornell University, Ithaca, NY, USA

4 Meinig School of Biomedical Engineering, Cornell University, Ithaca, NY, USA

5 Bone Biology Program, The Garvan Institute of Medical Research, Sydney, Australia

6 Hospital for Special Surgery, New York, United States

* **Corresponding author and reprint address:**

David G Little

Orthopaedic Research and Biotechnology

The Children's Hospital at Westmead

Locked Bag 4001,

Westmead, NSW, 2145, Australia

Email: david.little@health.nsw.gov.au

Phone: +61-2-98450117

Fax: +61-2-98453078

Author's contribution statement:

Study design: DGL, AM. Study conduct and data collection: AM, FK, LL. Data interpretation: AM. Drafting manuscript: AM. Revising manuscript content: AS, DGL, MMM, MVDM. Approving final and submitted version of manuscript: all authors. AM takes responsibility for the integrity of the data analysis.

Disclosure

Prof. Little has received funding support from Novartis Pharma, Amgen Inc. and Celgene for studies unrelated to this submission. Dr Schindeler has received funding support from Celgene and N8 Medical for studies unrelated to this submission and speaking fees from Amgen Inc. Dr McDonald has received funding from The Kay Ibbertson Cancer Council Project grant.

ABSTRACT

A viable *Dkk1* knockout (KO) mouse strain where embryonic lethality is rescued by developmental *Wnt3* heterozygosity *(Dkk1$^{-/-}$:Wnt3$^{+/-}$)* exhibits increased bone formation and a high bone mass phenotype. We hypothesized that biomechanical loading would further augment the bone formation response in *Dkk1* KO mice, comparable to results from *Sost* KO mice.

A cyclic loading protocol was applied to *Dkk1* KO mice, wild type mice (WT; *Dkk1$^{+/+}$:Wnt3$^{+/+}$*), and *Wnt3* heterozygote (*Wnt3$^{+/-}$*; *Dkk1$^{+/+}$:Wnt3$^{+/-}$)* controls. The left tibiae of 10 week old female mice were loaded *in vivo* with -7N compressive force 5 days/week for 2 weeks. *Dkk1* KO bones showed a significantly higher stiffness and so an additional group of *Dkk1* KO received -12N compressive force, which achieved an equivalent +1200με strain on the mid-diaphysis. MicroCT and bone histomorphometry analyses were subsequently performed.

All mouse groups responded to tibial loading with increased mid-diaphyseal bone volume, with the largest effect size seen in the *Dkk1* KO -12N group. Thus *Dkk1* KO animals showed enhanced sensitivity to biomechanical loading. Increases in cortical bone volume correlated with increased periosteal bone formation. Bone volume and formation were not altered between WT and *Wnt3$^{+/-}$* controls. These data support the concept that agonists of Wnt/β-catenin signaling can act synergistically with load-bearing exercise. Notably, *Sost* expression decreased with loading in *Dkk1* KO and WT genotypes, however did not significantly differ based on genotype. These data suggest that a compensatory downregulation of *Sost* in *Dkk1* KO mice is not likely to be the primary mechanism for the augmented response to biomechanical load.

Keywords: Dkk1, mechanotransduction, bone loading, Wnt, bone anabolism.

Abbreviations: WT (wild type), *Dkk1* KO (*Dkk1$^{-/-}$:Wnt3$^{+/-}$*)

INTRODUCTION

Bone is mechanosensitive with bone mass increasing in response to dynamic loading and decreasing with disuse (1). This has been displayed in animal models of increased and decreased mechanical load and in clinical studies (2-6). Mechanotransduction describes the cell signaling and effector biological response that occurs as a result of mechanical force applied to the bone compartment (7). Understanding and harnessing this process will be important in furthering our capacity to treat diseases involving low bone mass and/or uncoupled bone remodeling.

Though the processes of cellular signaling involved in bone mechanotransduction have yet to be fully elucidated, it is likely that multiple intersecting pathways are involved (8-11). Amongst these signaling pathways, Wnt/β-catenin signaling has emerged as being highly modulated by loading and unloading (12-15). Intact Wnt/β-catenin signaling, with a minimal threshold of β-catenin expression, is necessary for the bone anabolic response to mechanical loading (16). Moreover, increased activation of the Wnt/β-catenin pathway caused by deficiency in the Wnt antagonist sclerostin augments the bone to dynamic loading. Both sclerostin-deficient (*Sost*$^{-/-}$) mice and C57Bl/6 mice treated with a neutralizing anti-sclerostin antibody show increases in cyclic loading-induced bone formation that are enhanced compared to wild type/untreated mice (17, 18). These data further support the concept that in addition to Wnt/β-catenin other, as yet undefined, signaling pathways regulate mechanotransduction in these models.

Dickkopf WNT Signaling Pathway Inhibitor 1 (dickkopf-1/DKK1) is a soluble protein expressed and secreted within the bone microenvironment (14), and has a modulating role within the bone compartment. Overexpression of *Dkk1* within osteoblasts results in osteopenia in mice (19-21). Heterozygous and homozygous deletion of *Dkk1* results in a dose dependent increase of bone mass, due to an increase in bone formation and no alteration of bone resorption (22-24). Like sclerostin, DKK1 has a role within bone mechanotransduction. In particular, a suppression of both sclerostin and DKK1 expression is seen following an increase in mechanical bone loading within rodent models (14, 15, 25).

It was hypothesized that, as seen with sclerostin deficiency (17, 18), a loss of DKK1 could also augment the anabolic response of bone to increased mechanical loading. Neutralizing antibodies to DKK1 have been developed and such antibodies have been validated to augment bone

anabolism via increasing osteoblast-driven bone mass (26, 27). As with anti-sclerostin antibodies, anti-DKK1 antibodies may have clinical utility in promoting increased bone mass, however the interaction of these bioactive agents with load-based exercise remains ill-defined.

We aimed to investigate the effect of DKK1 deficiency on the anabolic response of bone to increased mechanical loading. This study utilized a unique mouse model of *Dkk1* deficiency where embryonic lethality is prevented by developmental knockdown of *Wnt3* expression. One challenge with analyzing this model is that the high bone mass phenotype considerably affects bone stiffness. There is no gold standard for the biomechanical loading of bones, with groups currently debating whether force-matched or strain-matched controls are more relevant. In this study, two groups of *Dkk1* KO mice were loaded with identical forces or strains and compared versus wild type (WT) and $Wnt3^{+/-}$ controls. Bone volume and formation changes were examined within the mid-diaphysis using a combination of radiographic and dynamic histomorphometry outcome measures. Potential compensatory effects of sclerostin in the absence of DKK1 were assessed by quantitative PCR.

METHODS AND MATERIALS

Dkk1 knockout mice

A *Dkk1*$^{-/-}$:*Wnt3*$^{+/-}$ mouse colony was gifted by Prof. Patrick Tam and was used and maintained on its original mixed 129J×C57Bl/6 background (28). The original cross was generated by breeding *Wnt3*$^{+/-}$ and *Dkk1*$^{+/-}$ strains with a further generation of *Dkk1*$^{+/-}$ backcrossing (29, 30). Wild type (WT; *Dkk1*$^{+/+}$:*Wnt3*$^{+/+}$) and *Wnt3* knockdown (*Wnt3*$^{+/-}$; *Dkk1*$^{+/+}$:*Wnt3*$^{+/-}$) mice were sourced from the *Wnt3*$^{+/-}$ × *Dkk1*$^{+/-}$ cross colony. Animal experiments were approved and performed under the Western Sydney LHD Animal Ethics Committee, protocol 4174.

Animals were bred in house at the Westmead Animal Holdings facility. Mice were given access to rodent chow and water ad libitum, and were housed with littermates with a maximum of 4 mice/cage. Genotyping was performed on DNA from ear punches using DirectPCR (Viagen Biotech, Los Angeles, CA, USA). PCR reactions were performed for the *Dkk1* wild type gene, the *Dkk1 neo* mutant allele and the *Wnt3* allele (29, 30).

For control mice that did not undergo loading protocols, tibiae from N=6-8 female mice of each genotype were collected for radiographic assessment at 12 weeks of age.

Tibial mid-diaphyseal strain gauging

Strain gauging of the mid-diaphysis was performed on the right and left tibiae for all genotypes (4-5 mice/genotype). Strain (bone tissue deformation) levels at the mid-diaphysis was measured in 10 week old female mice as previously described (17, 31, 32). Briefly, mice were anesthetized via isoflourane inhalation and a small incision made in the skin at the anterior tibia, half way down the bone. Muscle and periosteum were scraped away to expose the diaphysis, and the bone was cleaned and dried with a swab of methyl ethyl ketone. A miniature single element strain gauge (EA-06-015LA-120, Vishay Micromeasurements, NC, USA) was attached to the medial mid-diaphysis aligned with the bone's longitudinal axis. The limb was placed into a custom made loading apparatus so that the heel and knee were cupped and held securely. A range of cyclic axial compressive loads (-3N to -13N) were applied using 4Hz haversine waveform. No tibial failures

occurred with this load range. The strain at each load increment was recorded (National Instruments, Labview v8.2). Mice were euthanized following all measurements.

Cyclic tibial loading

Commencing on D1, 10 week old female *Dkk1* KO, WT, and *Wnt3*$^{+/-}$ mice (N=7-8/genotype) underwent unilateral cyclic axial compression of the left tibia, as described by Melville *et al*. (33). Briefly, 1200 cycles were applied daily, 5 days/week for 2 weeks, with rest days on D6, D7, D13, and D14. The loads applied for *Dkk1* KO (-12.0N), WT (-7.0N), and *Wnt3*$^{+/-}$ (-7.0N) mice achieved +1200με on the mid-shaft. A separate group of *Dkk1* KO mice also received -7.0N of load to directly compare force-matched responses between the genotypes. Mice were euthanized at D15 (12 weeks age) for assessment of macroscopic bone parameters, such as bone volume, density, microarchitecture, and dynamic bone histomorphometry. Mice were injected with calcein (10mg/kg, Sigma-Aldrich, MO, USA) at 3 and 10 days before euthanasia. Bones were fixed in 10% formalin for 24hrs (3hr room temperature, then the remainder at 4°C) then stored in 70% ethanol.

Microcomputed tomography

Right and left tibiae were measured *ex vivo* by microcomputed tomography (microCT; Skyscan 1174 2; Skyscan NV, Kontich, Belgium) using 12 μm isotropic voxel resolution, 0.5 mm aluminium filter, 50 kV X-ray tube voltage, 800μA tube electric current, and 4500ms exposure time. Images were reconstructed using a scale of 0-0.1 (NRecon version 1.6.1.7; Skyscan NV) and analyzed using CTAnalyser (Skyscan NV). The minimum threshold for bone was 0.4 g/cm^3, correlated to phantoms of known density. All microCT analysis excluded the fibula. A total of N=5 tibiae were excluded from microCT analysis as images showed poor focus.

A volume of interest (VOI) denoted “7.8 mm VOI” was selected, commencing 0.5mm below the growth plate and finishing 7.8 mm distally, proximal to the tibia-fibula joint (Fig 1A). Consecutive VOIs of height 0.06 mm were assessed along the 7.8 mm VOI and plotted on a histogram to visualize bone volume change following loading (loaded BV-control BV) for all genotypes.

Sub-regional analysis was performed within the diaphysis (Fig 1A). A VOI of height 0.5 mm was assessed commencing 37% down the tibia from the proximal end. This VOI corresponds with other published studies that examine the response to increased load in the tibia (17, 18, 31, 34-36). It also provides regional analysis of bone that received the same strain. A second VOI of the same height but 50% down the tibia was also analyzed to provide additional analysis of the strain-matched region, and results are supplied as supplementary data. Bone parameters assessed included cortical BV, cortical thickness (Ct.Th), tissue mineral density (TMD) and polar moment of inertia (*J*), a geometric predictor of whole bone strength. Representative (median BV) three-dimensional (3D) reconstructions were created using CTAnalyser.

Sub-regional of the metaphysis was also performed. A VOI of height 1.2 mm commencing 0.5 mm below the growth plate was selected to represent the secondary spongiosa (Fig 1A). Within this metaphyseal VOI both cancellous bone and cortical bone were assessed separately and together as a total bone VOI, as seen before (17). Bone parameters assessed within cancellous VOIs were BV, tissue volume (TV), trabecular bone volume/total volume (BV/TV), and tissue mineral density (TMD), as well as microarchitecture parameters of trabecular thickness (Tb.Th), number (Tb.N) and separation (Tb.Sp).

Dynamic bone histomorphometry

The tibiae were transversely cut using a diamond saw at the region of interest (ROI) within the tibial mid-diaphysis: 37% from the proximal end of the tibiae. The cross-sectional surface was smoothed using sand paper with grit designation of P1200 and cleaned in 70% ethanol. Samples were placed with the cross-sectional area of interest facing flat down on a plastic dish in 70% ethanol. The entire cross-sectional area was scanned and imaged using Leica TCS SP5 confocal microscope at 20x magnification (Leica Microsystems, NSW, Australia). The exposure time, z-stack, gain and offset remained consistent for all specimens. The endosteal and periosteal surfaces of each cross-sectional sample were analyzed for daily mineral apposition rate (MAR), mineralizing surface/bone surface (MS/BS) and bone formation rate/bone surface (BFR/BS) using BIOQUANT measure 32 Nova Prime (Nashville, TN, USA). Diaphyseal dynamic bone measures from a transverse tibial ROI 50% down the bone are supplied as supplementary data.

RNA extraction and quantitative reverse-transcription polymerase chain reaction

At 10 weeks age, an additional 23 mice (N=9 WT, N=14 *Dkk1* KO) underwent two days of strain-matched cyclic axial compression of the left tibia under the same conditions as the mice for radiographic/bone formation assessment. WT mice received a force of -7.0N, whilst *Dkk1* KO mice received a force of -12.0N. Euthanasia (cervical dislocation) was 24hrs later on D3. Dissected tibiae were cleaned of soft tissue, proximal and distal ends removed to leave the bone shaft, and flushed of marrow. The bone shaft was homogenized in Trizol using the Polytron PT2100 (Kinematica, Lucerne, Switzerland). Total RNA was isolated using chloroform separation and the miRNeasy Mini Kit (Qiagen, USA). RNA quality and concentration was verified by Nanodrop ND-2000 (Nanodrop Technologies, Delaware, USA). RNA of highest concentration and quality (260/280>1.8) was used for reverse-transcription using Superscript II Reverse Transcriptase (Thermo-Fisher). Duplicate/triplicate RTs were transcribed, along with a negative RT, for each sample.

Gene expression of *Sost* was determined on the Rotorgene Gene-Q (Qiagen) using Immolase DNA Polymerase (Bioline, London, UK), and normalized to *Gapdh*. Primers were designed to be intron-spanning (*Sost* forward: 5' TCC TCC TGA GAA CAA CCA GAC 3'; *Sost* reverse: 5' TGT CAG GAA GCG GGT GTA GTG 3'; *Gapdh* forward: 5' TGG TGA AGG TCG GTG TGA AC 3'; *Gapdh* reverse: 5' ATG GGC TTC CCG TTG ATG AC 3'). Reactions were performed in triplicate for each RT. For each condition, 3-5 animals were analyzed. Relative expression was calculated using the delta-delta Ct method.

Statistical analysis

Statistical analysis of stiffness between mouse genotypes from strain gauge testing was performed using a one-way ANOVA with LSD post-hoc testing. For microCT and dynamic bone formation analyses, the within-subject effect of loading (control, loaded limbs) and the between-subject effect of genotype (wild type, *Wnt3*$^{+/-}$, *Dkk1* KO) as well as the interactions between these terms were assessed using a mixed ANOVA. Sub-analyses between genotype groups was performed

using one way ANOVA and LSD post-hoc analysis. Analysis of contralateral tibiae (control versus loaded within each genotype) was performed using parametric paired samples test with a 95% confidence interval. Data assessed and presented are for load related changes within each genotype, and genotype related changes within loaded or control tibiae. Mean and standard deviation are presented within graphs and tables. Statistical analyses of qPCR analysis was performed on ΔCt values using non-parametric Mann-Whitney U. Mean fold-change and SEM are presented within graphs of qPCR results. For all testing a value of $p<0.05$ was considered significant. All analysis was performed using IBM SPSS Statistics 24 (SPSS Inc., Chicago, IL, USA) and graphed with GraphPad Prism 7 (GraphPad Software, La Jolla, CA, USA).

RESULTS

Bone volume is increased with *Dkk1* deficiency

MicroCT analyses of bone volume in non-loaded *Dkk1* KO mice confirmed an increase in tibial BV at 12 weeks of age compared to non-loaded WT controls (Fig 1B). BV was significantly increased within the proximal metaphysis, with 23-24% more BV in *Dkk1* KO mice compared with WT and *Wnt3*$^{+/-}$ mice ($p<0.01$). A small but significant BV increase was seen in *Dkk1* KO mice compared to *Wnt3*$^{+/-}$ mice, within the VOI located 50% down the tibiae (+9%, $p<0.05$). A similar BV increase was seen above WT mice (+8%), however was not significant ($p=0.06$).

Dkk1 KO bones require greater force to achieve identical bone strain

The relationship between the axial force applied and the strain on the tibial mid-diaphysis was determined for each genotype. The *Dkk1* KO tibiae demonstrated a 1.7-fold increase in stiffness over WT mice, and a 1.8-fold increase over *Wnt3*$^{+/-}$ control mice, under the same compressive cyclic loading force ($p<0.01$, Fig 2). WT and *Wnt3*$^{+/-}$ control tibiae had similar stiffness. These data were used to calculate the load/force required to achieve +1200με strain at the tibial mid-diaphysis for each of the mouse genotypes. Thus subsequent studies included strain-matched (-12N) and force-matched (-7N) *Dkk1* KO groups.

Increased bone volume response to mechanical loading greater in the *Dkk1* KO mouse

Following tibial loading, microCT was used to assess bone volume changes in a 7.8mm VOI running the length of the proximal tibiae. Significant effects were seen for both genotype and loading, along with the interaction of the two (genotype:loading) ($p<0.01$, Fig 3). Sub-analyses confirmed baseline data that *Dkk1* KO mice had greater BV than WT within non-loaded tibiae (8-9%, $p<0.05$). The loading regimen led to significant increases in BV in all genotypes, compared to matching contralateral non-loaded tibiae ($p<0.01$, Fig 3A). The BV increases were however greater in the strain-matched *Dkk1* KO mice (*Dkk1* KO -12N, +30%), than the WT (+8%), *Wnt3*$^{+/-}$ mice (+8%) and the force-matched *Dkk1* KO mice (*Dkk1* KO -7N, +10%). BV of *Dkk1* KO -12N

loaded tibiae was significantly greater than the loaded tibiae from all other groups (WT +32%, *Wnt3*$^{+/-}$ +25%, *Dkk1* KO -7N +19%, $p<0.01$). This data suggests that the BV response to loading was significantly enhanced within the *Dkk1* KO -12N mice. Notably, the BV of the loaded tibiae in the force-matched *Dkk1* KO mice (-7N) was also significantly greater than WT (+10%, $p<0.01$, Fig 3A). There were no differences in BV between WT and *Wnt3*$^{+/-}$ loaded tibiae. BV change due to loading was visualized by histogram along the 7.8mm VOI and indicate that the BV response to load exists along this entire region of the tibiae (Fig 3B).

Sub-regional analysis of microCT scans provided more insight into bone response within the mid-diaphysis, which was the zone of known strain (Fig 4). A VOI commencing 37% down from the proximal end of the tibiae was assessed. Significant effects within BV ($p<0.00001$), Ct.Th ($p<0.001$) and polar moment of inertia ($p<0.05$) were seen for both genotype and loading, along with the interaction of the two (genotype:loading) (Fig 4). Sub-analyses showed that all genotypes responded to load with increased BV in their loaded tibiae compared to their contralateral tibiae (WT +7%, $p<0.01$, *Wnt3*$^{+/-}$ +9%, $p<0.05$, *Dkk1* KO -12N +36%, $p<0.01$, *Dkk1* KO -7N +8%, $p<0.01$, Fig 4A). An enhanced loading response was seen within the strain-matched *Dkk1* KO (-12N) mice with significant increases over the loaded tibiae of all other groups ($p<0.01$). Increases were seen in BV (WT +35%, *Wnt3*$^{+/-}$ +28%, *Dkk1* KO -7N +32%), Ct.Th (WT +25%, *Wnt3*$^{+/-}$ +23%, *Dkk1* KO -7N +23%), and polar moment of inertia (WT +49%, *Wnt3*$^{+/-}$ +35%, *Dkk1* KO -7N +43%) for the *Dkk1* KO -12N mice. Similar results were seen in the additional mid-diaphyseal VOI assessed, 50% down the tibiae (Supplementary Fig 1).

The tibial proximal metaphysis was also assessed by microCT (Table 1). An effect of loading was seen for total metaphyseal TV, BV and TMD ($p<0.01$). The effect of genotype, and also the interaction of genotype:loading was also seen for metaphyseal BV ($p<0.01$). Sub-analyses showed that BV was increased with loading above contralateral non-loaded controls for all groups, and this effect was more enhanced within the strain-matched *Dkk1* KO mice (WT +11%, *Wnt3*$^{+/-}$ +11%, *Dkk1* KO -12N +33%, *Dkk1* KO -7N +18%, $p<0.01$). Overall, BV within the loaded tibiae was significantly greater for the strain-matched *Dkk1* KO (-12N) mice than all other loaded tibiae ($p<0.01$). Notably BV was also significantly greater in the loaded tibiae of force-matched *Dkk1* KO (-7N) mice compared to WT and *Wnt3*$^{+/-}$ loaded tibiae ($p<0.01$).

Break-down of the metaphysis into cortical and cancellous bone compartments found significant effects in genotype, loading, and the interaction of genotype:loading within cortical BV and thickness, and cancellous BV/TV and trabecular thickness ($p<0.05$, Table 1). This suggests that the response to loading was dependent on the group.

Sub-analyses showed that loading increased cortical BV and Ct.Th within all groups (BV: WT +11%, *Wnt3*$^{+/-}$ +10%, *Dkk1* KO -12N +32%, *Dkk1* KO -7N +19%, $p<0.01$; Ct.Th: WT +7% $p<0.05$, *Wnt3*$^{+/-}$ +10% $p<0.05$, *Dkk1* KO -12N +27% $p<0.01$, *Dkk1* KO -7N +13% $p<0.01$). Both strain-matched and force-matched loading of *Dkk1* KO tibiae resulted in significant increases in cortical BV over WT and *Wnt3*$^{+/-}$ loaded tibiae (*Dkk1* KO -12N vs WT and *Wnt3*$^{+/-}$ $p<0.01$; *Dkk1* KO -7N, vs WT $p<0.01$, vs *Wnt3*$^{+/-}$ $p<0.05$). However, the strain-matched loading of *Dkk1* mice elicited a greater BV response than force-matched ($p<0.01$). The cancellous bone saw less marked changes between contralateral tibiae following loading (*Dkk1* KO -12N: BV/TV and Tb.Th, $p<0.05$; *Wnt3*$^{+/-}$: BV and Tb.N, $p<0.05$).

Bone formation is augmented following mechanical tibial loading in the *Dkk1* KO mouse

Dynamic histomorphometry of non-loaded contralateral control tibiae showed that periosteal and endosteal bone formation in the mid-diaphysis (37% cortical ROI) of *Dkk1* KO (-7N and -12N) mice approached that of WT and *Wnt3*$^{+/-}$ mice by 12 weeks of age (Fig 5A-B).

Significant effects were seen for genotype, genotype:loading, and loading for periosteal MAR and BFR/BS ($p<0.01$). The effect of loading was significant for periosteal MS/BS. Sub-analyses showed that following tibial loading periosteal MAR was significantly increased over contralateral control in *Wnt3*$^{+/-}$ (+334%, $p<0.05$), *Dkk1* KO -12N (+330%, $p<0.01$) and *Dkk1* KO -7N mice (229%, $p<0.01$) (Fig 5A). Periosteal MS/BS was also significantly increased in *Wnt3*$^{+/-}$ (+68%, $p<0.05$), *Dkk1* KO -12N (+72%, $p<0.01$) loaded tibiae over control tibiae. This resulted in large increases in periosteal BFR/BS for *Wnt3*$^{+/-}$ (+439%, $p<0.05$), *Dkk1* KO -12N (+398%, $p<0.01$), and *Dkk1* KO -7N (453%, $p<0.01$) loaded tibiae compared to contralateral control tibiae.

Strain-matched loading of *Dkk1* KO mice (-12N) demonstrated increased periosteal bone formation above the loaded tibiae of all other groups (Fig 5A). Significant increases in *Dkk1* KO -12N loaded tibiae periosteal MAR (WT +166%, *Wnt3*$^{+/-}$ +95%, *Dkk1* KO -7N +131%) and

BFR/BS (WT +167%, *Wnt3*$^{+/-}$ +102%, *Dkk1* KO -7N +93%) were seen ($p<0.01$). WT, *Wnt3*$^{+/-}$ and *Dkk1* KO -7N loaded tibiae all had similar periosteal bone formation parameters.

Less marked responses were seen on the endosteal surface of the mid-diaphysis, however significant effects were seen with genotype:loading and loading for endosteal MAR and BFR/BS ($p<0.05$). Sub-analyses showed that significant increases in endosteal MAR and BFR/BS were seen for both the force-matched (MAR: +58%; BFR/BS: +77%, $p<0.05$) and strain-matched (MAR: +85%; BFR/BS: +82%, $p<0.01$) *Dkk1* KO mice, compared to their contralateral control tibiae (Fig 5B). MAR and BFR/BS were not altered with loading in the WT and *Wnt3*$^{+/-}$ mice. Between genotype comparisons showed that strain-matched loading of *Dkk1* KO mice resulted in significantly greater endosteal MAR above the loaded tibiae of the other groups (WT +34%, $p<0.05$; *Wnt3*$^{+/-}$ +55%, $p<0.01$; *Dkk1* KO -7N +40%, $p<0.05$). Similar periosteal and endosteal bone formation changes were seen within the second mid-diaphyseal ROI, assessed 50% down the tibiae (Supplementary Fig 2).

Sost expression is not altered within *Dkk1* KO mice, however decreases with loading

The expression of *Sost* within the mid-shaft of *Dkk1* KO non-loaded tibiae mice was not significantly altered compared to WT non-loaded tibiae (Fig 6A). The expression of *Sost* was also similar within the strain-matched loaded tibiae of both *Dkk1* KO and WT mice. Notably, *Sost* expression was similarly decreased with loading in both WT (0.55 fold-change, $p<0.01$) and *Dkk1* KO mice (0.68 fold-change, $p<0.01$, Fig 6B).

DISCUSSION

This study investigated the response of a *Dkk1* KO mouse line to cyclic compressive tibial loading. As hypothesized, the deficiency of DKK1 protein in these mice did not impair the anabolic response of bone to load, but rather augmented this response. All mice showed increased bone formation and bone volume as a result of the cyclic compressive loading protocol of the tibiae. The cortical bone volume response correlated with an increased periosteal bone formation response. These responses showed the greatest effect size within the *Dkk1* KO mice matched for strain in the cyclic loading protocol. This was the case for the BV response in all of VOIs measured. A variety of regions were measured due to a lack of standardization for regional analysis in the biomechanical testing field.

Non-loaded tibiae of *Dkk1* KO mice had greater bone volume compared to non-loaded tibiae of WT and *Wnt3*$^{+/-}$ control mice, which has been previously reported (24). Not only did WT and *Wnt3*$^{+/-}$ mice show comparable bone mass, *Wnt3*$^{+/-}$ mice also responded to loading similarly to WT. This was as anticipated as *Wnt3*$^{+/-}$ mice exhibit no independent bone phenotype, nor has *Wnt3* found to be expressed within the bone compartment (24, 37). Critically, this study showed that complete deletion of DKK1 does not result in maximal bone anabolism, as bone formation and bone volume were augmented with increased mechanical loading. Thus while *Dkk1* expression can be regulated by load (14, 25), these data confirm that DKK1 is not essential for transducing the response to cyclic loading.

Previous work investigating dynamic loading in animal models show that periosteal bone formation response is proportional to the local surface strain (38-40). With our *Dkk1* KO mouse model it was therefore necessary to undertake a strain-matched loading regimen to directly compare the loading-induced bone response to wild type controls. An enhanced bone response within the *Dkk1* KO mice was seen within the local region of equal strain with dynamic loading. Though these data support further clinical research into combining load-based exercise alongside anabolic drugs that enhance Wnt/β-catenin signaling, we must be mindful that such exercise would not easily control for the strain engendered upon the bone. However, our study included a force-matched loaded *Dkk1* KO mouse group, which provides additional insight. The force-matched *Dkk1* KO mice displayed analogous responses to wild type mice within the mid-diaphyseal cortical bone, a region we know would have received a lower strain within the force-matched *Dkk1* KO

mice. Further, the metaphyseal total bone volume response was greater in the force-matched *Dkk1* KO mice than wild type.

This study is consistent with our prior findings that increased Wnt/β-catenin signaling (instigated by decreased sclerostin activity) augments the bone response to mechanical loading (17, 18). One favored scenario was that sclerostin and DKK1 could compensate for each other within the bone compartment in such situations of deficiency (17). *Dkk1* has previously been shown to be elevated with sclerostin deficiency (41-43), however the converse remained untested. Sclerostin itself is sensitive to load, and is down-regulated under conditions of increased loading (14, 25). In this study, *Dkk1* KO tibiae showed no compensatory up-regulation of sclerostin expression, contrary to our initial hypothesis.

Despite similar functions as Wnt antagonists, DKK1 may have a less important role than sclerostin in regulating bone mass. The limited anabolic effect of monoclonal antibodies to DKK1 within adult rodents has been suggested to potentially result from a reduction in DKK1 expression within adult bone (44, 45). Therefore, ubiquitous deficiency in DKK1 may not induce the same compensatory feedback within adult bone as seen with sclerostin deficiency. *Sost* expression was similarly decreased with loading in both wild type and *Dkk1* KO mice, further suggesting that the augmented anabolic response to loading in the *Dkk1* KO mouse could not be directly attributable to *Sost* down-regulation.

It is likely that mechanotransduction within bone involves multiple signaling pathways intersecting with the Wnt/β-catenin pathway (8-11). As an anabolic bone response following mechanical loading requires intact Wnt/β-catenin signaling and a minimum threshold of β-catenin (15, 16, 46), the augmented loading response seen with DKK1 deficiency may result from heightened Wnt/β-catenin signaling potentiated by intersecting pathways and signal transducers. Further gene expression exploration following loading stimulation may help to elucidate the mechanism of action behind the heightened anabolic response to loading in DKK1 deficient mice.

In conclusion, this study provides novel information about mechanotransduction in bone. The anabolic bone response to dynamic tibial loading was augmented within mice lacking DKK1 expression. Though the exact mechanisms for sensing and transducing mechanotransduction signals have yet to be fully elucidated, these data support the paradigm that pharmacotherapy

targeting Wnt/β-catenin signaling may be useful in conjunction with load-bearing exercise. This remains an unexplored avenue for future clinical research investigating exercise alongside the use of neutralizing antibodies to DKK1 or sclerostin, and may have specific benefits in the management of osteoporosis.

FIGURES

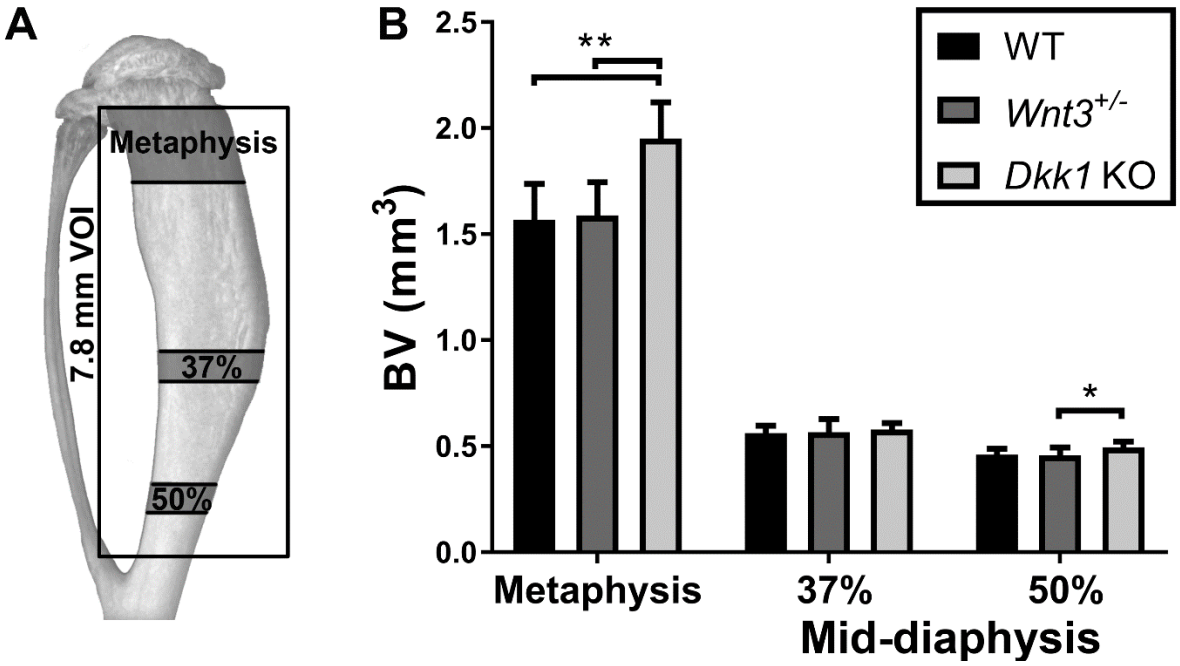

Figure 1: (A) Volume of interests (VOIs) measured by microCT. Metaphysis: a 1.2mm height VOI commencing 0.5mm below the growth plate. 37%: mid-diaphyseal 0.5mm height VOI commencing 37% down the tibiae. 50%: mid-diaphyseal 0.5mm height VOI commencing 50% down the tibiae. 7.8mm VOI: commencing 0.5mm below the growth plate and of height 7.8mm. All microCT analysis excluded the fibula. **(B)** Bone volume (BV) by microCT of female wild type (WT), *Wnt3*$^{+/-}$ and *Dkk1* KO mice aged 12 weeks, which did not undergo any loading regimen. Metaphyseal and mid-diaphyseal, 37% and 50%, VOIs were assessed. * $p<0.05$, ** $p<0.01$.

A

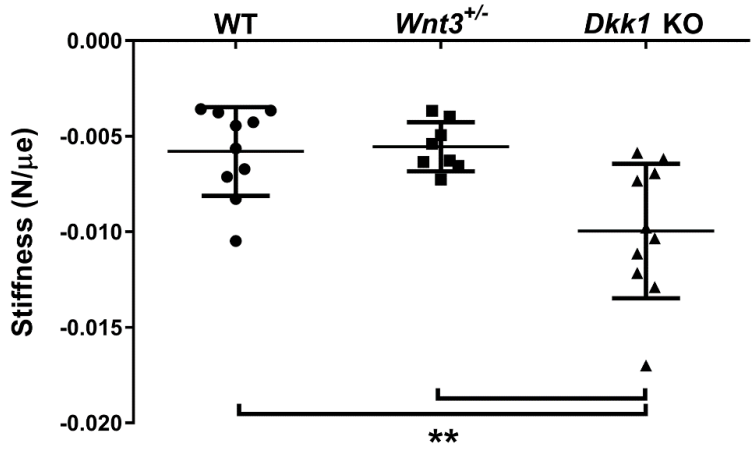

B

	N	Stiffness		Desired strain	Required Load (N)
		Mean	SD		
WT	5	-5.79E-03	1.82E-03	1200	-6.95
***Wnt3*$^{+/-}$**	4	-5.55E-03	1.28E-03	1200	-6.66
***Dkk1* KO**	5	-9.96E-03	3.30E-03	1200	-11.95

Figure 2: (A) *In vivo* strain measurements were performed on the medial mid-diaphysis of right and left tibiae of 10 week old female wild type (WT), *Wnt3*$^{+/-}$ and *Dkk1* KO mice (N=4-5 mice/genotype). Bars represent means ± SD stiffness. ** $p<0.01$. **(B)** The relationship between the axial force applied and the strain on the tibial mid-diaphysis was determined for each genotype. This was used to calculate the load required to achieve +1200με at the tibial mid-diaphysis each genotype, as shown.

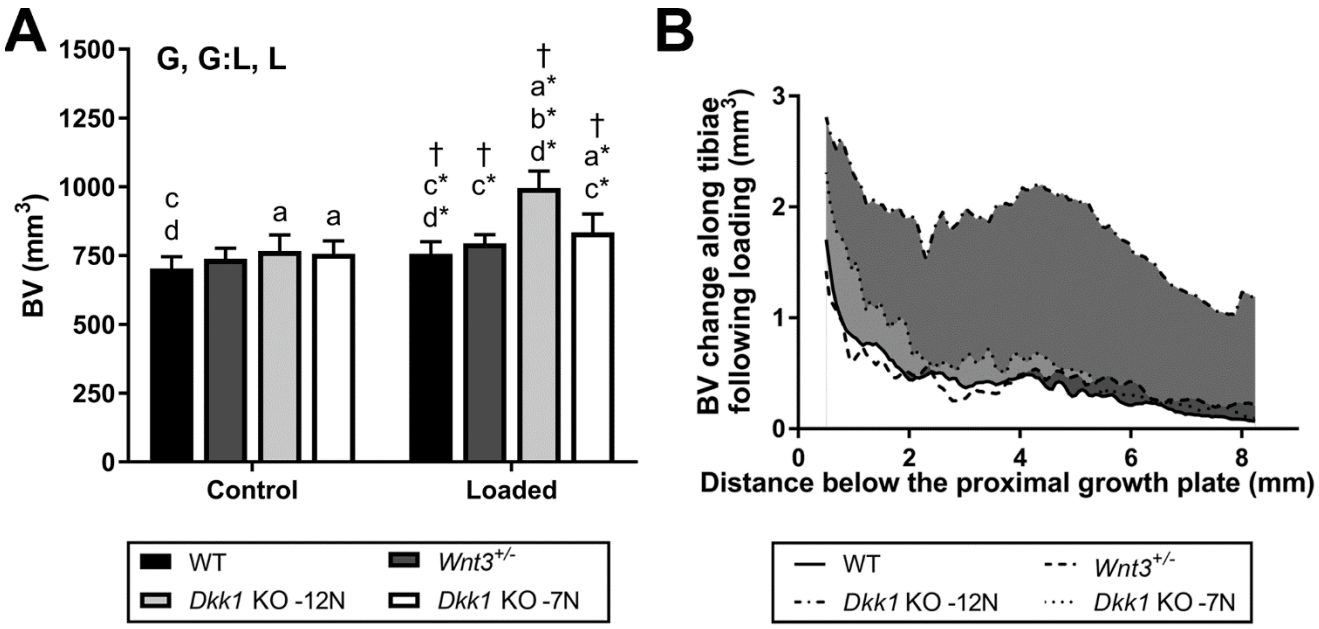

Figure 3: (A) Bone volume (BV) of control and loaded tibiae within the 7.8mm height VOI assessed by microCT. Groups assessed included wild type (WT), *Wnt3*$^{+/-}$, *Dkk1* KO -12N and *Dkk1* KO -7N. Mixed ANOVA: indicates an effect of (G) genotype, (G:L) genotype:loading, (L) loading, $p<0.00001$. Sub-analyses: † = $p<0.01$ loaded tibiae significant compared to contralateral control tibiae. a = $p<0.05$ compared to WT; b = $p<0.05$ compared to *Wnt3*$^{+/-}$; c = $p<0.05$ compared to *Dkk1* KO -12N; d = $p<0.05$ compared to *Dkk1* KO -7N; within loaded or control tibiae. * indicates stronger significance of $p<0.01$ for between genotype comparisons. **(B)** BV change with loading along the tibiae, assessed by microCT. The increase in BV for each loaded tibia was determined from their own contralateral control tibia and the mean change plotted for all groups: WT, *Wnt3*$^{+/-}$, *Dkk1* KO -12N and *Dkk1* KO -7N.

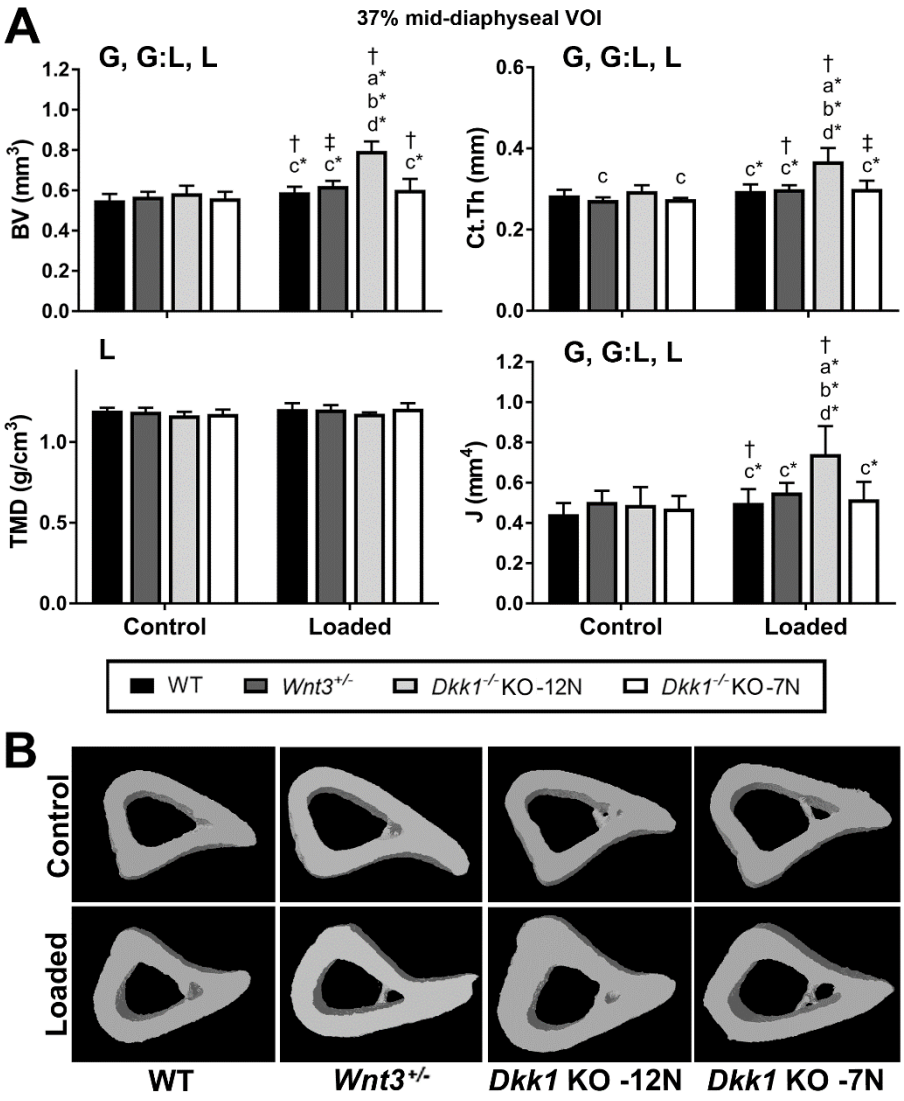

Figure 4: MicroCT assessment of the mid-diaphyseal VOI located 37% down the bone from the proximal end, for both control and loaded tibiae of all groups: wild type (WT), *Wnt3*$^{+/-}$, *Dkk1* KO -12N, *Dkk1* KO -7N. **(A)** Bone volume (BV), cortical thickness (Ct.Th), tissue mineral density (TMD) and polar moment of inertia (J) were assessed for each tibiae. Mixed ANOVA: indicates an effect of (G) genotype, (G:L) genotype:loading, (L) loading, $p<0.05$. Sub-analyses: † = $p<0.01$, ǂ = $p<0.05$ loaded tibiae significant compared to contralateral control tibiae. a = $p<0.05$ compared to WT; b = $p<0.05$ compared to *Wnt3*$^{+/-}$; c = $p<0.05$ compared to *Dkk1* KO -12N; d = $p<0.05$ compared to *Dkk1* KO -7N; within loaded or control tibiae. * indicates stronger significance of $p<0.01$ for between genotype comparisons. **(B)** 3D models of the median BV within the mid-diaphyseal 37% VOI for all groups.

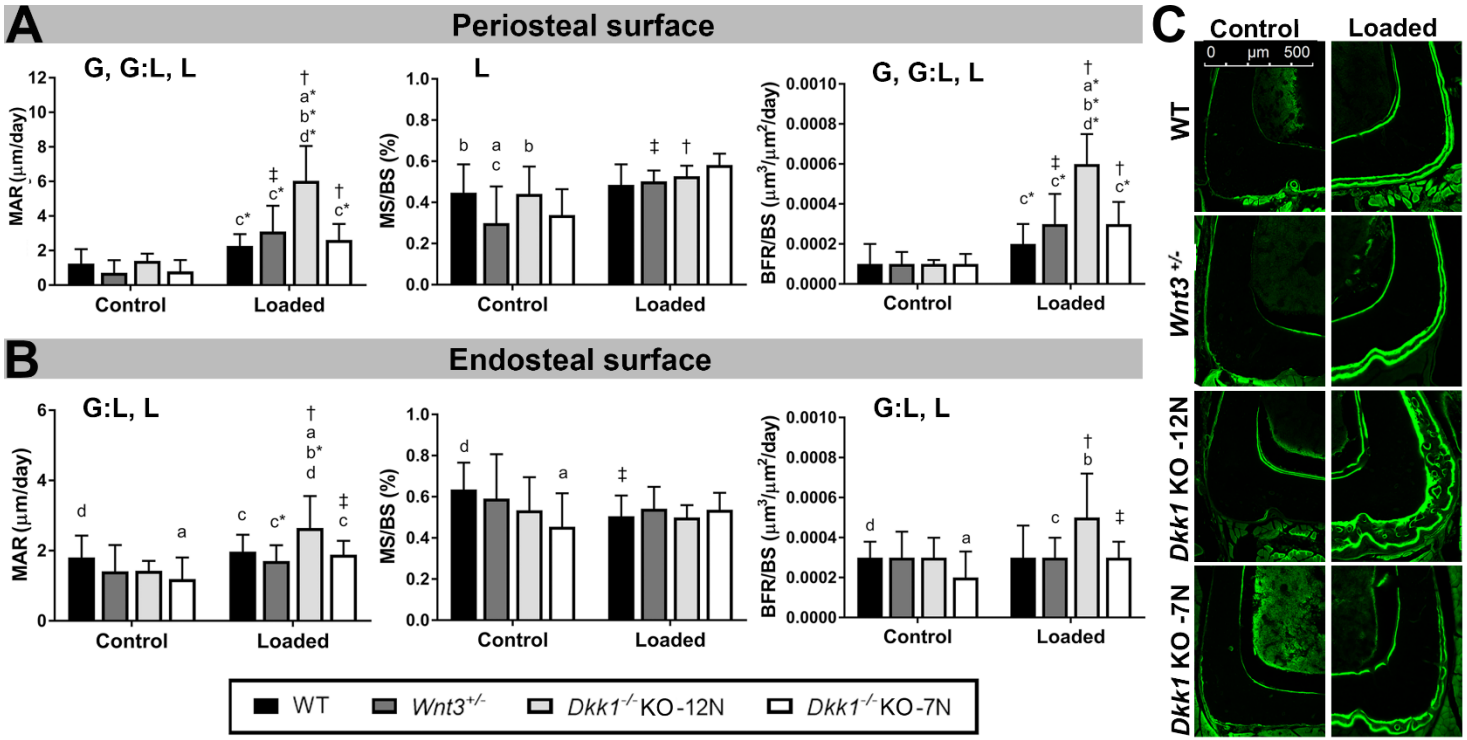

Figure 5: Dynamic histomorphometry of bone formation within the mid-diaphyseal VOI located 37% down the bone from the proximal end, for control and loaded tibiae of all genotypes: wild type (WT), *Wnt3*$^{+/-}$, *Dkk1* KO -12N, *Dkk1* KO -7N. **(A)** Analysis of the periosteal surface: mineral apposition rate (MAR/day), mineralizing surface/bone surface (MS/BS), bone formation rate/bone surface (BFR/BS). **(B)** Analysis of the endosteal surface: MAR/day, MS/BS, BFR/BS. Mixed ANOVA: indicates an effect of (G) genotype, (G:L) genotype:loading, (L) loading, $p<0.05$. Sub-analyses: † = $p<0.01$, ǂ = $p<0.05$ loaded tibiae significant compared to contralateral control tibiae. a = $p<0.05$ compared to WT; b = $p<0.05$ compared to *Wnt3*$^{+/-}$; c = $p<0.05$ compared to *Dkk1* KO -12N; d = $p<0.05$ compared to *Dkk1* KO -7N; within loaded or control tibiae. * indicates stronger significance of $p<0.01$ for between genotype comparisons. **(C)** Representative images of median MAR within the mid-diaphyseal 37% VOI for all groups.

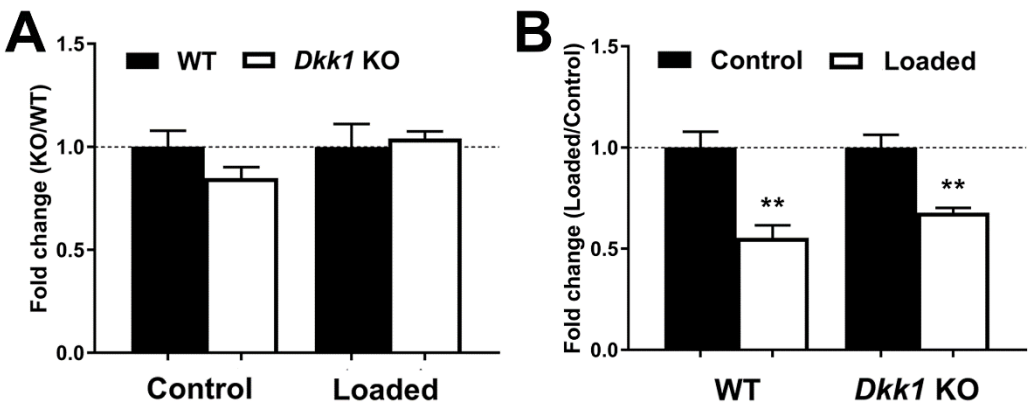

Figure 6: Gene expression of *Sost* measured at D3, 24 hrs following the second of two daily loading sessions. Control and loaded mid-shaft tibiae were assessed within wild type (WT) and strain-matched *Dkk1* KO (-12N) mice. (A) Fold-change of *Dkk1* KO mice normalized to WT, within control or loaded tibiae. (B) Fold-change of loaded tibiae normalized to control tibiae, within WT or *Dkk1* KO mice. Mean + SEM shown. ** = $p<0.01$.

TABLES

Table 1: MicroCT assessment of the tibial proximal metaphysis.

			WT		*Wnt3* $^{+/-}$		*Dkk1* KO -12N		*Dkk1* KO -7N	
VOI	Parameters	Effect	Control	Loaded	Control	Loaded	Control	Loaded	Control	Loaded
Cancellous	TV (mm^3)		1.18 ± 0.28	1.26 ± 0.29	1.30 ± 0.22	1.25 ± 0.16	1.34 ± 0.29	1.41 ± 0.30	1.41 ± 0.08	1.42 ± 0.12
	BV (mm^3)	G, L	0.05 ± 0.04 c* d*	0.05 ± 0.04 c* d*	0.12 ± 0.04 c d*	0.14 ± 0.06 † c* d*	0.24 ± 0.10 a* b	0.34 ± 0.11 a* b*	0.29 ± 0.11 a* b*	0.32 ± 0.11 a* b*
	BV/TV (%)	G, G:L, L	3.65 ± 2.16 c* d*	4.08 ± 1.96 b c* d*	9.02 ± 1.81 c* d*	10.92 ± 4.32 a c* d*	17.54 ± 5.08 a* b*	23.82 ± 5.53 † a* b*	20.46 ± 7.79 a* b*	22.36 ± 6.96 a* b*
	Tb.Th (mm)	G, G:L, L	0.07 ± 0.01 c* d*	0.08 ± 0.01 b* c* d*	0.08 ± 0.00	0.09 ± 0.01 a* c*	0.09 ± 0.01 a*	0.11 ± 0.01 †* a* b* d*	0.09 ± 0.01 a*	0.09 ± 0.01 a* c*
	Tb.Sp (mm)	G	0.61 ± 0.06 b* c* d*	0.65 ± 0.04 b* c* d*	0.51 ± 0.04 a* c* d*	0.50 ± 0.08 a* c* d*	0.32 ± 0.06 a* b*	0.30 ± 0.09 a* b*	0.24 ± 0.07 a* b* c	0.25 ± 0.07 a* b*
	Tb.N (mm^{-1})	G	0.48 ± 0.22 b c* d*	0.51 ± 0.20 b c* d*	1.12 ± 0.19 a c* d*	1.18 ± 0.38 † a c* d*	2.00 ± 0.47 a* b*	2.21 ± 0.51 a* b*	2.32 ± 0.74 a* b*	2.38 ± 0.66 a* b*
	TMD (g/cm^3)		0.65 ± 0.05	0.65 ± 0.04 c*	0.65 ± 0.02	0.66 ± 0.04 c	0.64 ± 0.03	0.71 ± 0.03 † a* b d*	0.63 ± 0.03	0.64 ± 0.03 c*
Cortical	BV (mm)	G, G:L, L	1.43 ± 0.11	1.58 ± 0.13 †* c* d*	1.50 ± 0.10	1.65 ± 0.07 †* c* d	1.52 ± 0.08	2.01 ± 0.05 †* a* b* d*	1.50 ± 0.06	1.79 ± 0.12 †* a* b c*
	Ct.Th (mm)	G, G:L, L	0.24 ± 0.01	0.25 ± 0.02 † c* d*	0.24 ± 0.01	0.26 ± 0.01 † c*	0.24 ± 0.01	0.31 ± 0.03 †* a* b* d*	0.24 ± 0.01	0.27 ± 0.01 †* a* c*
	TMD (g/cm^3)	G, L	1.08 ± 0.03 d*	1.11 ± 0.04	1.09 ± 0.01 d	1.10 ± 0.02	1.10 ± 0.03	1.11 ± 0.04 d	1.13 ± 0.03 a* b	1.16 ± 0.02 a* b* c
All Bone	TV (mm^3)	L	2.82 ± 0.39	3.09 ± 0.46 †* c	2.99 ± 0.32	3.09 ± 0.21 †* c	3.01 ± 0.36	3.57 ± 0.34 †* a b	3.08 ± 0.14	3.41 ± 0.23 †*
	BV (mm^3)	G, G:L, L	1.48 ± 0.15 c* d*	1.64 ± 0.16 †* c* d*	1.62 ± 0.13 d	1.79 ± 0.13 †* c* d*	1.76 ± 0.15 a	2.35 ± 0.13 †* a* b* d*	1.79 ± 0.15 a* b	2.11 ± 0.21 †* a* b* c*
	TMD (g/cm^3)	L	1.07 ± 0.03	1.09 ± 0.04 c	1.06 ± 0.01	1.07 ± 0.02	1.04 ± 0.04	1.05 ± 0.04 a	1.05 ± 0.02	1.08 ± 0.03
n			7	7	6	6	7	5	8	8

MicroCT assessment of the proximal tibial metaphysis for both control and loaded tibiae of all groups: wild type (WT), *Wnt3* $^{+/-}$, *Dkk1* KO -12N, *Dkk1* KO -7N. Cancellous and cortical compartments of the metaphysis was assessed separately, along with these compartments combined (All Bone). Mean ± SD are shown. Mixed ANOVA: indicates an effect of (G) genotype, (G:L) genotype:loading, (L) loading, $p<0.05$. Sub-analyses: † = $p<0.05$ compared to contralateral tibia of the same genotype, a = $p<0.05$ compared to WT tibiae that underwent same control/loaded treatment, b = $p<0.05$ compared to *Wnt3* $^{+/-}$ tibiae that underwent same control/loaded treatment, c = $p<0.05$ compared to *Dkk1* KO -12N tibiae that underwent same control/loaded treatment, d = $p<0.05$ compared to *Dkk1* KO -7N tibiae that underwent same control/loaded treatment. * indicates stronger significance of $p<0.01$ for the above sub-analyses.

SUPPLEMENTARY FIGURES

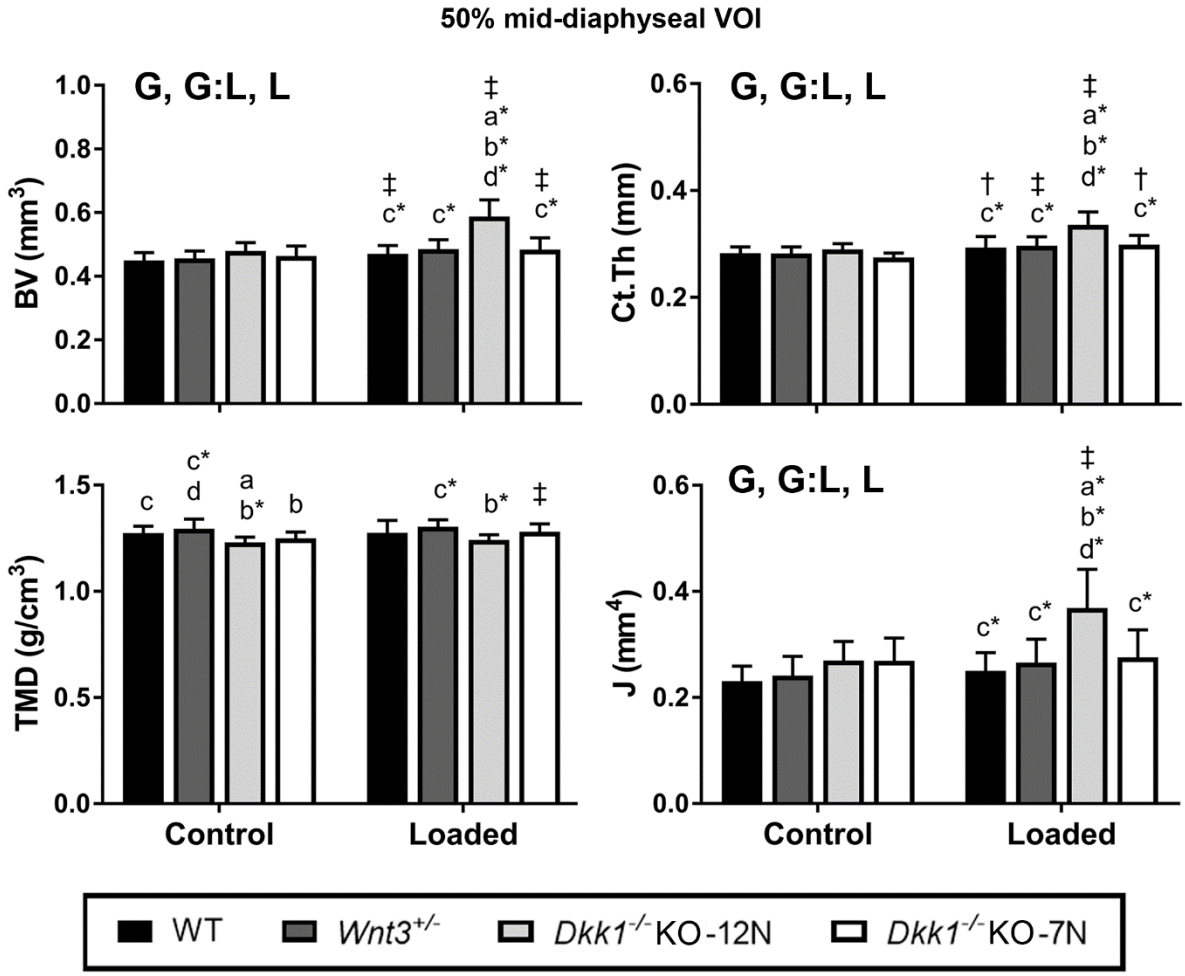

Supplementary Figure 1: MicroCT assessment of the mid-diaphyseal VOI located 50% down the bone from the proximal end, for both control and loaded tibiae of all groups: wild type (WT), *Wnt3*$^{+/-}$, *Dkk1* KO -12N, *Dkk1* KO -7N. Bone volume (BV), cortical thickness (Ct.Th), tissue mineral density (TMD) and polar moment of inertia (J) were assessed for each tibiae. Mixed ANOVA: indicates an effect of (G) genotype, (G:L) genotype:loading, (L) loading, $p<0.05$. Sub-analyses: † = $p<0.01$, ǂ = $p<0.05$ loaded tibiae significant compared to contralateral control tibiae. a = $p<0.05$ compared to WT; b = $p<0.05$ compared to *Wnt3*$^{+/-}$; c = $p<0.05$ compared to *Dkk1* KO -12N; d = $p<0.05$ compared to *Dkk1* KO -7N; within loaded or control tibiae. * indicates stronger significance of $p<0.01$ for between genotype comparisons.

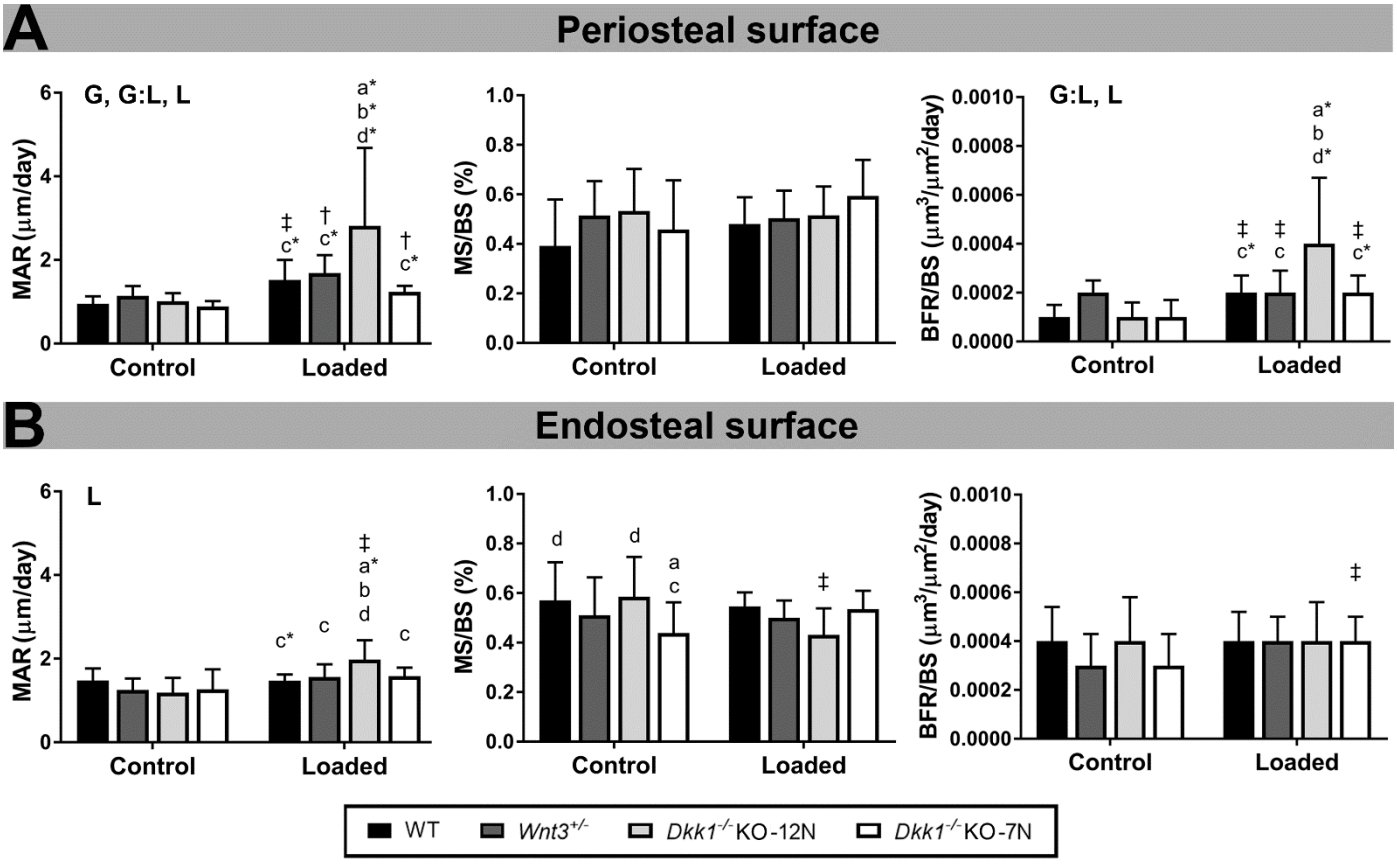

Supplementary Figure 2: Dynamic histomorphometry of bone formation within the mid-diaphyseal VOI located 50% down the bone from the proximal end, for control and loaded tibiae of all genotypes: wild type (WT), *Wnt3*$^{+/-}$, *Dkk1* KO -12N, *Dkk1* KO -7N. **(A)** Analysis of the periosteal surface: mineral apposition rate (MAR/day), mineralizing surface/bone surface (MS/BS), bone formation rate/bone surface (BFR/BS). **(B)** Analysis of the endosteal surface: MAR/day, MS/BS, BFR/BS. Mixed ANOVA: indicates an effect of (G) genotype, (G:L) genotype:loading, (L) loading, $p<0.05$. Sub-analyses: † = $p<0.01$, ǂ = $p<0.05$ loaded tibiae significant compared to contralateral control tibiae. a = $p<0.05$ compared to WT; b = $p<0.05$ compared to *Wnt3*$^{+/-}$; c = $p<0.05$ compared to *Dkk1* KO -12N; d = $p<0.05$ compared to *Dkk1* KO -7N; within loaded or control tibiae. * indicates stronger significance of $p<0.01$ for between genotype comparisons.

REFERENCES

1. Frost HM. Bone "mass" and the "mechanostat": a proposal. The Anatomical record. 1987;219(1):1-9.

2. Collet P, Uebelhart D, Vico L, Moro L, Hartmann D, Roth M, et al. Effects of 1- and 6-month spaceflight on bone mass and biochemistry in two humans. Bone. 1997;20(6):547-51.

3. Uhthoff HK, Jaworski ZF. Bone loss in response to long-term immobilisation. The Journal of bone and joint surgery British volume. 1978;60-b(3):420-9.

4. Skerry TM, Lanyon LE. Interruption of disuse by short duration walking exercise does not prevent bone loss in the sheep calcaneus. Bone. 1995;16(2):269-74.

5. Kontulainen S, Sievanen H, Kannus P, Pasanen M, Vuori I. Effect of long-term impact-loading on mass, size, and estimated strength of humerus and radius of female racquet-sports players: a peripheral quantitative computed tomography study between young and old starters and controls. J Bone Miner Res. 2003;18(2):352-9.

6. De Souza RL, Matsuura M, Eckstein F, Rawlinson SC, Lanyon LE, Pitsillides AA. Non-invasive axial loading of mouse tibiae increases cortical bone formation and modifies trabecular organization: a new model to study cortical and cancellous compartments in a single loaded element. Bone. 2005;37(6):810-8.

7. Duncan RL, Turner CH. Mechanotransduction and the functional response of bone to mechanical strain. Calcif Tissue Int. 1995;57(5):344-58.

8. Papachroni KK, Karatzas DN, Papavassiliou KA, Basdra EK, Papavassiliou AG. Mechanotransduction in osteoblast regulation and bone disease. Trends in molecular medicine. 2009;15(5):208-16.

9. Thompson WR, Rubin CT, Rubin J. Mechanical regulation of signaling pathways in bone. Gene. 2012;503(2):179-93.

10. Liedert A, Kaspar D, Augat P, Ignatius A, Claes L. Mechanobiology of Bone Tissue and Bone Cells. In: Kamkin A, Kiseleva I, editors. Mechanosensitivity in Cells and Tissues. Moscow: Academia, Academia Publishing House Ltd.; 2005.

11. Yavropoulou MP, Yovos JG. The molecular basis of bone mechanotransduction. J Musculoskelet Neuronal Interact. 2016;16(3):221-36.

12. Sunters A, Armstrong VJ, Zaman G, Kypta RM, Kawano Y, Lanyon LE, et al. Mechano-transduction in osteoblastic cells involves strain-regulated estrogen receptor alpha-mediated control of insulin-like growth factor (IGF) I receptor sensitivity to Ambient IGF, leading to phosphatidylinositol 3-kinase/AKT-dependent Wnt/LRP5 receptor-independent activation of beta-catenin signaling. J Biol Chem. 2010;285(12):8743-58.

13. Santos A, Bakker AD, Zandieh-Doulabi B, de Blieck-Hogervorst JM, Klein-Nulend J. Early activation of the beta-catenin pathway in osteocytes is mediated by nitric oxide, phosphatidyl inositol-3 kinase/Akt, and focal adhesion kinase. Biochem Biophys Res Commun. 2010;391(1):364-9.

14. Robling AG, Niziolek PJ, Baldridge LA, Condon KW, Allen MR, Alam I, et al. Mechanical stimulation of bone in vivo reduces osteocyte expression of Sost/sclerostin. J Biol Chem. 2008;283(9):5866-75.

15. Tu X, Rhee Y, Condon KW, Bivi N, Allen MR, Dwyer D, et al. Sost downregulation and local Wnt signaling are required for the osteogenic response to mechanical loading. Bone. 2012;50(1):209-17.

16. Javaheri B, Stern AR, Lara N, Dallas M, Zhao H, Liu Y, et al. Deletion of a single beta-catenin allele in osteocytes abolishes the bone anabolic response to loading. J Bone Miner Res. 2014;29(3):705-15.

17. Morse A, McDonald MM, Kelly NH, Melville KM, Schindeler A, Kramer I, et al. Mechanical load increases in bone formation via a sclerostin-independent pathway. J Bone Miner Res. 2014;29(11):2456-67.

18. Morse A, Schindeler A, McDonald MM, Kneissel M, Kramer I, Little DG. Sclerostin antibody augments the anabolic bone formation response in a mouse model of mechanical tibial loading. J Bone Miner Res. 2017. [Epub ahead of print].

19. Li J, Sarosi I, Cattley RC, Pretorius J, Asuncion F, Grisanti M, et al. Dkk1-mediated inhibition of Wnt signaling in bone results in osteopenia. Bone. 2006;39(4):754-66.

20. Guo J, Liu M, Yang D, Bouxsein ML, Saito H, Galvin RJ, et al. Suppression of Wnt signaling by Dkk1 attenuates PTH-mediated stromal cell response and new bone formation. Cell Metab. 2010;11(2):161-71.

21. Yao GQ, Wu JJ, Troiano N, Insogna K. Targeted overexpression of Dkk1 in osteoblasts reduces bone mass but does not impair the anabolic response to intermittent PTH treatment in mice. Journal of bone and mineral metabolism. 2011;29(2):141-8.

22. Morvan F, Boulukos K, Clement-Lacroix P, Roman Roman S, Suc-Royer I, Vayssiere B, et al. Deletion of a single allele of the Dkk1 gene leads to an increase in bone formation and bone mass. J Bone Miner Res. 2006;21(6):934-45.

23. MacDonald BT, Joiner DM, Oyserman SM, Sharma P, Goldstein SA, He X, et al. Bone mass is inversely proportional to Dkk1 levels in mice. Bone. 2007;41(3):331-9.

24. McDonald MM, Morse A, Schindeler A, Mikulec K, Peacock L, Cheng T, et al. Homozygous Dkk1 Knockout Mice Exhibit High Bone Mass Phenotype Due to Increased Bone Formation. Calcif Tissue Int. 2017. [Epub ahead of print].

25. Holguin N, Brodt MD, Silva MJ. Activation of Wnt Signaling by Mechanical Loading Is Impaired in the Bone of Old Mice. J Bone Miner Res. 2016;31(12):2215-26.

26. Glantschnig H, Hampton RA, Lu P, Zhao JZ, Vitelli S, Huang L, et al. Generation and selection of novel fully human monoclonal antibodies that neutralize Dickkopf-1 (DKK1) inhibitory function in vitro and increase bone mass in vivo. J Biol Chem. 2010;285(51):40135-47.

27. Glantschnig H, Scott K, Hampton R, Wei N, McCracken P, Nantermet P, et al. A rate-limiting role for Dickkopf-1 in bone formation and the remediation of bone loss in mouse and primate models of postmenopausal osteoporosis by an experimental therapeutic antibody. The Journal of pharmacology and experimental therapeutics. 2011;338(2):568-78.

28. Lewis SL, Khoo PL, De Young RA, Steiner K, Wilcock C, Mukhopadhyay M, et al. Dkk1 and Wnt3 interact to control head morphogenesis in the mouse. Development. 2008;135(10):1791-801.

29. Mukhopadhyay M, Shtrom S, Rodriguez-Esteban C, Chen L, Tsukui T, Gomer L, et al. Dickkopf1 is required for embryonic head induction and limb morphogenesis in the mouse. Dev Cell. 2001;1(3):423-34.

30. Liu P, Wakamiya M, Shea MJ, Albrecht U, Behringer RR, Bradley A. Requirement for Wnt3 in vertebrate axis formation. Nature genetics. 1999;22(4):361-5.

31. Lynch ME, Main RP, Xu Q, Walsh DJ, Schaffler MB, Wright TM, et al. Cancellous bone adaptation to tibial compression is not sex dependent in growing mice. J Appl Physiol. 2010;109(3):685-91.

32. Melville KM, Kelly NH, Surita G, Buchalter DB, Schimenti JC, Main RP, et al. Effects of Deletion of ERalpha in Osteoblast-Lineage Cells on Bone Mass and Adaptation to Mechanical Loading Differ in Female and Male Mice. J Bone Miner Res. 2015;30(8):1468-80.

33. Melville KM, Robling AG, van der Meulen MC. In vivo axial loading of the mouse tibia. Methods in molecular biology (Clifton, NJ). 2015;1226:99-115.

34. Moustafa A, Sugiyama T, Prasad J, Zaman G, Gross T, Lanyon L, et al. Mechanical loading-related changes in osteocyte sclerostin expression in mice are more closely associated with the subsequent osteogenic response than the peak strains engendered. Osteoporosis International. 2011:1-10.

35. Fritton JC, Myers ER, Wright TM, van der Meulen MC. Loading induces site-specific increases in mineral content assessed by microcomputed tomography of the mouse tibia. Bone. 2005;36(6):1030-8.

36. Fritton JC, Myers ER, Wright TM, van der Meulen MC. Bone mass is preserved and cancellous architecture altered due to cyclic loading of the mouse tibia after orchidectomy. J Bone Miner Res. 2008;23(5):663-71.

37. Koide M, Kobayashi Y, Yamashita T, Uehara S, Nakamura M, Hiraoka BY, et al. Bone formation is coupled to resorption via suppression of sclerostin expression by osteoclasts. J Bone Miner Res. 2017. [Epub ahead of print].

38. Torrance AG, Mosley JR, Suswillo RF, Lanyon LE. Noninvasive loading of the rat ulna in vivo induces a strain-related modeling response uncomplicated by trauma or periostal pressure. Calcif Tissue Int. 1994;54(3):241-7.

39. Mosley JR, March BM, Lynch J, Lanyon LE. Strain magnitude related changes in whole bone architecture in growing rats. Bone. 1997;20(3):191-8.

40. Gross TS, Edwards JL, McLeod KJ, Rubin CT. Strain gradients correlate with sites of periosteal bone formation. J Bone Miner Res. 1997;12(6):982-8.

41. Chang MK, Kramer I, Keller H, Gooi JH, Collett C, Jenkins D, et al. Reversing LRP5-dependent osteoporosis and SOST-deficiency induced sclerosing bone disorders by altering WNT signaling activity. J Bone Miner Res. 2014;29(1):29-42.

42. van Lierop A, Moester M, Hamdy N, Papapoulos S. Serum Dickkopf 1 Levels in Sclerostin Deficiency. J Clin Endocrinol Metab. 2014;99(2):E252-6.

43. Florio M, Gunasekaran K, Stolina M, Li X, Liu L, Tipton B, et al. A bispecific antibody targeting sclerostin and DKK-1 promotes bone mass accrual and fracture repair. Nature communications. 2016;7:11505.

44. Ke HZ, Richards WG, Li X, Ominsky MS. Sclerostin and Dickkopf-1 as therapeutic targets in bone diseases. Endocrine reviews. 2012;33(5):747-83.

45. Li X, Grisanti M, Fan W, Asuncion FJ, Tan HL, Dwyer D, et al. Dickkopf-1 regulates bone formation in young growing rodents and upon traumatic injury. J Bone Miner Res. 2011;26(11):2610-21.

46. Sawakami K, Robling AG, Ai M, Pitner ND, Liu D, Warden SJ, et al. The Wnt co-receptor LRP5 is essential for skeletal mechanotransduction but not for the anabolic bone response to parathyroid hormone treatment. J Biol Chem. 2006;281(33):23698-711.

Chapter 4. *Dkk1* KO mice treated with sclerostin antibody have additional increases in bone volume

This chapter has been published as:

Morse A, Cheng TL, Schindeler A, McDonald MM, Mohanty S, Kneissel M, Kramer I, Little DG. *Dkk1* KO mice treated with sclerostin antibody have additional increases in bone volume. Calcif Tissue Int. 2018 May 29. [Epub ahead of print]

Title: *Dkk1* KO mice treated with sclerostin antibody have additional increases in bone volume.

Running Title: Additional bone volume with Scl-Ab in *Dkk1* KO mice

Authors: Alyson Morse, BBiotech [1,2]; Tegan L Cheng, PhD [1,2]; Aaron Schindeler, PhD [1,2]; Michelle M McDonald, PhD [3]; Sindhu T Mohanty, PhD [3]; Michaela Kneissel, PhD [4]; Ina Kramer, PhD [4]; and David G Little, MBBS FRACS(Orth) PhD [1,2] *

Affiliations:

[1] Orthopaedic Research & Biotechnology Unit, The Children's Hospital at Westmead, Sydney, Australia

[2] Discipline of Paediatrics and Child Health, Faculty of Medicine, University of Sydney, Sydney, Australia

[3] Bone Biology Program, The Garvan Institute of Medical Research, Sydney, Australia

[4] Novartis Pharma AG, Basel, Switzerland

* **Corresponding author and reprint address:**

Orthopaedic Research & Biotechnology Unit

The Children's Hospital at Westmead

Locked Bag 4001

Westmead, NSW 2145, Australia

Phone: +61-4-19481125

Fax: +61-2-98453078

Email: david.little@health.nsw.gov.au

Acknowledgments

The authors received materials support (Scl-Ab) for this study from Novartis Pharma AG (Basel, Switzerland) and Mereo BioPharma (London, UK). Prof. Little and A/Prof Schindeler have received funding support from Novartis Pharma, Amgen Inc. UCB Pharma, Celgene, and N8 Medical for studies unrelated to this submission. Prof. Little is a consultant for Orthopaediatrics. Dr McDonald has received funding from The Kay Ibbertson Cancer Council Project grant. Dr Kramer and Dr Kneissel are employees of Novartis Pharma AG.

Author contribution statement: Study design: AM, DGL, MMM, MK, IK. Study conduct: AM, TLC, SM. Data collection: AM, TLC. Data interpretation: AM, TLC, DGL. Drafting manuscript: AM. Revising manuscript content and approving final version of manuscript: all authors. AM takes responsibility for the integrity of the data analysis. We thank Lauren Peacock and Kathy Mikulec for their assistance in animal dosing. We thank Dr. Ciara Murphy for her assistance in developing methods for confocal imaging.

ABSTRACT

Dickkopf-1 (DKK1) and sclerostin are antagonists of the Wnt/β-catenin pathway and decreased expression of either increases bone formation and mass. As both affect the same signalling pathway, we aimed to elucidate redundancy and/or compensation of sclerostin and DKK1. Weekly sclerostin antibody (Scl-Ab) was administered to 9 week old female *Dkk1* KO (*Dkk1*$^{-/-}$*:Wnt3*$^{+/-}$*)* mice and compared to Scl-Ab treated wild type mice, as well as vehicle-treated *Dkk1 KO* and wild type animals. While *Wnt3* heterozygote (*Wnt3*$^{+/-}$*)* mice show no bone phenotype, Scl-Ab and vehicle-treated control groups of this genotype were included. Specimens were harvested after 3 weeks for micro-computed tomography, histomorphometry, anti-sclerostin immunohistochemistry, and biomechanical testing.

Scl-Ab enhanced bone anabolism in all treatment groups, with synergistic enhancement seen in the cancellous compartment of *Dkk1* KO mice (bone volume +55% *Dkk1* KO $p<0.01$; +22% wild type $p<0.05$). Scl-Ab treatment produced less marked increases in cortical bone of the tibiae, with anabolic effects similar across genotypes. Mechanical testing confirmed that Scl-Ab improved strength across all genotypes, however no enhancement was seen within *Dkk1* KO mice. Scl-Ab treatment was associated with increased bone formation, regardless of genotype. Immunohistochemical staining for sclerostin protein indicated no differences in the *Dkk1* KO mice, suggesting increased Wnt signaling associated with DKK1 deficiency was not compensated by upregulation of sclerostin protein.

These data suggest complex interactions between Wnt signaling factors in bone, but critically illustrate synergy between DKK1 deficiency and Scl-Ab treatment within cancellous bone. These data support the application of dual-targeted therapeutics in the modulation of bone anabolism.

Keywords: Sclerostin; Sost; DKK1; anabolism; WNT antagonism

INTRODUCTION

Dickkopf-1 (DKK1) and sclerostin, encoded by *Dkk1* and *Sost* respectively, are soluble antagonists of the Wnt/β-catenin pathway, both of which target LRP5/6 receptors and inhibit Wnt binding (1). Both proteins are expressed and secreted within the bone microenvironment and regulate bone formation and resorption via modulation of Wnt/β-catenin signalling (2). In mice, overexpression of DKK1 or sclerostin within osteocytes or osteoblasts results in osteopenia (3-8). Conversely, heterozygous and homozygous deletion of *Dkk1* or *Sost* leads to increased bone formation and greater bone mass (9-12). In humans, mutations within the *Sost* gene are associated with Sclerosteosis and van Buchem's, conditions displaying characteristically high bone mass due to increased bone formation (6, 13-15).

Redundancy and/or compensation between sclerostin and DKK1 within the bone compartment has been suggested. *Dkk1* expression has been reported to increase when sclerostin is deficient, potentially via a negative feed-back mechanism. This has been seen within human and mouse conditions of *Sost* knock-out and also with the use of neutralizing antibodies to sclerostin (16-18). Ovariectomized rats treated weekly with anti-sclerostin antibody (Scl-Ab) for 26 weeks similarly displayed rapid but transient increases in bone anabolism (19). Notably, the anti-resorptive effects of Scl-Ab persisted throughout the treatment period. Similar diminution of upregulated bone anabolism has been observed in patients with Sclerosteosis (20). This suggests a compensatory mechanism during the absence of active sclerostin.

Recently, a bispecific antibody targeting both DKK1 and sclerostin was tested extensively within rodent and primate animals (18). This bispecific antibody yielded improved bone formation above either singular therapy. Inhibiting both of these Wnt antagonists was presumed to further increase Wnt/β-catenin signaling. However, the high efficacy of dual therapy may be due to a secondary mechanism – the suppression of compensation and/or redundancy that exists between DKK1 and sclerostin. Notably, animals treated with Scl-Ab alone did show elevated *Dkk1* expression (18).

In this study we aimed to explore the regulatory interaction between DKK1 and sclerostin. This employed a *Dkk1* KO mouse model treated for 3 weeks with Scl-Ab. Loss of DKK1 has been previously shown to be embryonic lethal, however a developmental knockdown of *Wnt3* expression has been found to create viable mice (21). *Dkk1* KO mice were treated with Scl-Ab or

vehicle and compared with wild type and *Wnt3*$^{+/-}$ genotype control mice similarly treated. We hypothesized that an enhanced anabolic response would be seen following Scl-Ab treatment within the *Dkk1* KO mice. Bone volume, bone formation and bone strength changes were examined within the tibial mid-diaphysis, proximal tibial metaphysis, and lumbar vertebrae using radiographic, dynamic histomorphometry, and mechanical testing outcome measures. *Sost* expression was also examined via immunohistochemistry staining.

METHODS AND MATERIALS

Dkk1 knockout mice

A *Dkk1*$^{-/-}$*:Wnt3*$^{+/-}$ mouse colony was originally generated by crossing *Wnt3*$^{+/-}$ and *Dkk1*$^{+/-}$ strains with a further generation of *Dkk1*$^{+/-}$ backcrossing (22, 23). The colony was gifted by Prof. Patrick Tam, and was maintained and utilized on its original mixed 129J×C57Bl/6 background (28). The wild type (*Dkk1*$^{+/+}$*:Wnt3*$^{+/+}$) and *Wnt3* knockdown (*Wnt3*$^{+/-}$*; Dkk1*$^{+/+}$*:Wnt3*$^{+/-}$) mice were sourced from the *Wnt3*$^{+/-}$ × *Dkk1*$^{+/-}$ cross colony. Animal experiments were approved and performed under the Western Sydney LHD Animal Ethics Committee protocol 4174 and CMRI/CHW animal ethics protocol K338.

Animals were bred in house at the Westmead Animal Holdings facility and Kid's Research Institute Transgenic Facility. Mice were housed with littermates with a maximum of 4 mice/cage, and were given access to rodent chow and water *ad libitum*. Genotyping on DNA from ear punches was performed using DirectPCR (Viagen Biotech, Los Angeles, CA, USA), for the *Dkk1* wild type gene, the *Dkk1 neo* mutant allele and the *Wnt3* allele using published methods (22, 23).

Biologicals and study design

A total of 96 mice were included within the study (N=16-18/group). A monoclonal antibody to sclerostin (sclerostin antibody/Scl-Ab) was gifted by Novartis Pharma AG (Basel, Switzerland) and Mereo BioPharma (London, UK). At 9 weeks of age, on day (D)0, mice were intravenously injected with vehicle (isotonic buffer pH 5.3) or 100mg/kg Scl-Ab, a concentration previously shown to be effective in mice (24, 25). Second and third doses were administered at D7 and D14. Mice were subcutaneously injected with calcein (10mg/kg, Sigma-Aldrich, MO, USA) 3 and 10 days prior to euthanasia. Mice were euthanized on D21, at 12 weeks of age. Tibiae and spine were harvested. Specimens for histology were fixed in 10% formalin for 24hrs and stored in 70% ethanol. Specimens for mechanical testing were stored (unfixed) wrapped in saline-soaked gauze at -80°C.

Micro-computed tomography

The right tibiae and lumbar vertebrae were microCT scanned *ex vivo* using 12 μm and 14.7 μm isotropic voxel resolutions respectively (50 kV, 800 μA; Skyscan 1174 2; Skyscan NV, Kontich, Belgium). Images were reconstructed (0-0.1; NRecon v1.6.1.7; Skyscan NV) and analyzed with CTAnalyser (Skyscan NV). Bone was set at minimum 0.4 g/cm^3, correlated to phantoms of known density. All three-dimensional (3D) reconstructions were created on CTVol (Skyscan NV).

All tibial analysis excluded the fibula. Within the proximal metaphysis a VOI of height 1.2 mm commencing 0.5 mm below the growth plate was selected to represent the secondary spongiosa. All bone within this region was assessed, and cancellous and cortical bone compartments were also assessed separately, as seen before (26). Bone parameters assessed included bone volume (BV), total volume (TV), BV/TV, tissue mineral density (TMD). As well as trabecular thickness (Tb.Th), trabecular separation (Tb.Sp), and trabecular number (Tb.N) within the cancellous bone compartment, and cortical thickness (Ct.Th), periosteal surface (Ps), and endocortical surface (Ec) within the cortical bone compartment.

Within the tibial diaphysis, a 0.5 mm height VOI was assessed commencing half-way down the tibia from the proximal end, as corresponds with microCT assessment studies of murine tibiae (25-29). Bone parameters included BV, TV, TMD, Ct.Th, Ps, Ec, polar moment of inertia (*J*), and moment of inertia about the anteroposterior axis (*Iap*), the latter two being geometric predictors of whole bone strength. A second diaphyseal VOI of height 0.5 mm, starting 37% down from the proximal end of the tibiae was also assessed for direct comparison to published *in vivo* mechanotransduction studies (25-27). Data is provided as supplementary material.

Within the lumbar vertebrae, the body of L1 was isolated for assessment and the posterior vertebral arch excluded. A VOI of height 1.8 mm was assessed centered within the body, and the cortical sheath and cancellous bone compartments were assessed separately. Parameters assessed were the same as for the tibial metaphysis.

Bone histomorphometry

Using a diamond saw, the left tibiae were transversely cut at 37% and 50% down the tibiae. The cross-sectional surface at the 50% region of interest (ROI) was smoothed using sand paper of grit P1200 and cleaned in 70% ethanol. Samples were placed with the cross-sectional area of interest facing down on a plastic dish in 70% ethanol and were scanned and imaged using Leica TCS SP5 confocal microscope at 20x magnification (Leica Microsystems, NSW, Australia). The exposure time, *z*-stack, gain and offset remained consistent for all specimens. The endosteal and periosteal surfaces of each cross-sectional sample were analyzed for daily mineral apposition rate (MAR), mineralizing surface/bone surface (MS/BS) and bone formation rate/bone surface (BFR/BS).

The proximal (0-37%) portion of the tibiae were cryo-sectioned mineralized using Cryofilm type IIC(10) (Section-Lab Co., Hiroshima, Japan). Coronal sections (5 µm) were cut to assess the proximal metaphysis. Images were captured using Aperio Scanscope FL and Aperio Imagescope v11.2.0.780 (Aperio, Vista, CA, USA). A cancellous ROI of 1.2 mm height, commencing 0.5mm below the proximal growth plate was measured for daily mineral apposition rate (MAR), mineralizing surface/bone surface (MS/BS), and bone formation rate (BFR/BS). Tibiae were then decalcified in EDTA and embedded in paraffin. Coronal sections (5 µm) were stained for tartrate-resistant acid phosphatase (TRAP), and imaged using Scanscope CS2 (Aperio). The cancellous ROI within the proximal tibial metaphysis was again assessed for number of osteoclasts (N.Oc), osteoclast number/bone surface (N.Oc/BS), osteoclast surface/bone surface (Oc.S/BS), and osteoclast surface/osteoclast number (Oc.S/N.Oc). All analyses were performed using BIOQUANT measure 32 Nova Prime (Nashville, TN, USA).

Mechanical testing

Right tibiae and L1 lumbar vertebrae underwent mechanical testing to failure using an Instron 5944 (Massachusetts, USA), with data collected using BlueHill 3 software. L1 vertebrae were chosen as more distal lumber vertebrae were commonly misshapen and/or fused within the *Dkk1* KO mice. Bones were stored at -80°C and allowed to thaw to room temperature prior to testing. Tibia were mechanically tested by four point bending to failure. Tibiae were positioned so that the

medial side was resting across the bottom spans. The support span was 12 mm, and the upper span measured 5 mm. Samples were pre-loaded at 0.25 mm/min until a load of 1N was reached, at which point the loading rate increased to 0.5 mm/min until failure. L1 vertebrae were tested by compression until failure along the cephalocaudal axis. The superior end facing up and processes removed prior to testing and the specimens placed on a custom jig, designed with a pin attachment to allow for placement through the neural canal to stabilize the upper and lower plates. The compression testing was performed at 3 mm/min until failure. For both the tibial and vertebral testing, maximum load (N) was the maximum recorded load for a specimen, and stiffness (N/mm) was calculated as the gradient of the linear portion of the load-displacement curve.

Immunohistochemistry

Immunohistochemical staining to identify sclerostin expression was performed on vehicle and Scl-Ab treated *Dkk1* KO and wild type tibiae collected at the 12-week end-point. In brief, paraffin sections were dewaxed in xylenes and rehydrated through a decreasing gradient of ethanol. All washes between incubations/treatments were performed with Wash Buffer (S300685, DAKO/Agilent Pathology Solutions, CA, USA). Antigen retrieval was performed using Carezyme II:Pepsin (BIC-PEP956H, Metagene Pty Ltd, QLD, Australia), followed by quenching of endogenous peroxidase with 3% H_2O_2, and blocked with Protein Block (X09093, DAKO/Agilent). Primary (1ng/ml; Anti-Mouse SOST antibody AF1589; R&D Systems, MN, USA) and secondary (1:200 dilution, Biotinylated-Horse Anti-Goat BA-9500; Vector Laboratories, CA, USA) antibodies were used. The signal by bound antibodies were amplified by Vectastain Elite ABC (Vector Laboratories) and visualized by DAB substrate (DAKO/Agilent). Sections were counterstained with hematoxylin and imaged using Aperio CS2 slide scanner (Leica, Germany). Control sections were included within the immunohistochemistry which omitted the primary antibody incubation to ensure that no non-specific binding was occurring.

Statistical analysis

The between subjects effects of drug treatment (vehicle, Scl-Ab) and genotype (wild type, *Wnt3*$^{+/-}$, *Dkk1* KO) as well as the interactions between these terms were assessed using a two-way ANOVA. Post-hoc Tukey HSD testing was performed on the between-subject effect of genotype to outline what genotypes were significantly different. Sub-analyses between groups was performed using one way ANOVA and LSD post-hoc analysis to determine what specific groups (genotype and drug treatment) were significantly altered. Data assessed and presented are for drug related changes within each genotype, and genotype related changes within a drug treatment. Mean and standard deviation are presented within graphs and tables. *n* assessed are listed within tables or figure legends. For all testing a value of $p<0.05$ was considered significant. All analysis was performed using IBM SPSS Statistics 24 (SPSS Inc., Chicago, IL, USA) and graphs created using GraphPad Prism 7 (GraphPad Software, La Jolla, CA, USA).

RESULTS

Bone volume is increased with *Dkk1* deficiency

MicroCT analyses of the tibiae and L1 vertebrae confirmed that *Dkk1* KO mice showed an increased bone volume phenotype at 12 weeks of age compared to wild type and $Wnt3^{+/-}$ control mice (Tables 1-3). *Dkk1* KO mice showed considerable increases within cancellous bone of the tibiae and L1 vertebrae. Within the proximal tibial metaphysis, cancellous BV/TV was significantly increased in *Dkk1* KO vehicle treated mice over both wild type (+123%, $p<0.05$) and $Wnt3^{+/-}$ mice (+180%, $p<0.01$) (Table 1). Tb.N was also significantly increased in *Dkk1* KO vehicle treated mice over both wild type (+117%, $p<0.01$) and $Wnt3^{+/-}$ mice (+150%, $p<0.01$). Similarly, within the bone of the L1 vertebrae, cancellous BV/TV and Tb.N were significantly increased in *Dkk1* KO vehicle treated mice over both wild type (BV/TV: +30%; Tb.N: +162%, $p<0.01$) and $Wnt3^{+/-}$ mice (BV/TV: +65%; Tb.N: +162%, $p<0.01$) (Table 3). Cortical bone volume however was not increased in the *Dkk1* KO mice within the proximal tibial metaphysis, the L1 vertebrae, and also of the tibial mid-diaphysis. However within a VOI measured half-way down the tibiae (mid-diaphysis) there were significant increases in *Dkk1* KO vehicle treated mice compared to control genotypes in BV (wild type: +14%; $Wnt3^{+/-}$: +25%; $p<0.01$), Ct.Th (wild type: +7%, $p<0.05$; $Wnt3^{+/-}$: +15%, $p<0.01$), and Ps (wild type: +9%; $Wnt3^{+/-}$: +13%; $p<0.01$) (Table 2).

Scl-Ab treatment synergizes with *Dkk1* deficiency in the proximal tibia

When assessing all bone within the tibial proximal metaphysis by microCT, the interaction of genotype:drug was significant for BV ($p<0.01$) and TV ($p<0.05$) (Table 1). The effects of genotype and drug treatment were both separately significant for all parameters measured (BV, TV, BV/TV and TMD, $p<0.01$). Sub-analyses showed that BV and BV/TV were significantly increased with Scl-Ab treatment for all genotypes compared to vehicle treated tibiae of the same genotype. These BV and BV/TV increases were greater in the *Dkk1* KO mice (BV +55%, BV/TV +27%, $p<0.01$), than the wild type (BV +22%, $p<0.05$ and BV/TV +20%, $p<0.01$) and the $Wnt3^{+/-}$ (BV +28%, BV/TV +15%, $p<0.01$) mice. BV and BV/TV were significantly greater within the Scl-Ab treated *Dkk1* KO mice than for Scl-Ab treated mice of the other genotypes (increase over wild type: BV

+42%, BV/TV +17%; increase over *Wnt3*$^{+/-}$: BV +52%, BV/TV +25%; p<0.01). There were no differences in bone parameters between Scl-Ab treated wild type and Scl-Ab treated *Wnt3*$^{+/-}$ mice.

The cancellous and cortical bone compartments were assessed separately within the proximal tibial metaphysis to better understand the response of the individual compartments to Scl-Ab treatment. Within the cancellous bone compartment the interaction of genotype:drug was significant for BV, TV, BV/TV, TMD, and Tb.Th (p<0.05, Table 1). The effects of genotype and drug treatment were both separately significant for BV, BV/TV, Tb.Th, Tb.Sp, and Tb.N (p<0.01). Sub-analyses revealed that Scl-Ab treatment resulted in increases in TMD and Tb.Th across all genotypes, when compared to vehicle treated mice of the same genotype (p<0.01). These increases were greater for the *Dkk1* KO mouse (TMD +21%, Tb.Th +56%) than for the wild type (TMD +11%, Tb.Th +22%) and *Wnt3*$^{+/-}$ (TMD +11%, Tb.Th +38%) mice. BV/TV was significantly increased following Scl-Ab treatment for wild type (+130%, p<0.01) and *Dkk1* KO (+143%, p<0.01) mice. A +106% increase in BV/TV was also seen following Scl-Ab treatment within *Wnt3*$^{+/-}$ mice, however did not reach significance (p=0.08). Notably, BV and TV were not significantly altered with Scl-Ab treatment in the wild type or *Wnt3*$^{+/-}$ mice, however significant increases were seen within the *Dkk1* KO mice following Scl-Ab treatment (BV +187%, p<0.01; TV +18%, p<0.05). Three-dimensional (3D) reconstructions of the median cancellous BV within the tibial metaphysis are shown for each group (Figure 1A).

Within the cortical bone compartment of the proximal tibial metaphysis TV only was significant for the interaction of genotype:drug (p<0.05, Table 1). The effect of genotype was significant for BV, Ct.Th, Ps, and Ec (p<0.05), and drug treatment significant for all parameters except Ec (p<0.05). Sub-analyses showed that Scl-Ab treatment resulted in significant increases in BV, TMD and Ct.Th for all genotypes (p<0.01). The TMD and Ct.Th increases with Scl-Ab were similar across all genotypes (TMD +6-10%, Ct.Th +15-17%). BV increase due to Scl-Ab treatment was moderately enhanced in the *Dkk1* KO mice (+26%) compared to wild type (+14%) and *Wnt3*$^{+/-}$ (+20%) mice. TMD and Ct.Th was not different between Scl-Ab treated groups of any genotype, however BV was significantly greater in the Scl-Ab treated *Dkk1* KO mice than the Scl-Ab treated wild type (+13%, p<0.01) or *Wnt3*$^{+/-}$ (+17%, p<0.01) mice.

These data suggest that the anabolic response to Scl-Ab was enhanced within the tibial metaphysis of *Dkk1* KO mice, and synergistically within the cancellous bone compartment.

Scl-Ab treatment produces a less marked anabolic response in the tibial diaphysis

The mid-diaphysis was also assessed by microCT (Table 2). The effects of drug treatment and genotype were significant for TV, BV, Ct.Th, Ps and moment of inertia (polar and about the anteroposterior axis), with post-hoc testing detailing the genotype effects were between *Dkk1* KO mice and the control mice (wild type and *Wnt3*$^{+/-}$) ($p<0.01$). The effect of genotype was significant for Ec also, and drug was significant for TMD. Sub-analyses showed that the response to Scl-Ab treatment was less marked than that seen within the metaphyseal cortical bone. However, notable increases due to Scl-Ab treatment within the mid-diaphyseal cortical bone were within BV, TMD and Ct.Th. Notably, these increases were greatest in the *Wnt3*$^{+/-}$ genotype (BV +25%, TMD +6%, Ct.Th +19%, $p<0.01$), however similar between wild type (BV +14% $p<0.01$, TMD +4% $p<0.05$, Ct.Th +14% $p<0.01$) and *Dkk1* KO (BV +18% $p<0.01$, TMD +4% $p<0.05$, Ct.Th +10% $p<0.01$) genotypes. Despite this, *Dkk1* KO Scl-Ab treated mice still had significantly higher values for BV and Ct.Th, along with Ps, Ec, and polar moment of inertia above Scl-Ab treated wild type and *Wnt3*$^{+/-}$ mice. However, vehicle treated *Dkk1* KO mice initially had significantly higher values for these parameters compared to vehicle treated wild type and *Wnt3*$^{+/-}$ mice. 3D reconstructions of the median BV within the mid-diaphysis are shown for each group (Figure 1B). A second diaphyseal VOI commencing 37% down the tibiae was also assessed. Results were similar to the mid-diaphyseal VOI and data is shown within Supplementary Table 1.

Anabolic response to Scl-Ab treatment in the L1 vertebrae body independent of genotype

Within the L1 vertebrae body, cancellous and cortical bone compartments were assessed by microCT (Table 3). Similar to results seen within the proximal metaphysis of the tibia, the most pronounced effects were seen within the cancellous compartment of the L1 vertebrae. The effects of genotype and drug were both significant for BV, TMD, Tb.Th, Tb.Sp, and Tb.N ($p<0.01$). The interaction of genotype:drug was significant for TMD, Tb.Th and Tb.N ($p<0.01$). Sub-analyses showed that the changes due to Scl-Ab treatment had a significant anabolic effect on all genotypes (BV/TV: wild type +62%, *Wnt3*$^{+/-}$ +68%, *Dkk1* KO +57%, $p<0.01$). The effect of Scl-Ab on TMD and the cancellous architecture was enhanced within the *Dkk1* KO mouse (TMD: wild type +43%,

Wnt3$^{+/-}$ +38%, *Dkk1* KO +70%, p<0.01; Tb.Th: wild type -27%, *Wnt3*$^{+/-}$ -23%, *Dkk1* KO -22%, p<0.01; Tb.N: wild type +27% p<0.01, *Wnt3*$^{+/-}$ +21% p<0.01, *Dkk1* KO +35% p<0.05). BV/TV, TMD and Tb.Th values were all significantly greater in the *Dkk1* KO Scl-Ab group, compared to wild type and *Wnt3*$^{+/-}$ Scl-Ab groups (p<0.01), however so were most of the values for the *Dkk1* KO vehicle group compared to wild type and *Wnt3*$^{+/-}$ vehicle groups (p<0.01).

The effect of drug treatment on the cortical bone of the L1 vertebrae was significant for BV and TV. Sub-analyses showed that similar increases in BV and TMD were seen with Scl-Ab treatment, compared to vehicle, across all genotypes (p<0.01). 3D reconstructions of the median cancellous BV within the L1 vertebrae body are shown for each group (Figure 1C).

Scl-Ab treatment enhances bone formation rates in the proximal tibia and tibial midshaft independent of genotype

Dynamic histomorphometry was assessed within the mid-diaphysis and proximal metaphysis of the tibiae (Figure 2). Within the mid-diaphysis, similar results were seen on the periosteal and endosteal surfaces (Figure 2A-B). The effect of genotype was not significant for any parameter, however drug treatment was for all (p<0.01). Sub-analyses confirmed that dynamic bone formation parameters on the periosteal and endosteal surfaces were not-significantly different between any genotype, regardless of drug treatment. Scl-Ab treatment resulted in significant increases in MS/BS and BFR/BS for all genotypes (*Dkk1* KO mice - MS/BS: periosteal +258%, endosteal +65%; BFR/BS: periosteal +375%, endosteal +118%; p<0.01) (wild type - MS/BS: periosteal +98%, endosteal +38%; BFR/BS: periosteal +129%, endosteal +61%; p<0.01) (*Wnt3*$^{+/-}$ - MS/BS: periosteal +209%, endosteal +43%; BFR/BS: periosteal +169%, endosteal +61%; p<0.01). Images representing the median periosteal BFR/BS are shown in Figure 2C.

Within the proximal metaphysis of the tibiae, again the effect of genotype was not significant for any parameter, however drug treatment was significant for all (p<0.05, Figure 2D). The interaction of genotype:drug treatment was also significant for MAR and BFR/BS (p<0.05). Sub-analyses revealed that *Dkk1* KO vehicle mice had increased MAR and MS/BS compared to wild type vehicle mice (MAR +259%, MS/BS +135%, p<0.01). Notably, the addition of Scl-Ab did not further increase MAR or MS/BS within the *Dkk1* KO mice, but rather these levels were similar for

all Scl-Ab treated mice, regardless of genotype. This suggests that a maximal MAR and MS/BS level was reached within either *Dkk1* KO vehicle mice or Scl-Ab treatment. BFR/BS within the tibial proximal metaphysis was similar for all groups, except for wild type Scl-Ab mice, which had significantly greater BFR/BS over all other groups. Images representing the median BFR/BS are shown in Figure 2E.

The number of osteoclasts and osteoclast surface activity were measured within this same metaphyseal ROI (Figure 2F). The effect of genotype was significant for N.Oc and Oc.S/N.Oc only, and the effect of drug was not significant for any parameter measured. Sub-analyses showed that there were a significantly greater number of osteoclasts within the *Dkk1* KO mice than in *Wnt3*$^{+/-}$ mice, regardless of drug treatment ($p<0.05$). Wild type mice had similarly low numbers of osteoclasts as *Wnt3*$^{+/-}$ mice, however the comparison to *Dkk1* KO mice did not reach significance (vehicle: $p=0.08$; Scl-Ab: $p=0.05$). Sub-analyses also showed that Oc.S/BS and Oc.S/N.Oc were not different between any group, suggesting that the osteoclast activity on the bone surface was not greatly altered by either DKK1 deficiency of Scl-Ab treatment.

Scl-Ab treatment enhances tibial mid-diaphyseal and lumbar vertebrae strength independent of genotype

Four-point bending was undertaken on the tibiae, assessing the strength of the mid-diaphyseal cortical bone (Figure 3A). The effect of drug treatment was significant for all parameters, whilst genotype was significant for stiffness only. However, sub-analyses showed that all genotypes of the same drug treatment, either vehicle or Scl-Ab, were similar in maximum load to failure, stiffness, and energy, except for a -16% decrease in stiffness in vehicle treated *Wnt3*$^{+/-}$ mice compared to wild type vehicle ($p<0.05$). Scl-Ab treatment had a significant effect for maximum load to failure only, where it was similarly improved with Scl-Ab treatment across all genotypes (wild type +16%, $p<0.05$; *Wnt3*$^{+/-}$ +23%, $p<0.05$; *Dkk1* KO +37%, $p<0.01$).

Compression testing of the L1 vertebrae was also performed (Figure 3B). The effect of genotype was significant for maximum load to failure ($p<0.05$), whilst drug treatment was significant for all parameters ($p<0.01$). Sub-analyses showed that vehicle treated *Dkk1* KO mice had greater

maximum load to failure compared to vehicle treated wild type (+48%) and *Wnt3*$^{+/-}$ (+54%) mice ($p<0.05$). Scl-Ab treatment significantly increased maximum load to failure within all genotypes (wild type +143%; *Wnt3*$^{+/-}$ +109%; *Dkk1* KO +58%, $p<0.01$). And a maximal strength was reached with Scl-Ab dosing, with all Scl-Ab genotypes having similar maximum load. Scl-Ab treatment only had an effect on stiffness within the wild type group (+68%, $p<0.01$), whilst energy to maximum load was increased following Scl-Ab treatment for all genotypes (wild type +240%, $p<0.01$; *Wnt3*$^{+/-}$ +192%, $p<0.01$; *Dkk1* KO +89%, $p<0.05$). The energy was similar for all Scl-Ab treated mice, suggesting again that a maximal threshold was reached with Scl-Ab treatment.

Sclerostin protein does not show compensatory upregulation in *Dkk1* KO mice

Sclerostin expression within the tibiae was identified by immunohistochemical staining (Figure 4). Considerable staining of sclerostin was seen in both cancellous (Figure 4A) and cortical (Figure 4B) bone compartments. Observational assessment revealed no evident alterations in sclerostin distribution or staining intensity between groups, regardless of genotype or drug treatment.

DISCUSSION

This study investigated the bone response of a *Dkk1* KO mouse line to short-term Scl-Ab therapy. As expected, there was no negative effect on bone anabolism with dual DKK1 and sclerostin deficiency, but rather there was a synergistic anabolic response to Scl-Ab treatment within the *Dkk1* KO mice. This synergistic response was limited to the cancellous bone compartment, with the anabolic effect on cortical bone equivalent across all genotypes. These data support the concept that inhibition of multiple Wnt antagonists can enhance bone anabolism in cancellous bone.

Vehicle treated *Dkk1* KO mice displayed a high bone mass phenotype compared to vehicle treated control wild type and *Wnt3*$^{+/-}$ mice. The most prominent increases were seen within the cancellous bone of the proximal metaphysis and vertebrae. This data is in agreement with prior findings within female adult *Dkk1* KO mice, where effects were primarily seen within cancellous bone (12). Further, we have shown that the strength of the L1 vertebrae was increased within non-treated *Dkk1* KO mice over genotype controls, confirming an improvement in cancellous bone strength in the *Dkk1* KO mice and confirming previously shown data (12). However, the strength of the tibial mid-diaphysis was not altered between genotypes, suggesting a limited role of DKK1 in regulating cortical bone within this region. This is consistent with prior suggestions that DKK1 may have a lesser role in regulating cortical bone (12), and that its expression may be limited within adult cortical bone (30).

Scl-Ab treatment had a significant anabolic effect on all mice. Within the cortical bone compartments (tibial mid-diaphyseal and metaphyseal cortical bone, and vertebral cortical bone), similar anabolic increases were seen across all genotypes with Scl-Ab treatment. Dynamic bone formation measures confirmed similar responses to Scl-Ab across all genotypes within the cortical bone of the tibial mid-diaphysis. However, the anabolic bone volume response to Scl-Ab was synergistically enhanced within the cancellous bone of the proximal tibiae of *Dkk1* KO mice. The response of vertebral cancellous bone to Scl-Ab was also improved within *Dkk1* KO mice. These data suggest that dual inhibition of DKK1 and sclerostin may enhance cancellous bone anabolism. Further, it supports the evidence that DKK1 expression may be more localized to cancellous bone (12, 30).

Despite the synergistic increases in bone parameters in the cancellous bone with *Dkk1* KO genotype and Scl-Ab treatment, there was no significant interaction between variables in terms of dynamic bone formation measures. This result was unexpected and could be justified by multiple explanations. The first possibility is that Scl-Ab or *Dkk1* KO could be affecting bone resorption rather than formation, however this is unlikely as osteoclast activity was not effected by either genotype or Scl-Ab treatment. A more likely alternate scenario is that the synergistic interaction is transient and the effects on cancellous bone anabolism are no longer detectable at 3 weeks.

There is building evidence on the transient effect of Scl-Ab on bone formation. The levels of bone formation markers following Scl-Ab therapy have been shown to be transient within Phase II and III clinical trials (31-33). Similarly, lessening of the strong anabolic effects within Sclerosteosis patients has also been observed (20). Recently, weekly Scl-Ab dosing of balb/c mice showed an attenuated serum P1NP response as early as the third dose, compared with mice being dosed for the first time (34). Further, *Col1a1* mRNA expression within bone was reduced by 6 weeks of dosing. Longer assessment of Scl-Ab treatment alongside DKK1 deficiency would be required to further elucidate the transient bone formation response in this setting of dual deficiency. Utilization of anti-catabolic agents, such as bisphosphonates, may also be investigated to harness any transient anabolic burst. Such follow-up bisphosphonate investigations have been previously undertaken in Scl-Ab (romosozumab, Amgen) Phase II clinical trials (35).

Contrary to our initial hypothesis, sclerostin expression in the tibiae was not upregulated in *Dkk1* KO bones. An important caveat is that *Dkk1* KO mice have had developmental and sustained DKK1 deficiency and compensatory upregulation of sclerostin protein may be transient. Moreover, while DKK1 levels have been shown to be elevated with sclerostin deficiency (16-18), the converse may not be true. This again may result from DKK1 having a less prominent regulatory role within the adult skeleton (30).

In conclusion, this study uses an alternative system to a prior report using a bispecific DKK1/sclerostin antibody (18) to examine the interaction between DKK1 and sclerostin in bone. Not only were *Dkk1 KO* mice capable of mounting an anabolic response to Scl-Ab treatment, this response within cancellous bone was synergistic compared to the response of wild type mice to Scl-Ab. Immunostaining indicated that compensatory upregulation of sclerostin protein in *Dkk1*

KO mice was not the underlying mechanism, and thus further studies are required to determine the complex interactions in Wnt signaling in cancellous bone. These data support the theory that dual agents targeting Wnt modulation have the potential for increased bone anabolism above a single agent.

Disclosure of financial conflicts of interest

The authors received materials support (Scl-Ab) for this study from Novartis Pharma AG (Basel, Switzerland) and Mereo BioPharma (London, UK). Prof Little has received additional funding and materials support from Novartis Pharma AG and Mereo BioPharma for pre-clinical research separate to this submission and is a consultant for Orthopediatrics. Prof Little and A/Prof Schindeler have received funding support from Amgen Inc., UCB Pharma, N8 Medical, and Celgene for pre-clinical research separate to this submission. Dr McDonald has received funding from The Kay Ibbertson Cancer Council Project grant. Authors Dr Kneissel and Dr Kramer are employees of Novartis Pharma AG.

FIGURES

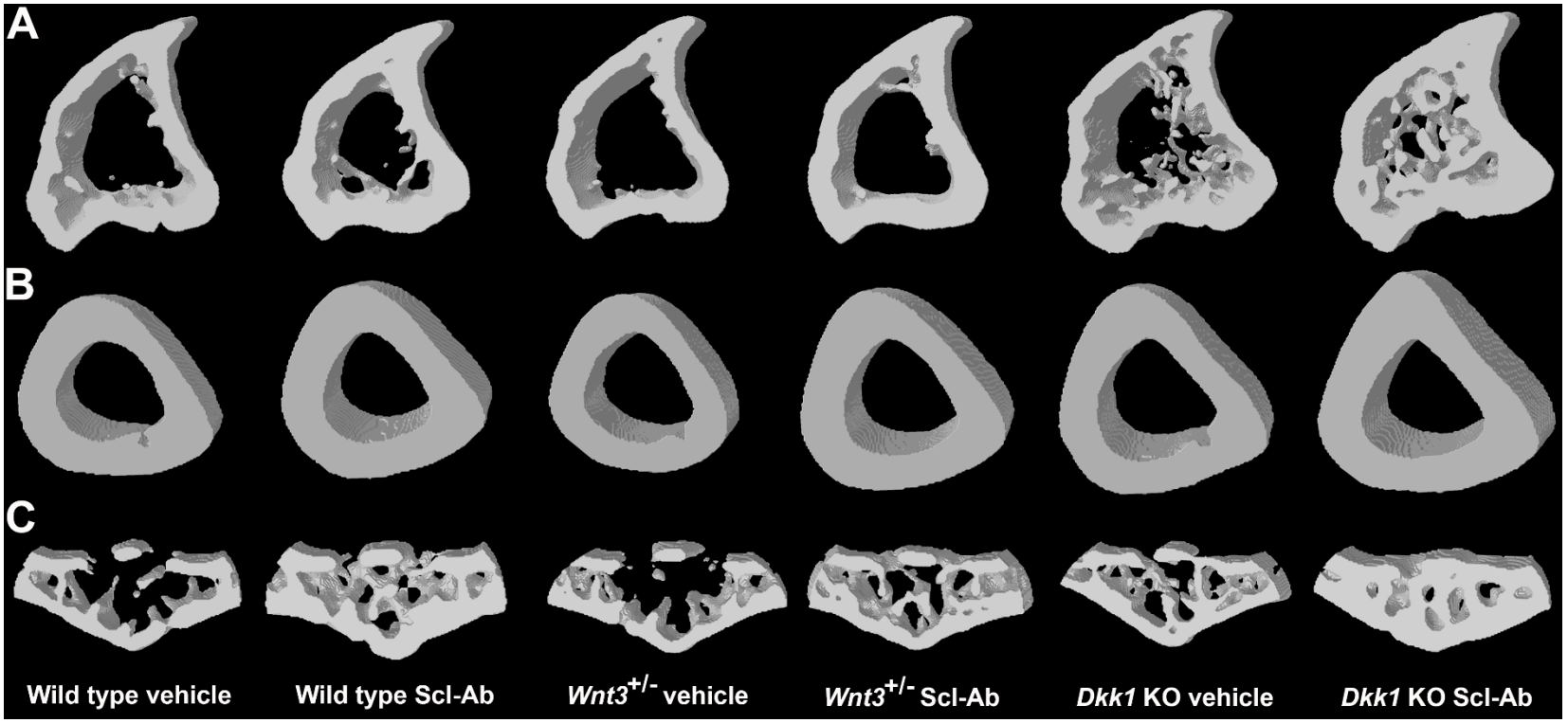

Figure 1: 3D models of bone specimens showing the median bone volume per group as measured by microCT**. (A)** Proximal tibial metaphysis. A 1.2mm volume of interest (VOI) was selected 0.5mm below the growth plate. **(B)** Tibial mid-diaphysis. A 0.5mm VOI was selected half-way down the tibia. **(C)** The body of the L1 vertebrae was isolated and a VOI of 1.8mm height assessed. A 0.5mm section centered within this VOI was selected for 3D modeling.

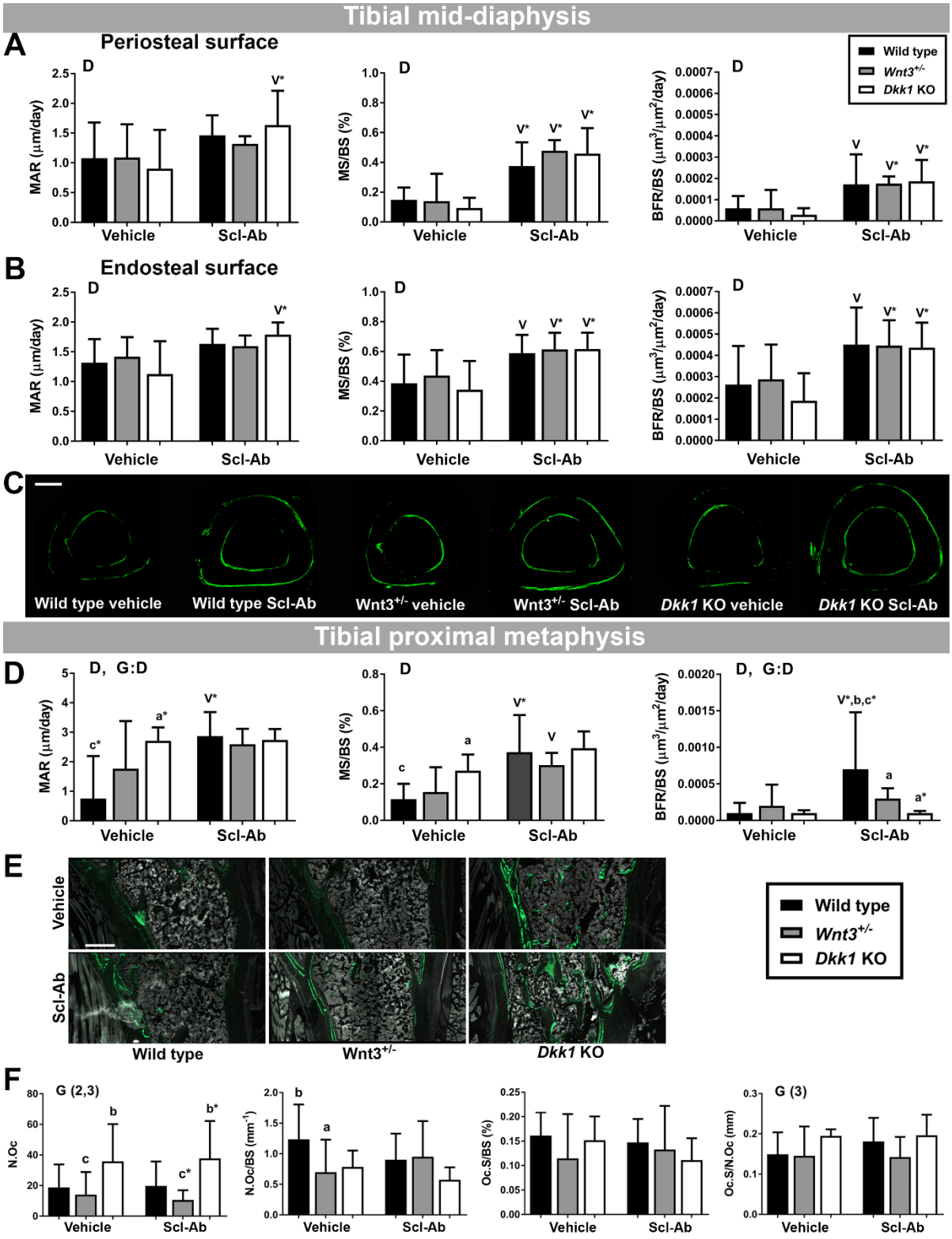

Figure 2: Histomorphometry of the tibiae of *Dkk1* KO and control (wild type and *Wnt3*$^{+/-}$**)** mice following three weeks treatment with vehicle or Scl-Ab. **(A-D)** Mineral apposition rate (MAR), mineralizing surface/bone surface (MS/BS), and bone formation rate (BFR/BS) were measured/calculated. **(A)** Dynamic bone formation of the periosteal surface of mid-diaphyseal

cortical bone at a ROI half way along the tibiae. *n*=8 **(B)** Dynamic bone formation of the endosteal surface of mid-diaphyseal cortical bone at a ROI half way along the tibiae. *n*=8 **(C)** Representative specimens of mid-diaphyseal ROI (median BFR/BS). Scale bar is 300µm. **(D)** Dynamic bone formation of the cancellous bone within the proximal metaphysis. *n*=5-8 **(E)** Representative specimens of the metaphyseal ROI (median BFR/BS). Scale bar is 400µm. **(F)** Number of osteoclasts (N.Oc), number of osteoclasts/bone surface (N.Oc/BS), Osteoclast surface/bone surface (Oc.S/BS), and osteoclast surface/number of osteoclasts were measured within cancellous bone of the proximal metaphysis. *n*=7-8. Data (bars) are Mean (SD). ANOVA: significant between-subjects effects of (G) genotype, (D) drug treatment, and the interaction of (G:D) genotype:drug ($p<0.05$). Tukey HSD post-hoc testing of between-subject effect of genotype: significance for (1) wild type vs *Wnt3*$^{+/-}$, (2) wild type vs *Dkk1* KO, (3) *Wnt3*$^{+/-}$ vs *Dkk1* KO ($p<0.05$). Sub-analyses: V = $p<0.05$ Scl-Ab compared to vehicle treatment of the same genotype, a = $p<0.05$ compared to wild type of same drug treatment, b = $p<0.05$ compared to *Wnt3*$^{+/-}$ of same drug treatment, c = $p<0.05$ compared to *Dkk1* KO of same drug treatment. * indicates stronger significance of $p<0.01$ for sub-analyses.

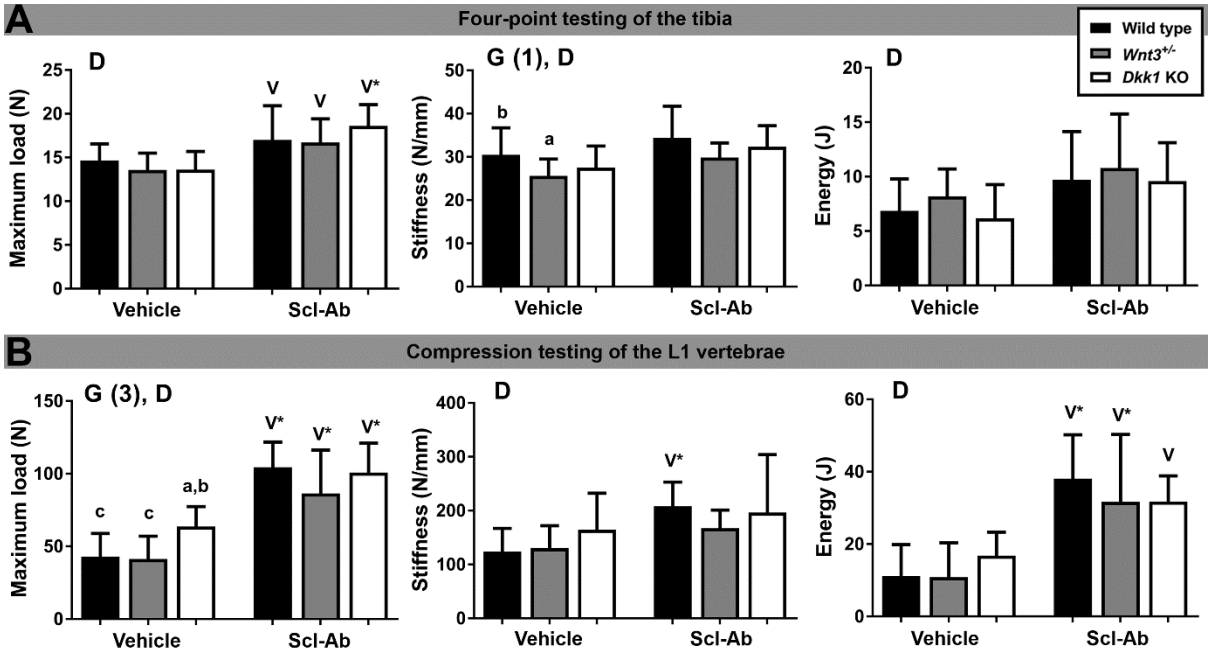

Figure 3: Mechanical testing of bones from *Dkk1* KO and control (wild type and *Wnt3*$^{+/-}$**)** mice following 3 weeks treatment with vehicle or Scl-Ab. Maximum load to failure (Maximum load), Stiffness, and energy until maximum load (Energy) were measured/calculated. **(A)** Four-point testing of tibiae. **(B)** Compression testing of L1 vertebrae. Data (bars) are Mean (SD). ANOVA: significant between-subjects effects of (G) genotype, (D) drug treatment, and the interaction of (G:D) genotype:drug ($p<0.05$). Tukey HSD post-hoc testing of between-subject effect of genotype: significance for (1) wild type vs *Wnt3*$^{+/-}$, (2) wild type vs *Dkk1* KO, (3) *Wnt3*$^{+/-}$ vs *Dkk1* KO ($p<0.05$). Sub-analyses: V = $p<0.05$ Scl-Ab compared to vehicle treatment of the same genotype, a = $p<0.05$ compared to wild type of same drug treatment, b = $p<0.05$ compared to *Wnt3*$^{+/-}$ of same drug treatment, c = $p<0.05$ compared to *Dkk1* KO of same drug treatment. * indicates stronger significance of $p<0.01$ for sub-analyses.

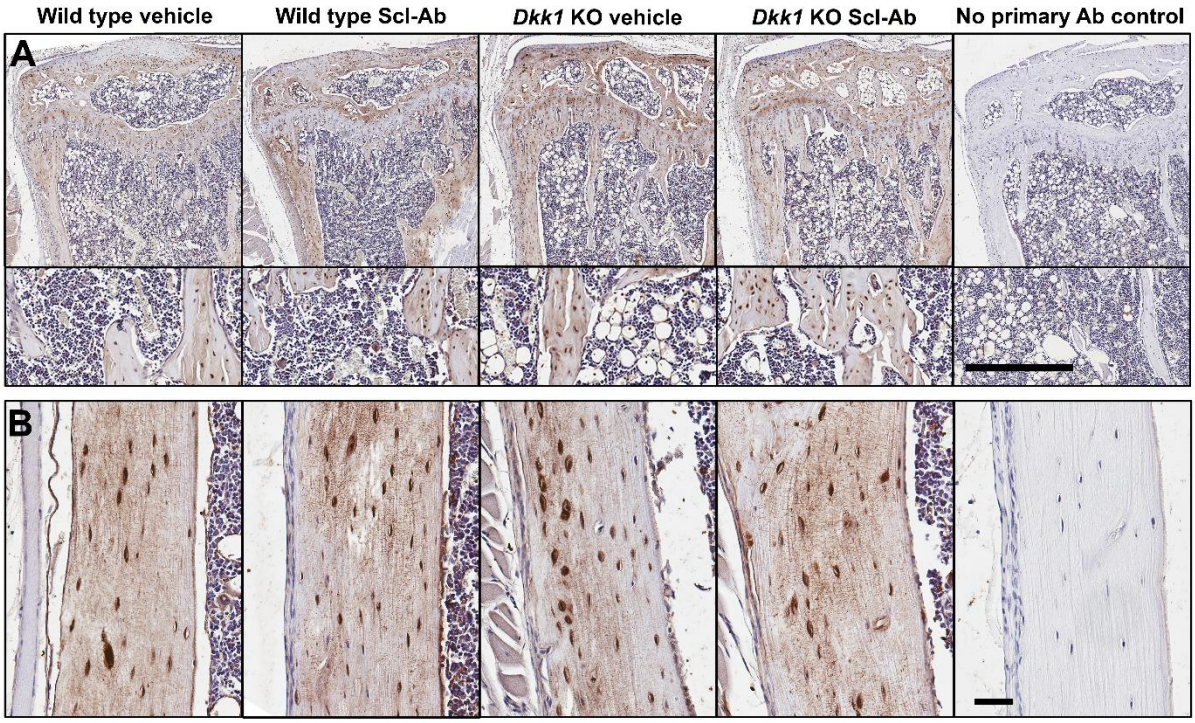

Figure 4: Immunohistochemistry for sclerostin in tibiae of vehicle and Scl-Ab treated wild type and *Dkk1* KO mice at the 12-week end-point. **(A)** Proximal metaphysis. The bottom panel is a region from the top panel in higher magnification. **(B)** Mid-diaphysis. Scale bar 50µm.

TABLES

Table 1: Bone parameters of the tibial metaphysis measured by microCT for wild type, *Wnt3*$^{+/-}$ and *Dkk1* KO mice, which underwent vehicle or Scl-Ab treatment.

			Wild type		*Wnt3*$^{+/-}$		*Dkk1* KO	
	Parameters	**Between-subjects effects**	**Vehicle**	**Scl-Ab**	**Vehicle**	**Scl-Ab**	**Vehicle**	**Scl-Ab**
All bone	BV (mm^3)	G (2,3), D, G:D	1.69 (0.25)	2.07 (0.29)^{V}	1.52 (0.15)	1.94 (0.14)^{V*}	1.90 (0.12)	2.94 (0.54)^{V*,a*,b*}
	TV (mm^3)	G (2,3), D, G:D	3.25 (0.47)	3.29 (0.32)	3.01 (0.21)	3.33 (0.31)^{V}	3.31 (0.17)	4.00 (0.36)^{V*,a*,b*}
	BV/TV (%)	G (2,3), D	52.16 (4.50)	62.72 (3.32)^{V*}	50.60 (3.37)	58.37 (4.70)^{V*}	57.40 (2.32)^{a,b*}	73.17 (7.88)^{V*,a*,b*}
	TMD (g/cm^3)	G (2,3), D	1.03 (0.04)	1.07 (0.04)^{V}	1.01 (0.03)	1.09 (0.04)^{V*}	0.99 (0.04)^{a}	1.03 (0.04)^{V,b*}
Cancellous bone	BV (mm^3)	G (2,3), D, G:D	0.13 (0.06)	0.28 (0.11)	0.10 (0.03)	0.20 (0.08)	0.31 (0.09)^{b}	0.89 (0.43)^{V*,a*,b*}
	TV (mm^3)	G (2,3), G:D	1.53 (0.31)	1.37 (0.14)	1.43 (0.14)	1.47 (0.22)	1.57 (0.12)	1.85 (0.26)^{V,a*,b*}
	BV/TV (%)	G (2,3), D, G:D	8.67 (2.89)	19.95 (6.33)^{V*}	6.90 (1.89)	14.26 (6.87)	19.31 (4.83)^{a,b*}	46.90 (16.75)^{V*,a*,b*}
	TMD (g/cm^3)	D, G:D	0.65 (0.02)	0.72 (0.03)^{V*}	0.65 (0.02)	0.72 (0.04)^{V*}	0.62 (0.02)^{b}	0.75 (0.05)^{V*,b}
	Tb.Th (mm)	G (2,3), D, G:D	0.09 (0.01)	0.11 (0.01)^{V*}	0.08 (0.00)	0.11 (0.01)^{V*}	0.09 (0.01)	0.14 (0.02)^{V*,a*,b*}
	Tb.Sp (mm)	G (1,2,3), D	0.57 (0.13)	0.45 (0.07)^{V}	0.64 (0.08)	0.55 (0.10)^{V}	0.28 (0.04)^{a*,b*}	0.21 (0.09)^{a*,b*}
	Tb.N (mm^{-1})	G (2,3), D	0.98 (0.23)	1.79 (0.47)^{V*}	0.85 (0.20)	1.31 (0.49)	2.13 (0.42)^{a*,b*}	3.27 (0.79)^{V*,a*,b*}
Cortical bone	BV (mm^3)	G (2,3), D	1.63 (0.21)	1.86 (0.20)^{V*}	1.49 (0.15)	1.79 (0.10)^{V*}	1.67 (0.08)	2.10 (0.13)^{V*,a*,b*}
	TV (mm^3)	G (2,3), D, G:D	3.22 (0.47)	3.26 (0.32)	2.98 (0.21)	3.31 (0.31)^{V}	3.29 (0.16)	3.98 (0.36)^{V*,a*,b*}
	TMD (g/cm^3)	D	1.03 (0.04)	1.09 (0.05)^{V*}	1.00 (0.03)	1.10 (0.03)^{V*}	1.02 (0.03)	1.12 (0.02)^{V*}
	Ct.Th (mm)	G (2,3), D	0.25 (0.02)	0.29 (0.02)^{V*}	0.24 (0.02)	0.28 (0.01)^{V*}	0.26 (0.02)^{b}	0.30 (0.01)^{V*}
	Ps (mm)	G (3), D	7.23 (0.46)	7.24 (0.37)	6.96 (0.26)	7.19 (0.31)	7.22 (0.21)	7.72 (0.28)^{V*,a*,b*}
	Ec (mm)	G (2,3)	4.97 (0.47)	4.84 (0.22)	4.81 (0.24)	4.83 (0.32)	5.10 (0.19)	5.47 (0.34)^{V,a*,b*}
	n		8	8	8	8	8	8

Data are Mean (SD). ANOVA: significant between-subjects effects of (G) genotype, (D) drug treatment, and the interaction of (G:D) genotype:drug ($p<0.05$). Tukey HSD post-hoc testing of between-subject effect of genotype: significance for (1) wild type vs *Wnt3*$^{+/-}$, (2) wild type vs *Dkk1* KO, (3) *Wnt3*$^{+/-}$ vs *Dkk1* KO ($p<0.05$). Sub-analyses: V=$p<0.05$ compared to vehicle treatment of same genotype; a=$p<0.05$ compared to wild type of same drug treatment; b=$p<0.05$ *Dkk1* KO compared to *Wnt3*$^{+/-}$ of same drug treatment; * indicates stronger significance of $p<0.01$ for sub-analyses.

Table 2: Cortical bone parameters of the tibial mid-diaphysis measured by microCT for wild type, *Wnt3*$^{+/-}$ and *Dkk1* KO mice, which underwent vehicle or Scl-Ab treatment.

	Between-subjects	Wild type		*Wnt3*$^{+/-}$		*Dkk1* KO	
Parameters	**effects**	**Vehicle**	**Scl-Ab**	**Vehicle**	**Scl-Ab**	**Vehicle**	**Scl-Ab**
BV (mm^3)	G (2,3), D	0.44 (0.05)	0.50 (0.06)^{V*}	0.40 (0.02)	0.50 (0.04)^{V*}	0.50 (0.02)^{a*,b*}	0.59 (0.05)^{V*,a*,b*}
TV (mm^3)	G (2,3), D	0.64 (0.10)	0.67 (0.07)	0.59 (0.05)	0.69 (0.06)^{V*}	0.73 (0.04)^{a,b*}	0.82 (0.06)^{V,a*,b*}
TMD (g/cm^3)	D	1.20 (0.03)	1.25 (0.04)^{V}	1.18 (0.03)	1.25 (0.05)^{V*}	1.19 (0.04)	1.24 (0.03)^{V}
Ct.Th (mm)	G (2,3), D	0.28 (0.01)	0.32 (0.02)^{V*}	0.26 (0.01)	0.31 (0.01)^{V*}	0.30 (0.01)^{a,b*}	0.33 (0.02)^{V*,a,b*}
Ps (mm)	G (2,3), D	4.29 (0.36)	4.40 (0.26)	4.14 (0.16)	4.48 (0.24)^{V*}	4.68 (0.15)^{a*,b*}	4.91 (0.21)^{a*,b*}
Ec (mm)	G (2,3)	2.44 (0.29)	2.28 (0.15)	2.36 (0.17)	2.35 (0.21)	2.63 (0.14)^{b*}	2.62 (0.09)^{a*,b*}
J (mm^4)	G (2,3), D	0.24 (0.08)	0.27 (0.06)	0.19 (0.05)	0.28 (0.05)^{V*}	0.31 (0.03)^{a,b*}	0.39 (0.06)^{V*,a*,b*}
*J*ap (mm^4)	G (2,3), D	0.12 (0.05)	0.14 (0.03)	0.10 (0.02)	0.15 (0.03)^{V*}	0.16 (0.02)^{a,b*}	0.20 (0.03)^{V,a*,b*}
n		8	8	8	8	8	8

Data are Mean (SD). ANOVA: significant between-subjects effects of (G) genotype, (D) drug treatment, and the interaction of (G:D) genotype:drug ($p<0.01$). Tukey HSD post-hoc testing of between-subject effect of genotype: significance for (1) wild type vs *Wnt3*$^{+/-}$, (2) wild type vs *Dkk1* KO, (3) *Wnt3*$^{+/-}$ vs *Dkk1* KO ($p<0.01$). Sub-analyses: V=$p<0.05$ compared to vehicle treatment of same genotype; a=$p<0.05$ compared to wild type of same drug treatment; b=$p<0.05$ *Dkk1* KO compared to *Wnt3*$^{+/-}$ of same drug treatment; * indicates stronger significance of $p<0.01$ for sub-analyses.

Table 3: Cancellous and cortical bone parameters of the L1 vertebrae measured by microCT for vehicle or Scl-Ab treated wild type, *Wnt3*$^{+/-}$ and *Dkk1* KO mice.

	Between-subjects effects	Parameters	Wild type		*Wnt3*$^{+/-}$		*Dkk1* KO	
			Vehicle	Scl-Ab	Vehicle	Scl-Ab	Vehicle	Scl-Ab
Cancellous bone	G (1,3), D	BV (mm³)	0.79 (0.18)	1.28 (0.23) ^{V*}	0.62 (0.08) ^{a}	1.04 (0.19) ^{V*,a*}	0.91 (0.16) ^{b*}	1.33 (0.10) ^{V*,b*}
	G (2,3)	TV (mm³)	2.01 (0.13)	1.99 (0.27)	1.99 (0.12)	1.99 (0.07)	1.78 (0.25) ^{a,b}	1.66 (0.17) ^{a*,b*}
	G (1,2,3), D	BV/TV (%)	39.55 (8.94)	64.08 (5.46) ^{V*}	31.03 (2.94) ^{a*}	52.16 (9.63) ^{V*,a*}	51.29 (7.89) ^{a*,b*}	80.48 (3.01) ^{V*,a*,b*}
	G (2,3), D, G:D	TMD (g/cm³)	0.12 (0.02)	0.17 (0.02) ^{V*}	0.11 (0.01)	0.15 (0.02) ^{V*}	0.13 (0.02) ^{a*,b*}	0.22 (0.01) ^{V*,a*,b*}
	G (1,2,3), D, G:D	Tb.Th (mm)	0.27 (0.04)	0.20 (0.02) ^{V*}	0.29 (0.02)	0.23 (0.03) ^{V*,a*}	0.20 (0.01) ^{b*}	0.16 (0.01) ^{V*,a*,b*}
	G (1,2,3), D	Tb.Sp (mm)	3.22 (0.38)	3.69 (0.18) ^{V*}	2.86 (0.20)	3.48 (0.26) ^{V*,a}	3.92 (0.2) ^{a*,b*}	3.61 (0.22) ^{V*,a*,b*}
	G (1,2,3), D, G:D	Tb.N (mm^{-1})	0.68 (0.03)	0.87 (0.05) ^{V*}	0.68 (0.03) ^{a*}	0.82 (0.05) ^{V*}	0.75 (0.08) ^{a*,b*}	1.02 (0.07) ^{V}
Cortical bone	G (3), D	BV (mm³)	1.02 (0.05)	1.25 (0.14) ^{V*}	0.98 (0.05)	1.18 (0.08) ^{V*}	1.07 (0.14)	1.27 (0.08) ^{V*}
	G (2), D	TV (mm³)	3.01 (0.20)	3.29 (0.36) ^{V}	3.02 (0.18)	3.22 (0.12)	2.88 (0.34)	2.95 (0.18) ^{a*,b}
	D	TMD (g/cm³)	1.06 (0.04)	1.23 (0.05) ^{V*}	1.06 (0.05)	1.20 (0.05) ^{V*}	1.08 (0.06)	1.27 (0.04) ^{V*,b}
	D	Ct.Th (mm)	0.16 (0.02)	0.16 (0.01)	0.15 (0.01) ^{a}	0.15 (0.01)	0.14 (0.00) ^{a*}	0.15 (0.02)
		Ps (mm)	6.09 (0.30)	6.14 (0.38)	6.03 (0.18)	6.10 (0.16)	5.99 (0.42)	5.81 (0.20)
	G (3), D	Ec (mm)	4.44 (0.45)	5.06 (0.28) ^{V*}	4.33 (0.41)	4.90 (0.25) ^{V*}	4.88 (0.33) ^{b*}	5.02 (0.17)
n			10	10	10	7	6	7

Data are Mean (SD). ANOVA: significant between-subjects effects of (G) genotype, (D) drug treatment, and the interaction of (G:D) genotype:drug ($p<0.05$). Tukey HSD post-hoc testing of between-subject effect of genotype: significance for (1) wild type vs *Wnt3*$^{+/-}$, (2) wild type vs *Dkk1* KO, (3) *Wnt3*$^{+/-}$ vs *Dkk1* KO ($p<0.05$). Sub-analyses: V=$p<0.05$ compared to vehicle treatment of same genotype; a=$p<0.05$ compared to wild type of same drug treatment; b=$p<0.05$ *Dkk1* KO compared to *Wnt3*$^{+/-}$ of same drug treatment; * indicates stronger significance of $p<0.01$ for sub-analyses.

SUPPLEMENTARY DATA

Supplementary Table 1: Cortical bone parameters of the tibial diaphysis, starting 37% down the tibia, measured by microCT for wild type, *Wnt3*$^{+/-}$ and *Dkk1* KO mice, which underwent vehicle or Scl-Ab treatment.

	Between-subjects	Wild type		*Wnt3*$^{+/-}$		*Dkk1* KO	
Parameters	**effects**	**Vehicle**	**Scl-Ab**	**Vehicle**	**Scl-Ab**	**Vehicle**	**Scl-Ab**
BV (mm^3)	G (2,3), D	0.54 (0.07)	0.60 (0.07)^{V}	0.50 (0.03)	0.61 (0.05)^{V*}	0.57 (0.02)^{b*}	0.69 (0.05)^{V*,a*,b*}
TV (mm^3)	G (2,3), D	0.87 (0.14)	0.86 (0.10)	0.78 (0.06)	0.90 (0.07)^{V}	0.88 (0.04)^{b}	1.02 (0.08)^{V*,a*,b*}
TMD (g/cm^3)	D	1.14 (0.03)	1.18 (0.04)^{V}	1.11 (0.02)	1.18 (0.04)^{V*}	1.12 (0.05)	1.16 (0.03)^{V}
Ct.Th (mm)	G (1,3), D	0.28 (0.01)	0.31 (0.02)^{V*}	0.26 (0.01)^{a}	0.31 (0.01)^{V*}	0.28 (0.01)^{b*}	0.32 (0.01)^{V*}
Ps (mm)	G (2,3), D	5.57 (0.49)	5.61 (0.35)	5.47 (0.23)	5.76 (0.26)	5.81 (0.17)^{b}	6.07 (0.26)^{a*}
Ec (mm)	G (2,3)	3.33 (0.45)	3.05 (0.27)	3.17 (0.19)	3.18 (0.19)	3.55 (0.18)^{b}	3.84 (0.47)^{a*,b*}
J (mm^4)	D	0.47 (0.16)	0.49 (0.11)	0.40 (0.06)	0.54 (0.09)^{V}	0.51 (0.04)	0.60 (0.16)
*I*ap (mm^4)	G (3), D	0.33 (0.11)	0.35 (0.08)	0.29 (0.05)	0.38 (0.07)^{V}	0.35 (0.04)	0.44 (0.07)^{V,a*}
n		8	8	8	8	8	8

Data are Mean (SD). ANOVA: significant between-subjects effects of (G) genotype, (D) drug treatment, and the interaction of (G:D) genotype:drug ($p<0.01$). Tukey HSD post-hoc testing of between-subject effect of genotype: significance for (1) wild type vs *Wnt3*$^{+/-}$, (2) wild type vs *Dkk1* KO, (3) *Wnt3*$^{+/-}$ vs *Dkk1* KO ($p<0.05$). Sub-analyses: V=$p<0.05$ compared to vehicle treatment of same genotype; a=$p<0.05$ compared to wild type of same drug treatment; b=$p<0.05$ *Dkk1* KO compared to *Wnt3*$^{+/-}$ of same drug treatment; * indicates stronger significance of $p<0.01$ for sub-analyses.

REFERENCES

1. Krishnan V, Bryant HU, Macdougald OA. Regulation of bone mass by Wnt signaling. The Journal of clinical investigation. 2006;116(5):1202-9.

2. Robling AG, Niziolek PJ, Baldridge LA, Condon KW, Allen MR, Alam I, et al. Mechanical stimulation of bone in vivo reduces osteocyte expression of Sost/sclerostin. J Biol Chem. 2008;283(9):5866-75.

3. Li J, Sarosi I, Cattley RC, Pretorius J, Asuncion F, Grisanti M, et al. Dkk1-mediated inhibition of Wnt signaling in bone results in osteopenia. Bone. 2006;39(4):754-66.

4. Guo J, Liu M, Yang D, Bouxsein ML, Saito H, Galvin RJ, et al. Suppression of Wnt signaling by Dkk1 attenuates PTH-mediated stromal cell response and new bone formation. Cell Metab. 2010;11(2):161-71.

5. Yao GQ, Wu JJ, Troiano N, Insogna K. Targeted overexpression of Dkk1 in osteoblasts reduces bone mass but does not impair the anabolic response to intermittent PTH treatment in mice. Journal of bone and mineral metabolism. 2011;29(2):141-8.

6. Loots GG, Kneissel M, Keller H, Baptist M, Chang J, Collette NM, et al. Genomic deletion of a long-range bone enhancer misregulates sclerostin in Van Buchem disease. Genome Res. 2005;15(7):928-35.

7. Rhee Y, Allen MR, Condon K, Lezcano V, Ronda AC, Galli C, et al. PTH receptor signaling in osteocytes governs periosteal bone formation and intracortical remodeling. J Bone Miner Res. 2011;26(5):1035-46.

8. Winkler DG, Sutherland MK, Geoghegan JC, Yu C, Hayes T, Skonier JE, et al. Osteocyte control of bone formation via sclerostin, a novel BMP antagonist. The EMBO journal. 2003;22(23):6267-76.

9. MacDonald BT, Joiner DM, Oyserman SM, Sharma P, Goldstein SA, He X, et al. Bone mass is inversely proportional to Dkk1 levels in mice. Bone. 2007;41(3):331-9.

10. Kramer I, Kneissel M. The high bone mass phenotype of Sost deficient mice is characterized by progressive increase in bone thickness, mineralization and predicted cortical bone strength in a gene dosage unrelated manner. Bone. 2008;42, Supplement 1(0):S57.

11. Li X, Ominsky MS, Niu QT, Sun N, Daugherty B, D'Agostin D, et al. Targeted deletion of the sclerostin gene in mice results in increased bone formation and bone strength. J Bone Miner Res. 2008;23(6):860-9.

12. McDonald MM, Morse A, Schindeler A, Mikulec K, Peacock L, Cheng T, et al. Homozygous Dkk1 Knockout Mice Exhibit High Bone Mass Phenotype Due to Increased Bone Formation. Calcif Tissue Int. 2017. [Epub ahead of print].

13. Staehling-Hampton K, Proll S, Paeper BW, Zhao L, Charmley P, Brown A, et al. A 52-kb deletion in the SOST-MEOX1 intergenic region on 17q12-q21 is associated with van Buchem disease in the Dutch population. American journal of medical genetics. 2002;110(2):144-52.

14. Balemans W, Ebeling M, Patel N, Van Hul E, Olson P, Dioszegi M, et al. Increased bone density in sclerosteosis is due to the deficiency of a novel secreted protein (SOST). Human molecular genetics. 2001;10(5):537-43.

15. Gardner JC, van Bezooijen RL, Mervis B, Hamdy NA, Lowik CW, Hamersma H, et al. Bone mineral density in sclerosteosis; affected individuals and gene carriers. J Clin Endocrinol Metab. 2005;90(12):6392-5.

16. Chang MK, Kramer I, Keller H, Gooi JH, Collett C, Jenkins D, et al. Reversing LRP5-dependent osteoporosis and SOST-deficiency induced sclerosing bone disorders by altering WNT signaling activity. J Bone Miner Res. 2014;29(1):29-42.

17. van Lierop A, Moester M, Hamdy N, Papapoulos S. Serum Dickkopf 1 Levels in Sclerostin Deficiency. J Clin Endocrinol Metab. 2014;99(2):E252-6.

18. Florio M, Gunasekaran K, Stolina M, Li X, Liu L, Tipton B, et al. A bispecific antibody targeting sclerostin and DKK-1 promotes bone mass accrual and fracture repair. Nature communications. 2016;7:11505.

19. Ominsky M SR, Jolette J, et. al. . Long-term Sclerostin Antibody Treatment in Cynomolgus Monkeys: Sustained Improvements in Vertebral Microarchitecture and Bone Strength Following a Temporal Increase in Cancellous Bone Formation. Journal of Bone and Mineral Research. 2012;27(S1):S1-S.

20. van Lierop AH, Hamdy NA, Hamersma H, van Bezooijen RL, Power J, Loveridge N, et al. Patients with sclerosteosis and disease carriers: human models of the effect of sclerostin on bone turnover. J Bone Miner Res. 2011;26(12):2804-11.

21. Lewis SL, Khoo PL, De Young RA, Steiner K, Wilcock C, Mukhopadhyay M, et al. Dkk1 and Wnt3 interact to control head morphogenesis in the mouse. Development. 2008;135(10):1791-801.

22. Mukhopadhyay M, Shtrom S, Rodriguez-Esteban C, Chen L, Tsukui T, Gomer L, et al. Dickkopf1 is required for embryonic head induction and limb morphogenesis in the mouse. Dev Cell. 2001;1(3):423-34.

23. Liu P, Wakamiya M, Shea MJ, Albrecht U, Behringer RR, Bradley A. Requirement for Wnt3 in vertebrate axis formation. Nature genetics. 1999;22(4):361-5.

24. Chandra A, Lin T, Young T, Tong W, Ma X, Tseng WJ, et al. Suppression of Sclerostin Alleviates Radiation-Induced Bone Loss by Protecting Bone-Forming Cells and Their Progenitors Through Distinct Mechanisms. J Bone Miner Res. 2017;32(2):360-72.

25. Morse A, Schindeler A, McDonald MM, Kneissel M, Kramer I, Little DG. Sclerostin antibody augments the anabolic bone formation response in a mouse model of mechanical tibial loading. J Bone Miner Res. 2017. [Epub ahead of print].

26. Morse A, McDonald MM, Kelly NH, Melville KM, Schindeler A, Kramer I, et al. Mechanical load increases in bone formation via a sclerostin-independent pathway. J Bone Miner Res. 2014;29(11):2456-67.

27. Moustafa A, Sugiyama T, Prasad J, Zaman G, Gross T, Lanyon L, et al. Mechanical loading-related changes in osteocyte sclerostin expression in mice are more closely associated with the subsequent osteogenic response than the peak strains engendered. Osteoporosis International. 2012;23(4):1225-34

28. Lynch ME, Main RP, Xu Q, Walsh DJ, Schaffler MB, Wright TM, et al. Cancellous bone adaptation to tibial compression is not sex dependent in growing mice. J Appl Physiol. 2010;109(3):685-91.

29. Fritton JC, Myers ER, Wright TM, van der Meulen MC. Loading induces site-specific increases in mineral content assessed by microcomputed tomography of the mouse tibia. Bone. 2005;36(6):1030-8.

30. Li X, Grisanti M, Fan W, Asuncion FJ, Tan HL, Dwyer D, et al. Dickkopf-1 regulates bone formation in young growing rodents and upon traumatic injury. J Bone Miner Res. 2011;26(11):2610-21.

31. McClung MR, Grauer A, Boonen S, Bolognese MA, Brown JP, Diez-Perez A, et al. Romosozumab in Postmenopausal Women with Low Bone Mineral Density. The New England journal of medicine. 2014;370(5):412-20.

32. Recker RR, Benson CT, Matsumoto T, Bolognese MA, Robins DA, Alam J, et al. A randomized, double-blind phase 2 clinical trial of blosozumab, a sclerostin antibody, in postmenopausal women with low bone mineral density. J Bone Miner Res. 2015;30(2):216-24.

33. Cosman F, Crittenden DB, Adachi JD, Binkley N, Czerwinski E, Ferrari S, et al. Romosozumab Treatment in Postmenopausal Women with Osteoporosis. The New England journal of medicine. 2016;375(16):1532-43.

34. Holdsworth G, Greenslade K, Jose J, Stencel Z, Kirby H, Moore A, et al. Dampening of the bone formation response following repeat dosing with sclerostin antibody in mice is associated with up-regulation of Wnt antagonists. Bone. 2017;107:93-103.

35. McClung MR CA, Brown JP, Diez-Perez A, Resch H, Caminis J, Bolognese MA, Goemaere S, Bone HG, Zanchetta JR, Maddox J, Rosen O, Bray S, Grauer A, . OP0251 Effects of 2 Years of Treatment with Romosozumab Followed by 1 Year of Denosumab or Placebo in Postmenopausal Women with Low Bone Mineral Density. Annals of the Rheumatic Diseases. 2015;74(Suppl 2):166-7.

Chapter 5. Sclerostin antibody augments the anabolic bone formation response in a mouse model of mechanical tibial loading

This chapter has been published as:

Morse A, Schindeler A, McDonald MM, Kneissel M, Kramer I, Little DG. Sclerostin antibody augments the anabolic bone formation response in a mouse model of mechanical tibial loading. J Bone Miner Res. 2017 Nov 1 [Epub ahead of print].

ORIGINAL ARTICLE

JBMR®

Sclerostin Antibody Augments the Anabolic Bone Formation Response in a Mouse Model of Mechanical Tibial Loading

Alyson Morse,[1,2] Aaron Schindeler,[1,2] Michelle M McDonald,[3] Michaela Kneissel,[4] Ina Kramer,[4] and David G Little[1,2]

[1]Orthopaedic Research & Biotechnology Unit, The Children's Hospital at Westmead, Westmead, Australia
[2]Discipline of Paediatrics and Child Health, Sydney Medical School, University of Sydney, Sydney, Australia
[3]Bone Biology Program, The Garvan Institute of Medical Research, Darlinghurst, Australia
[4]Novartis Pharma, Basel, Switzerland

ABSTRACT

Decreased activity or expression of sclerostin, an endogenous inhibitor of Wnt/β-catenin signaling, results in increased bone formation and mass. Antibodies targeting and neutralizing sclerostin (Scl-Ab) have been shown to increase bone mass and reduce fracture risk. Sclerostin is also important in modulating the response of bone to changes in its biomechanical environment. However, the effects of Scl-Ab on mechanotransduction are unclear, and it was speculated that the loading response may be altered for individuals receiving Scl-Ab therapy. To address this, we carried out a 2-week study of tibial cyclic compressive loading on C57Bl/6 mice treated with vehicle or 100 mg/kg/wk Scl-Ab. Increases in bone volume, density, and dynamic bone formation were found with loading, and the anabolic response was further increased by the combination of load and Scl-Ab. To investigate the underlying mechanism, gene profiling by RNA sequencing (RNAseq) was performed on tibias isolated from mice from all four experimental groups. Major alterations in Wnt/β-catenin gene expression were found with tibial loading, however not with Scl-Ab treatment alone. Notably, the combination of load and Scl-Ab elicited a synergistic response from a number of specific Wnt-related and mechanotransduction factors. An unexpected finding was significant upregulation of factors in the Rho GTPase signaling pathway with combination treatment. In summary, combination therapy had a more profound anabolic response than either Scl-Ab or loading treatment alone. The Wnt/β-catenin and Rho GTPase pathways were implicated within bone mechanotransduction and support the concept that bone mechanotransduction is likely to encompass a number of interconnected signaling pathways. © 2017 American Society for Bone and Mineral Research.

KEY WORDS: WNT/β-CATENIN/LRPS; THERAPEUTICS; ANABOLICS; BONE QCT/μCT; PRECLINICAL STUDIES

Introduction

Osteoporosis is a prevalent and debilitating bone fragility disorder where a reduction in bone mass leads to an increase in fracture risk. Osteoporosis is most common in postmenopausal women; however, it can affect men and women of any age. Some pediatric bone disorders can also lead to bone fragility (eg, osteogenesis imperfecta), but individuals with disuse osteopenia and cerebral palsy also show increased fracture risk.[1–3] Antiresorptive drugs, particularly bisphosphonates, are the mainstay of current therapeutic interventions for bone fragility. These agents may have limited therapeutic benefit, however, in situations where anabolism is deficient.[2,4,5]

As a nonpharmaceutical intervention, exercise featuring bone loading has been demonstrated to increase bone mass and resistance to fracture.[6–8] Although such treatments capitalize on the biomechanical responsiveness of bone, this is not suitable for all patients. Thus, drugs that promote increased bone formation have been developed as an alternative or adjunctive treatment. Parathyroid hormone (PTH) analogs teriparatide and, more recently, abaloparatide have been shown to increase bone mineral density (BMD) and decrease fracture rate in clinical trials.[9–11] Neutralizing antibodies to sclerostin (Scl-Ab) are another bone anabolic therapeutic principle that targets the sclerostin protein and abrogates its inhibition of Wnt/β-catenin signaling.[12] Sclerostin is expressed chiefly by osteocytes[13–15] and acts upon osteoblasts in a paracrine manner. The major effect of Scl-Ab is the stimulation of bone formation;[16] however, human clinical trials of Scl-Ab have also shown decreases in bone resorption alongside increased bone formation.[17]

Received in original form July 27, 2017; revised form October 11, 2017; accepted October 29, 2017. Accepted manuscript online November 1, 2017.
Address correspondence to: David Little, FRACS(Orth), PhD, Orthopaedic Research and Biotechnology, The Children's Hospital at Westmead, Locked Bag 4001, Westmead, NSW, 2145, Australia. E-mail: david.little@health.nsw.gov.au
Additional Supporting Information may be found in the online version of this article.
Journal of Bone and Mineral Research, Vol. 33, No. xx, Month 2018, pp 1–13
DOI: 10.1002/jbmr.3330

Sclerostin plays a major role in mechanotransduction within bone. Both acute and chronic deficiency in sclerostin can prevent bone loss associated with reduced loading.[18–20] Conversely, upregulation of sclerostin has been shown to prevent the added bone anabolism associated with increased loading.[21] However, it is not clear whether Scl-Ab therapy and increased mechanical stimulation of bone are redundant. If so, there would be expected to be no additional benefit to recommending biomechanical loading exercise to individuals on Scl-Ab for treatment of low bone mass or bone mineral density (BMD).

In a recent study, we analyzed mechanical loading in a genetic knockout mouse model of sclerostin gene (*Sost*) deficiency.[20] In this model, there was no attenuation of the response to cyclic compressive loading in the *Sost* knockout mice. Indeed, the combination of loading and *Sost* deficiency resulted in an augmentation of the anabolic response. It was hypothesized that these findings may translate to short-term Scl-Ab therapy, which may show synergistic benefits with exercise-based loading programs.

In this study, we tested this concept in C57Bl/6 mice via 2 weeks of cyclic compressive loading of the tibia. Mice were treated with vehicle or 100 mg/kg/wk Scl-Ab in parallel during this period of biomechanical loading. Radiographic and histomorphometric measures were used to investigate functional changes in bone volume and bone formation, and RNASeq was used to investigate mechanistic changes in gene expression.

Materials and Methods

Animals and Scl-Ab treatment

A total of 36 female 9-week-old C57BL/6J mice ($n = 18$ vehicle/Scl-Ab treatment) were sourced from Animal Resources Centre (Murdoch, Australia) and acclimatized for 1 week before treatment. Animals were housed 4/cage and given water and rodent chow *ad libitum*. Studies were approved under South Western Area Health Service (SWAHS) ethics protocol 4174.

A neutralizing human monoclonal antibody to sclerostin (sclerostin antibody/Scl-Ab) that binds human and mouse sclerostin was gifted by Novartis Pharma AG (Basel, Switzerland). At 10 weeks of age, on day (D)0, randomly allocated mice were intravenously injected with vehicle (isotonic buffer pH 5.3) or 100 mg/kg Scl-Ab, a concentration previously shown to be effective in mice.[22] A second dose was administered at D7. An overview of the study design, including dosing, dual-energy X-ray absorptiometry (DXA), tibial loading, and euthanasia, is summarized in Fig. 1*A* and is described in detail below.

In vivo tibial mechanical loading for radiographic and bone formation assessment

Mice commenced unilateral cyclic axial compression of the left tibia at D1 ($n = 8$ for vehicle and Scl-Ab antibody treatment). Briefly, 1200 cycles were applied at a rate of 4 Hz, 5 d/wk for

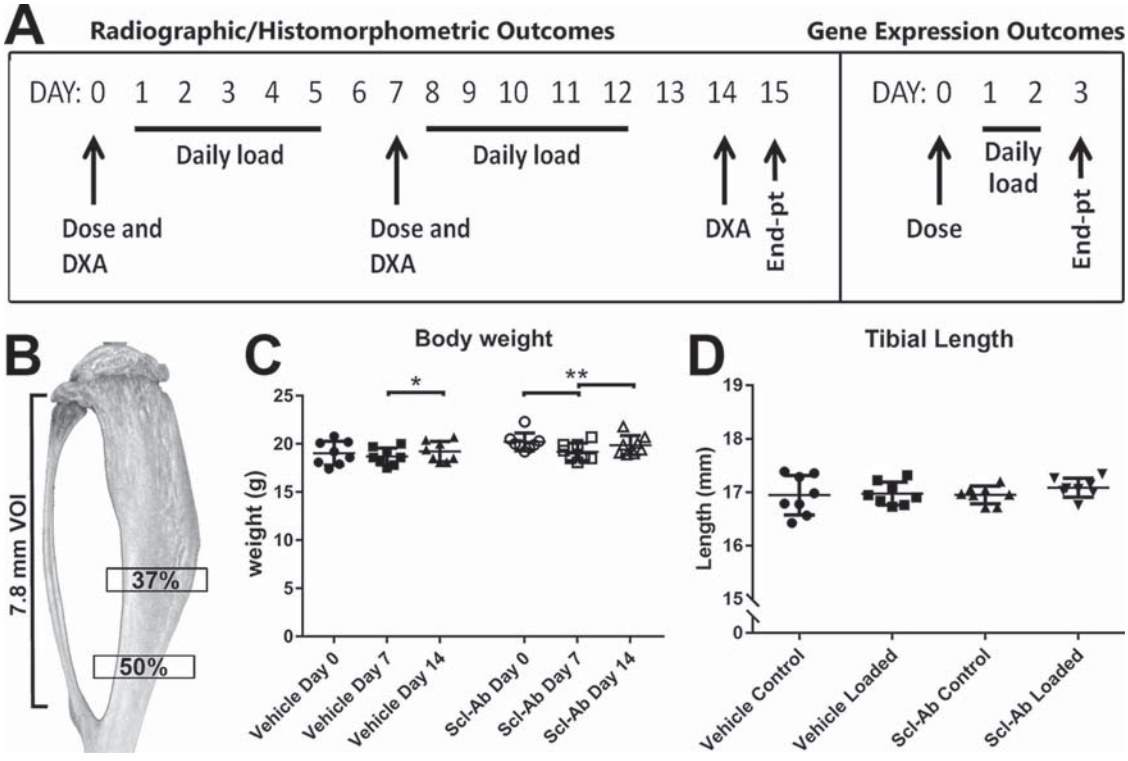

Fig. 1. (*A*) Study design for radiographic/histomorphometry outcomes ($n = 8$) and gene expression outcomes ($n = 10$). For each mouse, vehicle/Scl-Ab (100 mg/kg iv) dosing was administered on D0 and D7. DXA was performed on D0, D7, and D14. Tibial compressive cyclic loading of the left tibia was performed D1–5 and D8–12. Endpoint was D15 for radiographic/histomorphometry outcomes and D3 for gene expression outcomes. (*B*) Graphical depiction of the VOIs assessed by μCT (fibula excluded from all analysis). A 7.8 mm height VOI was used to assess the tibia from 0.5 mm below the growth plate to above the tibia-fibula junction. A 0.5 mm height VOI was used to assess the mid-diaphysis of the tibias, 37% and 50% down the length of the tibias from the proximal end. (*C*) Weekly body weights for the mice that underwent 2 weeks of tibial loading. Between-group analyses (*t* test): $^{*}p < 0.05$, $^{**}p < 0.01$. (*D*) Left tibia length of each mouse after 2 weeks of tibial loading.

2 weeks, with rest on D6, D7, D13, and D14. Cycles were in a triangular waveform with a peak load of −9.0 N to engender 1200 με on the midshaft of 10-week-old C57Bl/6J mice, as previously described.[20,23] Right tibias behaved as contralateral non-loaded controls. Mice were monitored and weighed daily, and weekly body weights were recorded.

Mice were subcutaneously injected with calcein (10 mg/kg, Sigma, St. Louis, MO, USA) 10 and 3 days before euthanization. Mice were euthanized at D15 by CO_2 asphyxiation. Right (control) and left (loaded) tibias were dissected and fixed for 24 hr in 10% formalin and stored in 70% ethanol. Right and left tibias were X-rayed and their length measured (Faxitron X-ray Corp., Wheeling, IL, USA).

Dual-energy X-ray absorptiometry

DXA (GE Lunar PIXImus; Lunar Piximus Corp., Madison, WI, USA) was performed at D0, D7, and D14 under inhaled isoflurane anesthesia. Blinded to drug treatment but not load, a region of interest of 30 × 13 (LxW) pixels was analyzed in the diaphysis, centered halfway along the tibia. BMD and bone mineral content (BMC) were obtained and fold-change from D0 assessed at each time point.

Microcomputed tomography

Right and left tibias were μCT scanned ex vivo (Skyscan 1174 2; Skyscan NV, Kontich, Belgium) using 12 μm isotropic voxel resolution, 0.5 mm aluminum filter, 50 kV X-ray tube voltage, 800 μA tube electric current, and 4500 ms exposure time. Images were reconstructed using a 0–0.1 greyscale (NRecon v1.6.1.7; Skyscan NV) and analyzed with CTAnalyser (Skyscan NV). The minimum threshold for bone was 0.4 g/cm^3, correlated to phantoms of known density.

All analyses excluded the fibula and were performed blinded to drug treatment but not load. A volume of interest (VOI) denoted "7.8 mm VOI" was selected, commencing 0.5 mm below the growth plate and finishing 7.8 mm distally, proximal to the tibia-fibula joint (Fig. 1*B*). Consecutive VOIs of height 0.06 mm were assessed along the 7.8 mm VOI and plotted on a histogram to visualize bone volume change along the bone after loading (loaded BV-control BV) for Scl-Ab- and vehicle-treated mice.

Subregional analysis within the diaphysis was performed on a VOI of height 0.5 mm commencing 37% down the tibia from the proximal end (Fig. 1*B*). This VOI corresponds with other published studies examining dynamic loading of murine tibias.[20,24–26] A second VOI of the same height but 50% down the tibia was also analyzed and supplied as supplemental data. A metaphyseal region representing the secondary spongiosa was assessed; VOI height 1.2 mm, commencing 0.5 mm below the proximal growth plate. All bone was assessed, as well as separate subanalyses of trabecular and cortical bone compartments. Bone parameters assessed included bone volume (BV), total volume (TV), BV/TV, tissue mineral density (TMD), as well as trabecular thickness (Tb.Th), within the trabecular bone compartment, and cortical thickness (Ct.Th), periosteal surface (Ps), endocortical surface (Ec), and polar moment of inertia (J) within the cortical bone compartment.

Dynamic bone histomorphometry

Using a diamond saw, the tibias were transversely cut 37% down from the proximal end of the tibias. The cross-sectional surface was smoothed using sandpaper of grit P1200 and cleaned in 70% ethanol. Samples were placed with the cross-sectional area of interest facing down on a plastic dish in 70% ethanol and were scanned and imaged using Leica TCS SP5 confocal microscope at 20× magnification (Leica Microsystems, North Ryde, Australia). The exposure time, *z*-stack, gain, and offset remained consistent for all specimens. The endosteal and periosteal surfaces of each cross-sectional sample were analyzed for daily mineral apposition rate (MAR), mineralizing surface/bone surface (MS/BS), and bone formation rate/bone surface (BFR/BS) using BIOQUANT measure 32 Nova Prime (Nashville, TN, USA). Analyses were performed blinded to drug treatment but not load. The tibias were also transversely cut 50% down the bone and similarly prepared and analyzed (supplied as supplemental data).

Statistical analysis

The within-subject effect of loading (control, loaded limbs) and the between-subject effect of drug treatment (vehicle, Scl-Ab) as well as the interactions between these terms were assessed using a mixed ANOVA. For DXA analyses, the interactions between the terms of time (D0, D7, D14) and drug treatment and between time and loading were respectively assessed by mixed and two-way repeated measures ANOVAs. Subanalyses between drug treatment groups was performed using parametric independent samples *t* test. Analysis of contralateral tibiae (control versus loaded within treatment groups) was performed using parametric paired samples *t* test. For all testing, a value of $p < 0.05$ was considered significant. All analysis was performed using IBM SPSS Statistics 20 (SPSS Inc., Chicago, IL, USA) and graphed with GraphPad Prism 7 (GraphPad Software, La Jolla, CA, USA).

Specimen preparation for RNA sequencing (RNAseq) studies

At age 10 weeks, on D1 (1 day after vehicle/Scl-Ab treatment), 20 mice ($n = 10$ vehicle/Scl-Ab) commenced unilateral cyclic axial compression of the left tibia under the same conditions as the mice for radiographic/bone formation assessment. However, these mice received loading on D1 and D2 only and were euthanized 24 hr later on D3 (Fig. 1*A*). Euthanasia (cervical dislocation) was just before tibial dissection. The right (control) tibia was dissected quickly and within an RNase-free environment. The tibia was cleaned thoroughly of soft tissue and the bone scraped clean using a scalpel. The proximal and distal ends of the bone were cut off to leave the bone shaft. The shaft was flushed of marrow using DEPC-treated water, and the clean bone was placed in 2 mL Trizol, homogenized using a Polytron PT2100 (Kinematica, Lucerne, Switzerland) and placed on dry ice immediately. This was repeated for the left (loaded) tibia of the same mouse. The entire process of euthanasia and dissection was repeated for each mouse in turn and the homogenizer was cleaned thoroughly between each tibia. The homogenized samples in Trizol were stored at −80°C.

RNA isolation and whole transcriptome RNAseq

Samples were thawed on ice and total RNA isolated using chloroform separation and the miRNeasy Mini Kit (Qiagen, Valencia, CA, USA) per the manual instructions. Quality and concentration of RNA was accessed via the 2100 Bioanalyzer (Agilent Technologies, Santa Clara, USA). For RNAseq, $n = 6$/group of the highest quality RNA was used. The RNA integrity number for all samples fell between 6.6 and 9.3.

RNAseq (100 bp single end reads) was performed via the Australian Genome Research Facility (AGRF, Parkville, Australia) using the Illumina HiSeq2000 (Illumina, Inc., San Diego, CA, USA). Image analysis was performed in real time by the HiSeq Control Software (HCS) v1.4.8 and Real Time Analysis (RTA) v1.18.61 (Illumina, Inc.). Primary sequence data were generated via Illumina CASAVA 1.8.2 pipeline (Illumina, Inc.), quality-checked by FastQC (per-base sequence quality >88% bases above Q30), and screened for Illumina adaptor/overrepresented sequences and cross-species contamination. Cleaned sequence reads were aligned against the Mus musculus genome (build version mm10) using Tophat aligner (v1.3.1).[27] Transcripts were assembled with the Cufflinks tool (v2.2.1) utilizing GENCODE annotation version M4 (http://www.gencodegenes.org) for the Mus musculus genome (build version mm10) and reference annotation based assembly option (RABT).

Assembled transcripts underwent quantification, normalization, and differential expression analysis using cluster profiler. Analysis of differentially expressed genes (DEGs) was undertaken using the bioconductor package edgeR.[28] A false-discovery rate (FDR, q value) <0.05 was used. Comparisons 1–4 assessed between groups are listed in Table 1. DEGs common and unique between comparisons were investigated and numbers represented in VENN diagrams.[29] Pathway enrichment analyses of gene sets were undertaken using Bioconductor Pathview package.[30] All data were compared with a list of genes possibly from contaminant tissue outside the bone compartment and of which may be present after murine diaphyseal tibial loading, as outlined by Ayturk and colleagues.[31]

Results

Scl-Ab and loading increase BMD, BMC, and BV along the length of the tibias

Compressive axial loading was performed on tibias of vehicle- and Scl-Ab-treated mice. All mice showed evidence of good health for the entirety of the study. A small decline in body weight was found during the first week of the study but normalized by the second week (Fig. 1*C*). Loading or drug treatment did not have any effect on tibial length (Fig. 1*D*).

Longitudinal DXA was performed on the tibia indicating anabolic responses due to both Scl-Ab and loading treatments (Fig. 2*A*). Significant BMC and BMD responses to loading and drug treatment were found by day 14. Further, the effect of drug treatment and time was significant for control (BMD) and loaded limbs (BMC, BMD). Significant effects of loading and time and of drug and time were also observed. Subanalyses showed significant increases in BMC and BMD with the combination of load and Scl-Ab treatment compared with all other groups. Notably, BMC and BMD were significantly greater with the combination therapy compared with Scl-Ab alone at both D7 and D14 ($p < 0.01$) and compared with loading alone (D7 $p < 0.05$, D14 $p < 0.01$). The Vehicle Loaded group showed increased BMD ($p < 0.01$) but not BMC at this time point compared with Vehicle Control. Similar trends were noted for D7 that only reached significance for the Scl-Ab Loaded group.

μCT analysis at D15, performed within a VOI spanning a 7.8 mm length of the tibias, showed significant effects in BV to loading and Scl-Ab treatments. Subanalyses showed that BV was significantly greater in Scl-Ab Loaded tibias compared with Vehicle Loaded tibias (+15%, $p < 0.01$; Fig 2*B*). Without loading, Scl-Ab treatment gave a 13% BV increase compared with Vehicle Control ($p < 0.01$). Loading increased BV within both vehicle- and Scl-Ab-treated mice (Loaded versus Control: +18% vehicle, +20% Scl-Ab, $p < 0.01$), and the loading-induced BV increases were found along the entire tibias in both vehicle- and Scl-Ab-treated mice (Fig. 2*C*).

Scl-Ab and loading increase cortical bone volume and thickness

Murine tibial loading studies commonly focus on the cortical bone, and a subregion within the mid-diaphyseal VOI (37% down the tibias) was selected for detailed μCT analysis (Fig. 3*A*). The effect of loading was significant across all parameters, and the effect of drug treatment was significant within BV, Ct.Th, and polar moment of inertia. Subanalyses showed that BV was significantly greater in Scl-Ab Loaded tibias above Vehicle Loaded tibias (+12%, $p < 0.01$) and Scl-Ab Control tibias (+22%, $p < 0.01$). This was likely driven by a periosteal response within the mid-diaphysis, with small but significant increases in periosteal surface (+7%, $p < 0.01$) and Ct.Th (+15%, $p < 0.01$) in Scl-Ab Loaded tibias above Scl-Ab Control. Strength as predicted by polar moment of inertia (J) was significantly enhanced by the combination therapy; Scl-Ab Loaded tibias were increased +16% and +33% compared with Vehicle Loaded and Scl-Ab non-loaded controls, respectively ($p < 0.05$). Scl-Ab treatment alone significantly increased BV and Ct.Th, confirming the anabolic efficacy of the drug (Vehicle Control versus Scl-Ab Control: +7% BV, $p < 0.05$; +8% Ct.Th, $p < 0.01$). Loading treatment alone also resulted in an anabolic response compared with non-loaded controls within vehicle-treated mice (+17% BV; +3% TMD; +5% Ct.Th; +26% J; $p < 0.01$). In summary, an increased anabolic response with the loading and Scl-Ab combination was found versus either treatment alone.

Representative 3D models for specimens representing the median BV values for each treatment group illustrated the quantitative findings (Fig. 3*B*). A comparable trend was found in the second mid-diaphyseal VOI, 50% down the bone (Supplemental Fig. S1).

A metaphyseal region was also assessed by μCT (Fig. 4). The effect of loading and drug treatment was significant for total (combined cortical and trabecular) BV, cortical BV, and cortical thickness. Subanalyses confirmed a greater loading response within this region within Scl-Ab-treated mice. Parameters including total BV (+60%, +26%, +29%) and BV/TV, trabecular BV (+116%, +58%, +25%), BV/TV, Tb.Th, and TMD, and cortical

Table 1. RNASeq Data Were Assessed for Multiple Comparisons

Comparison		Assessment of:
1	Vehicle Control versus Vehicle Loaded	Genes altered due to loading alone
2	Vehicle Control versus Scl-Ab Control	Genes altered due to Scl-Ab treatment
3	Scl-Ab Control versus Scl-Ab Loaded	Genes altered due to loading in the presence of Scl-Ab
4	Vehicle Loaded versus Scl-Ab Loaded	Genes altered in loaded bones due to Scl-Ab

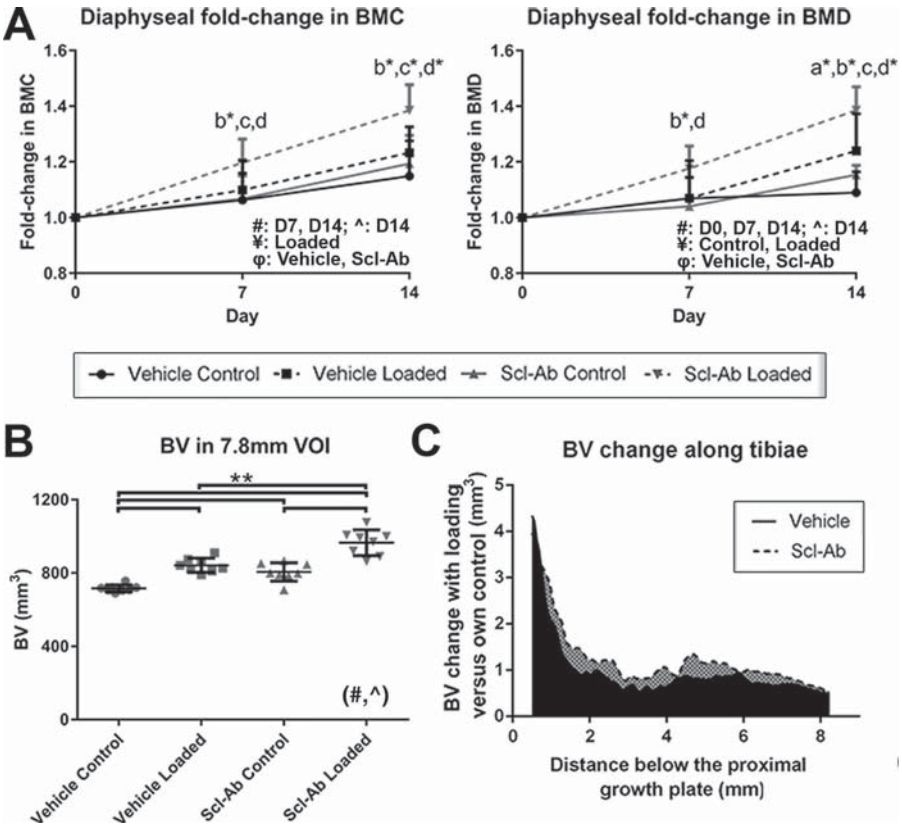

Fig. 2. (*A*) Dual-energy X-ray absorptiometry (DXA) was performed at D0, D7, and D14 on control and loaded tibias, and the mid-diaphysis assessed. Fold-change in bone mineral content (BMC) and bone mineral density (BMD) from D0 was determined for each mouse at D7 and D14, and the mean ± SD shown. ANOVA: bottom right-hand of each graph indicates an effect of (^) drug treatment, (#) loading, (†) loading and drug treatment at each time point, (¥) time and drug treatment for control/loaded limbs, φ) time and loading for each drug treatment. Subanalyses between groups at each time point (*t* test): a = $p < 0.05$ Vehicle Control versus Vehicle Loaded, b = $p < 0.05$ Scl-Ab Control versus Scl-Ab Loaded, c = $p < 0.05$ Vehicle Control versus Scl-Ab Loaded, and d = $p < 0.05$ Vehicle Loaded versus Scl-Ab Loaded. $^{*}p < 0.01$. All groups were compared; only comparisons that were significant are detailed. (*B*) Bone volume (BV) of control and loaded tibias within a 7.8 mm height VOI assessed by μCT. ANOVA: indicates an effect of (^) drug treatment, (#) loading, (†) loading and drug treatment. Subanalyses between groups (*t* test): $^{**}p < 0.01$. (*C*) BV change with loading along the tibias, assessed by μCT. Consecutive 0.06 mm VOIs were assessed along the 7.8 mm VOI for all tibias. The increase in BV for each loaded tibia was determined from their own contralateral control tibia and the mean change for vehicle and Scl-Ab treatment groups were plotted.

BV (+46%, +18%, +31%) and Ct.Th were all significantly greater with combination Scl-Ab and loading treatment, above Vehicle Control, Vehicle Loaded, and Scl-Ab Control, respectively.

The effect of loading on the metaphysis was significant for all parameters, omitting cortical TMD. The effect of drug treatment on the metaphysis was significant for all parameters, omitting total TMD and Ps. Notably, subanalyses showed that within the trabecular compartment, Scl-Ab had a greater anabolic response than loading above Vehicle Control (Vehicle Loaded: BV +37%, BV/TV +23%; Scl-Ab Control: BV +73%, BV/TV +60%). This was not found within the cortical compartment, whereby loading alone elicited a stronger response than Scl-Ab. This suggests a stronger response for Scl-Ab within the trabecular compartment. However, both treatment groups saw significant responses within all parameters, omitting total and cortical TMD, and Ps. These data confirm that both loading and Scl-Ab elicit anabolic responses within the metaphysis and that even greater responses were found with combination therapy.

Scl-Ab and loading increase bone anabolism

The effects of Scl-Ab and loading on mineralization and bone formation rate were analyzed using dynamic bone labeling within the mid-diaphysis, whereby the effect of load was of particular significance on the periosteal surface in all parameters assessed, and the effect of drug treatment was significant for periosteal MS/BS. Subanalyses observed that combination Scl-Ab and loading increased the periosteal response above Scl-Ab alone (+147% MAR; +115% MS/BS; +340% BFR/BS; $p < 0.01$; Fig. 5*A*). Scl-Ab therapy similarly increased the anabolic periosteal response in non-loaded tibias (Vehicle Control versus Scl-Ab Control: +131% MS/BS; +180% BFR/BS; $p < 0.05$). In untreated control animals, load also increased periosteal bone formation (Vehicle Control versus Vehicle Loaded: +259% MAR; +903 BFR; $p < 0.05$). There was no difference in periosteal bone formation between Scl-Ab Loaded and Vehicle Loaded tibias. In contrast, the endosteal response was muted and any changes of statistical significance were small in magnitude (Fig. 5*B*). Representative images are shown within Fig. 5*C*.

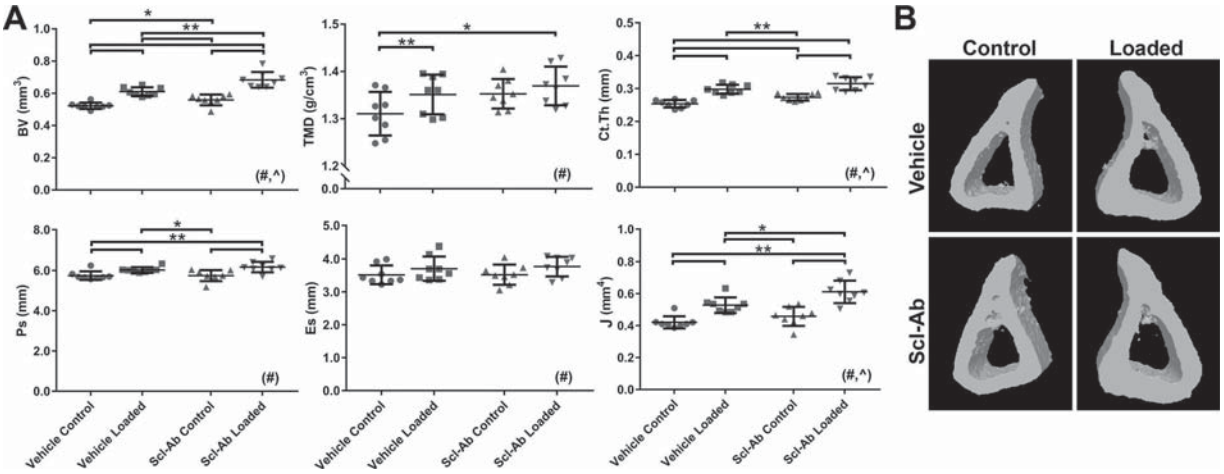

Fig. 3. μCT assessment of the mid-diaphyseal VOI located 37% down the bone from the proximal end, for both control and loaded tibias of all vehicle- and Scl-Ab-treated mice. (*A*) Bone volume (BV), tissue mineral density (TMD), cortical thickness (Ct.Th), periosteal perimeter (Ps), endosteal perimeter (Ec), and polar moment of inertia (J) were assessed for each tibia. ANOVA: indicates an effect of (^) drug treatment, (#) loading, (†) loading and drug treatment. Subanalyses between groups (*t* test): $^{*}p < 0.05$, $^{**}p < 0.01$. (*B*) Representative 3D models of the 37% VOI, located within the mid-diaphysis, for control and loaded tibias of vehicle and Scl-Ab treatment groups.

Differential gene expression in response to Scl-Ab and load

Radiographic and histological data indicated that sclerostin inhibition and cyclic compressive loading led to significant changes in bone volume, density, and formation. To investigate the underlying genetic mechanisms, RNAseq was undertaken using mRNA isolated from bones stripped of periosteum and flushed of marrow. The transcriptome profile, notionally enriched for osteocyte gene expression, were compared between all groups to determine all differentially expressed genes (DEGs; Supplemental Tables S1–S4).

The top 15 upregulated and downregulated genes were determined based on changes associated with load (Table 2) and related to Scl-Ab treatment (Table 3). For later discussion, it

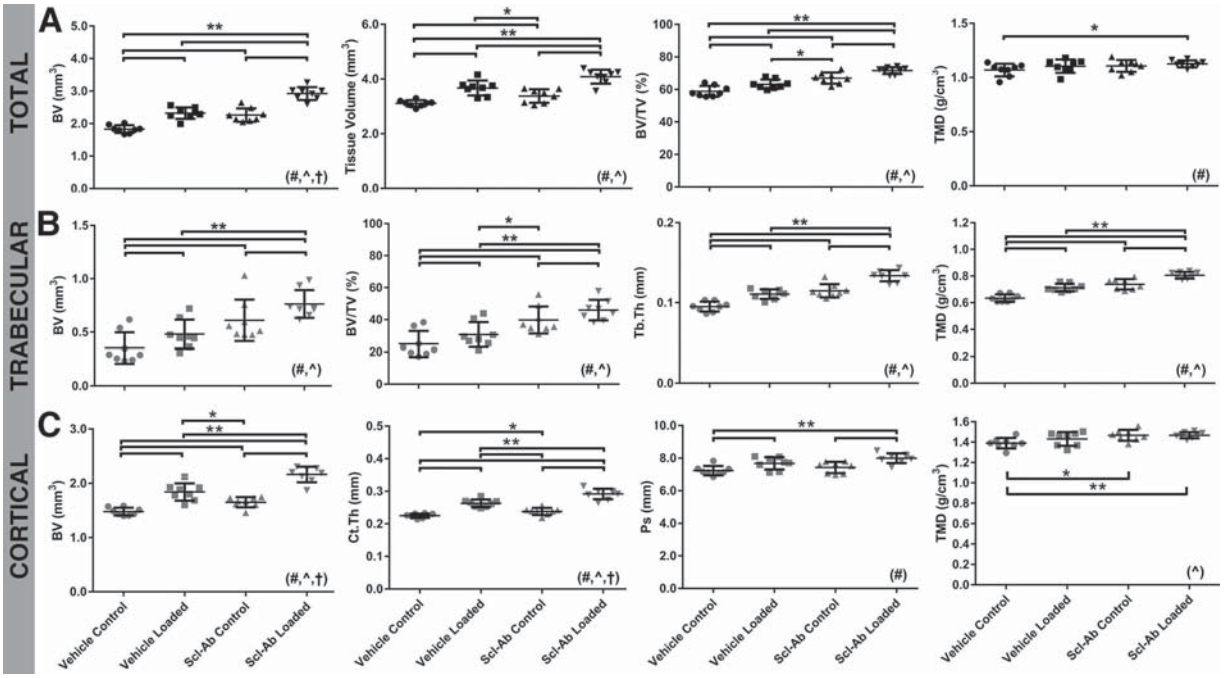

Fig. 4. μCT assessment of the proximal tibial metaphysis for control and loaded tibias of all vehicle- and Scl-Ab-treated mice. (*A*) Total metaphysis (trabecular and cortical compartments): bone volume (BV), tissue volume (TV), BV/TV, tissue mineral density (TMD). (*B*) Trabecular bone compartment: BV, BV/TV, trabecular thickness (Tb.Th), TMD. (*C*) Cortical bone compartment: BV, cortical thickness (Ct.Th), periosteal surface (Ps), TMD. ANOVA: indicates an effect of (^) drug treatment, (#) loading, (†) loading and drug treatment. Subanalyses between groups (*t* test): $^{*}p < 0.05$, $^{**}p < 0.01$.

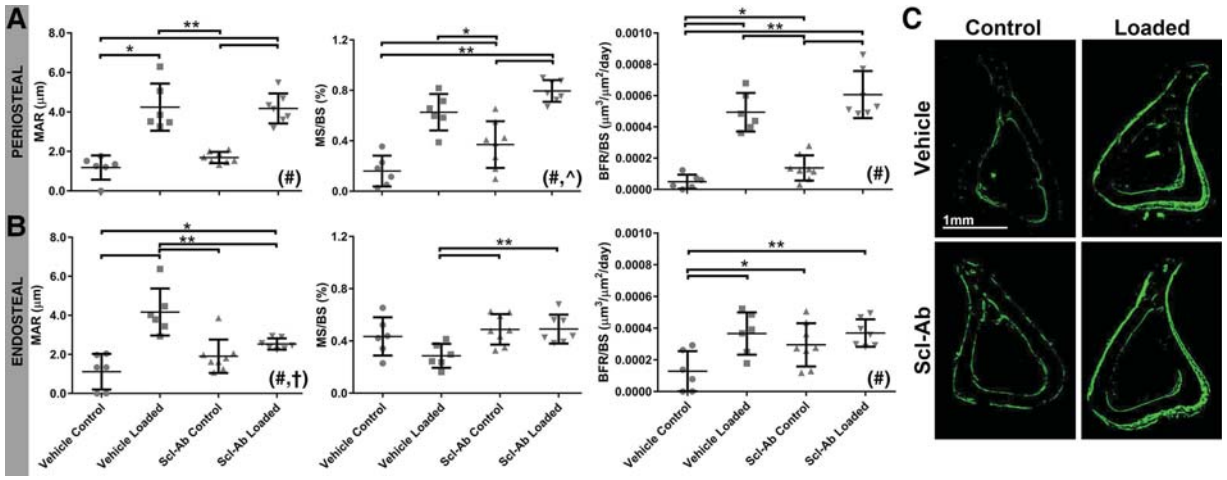

Fig. 5. Dynamic tissue histomorphometry of the mid-diaphyseal VOI located 37% down the bone from the proximal end, for both control and loaded tibias of all vehicle- and Scl-Ab-treated mice. Mineral apposition rate (MAR), mineralizing surface/bone surface (MS/BS), and bone formation rate (BFR/BS) were assessed for periosteal and endosteal surfaces of all tibias. ANOVA: indicates an effect of (^) drug treatment, (#) loading, (†) loading and drug treatment. Subanalyses between groups (*t* test): $^{*}p < 0.05$, $^{**}p < 0.01$. (*A*) Periosteal surface. (*B*) Endosteal surface. (*C*) Representative images of the 37% VOI for control and loaded tibias of Vehicle and Scl-Ab treatment groups.

Table 2. The Top 15 Up- and Downregulated DEGs Related to Loading in Vehicle- and Scl-Ab-Treated Mice

Vehicle Control versus Vehicle Loaded				Scl-Ab Control versus Scl-Ab Loaded			
Gene symbol	Fold change	*p* Value	*q* Value	Gene symbol	Fold change	*p* Value	*q* Value
Gm8034	10.42	5.00E-05	1.98E-03	Tfcp2l1	68.68	5.00E-05	4.42E-03
Gle1	8.61	5.00E-05	1.98E-03	Lonrf3	63.42	5.00E-05	4.42E-03
Rps16	7.80	5.00E-05	1.98E-03	1700030C10Rik,Gm28503, RP23-152O2.3	15.65	5.00E-05	4.42E-03
Igkv4-90	7.46	1.35E-03	3.20E-02	Lhx6	13.53	5.00E-05	4.42E-03
Gm27477,Gm27861,Gm27867, Gm27868,Hotairm1	7.38	5.00E-05	1.98E-03	BC024978	6.67	5.00E-05	4.42E-03
Car12	6.98	5.00E-05	1.98E-03	Gal	5.03	5.00E-05	4.42E-03
Sln	5.94	5.00E-04	1.41E-02	Kera	4.56	2.00E-04	1.36E-02
St7	5.57	5.00E-05	1.98E-03	Nell1	4.37	5.00E-05	4.42E-03
Ighv5-12	5.28	5.00E-05	1.98E-03	Auts2	3.76	5.00E-05	4.42E-03
Panx3	4.88	5.00E-05	1.98E-03	Aif1l	3.64	5.00E-05	4.42E-03
Wnt1	4.88	5.00E-05	1.98E-03	Ighv5-9-1	3.56	6.00E-04	3.14E-02
Serpina3n	4.85	5.00E-05	1.98E-03	Gm12519	3.40	5.00E-05	4.42E-03
Bcan	4.52	5.00E-05	1.98E-03	Ptgs2	3.29	5.00E-05	4.42E-03
Acan	4.51	5.00E-05	1.98E-03	Cfhr2	3.04	1.50E-04	1.11E-02
Thbs4	4.37	5.00E-05	1.98E-03	Nr4a2	2.94	5.00E-05	4.42E-03
2310014L17Rik	0.00	5.00E-05	1.98E-03	Hist1h2ac	0.04	5.00E-05	4.42E-03
Igkv6-13	0.07	5.00E-05	1.98E-03	Gm5269	0.04	5.50E-04	2.94E-02
Igkv3-1	0.10	5.00E-05	1.98E-03	Gm27477,Gm27861,Gm27867, Gm27868,Hotairm1	0.14	1.00E-04	7.94E-03
Ighv1-50	0.17	5.00E-05	1.98E-03	Ighv5-12	0.15	5.00E-05	4.42E-03
Ighv1-72	0.19	5.00E-05	1.98E-03	St7	0.21	5.00E-05	4.42E-03
Gm26397	0.19	5.00E-05	1.98E-03	Ighv14-1	0.21	5.00E-05	4.42E-03
Ighv1-85	0.20	3.00E-04	9.14E-03	Actc1	0.24	5.00E-05	4.42E-03
Igkv4-86	0.21	5.00E-05	1.98E-03	Cyp2e1	0.26	5.00E-05	4.42E-03
Prss30	0.21	5.00E-05	1.98E-03	Arhgap22	0.27	5.00E-05	4.42E-03
Ighv1-18	0.23	5.00E-05	1.98E-03	Igkv4-58	0.30	6.00E-04	3.14E-02
Igkv4-72	0.23	5.00E-05	1.98E-03	Rpl21	0.30	5.00E-05	4.42E-03
Igkv4-70	0.29	5.00E-05	1.98E-03	Shank2	0.32	5.00E-05	4.42E-03
Igkv8-30	0.30	5.50E-04	1.52E-02	Mpz	0.32	5.00E-05	4.42E-03
Igkv15-103	0.34	5.00E-05	1.98E-03	Myoc	0.34	5.00E-05	4.42E-03
Cytl1	0.35	1.00E-04	3.61E-03	Fam65a	0.34	5.00E-05	4.42E-03

Table 3. The Top 15 Up- and Downregulated Genes Related to Scl-Ab Treatment in Control or Loaded Tibias

Vehicle Control versus Scl-Ab Control				Vehicle Loaded versus Scl-Ab Loaded			
Gene symbol	Fold change	*p* Value	*q* Value	Gene symbol	Fold change	*p* Value	*q* Value
Cnga1	121.01	9.00E-04	4.40E-02	Pnpla3	93.58	5.00E-05	3.69E-03
Igkv1-88	49.11	5.00E-05	3.58E-03	Tfcp2l1	68.79	5.00E-05	3.69E-03
Hoxb4	31.15	5.00E-05	3.58E-03	Lonrf3	65.14	5.00E-05	3.69E-03
1700030C10Rik,Gm28503,RP23-152O2.3	13.73	5.00E-05	3.58E-03	1700030C10Rik,Gm28503, RP23-152O2.3	15.30	5.00E-05	3.69E-03
P2rx7	12.86	5.00E-05	3.58E-03	Lhx6	13.43	5.00E-05	3.69E-03
Cep131	10.89	5.00E-05	3.58E-03	BC024978	6.67	5.00E-05	3.69E-03
Med23	7.67	5.00E-05	3.58E-03	Gal	5.18	5.00E-05	3.69E-03
Gm27454,Gm27492,Gm27543, Gm27695,Gm28032,Hoxa11os	6.29	5.00E-05	3.58E-03	Kera	4.74	5.00E-05	3.69E-03
Zfp618	5.87	5.00E-05	3.58E-03	Nell1	4.41	5.00E-05	3.69E-03
Ighv5-16	5.85	5.00E-05	3.58E-03	Auts2	3.99	5.00E-05	3.69E-03
BC024978	5.52	5.00E-05	3.58E-03	Aif1l	3.92	3.00E-04	1.65E-02
Igkv8-27	5.20	5.00E-05	3.58E-03	Ighv5-9-1	3.67	1.00E-04	6.63E-03
Igkv4-69	4.79	2.50E-04	1.49E-02	Ptgs2	3.44	5.00E-05	3.69E-03
Rabl2	4.71	5.00E-05	3.58E-03	Gm12519	3.20	5.00E-05	3.69E-03
Igkv3-4	4.50	5.00E-05	3.58E-03	Cfhr2	3.16	5.00E-05	3.69E-03
2310014L17Rik	0.00	5.00E-05	3.58E-03	Gm5269	0.04	4.00E-04	2.05E-02
Hist1h2ac	0.01	5.00E-05	3.58E-03	Hist1h2ac	0.04	5.00E-05	3.69E-03
Tnni1	0.06	1.00E-04	6.59E-03	Gm8034	0.09	5.00E-05	3.69E-03
Gm26397	0.06	5.00E-05	3.58E-03	Rps16	0.14	5.00E-05	3.69E-03
Igkv3-1	0.10	5.00E-05	3.58E-03	Gm27477,Gm27861,Gm27867, Gm27868,Hotairm1	0.15	5.00E-05	3.69E-03
Igkv4-86	0.12	5.00E-05	3.58E-03	Ighv5-12	0.15	5.00E-05	3.69E-03
C5ar2	0.12	2.00E-04	1.23E-02	St7	0.21	5.00E-05	3.69E-03
Igkv6-13	0.19	5.00E-05	3.58E-03	Actc1	0.23	5.00E-05	3.69E-03
Ighv1-50	0.22	5.00E-05	3.58E-03	Igkv3-7	0.25	5.00E-05	3.69E-03
Myl2	0.24	5.00E-05	3.58E-03	Arhgap22	0.26	5.00E-05	3.69E-03
Ighv1-18	0.24	5.00E-05	3.58E-03	Cyp2e1	0.28	5.00E-05	3.69E-03
Igkv4-72	0.26	5.00E-05	3.58E-03	Rpl21	0.29	1.00E-04	6.63E-03
Ighv1-72	0.30	5.00E-05	3.58E-03	Igkv4-58	0.30	3.00E-04	1.65E-02
Fam65a	0.31	5.00E-05	3.58E-03	Syt8	0.31	5.00E-05	3.69E-03
Ighv1-58	0.32	4.00E-04	2.20E-02	Mpz	0.31	5.00E-05	3.69E-03

was noted that these lists of the greatest fold changes included genes involved with WNT signaling (*Wnt1, Tfcp2l1, Cyp2e1, MyoC, Med23*), inflammation (*Panx3, Ptgs2, Nr4a2, P2rx7*), and BMP signaling and osteogenic differentiation (*Kera, Nell1, MyoC, P2rx7, Med23*).

To further refine the analysis, the DEG list was compared with a list of potential contaminating sequences from outside the bone compartment.[31] These ranged from 0.3% to 2.9% of the DEGs for each of the comparisons (Supplemental Table S5). Of note, *Sln*, *Actn1*, and *Myl2* identified in Tables 2 and 3 may result from contaminant tissues.

Based on similar prior studies analyzing the response of the transcriptome to biomechanical loading, a candidate gene approach was also taken to examine changes in relative gene expression. This included genes with known roles in Wnt/β-catenin signaling as well as other orphan genes related to sensation of load.[32,33] Consistent with these genes and the Wnt/β-catenin pathway in general having key roles in Scl-Ab and load responses, significant changes in gene expression were found, particularly when comparing Vehicle Control and Vehicle Loaded groups (Fig. 6). In addition, several genes showed the greatest change in the Scl-Ab Loaded treatment group including *Wisp1, Dkk3, Cdh2, Sfrp5, Ptgs2,* and *Ptn*.

It was speculated that transcripts key to the load and Scl-Ab responses would be shared between sets of differentially expressed genes. A comparison of DEGs were made according to load response (Fig. 7*A*) and the Scl-Ab response (Fig. 7*B*). This identified 251 genes that were differentially expressed in response to load in both Vehicle- and Scl-Ab-treated mice. A total of 194 genes were differentially expressed in response to Scl-Ab in both control and loaded mice.

Conversely, 100 DEGs were found to be specifically upregulated due to load in Scl-Ab-treated mice but not control mice. A further 203 DEGs were specifically upregulated due to Scl-Ab treatment in loaded but not the non-loaded tibias. A further comparison of the two groups (Fig. 7*C*) highlighted 80 DEGs that were altered within both subgroups (Table 4). Noteworthy DEGs' potential key to the combined response of Scl-Ab and loading include *Ptgs2* (3.23; 3.44), *Enpp1* (1.66; 1.69), *Sox9* (2.19; 2.43), *Dkk1* (1.53; 1.58), *Nell1* (4.37; 4.41), *Nbl1* (1.49; 1.53), *Fam3c* (1.43; 1.47), *Gdpd2* (0.65; 0.66), *Ckb* (1.44; 1.40), *Klf4* (1.45; 1.48), and *Bmp7* (1.63; 1.64).

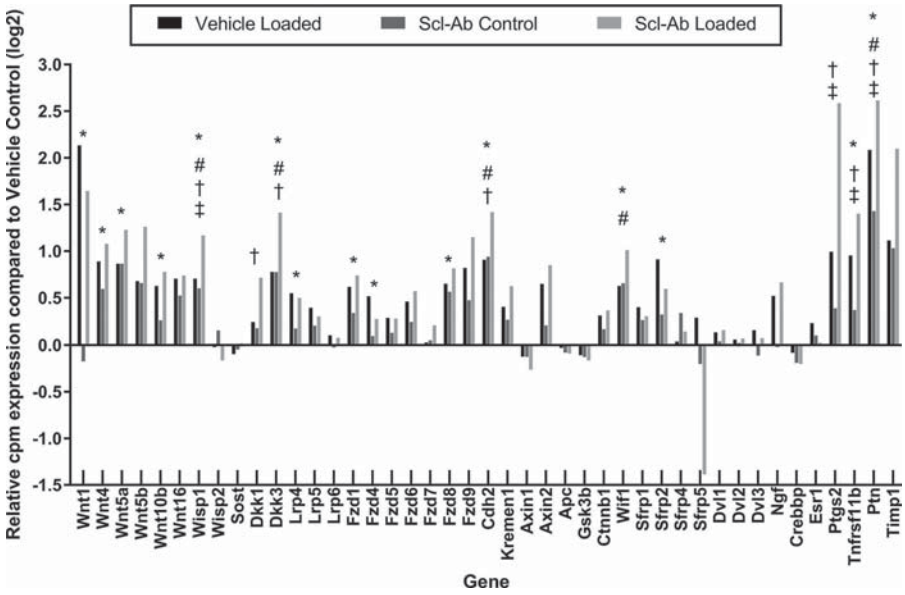

Fig. 6. Relative gene expression (counts per million/cpm) compared with the Vehicle Control group for Vehicle Loaded, Scl-Ab Control, and Scl-Ab Loaded groups. Genes graphed include Wnt/β-catenin signaling pathway factors and orphan genes of interest with known involvement in bone mechanotransduction. Significance (FDR < 0.05) for Comparisons 1–4 of differentially expressed genes (DEGs) shown: *Comparison 1; #Comparison 2; †Comparison 3; ‡Comparison 4. Unable to obtain *p* value within Comparison 1 and 2 for *Ptgs2* and Comparison 2 for *Wnt1* and so not tested.

Analysis of the genetic pathways responsive to Scl-Ab and load

Pathway enrichment analysis was performed in an effort to identify the genetic circuits represented by the DEGs for each of the group-wise comparisons. Pathway analysis identified many circuits that were common across all comparisons, which likely underlie the associated increase in bone formation response found in functional analyses. These include extracellular matrix organization and degradation, as well as collagen biosynthesis and formation. In addition, some pathways were specifically altered with loading or Scl-Ab treatment, however were not altered further with combination load and Scl-Ab therapy. These include ECM proteoglycans, integrin cell surface interactions, and collagen degradation, TCF-dependent WNT signaling, and other pathways involving cell-cell communication and matrix organization (Supplemental Table S6). An unexpected finding was alterations in Rho GTPase pathways that were associated with loading in Scl-Ab-treated mice as well as by Scl-Ab treatment in loaded mice. Key genes affected included *Arhgap22* (0.27; 0.26), *A2m* (0.56; 0.57), *Arhgap6* (0.51; 0.53), *Srgap1* (1.48; 1.53), *Chn1* (1.81; 1.89), and *Ngef* (1.82; 1.85).

Discussion

We have previously reported that *Sost* knockout mice show no impairment of the response to cyclic compressive loading but

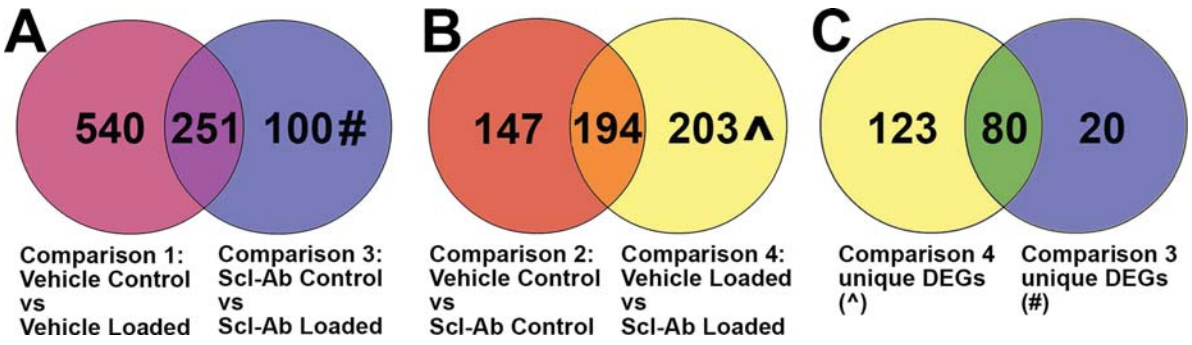

Fig. 7. VENN diagrams showing the number of differentially expressed genes (DEGs) common and unique within comparisons. (*A*) Load-related DEGs: Comparison 1 compared with Comparison 3. #Comparison 3 (loading in the presence of Scl-Ab treatment) unique DEGs. (*B*) Scl-Ab-related DEGs: Comparison 2 was compared with Comparison 4. ^Comparison 4 (Scl-Ab in the presence of loading) unique DEGs. (*C*) The DEGs unique to loading in the presence of Scl-Ab treatment (#) were compared with DEGs unique to Scl-Ab in the presence of loading (^).

Table 4. DEGs Common and Unique to a Comparison of DEGs Unique to Loading in the Presence of Scl-Ab Treatment (#) and DEGs Unique to Scl-Ab in the Presence of Loading (^)

Unique DEGs: for Comparison 4 unique DEGs (^)	Common DEGs	Unique DEGs: for Comparison 3 unique DEGs (#)
Pi15, 1700066M21Rik, Myoc, Mpz, Rftn2, Dcbld1, Adamts2, Metrnl, Grb10, Ighv5-12, Pxdc1, Arhgap22, Mmp14, Pnpla3, Tnfrsf11b, Tuba1a, Gm8034, Rom1, Prg3, Bmp2, Frzb, Hey1, Pcdh18, Gpx7, Bmp8a, Pcdh7, Msi1, Gm27477, Gm27861, Gm27867, Gm27868, Hotairm1, Igkv3-7, A2m, Igkv5-48, Pdzrn3, B4galnt3, Ptms, Acan, Ifitm5, Irx5, Pygo1, Cd109, Ryk, Fam46a, Wbp5, Aebp1, Gm5805, Rai14, Jam2, Pvrl3, Tmem45a, Tmem38b, Aplp1, Gsg1l, Fxyd6, Tceal8, Myoz1, Snai2, Rcan2, Acta2, Nnmt, Apln, Klf12, Smad9, Smarca1, Ppfia2, Tm4sf1, Peg10, Dlx5, Slc37a3, Hoxa10, Hoxa9, Tmem86a, Mrc2, Dap, Casc4, Yipf5, Fibin, Pdgfc, 5730409E04Rik, Dnm3os, Ube2e2, Chsy1, Sema5a, Emp2, Angpt4, Ccdc149, Gm6377, Sh3bgrl, Glrx5, Scara3, Polr3d, Hist2h2aa2, Hist2h3c1, Slc2a10, Abi2, Lbr, Dixdc1, Arl1, Rhbdl2, Cdk14, Aldh1a2, Lipc, Klhl13, Pdia5, Zfhx4, Mical3, Enpp6, Cd63, Anxa8, Fhod3, Efr3b, Rhpn2, Gnb5, Csnk1g3, Ift20, Frmd3, Igkv6-17, Kcnn1, Inhbb, Entpd1, Cilp	*Ackr3, Tfcp2l1, Ptgs2, Bend6, Dsel, Cfhr2, Kera, Enpp1, Sox9, Slc1a4, Epx, Ighv1-55, Ell2, Ear2, Ear6, Ear1, 3632451O06Rik, Dpysl2, H2-Pb, Gal, Dkk1, Csrnp3, Lhx6, Actc1, Lppr4, Gm12519, Zmpste24, Fras1, Ephx4, Auts2, Ggcx, Nell1, Vimp, Cyp2e1, Rplp2, Syt8, Jund, Cd97, Pgbd5, Gramd2, Susd5, Atp1b3, Lonrf3, Arhgap6, Rab11fip4, Ighv5-9-1, Sec61b, Klf4, Nbl1, Rpl21, Tmem97, Serf1, Afap1l2, Gale, Bcat1, Slc6a15, Srgap1, Nt5e, Adm, Aif1l, Unc5c, Igkv4-58, Fam3c, Gm5269, Gm10320, Pdgfa, Irx6, Basp1, Gdpd2, Gm8113, Tmem200a, Hspb7, Ttc26, Ngef, Ckb, Fbln7, Sdr9c7, Vit, Bmp7, Arl4d*	*Slc9a2, 1700030C10Rik, Gm28503, RP23-152O2.3, Gm266, Ighv14-1, Ighv4-1, Hist1h2ac, Igkv4-55, BC024978, Rpl27a, Shank2, Fam65a, Lrrc15, Dpep2, Arfgap3, Igkv4-57-1, Slc35a2, Adamtsl2, Tcerg1*

rather an increased anabolic response compared with wild-type mice.[20] A limitation of this prior study was that *Sost* knockout bones undergoing loading possessed a higher bone mass and thus altered biomechanical properties. In this study, Scl-Ab and loading interventions commenced simultaneously. It was hypothesized that this approach would better translate to the clinical scenario of combining drug- and exercise-based therapies.

Scl-Ab treatment for only a 2-week period produced significant increases in bone density, cortical and trabecular bone parameters, and bone anabolism in C57Bl/6 mice. The osteogenic response of Scl-Ab within cortical bone was less marked than that for loading treatment alone; however, Scl-Ab had a greater effect within trabecular bone. A longer period of Scl-Ab treatment may likely elicit a stronger osteogenic response within the cortical bone. However, this period of Scl-Ab treatment did not produce maximal bone anabolism within either bone compartment as it could be further enhanced by biomechanical loading. Notably, the interaction between Scl-Ab and the adaptive response to biomechanical load was only synergistic in the cortical bone compartment. This may be due to differential compensatory changes in gene regulation, however the precise mechanism remains unclear.

These data are highly relevant to the future clinical use of Scl-Ab in osteoporosis treatment and other conditions of bone loss. Monthly Scl-Ab treatment (Romosozumab) in postmenopausal osteoporotic women yielded decreases in vertebral fractures during the trial period, but nonvertebral fracture rate was unaffected.[34] It is possible that load-based exercise may increase the efficacy of Scl-Ab, particularly for outcomes such as reducing hip and long bone fractures.

A critical aim of this study was to examine the genetic pathways underlying both the response to load and to Scl-Ab treatment, to identify both commonalities and differences. Notably, the Wnt/β-catenin signaling pathway has been implicated both in the mechanism of sclerostin action[12] as well as for mechanotransduction in bone.[21,35–40] Indeed, a critical threshold of β-catenin and an intact Wnt/β-catenin pathway are requirements for the anabolic response of bone to mechanical loading.[38,41]

RNASeq was used to analyze the transcriptome and revealed information regarding both specific DEGs and affected pathways. Pathway analysis showed that biomechanical load caused significant alteration to the "TCF-dependent signaling in response to WNT" pathway. Upregulated genes included Wnt/β-catenin signaling agonists (*Wnt1, Wnt4, Wnt5a*) and receptors (*Fzd1, Fzd4*). *Wnt1* was one of the most highly upregulated genes after loading, in accordance with prior data.[33,42] Hypomorphic *Wnt1* alleles have been implicated in diseases of low bone density,[43–46] and thus increased *Wnt1* expression may conversely increase osteogenesis. Recently, osteocyte-expressed *Wnt1* has been shown to be important in bone development and homeostasis.[47] *Panx3*, also amongst the highly upregulated genes with loading, may also be important in the loading response; it has interactions with Wnt/β-catenin signaling and has roles in inhibiting osteoprogenitor proliferation and promoting cell cycle exit.[48]

In contrast to loading, Scl-Ab treatment did not comparably affect Wnt/β-catenin pathways or DEGs. One potential explanation is that loading upregulates expression of Wnt/β-catenin pathway factors on a transcriptional level, whereas Scl-Ab primarily modulates downstream activation of β-catenin-dependent gene

expression. Also, the short-term treatment of Scl-Ab and the less profound anabolic response compared with loading may also explain the reduced effect on the Wnt/β-catenin pathway.

A major goal of the RNAseq analysis was to examine DEGs and genetic circuits that could modulate the effects of dual treatment with Scl-Ab and mechanical loading. Candidate gene analysis found that load and Scl-Ab in combination yielded synergistic increases in the expression of Wnt-related genes including *Wisp1, Dkk3, Cdh2,* and *Sfrp5*. In addition, the combined treatment led to considerable upregulation of *Ptgs2, Tnfrsf11b,* and *Timp1*, factors previously associated with mechanotransduction.[32,33] Comparative analysis of genes identified by unbiased screening revealed 80 unique genes altered with the combination of Scl-Ab and load versus either treatment alone.

Of these 80 genes, *Nell1* and *Ptgs2* (also known as *Cox2*) were particularly of interest. *Nell1* encodes for a secreted protein that is critical for normal skeletal development; overexpression causes craniosynostosis[49,50] and deficiency results in cranial/vertebral defects and undermineralization.[51] Nell1 has been shown to regulate Wnt/β-catenin downstream of integrin receptor signaling to produce effects on osteoblastic differentiation and osteoclastic bone resorption.[52,53] Ptgs2/Cox2 is an isoform of cyclooxygenase and is thus involved in the production of prostaglandins.[54] Cox2 blockade has been shown to block lamellar bone formation in response to in vivo mechanical loading,[55] although in some situations it may be compensated for by Cox1.[56] Prostaglandins have been shown to affect Wnt/β-catenin signaling,[57,58] and Cox inhibition prevents sclerostin downregulation after biomechanical loading of bone.[59]

An unexpected outcome of pathway analysis was identifying significant alterations in the "Rho GTPase cycle" and "Signaling by Rho GTPases" pathways that was associated with combined treatment. Rho GTPases, a subgroup of the Ras superfamily of small guanine nucleotide-binding proteins, have known roles in mechanotransduction. This has been shown in aortic and vascular smooth muscle cells, cardiac myocytes,[60–63] and most recently osteoblasts.[64,65] There is evidence of Rho family proteins and Wnt/β-catenin signaling interactions within cancer cells, developing embryos, and embryonic cells,[66–69] and similar interactions within bone cells could be hypothesized.

A limitation of the RNAseq component of the study is that analysis was not performed on a single subset of cells. Importantly, the number of contaminating sequences from outside the bone compartment was below 3% for all samples based on a prior curated list.[31] Within the bone compartment, however, there are a combination of cells housed that may confound the data, such as osteoblasts, osteocytes, osteoclasts, bone lining cells, osteoprogenitor, and endothelial cells. However, because osteocytes comprise 90% to 95% of the cellular bone compartment,[70] we deduce the RNA to be from an osteocyte-rich population of cells.

In summary, this study examined the intersection between Scl-Ab and biomechanical loading, which both can act via the Wnt/β-catenin pathway. Combination therapy of loading and Scl-Ab treatment had a more profound anabolic response than either treatment alone. This may be clinically important for future use of Scl-Ab in treating low bone mass. Mechanistically, we have identified a number of genes belonging to Wnt family, downstream Wnt/β-catenin factors, as well as several notable novel circuits including Rho GTPase signaling. These data illustrate the complexity involved with the response to biomechanical loading but may reveal new avenues to target more powerful anabolic stimuli in bone.

Disclosures

The authors received materials support (sclerostin antibody) for this study from Novartis Pharma AG (Basel, Switzerland) and Mereo BioPharma (London, UK), along with additional funding and materials support for research separate to this submission. Prof. Little and A/Prof Schindeler have received funding support from Amgen Inc., UCB Pharma, Celgene, and N8 Medical. Prof. Little is a consultant for Orthopaediatrics. Dr. McDonald has received funding from IBMS Greg Mundy Fellowship. Dr Kramer and Dr Kneissel are employees of Novartis Pharma AG.

Acknowledgments

The authors thank Lauren Peacock and Kathy Mikulec for aid in animal dosing and Guy Smith for his help with DXA analysis. The authors also thank the AGRF Bioinformatics team, in particular Dr Sonika Tyagi, for their help in data analysis of RNAseq.

Authors' roles: Study design: DGL, AM, IK, and MK. Study conduct: AM. Data collection: AM. Data analysis: AM. Data interpretation: AM, DGL, and AS. Drafting manuscript: AM. Revising manuscript content: AM, DGL, AS, IK, MK, and MMM. Approving final version of manuscript: all authors. AM takes responsibility for the integrity of the data analysis.

References

1. Houlihan CM. Bone health in cerebral palsy: who's at risk and what to do about it? J Pediatr Rehabil Med. 2014;7(2):143–53.
2. Boyce AM, Tosi LL, Paul SM. Bisphosphonate treatment for children with disabling conditions. PMR. 2014;6(5):427–36.
3. Goemans N, Buyse G. Current treatment and management of dystrophinopathies. Curr Treat Options Neurol. 2014;16(5):287.
4. Meier RP, Perneger TV, Stern R, Rizzoli R, Peter RE. Increasing occurrence of atypical femoral fractures associated with bisphosphonate use. Arch Intern Med. 2012;172(12):930–6.
5. Shane E, Burr D, Ebeling PR, et al. Atypical subtrochanteric and diaphyseal femoral fractures: report of a task force of the American Society for Bone and Mineral Research. J Bone Miner Res. 2010;25(11):2267–94.
6. Al Wren T, Lee DC, Kay RM, Dorey FJ, Gilsanz V. Bone density and size in ambulatory children with cerebral palsy. Dev Med Child Neurol. 2011;53(2):137–41.
7. Chad KE, Bailey DA, McKay HA, Zello GA, Snyder RE. The effect of a weight-bearing physical activity program on bone mineral content and estimated volumetric density in children with spastic cerebral palsy. J Pediatr. 1999;135(1):115–7.
8. Fowler EG, Kolobe TH, Damiano DL, et al. Promotion of physical fitness and prevention of secondary conditions for children with cerebral palsy: section on pediatrics research summit proceedings. Phys Ther. 2007;87(11):1495–510.
9. Miller PD, Hattersley G, Riis BJ, et al. Effect of abaloparatide vs placebo on new vertebral fractures in postmenopausal women with osteoporosis: a randomized clinical trial. JAMA. 2016;316(7):722–33.
10. Iwata A, Kanayama M, Oha F, Hashimoto T, Iwasaki N. Effect of teriparatide (rh-PTH 1-34) versus bisphosphonate on the healing of osteoporotic vertebral compression fracture: a retrospective comparative study. BMC Musculoskel Disord. 2017;18(1):148.
11. Fujita T, Fukunaga M, Itabashi A, Tsutani K, Nakamura T. Once-weekly injection of low-dose teriparatide (28.2 mug) reduced the risk of vertebral fracture in patients with primary osteoporosis. Calcif Tissue Int. 2014;94(2):170–5.

12. Semenov M, Tamai K, He X. SOST is a ligand for LRP5/LRP6 and a Wnt signaling inhibitor. J Biol Chem. 2005;280(29):26770–5.
13. Poole KE, van Bezooijen RL, Loveridge N, et al. Sclerostin is a delayed secreted product of osteocytes that inhibits bone formation. FASEB J. 2005;19(13):1842–4.
14. Jager A, Gotz W, Lossdorfer S, Rath-Deschner B. Localization of SOST/sclerostin in cementocytes in vivo and in mineralizing periodontal ligament cells in vitro. J Periodontal Res. 2010;45(2):246–54.
15. van Bezooijen RL, Roelen BA, Visser A, et al. Sclerostin is an osteocyte-expressed negative regulator of bone formation, but not a classical BMP antagonist. J Exp Med. 2004;199(6):805–14.
16. Clarke BL. Anti-sclerostin antibodies: utility in treatment of osteoporosis. Maturitas. 2014;78(3):199–204.
17. McClung MR, Grauer A, Boonen S, et al. Romosozumab in postmenopausal women with low bone mineral density. N Engl J Med. 2014;370(5):412–20.
18. Lin C, Jiang X, Dai Z, et al. Sclerostin mediates bone response to mechanical unloading through antagonizing Wnt/beta-catenin signaling. J Bone Miner Res. 2009;24(10):1651–61.
19. Spatz JM, Ellman R, Cloutier AM, et al. Sclerostin antibody inhibits skeletal deterioration due to reduced mechanical loading. J Bone Miner Res. 2013;28(4):865–74.
20. Morse A, McDonald MM, Kelly NH, et al. Mechanical load increases in bone formation via a sclerostin-independent pathway. J Bone Miner Res. 2014;29(11):2456–67.
21. Tu X, Rhee Y, Condon KW, et al. Sost downregulation and local Wnt signaling are required for the osteogenic response to mechanical loading. Bone. 2012;50(1):209–17.
22. Chandra A, Lin T, Young T, et al. Suppression of sclerostin alleviates radiation-induced bone loss by protecting bone-forming cells and their progenitors through distinct mechanisms. J Bone Miner Res. 2017;32(2):360–72.
23. Melville KM, Kelly NH, Surita G, et al. Effects of deletion of ERalpha in osteoblast-lineage cells on bone mass and adaptation to mechanical loading differ in female and male mice. J Bone Miner Res. 2015;30(8):1468–80.
24. Moustafa A, Sugiyama T, Prasad J, et al. Mechanical loading-related changes in osteocyte sclerostin expression in mice are more closely associated with the subsequent osteogenic response than the peak strains engendered. Osteoporos Int. 2012;23(4):1225–34.
25. Lynch ME, Main RP, Xu Q, et al. Cancellous bone adaptation to tibial compression is not sex dependent in growing mice. J Appl Physiol. 2010;109(3):685–91.
26. Fritton JC, Myers ER, Wright TM, van der Meulen MC. Loading induces site-specific increases in mineral content assessed by microcomputed tomography of the mouse tibia. Bone. 2005;36(6):1030–8.
27. Trapnell C, Roberts A, Goff L, et al. Differential gene and transcript expression analysis of RNA-seq experiments with TopHat and Cufflinks. Nat Protoc. 2012;7(3):562–78.
28. Robinson MD, McCarthy DJ, Smyth GK. edgeR: a bioconductor package for differential expression analysis of digital gene expression data. Bioinformatics. 2010;26(1):139–40.
29. Oliveros JC. Venny. An interactive tool for comparing lists with Venn's diagrams. 2007–2015 [Internet]. Available from: http://bioinfogp.cnb.csic.es/tools/venny/index.html.
30. Luo W, Brouwer C. Pathview: an R/Bioconductor package for pathway-based data integration and visualization. Bioinformatics. 2013;29(14):1830–1.
31. Ayturk UM, Jacobsen CM, Christodoulou DC, et al. An RNA-seq protocol to identify mRNA expression changes in mouse diaphyseal bone: applications in mice with bone property altering Lrp5 mutations. J Bone Miner Res. 2013;28(10):2081–93.
32. Zaman G, Saxon LK, Sunters A, et al. Loading-related regulation of gene expression in bone in the contexts of estrogen deficiency, lack of estrogen receptor alpha and disuse. Bone. 2010;46(3):628–42.
33. Kelly NH, Schimenti JC, Ross FP, van der Meulen MC. Transcriptional profiling of cortical versus cancellous bone from mechanically-loaded murine tibiae reveals differential gene expression. Bone. 2016;86:22–9.
34. Cosman F, Crittenden DB, Adachi JD, et al. Romosozumab treatment in postmenopausal women with osteoporosis. N Engl J Med. 2016;375(16):1532–43.
35. Sunters A, Armstrong VJ, Zaman G, et al. Mechano-transduction in osteoblastic cells involves strain-regulated estrogen receptor alpha-mediated control of insulin-like growth factor (IGF) I receptor sensitivity to Ambient IGF, leading to phosphatidylinositol 3-kinase/AKT-dependent Wnt/LRP5 receptor-independent activation of beta-catenin signaling. J Biol Chem. 2010;285(12):8743–58.
36. Santos A, Bakker AD, Zandieh-Doulabi B, de Blieck-Hogervorst JM, Klein-Nulend J. Early activation of the beta-catenin pathway in osteocytes is mediated by nitric oxide, phosphatidyl inositol-3 kinase/Akt, and focal adhesion kinase. Biochem Biophys Res Commun. 2010;391(1):364–9.
37. Case N, Ma M, Sen B, Xie Z, Gross TS, Rubin J. Beta-catenin levels influence rapid mechanical responses in osteoblasts. J Biol Chem. 2008;283(43):29196–205.
38. Sawakami K, Robling AG, Ai M, et al. The Wnt co-receptor LRP5 is essential for skeletal mechanotransduction but not for the anabolic bone response to parathyroid hormone treatment. J Biol Chem. 2006;281(33):23698–711.
39. Robling AG, Niziolek PJ, Baldridge LA, et al. Mechanical stimulation of bone in vivo reduces osteocyte expression of Sost/sclerostin. J Biol Chem. 2008;283(9):5866–75.
40. Robinson JA, Chatterjee-Kishore M, Yaworsky PJ, et al. Wnt/beta-catenin signaling is a normal physiological response to mechanical loading in bone. J Biol Chem. 2006;281(42):31720–8.
41. Javaheri B, Stern AR, Lara N, et al. Deletion of a single beta-catenin allele in osteocytes abolishes the bone anabolic response to loading. J Bone Miner Res. 2014;29(3):705–15.
42. Holguin N, Brodt MD, Silva MJ. Activation of Wnt signaling by mechanical loading is impaired in the bone of old mice. J Bone Miner Res. 2016;31(12):2215–26.
43. Fahiminiya S, Majewski J, Mort J, Moffatt P, Glorieux FH, Rauch F. Mutations in WNT1 are a cause of osteogenesis imperfecta. J Med Genet. 2013;50(5):345–8.
44. Keupp K, Beleggia F, Kayserili H, et al. Mutations in WNT1 cause different forms of bone fragility. Am J Hum Genet. 2013;92(4):565–74.
45. Laine CM, Joeng KS, Campeau PM, et al. WNT1 mutations in early-onset osteoporosis and osteogenesis imperfecta. N Engl J Med. 2013;368(19):1809–16.
46. Pyott SM, Tran TT, Leistritz DF, et al. WNT1 mutations in families affected by moderately severe and progressive recessive osteogenesis imperfecta. Am J Hum Genet. 2013;92(4):590–7.
47. Joeng KS, Lee YC, Lim J, et al. Osteocyte-specific WNT1 regulates osteoblast function during bone homeostasis. J Clin Invest. 2017;127(7):2678–88.
48. Ishikawa M, Iwamoto T, Fukumoto S, Yamada Y. Pannexin 3 inhibits proliferation of osteoprogenitor cells by regulating Wnt and p21 signaling. J Biol Chem. 2014;289(5):2839–51.
49. Ting K, Vastardis H, Mulliken JB, et al. Human NELL-1 expressed in unilateral coronal synostosis. J Bone Miner Res. 1999;14(1):80–9.
50. Zhang X, Kuroda S, Carpenter D, et al. Craniosynostosis in transgenic mice overexpressing Nell-1. J Clin Invest. 2002;110(6):861–70.
51. Desai J, Shannon ME, Johnson MD, et al. Nell1-deficient mice have reduced expression of extracellular matrix proteins causing cranial and vertebral defects. Hum Mol Genet. 2006;15(8):1329–41.
52. Shen J, James AW, Chung J, et al. NELL-1 promotes cell adhesion and differentiation via Integrinbeta1. J Cell Biochem. 2012;113(12):3620–8.
53. James AW, Shen J, Zhang X, et al. NELL-1 in the treatment of osteoporotic bone loss. Nat Commun. 2015;6:7362.
54. Smith WL, Garavito RM, DeWitt DL. Prostaglandin endoperoxide H synthases (cyclooxygenases)-1 and -2. J Biol Chem. 1996;271(52):33157–60.
55. Forwood MR. Inducible cyclo-oxygenase (COX-2) mediates the induction of bone formation by mechanical loading in vivo. J Bone Miner Res. 1996;11(11):1688–93.

56. Alam I, Warden SJ, Robling AG, Turner CH. Mechanotransduction in bone does not require a functional cyclooxygenase-2 (COX-2) gene. J Bone Miner Res. 2005;20(3):438–46.

57. Kamel MA, Picconi JL, Lara-Castillo N, Johnson ML. Activation of beta-catenin signaling in MLO-Y4 osteocytic cells versus 2T3 osteoblastic cells by fluid flow shear stress and PGE2: implications for the study of mechanosensation in bone. Bone. 2010;47(5): 872–81.

58. Kitase Y, Barragan L, Qing H, et al. Mechanical induction of PGE2 in osteocytes blocks glucocorticoid-induced apoptosis through both the beta-catenin and PKA pathways. J Bone Miner Res. 2010;25(12): 2657–68.

59. Lara-Castillo N, Kim-Weroha NA, Kamel MA, et al. In vivo mechanical loading rapidly activates beta-catenin signaling in osteocytes through a prostaglandin mediated mechanism. Bone. 2015;76: 58–66.

60. Putnam AJ, Cunningham JJ, Pillemer BB, Mooney DJ. External mechanical strain regulates membrane targeting of Rho GTPases by controlling microtubule assembly. Am J Physiol Cell Physiol. 2003;284(3):C627–39.

61. Aikawa R, Komuro I, Yamazaki T, et al. Rho family small G proteins play critical roles in mechanical stress-induced hypertrophic responses in cardiac myocytes. Circ Res. 1999;84(4):458–66.

62. Katsumi A, Milanini J, Kiosses WB, et al. Effects of cell tension on the small GTPase Rac. J Cell Biol. 2002;158(1):153–64.

63. Numaguchi K, Eguchi S, Yamakawa T, Motley ED, Inagami T. Mechanotransduction of rat aortic vascular smooth muscle cells requires RhoA and intact actin filaments. Circ Res. 1999;85(1):5–11.

64. Arnsdorf EJ, Tummala P, Kwon RY, Jacobs CR. Mechanically induced osteogenic differentiation—the role of RhoA, ROCKII and cytoskeletal dynamics. J Cell Sci. 2009;122(Pt 4):546–53.

65. Hamamura K, Swarnkar G, Tanjung N, et al. RhoA-mediated signaling in mechanotransduction of osteoblasts. Connect Tissue Res. 2012; 53(5):398–406.

66. Esufali S, Bapat B. Cross-talk between Rac1 GTPase and dysregulated Wnt signaling pathway leads to cellular redistribution of beta-catenin and TCF/LEF-mediated transcriptional activation. Oncogene. 2004;23(50):8260–71.

67. Jones WM, Bejsovec A. RacGap50C negatively regulates wingless pathway activity during Drosophila embryonic development. Genetics. 2005;169(4):2075–86.

68. Wu X, Tu X, Joeng KS, Hilton MJ, Williams DA, Long F. Rac1 activation controls nuclear localization of beta-catenin during canonical Wnt signaling. Cell. 2008;133(2):340–53.

69. Habas R, Dawid IB, He X. Coactivation of Rac and Rho by Wnt/Frizzled signaling is required for vertebrate gastrulation. Genes Dev. 2003; 17(2):295–309.

70. Florencio-Silva R, Sasso GR, Sasso-Cerri E, Simoes MJ, Cerri PS. Biology of bone tissue: structure, function, and factors that influence bone cells. BioMed Res Int. 2015;2015:421746.

Chapter 6. Discussion

1. Summary of novel findings

Sclerostin and other Wnt-family antagonists have a critical role in bone formation and homeostasis. Consequently, significant academic and industry resources have been invested to target sclerostin as a means of promoting bone formation to treat osteoporosis and other conditions of low bone mass. Despite the promising findings from phase II and phase III trials for anti-sclerostin antibody therapy (Scl-Ab) (1-3), there are considerable gaps in our knowledge regarding the mechanism of action of sclerostin and how it interacts with environmental conditions, such as biomechanical loading. This thesis describes a series of preclinical studies aimed to tackle these research questions.

Chapter 2 investigated the effect of the ubiquitous genetic deletion of sclerostin on the bone's response to changes in mechanical loading. Tibial unloading (disuse) and strain- and force-matched biomechanical loading (axial cyclic compression) were applied to a *Sost* KO mouse line. Sclerostin was found to be essential for the bone response to unloading; *Sost* KO unloaded tibiae did not exhibit the bone loss seen in unloaded wild type tibiae. However, in an experiment of increased tibial loading, sclerostin was not required for an anabolic response within bone. Moreover, *Sost* KO tibiae showed an augmented anabolic response to mechanical loading that featured increased bone volume and formation.

DKK1 is another Wnt-family antagonist that has potential as a bone therapeutic target. Chapter 3 examined strain-matched and force-matched bone loading (axial compression) in the tibiae of *Dkk1* KO mice. Non-loaded *Dkk1* KO tibiae had an increased bone volume compared to wild type controls. Critically, complete deletion of DKK1 did not result in maximal bone anabolism, as the high bone formation and bone volume of *Dkk1* KO mice were augmented with increased mechanical loading. Thus while DKK1 expression can be regulated by load, these data confirm that DKK1 is not essential for transducing the response to cyclic loading. Notably, *Sost* expression was not altered by DKK1 deficiency, however was similarly down-regulated by loading.

In Chapter 4, *Dkk1* KO mice were treated with a murine neutralizing antibody to sclerostin (Scl-Ab) to induce dual deficiency of both Wnt antagonists, DKK1 and sclerostin. These were compared to genotype control mice treated with Scl-Ab, and also mice of all genotypes treated with vehicle. Both the *Dkk1* KO mouse and Scl-Ab treatment resulted in increased bone volume, with Scl-Ab treatment having a greater effect on bone volume and density compared to DKK1

deficiency. Additional increases in bone volume were seen with the dual deficiency, with prominent and synergistic effects seen within cancellous bone. Bone formation was increased with Scl-Ab treatment, however no additive effect was seen within *Dkk1* KO mice. Sclerostin expression was not observed to be altered by DKK1 deficiency or Scl-Ab treatment.

Chapter 5 continued the theme of characterizing the nexus between mechanical loading and sclerostin deficiency. Short-term deficiency of sclerostin was induced via the administration of Scl-Ab, and mice received concomitant tibial axial compressive loading. Both interventions – Scl-Ab treatment and loading – resulted in increased bone volume and formation. The combination produced additional increases, confirming the critical information that sclerostin antagonism and loading are not functionally redundant.

Next, RNA sequencing (RNAseq) findings were presented describing gene expression in the cortical bone of the mid-diaphysis of loaded and non-loaded tibiae from Scl-Ab and vehicle treated mice. Notably, loading alone caused significant alteration to the "TCF dependent signalling in response to WNT" pathway, including Wnt/β-catenin signalling agonists (*Wnt1, Wnt4, Wnt5a*) and receptors (*Fzd1, Fzd4*). DKK1 expression, along with other Wnt factors, showed compensatory increases with Scl-Ab and loading, alone or in combination. This increase in DKK1 expression was significant with loading in the Scl-Ab treated mice, and not altered with loading in vehicle treated mice. Numerous genes were found to be specifically altered following two days of combination Scl-Ab and mechanical loading therapy. These included Wnt family members, some of which were synergistically increased over either monotherapy. The Rho GTPase signalling pathway was also highlighted to be significantly altered with combination loading and Scl-Ab.

2. Thesis themes, limitations, strengths, and potential clinical impact

This thesis develops several key concepts within the field of bone mechanobiology and modulating the Wnt/β-catenin pathway.

2.1. Sclerostin deficiency attenuates disuse-induced bone loss

Unloading due to BTX-induced disuse decreased cortical bone volume and thickness, and trabecular bone volume and number, within wild type mice. In contrast, in *Sost* KO mice the bone losses associated with unloading were abrogated. These data confirm that sclerostin expression and the subsequent blockade of Wnt/β-catenin signalling are required for decreased bone volume associated with disuse, substantiating previous studies. Prior reports had shown that genetic knock-out mice (4), and mice under short-term treatment with neutralising antibodies to sclerostin (5), display less bone loss with hind-limb suspension. Subsequent to our studies, comparable results were also presented in a hind-limb suspension disuse model in *Sost* KO mice (6).

The confirmation of outcomes from the BTX-induced disuse study was important due to limitations in both hind-limb suspension and BTX-induced disuse models. Tail suspension decreases locomotion and exploration, and increases anxiety (7). Additionally there is some added mouse numbers as contralateral limbs cannot be used as controls and some wasted mice as they can get free from the suspension apparatus. The BTX model is not without its own caveats, as there potentially may be secondary effects due to myokines associated with muscle wastage (8). Further BTX effects wear off over a time.

Prior studies examining disuse-induced bone loss and the protective effects of sclerostin deficiency have lacked a thorough assessment of resorption. It has been widely shown that unloading significantly elevates osteoclastic activity and bone resorption (9-16). However, within my data no alteration was seen in osteoclast number, or the proportion of the bone surface bound by osteoclasts, with unloading in either wild type or *Sost* KO genotypes (Chapter 2). Notably, the proportion of the bone surface bound by osteoclasts was significantly reduced in *Sost* KO mice though (control and unloaded tibiae). This does suggest a reduction in osteoclast activity, however may also be reasoned by the increased bone volume seen in the *Sost* KO mice.

It is unclear whether a reduction in bone catabolism is the sole mechanism in preventing bone loss in disuse in *Sost* KO mice, or whether an increase in bone formation is involved. Other papers investigating bone catabolism have analysed the dimensions of osteocyte resorption cavities (17), although we did not undertake such studies. Nevertheless, the lack of any measurable impact on bone anabolism in unloaded wild type and *Sost* KO tibiae suggests that effects on osteoblasts and osteocytes do not represent the primary mechanism. This contrasts data from a murine model of bilateral hind limb disuse (tail suspension), where a reduction in bone formation parameters were seen in wild type unloaded mice but not *Sost* KO mice (4). Yet in this study, resorption parameters were not assessed at all, making it impossible to conclude that anabolic changes were the sole cause.

Importantly for clinical translation, my findings support trialling neutralising antibodies to sclerostin as a clinical therapy for preventing bone loss caused by disuse osteopenia.

2.2. Wnt antagonist deficiency augments the response to loading

The anabolic response of bone to mechanical loading was significantly increased with deficiency in Wnt antagonists. This finding was one of the most consistent across all of my research studies – being seen in *Sost* KO mice, *Dkk1* KO mice, and also within C57Bl/6 mice treated with Scl-Ab. Thus my initial hypothesis – that exercise would be redundant with Wnt/β-catenin activating therapy – was disproven. Critically, these data also provide new mechanistic information regarding combining Wnt/β-catenin pathway activation and mechanical stimulation. Review of the recent literature also shows agreement with data from LRP5 gain-of-function mutation studies, which show an increased response to mechanical stimulation (18-20). The finding of mechanical loading having increased effects in *Sost* KO mice has also been since confirmed by another group (21).

Notably, the statistical interaction between loading and genotype was significantly stronger for bone formation in the *Sost* KO and *Dkk1* KO mice than in wild type mice. This confirms a synergistic response of sclerostin/DKK1 deficiency and increased mechanical bone loading. A mixed ANOVA analysis of data from Chapter 2 was performed subsequent to publication to assess the interactions between the between-subject effect of genotype (wild type, *Sost* KO) and the within-subject effect of loading (control, loaded limbs). These data are shown in Table 1 below. Conspicuously, the genotype:loading interaction was significant for bone volume within all

Table 1: Mixed ANOVA analysis of microCT and dynamic histomorphometry data, assessing the interaction between the between-subject effect of genotype (wild type, *Sost* KO) and the within-subject effect of loading (control, loaded limbs).

Region of interest		MicroCT		Dynamic histolomorphometry	
		Parameter	G:L	Parameter	G:L
7.8mm VOI		BV	p<0.01		
Proximal metaphysis	Canc + Cort	TV	p<0.01		
		BV	p<0.01		
	Cancellous	TV	n.s.		
		BV	p<0.01		
		BV/TV	p<0.01		
		Tb.Th	n.s.		
		Tb.Sp	p<0.01		
		Tb.N	p<0.01		
		TMD	n.s.		
	Cortical	TV	p<0.01		
		BV	p<0.01		
		Ct.Th	p<0.01		
		Ps	n.s.		
		Ec	n.s.		
		TMD	n.s.		
Mid-diaphysis	37% VOI	TV	p<0.05	Periosteal MAR	n.s.
		BV	p<0.01	Periosteal MS/BS	p<0.01
		Tb.Th	n.s.	Periosteal BFR/BS	p<0.01
		Ps	n.s.	Endosteal MAR	n.s.
		Ec	n.s.	Endosteal MS/BS	n.s.
		J	p<0.01	Endosteal BFR/BS	n.s.
		TMD	n.s.		
	50% VOI	TV	n.s.	Periosteal MAR	n.s.
		BV	n.s.	Periosteal MS/BS	n.s.
		Tb.Th	n.s.	Periosteal BFR/BS	n.s.
		Ps	n.s.	Endosteal MAR	p<0.05
		Ec	n.s.	Endosteal MS/BS	n.s.
		J	n.s.	Endosteal BFR/BS	n.s.
		TMD	n.s.		

(G:L): the interaction of genotype:load by mixed ANOVA analyses. P-values listed for each parameter assessed for microCT and dynamic histomorphometry analysis, and n.s. denotes no significance. BV (bone volume), TV (total volume), Tb.Th (trabecular thickness), Tb.Sp (trabecular separation), Tb.N (trabecular number), TMD (total mineral density), Ps (periosteal perimeter), Ec (endocortical perimeter), and J (polar moment of inertia).

metaphyseal compartments, along with the mid-diaphyseal regions located 37% down the tibiae ($p<0.01$). The genotype:loading interaction were also significant for MS/BS and BFR/BS within the 37% cortical VOI, as assessed by dynamic histomorphometry ($p<0.01$).

The anabolic increases seen within the loaded mice administered with Scl-Ab were however considerably less marked than for the genetically modified *Sost* KO mice. The osteogenic effect of neutralising antibodies to sclerostin was dose-related in Phase I clinical trials (22, 23). It may be that a higher dose rate of Scl-Ab or a longer dosing regimen alongside exercise could induce the synergistic anabolic response witnessed in the loaded tibiae of *Sost* KO mice.

Of clinical relevance, these data advocate that load-based exercise may increase the efficacy of therapy with neutralising antibodies to sclerostin. This has promising implications for the treatment of low bone mass disease, such as osteoporosis.

2.3. Combined deficiency of DKK1 and sclerostin

To investigate any compensatory or redundancy effects to bone anabolism with deficiency in more than one Wnt antagonist, deficiency in both sclerostin and DKK1 were investigated (Chapter 4). The addition of Scl-Ab to the *Dkk1* KO mouse increased bone volume above either single deficiency. Prominent and synergistic effects were seen within cancellous bone. This agrees with the hypothesis that combined Wnt/β-catenin activating therapies would have synergistic effects.

Emerging data has shown that Wnt antagonists may be up-regulated to compensate for a deficiency in other family members (24-26). Thus combining Wnt/β-catenin activating treatments could overcome this negative feedback. Synergism with *Dkk1* KO and Scl-Ab was seen mainly within the cancellous bone however. This may be a result of a more localised expression of DKK1 within cancellous bone, as has previously been suggested (27). Further, there is emerging evidence that DKK1 has limited expression throughout cancellous and cortical bone of the adult skeleton, unless stimulated by trauma (28).

A recent study in ovariectomised (OVX) rats and intact mice examined the combination of sclerostin and DKK1 inhibition (26). OVX rats received a combination of sclerostin and DKK1 neutralising antibodies, whereas mice received a unique bispecific antibody, neutralising both DKK1 and sclerostin. In both cases, treatments were compared to vehicle controls and animals

receiving a monotherapy. Areal BMD was increased in Scl-Ab/DKK1-Ab treated OVX rats compared to vehicle or monotherapy, and bone formation was synergistically increased. Closed fracture studies were also assessed following treatment of combination Scl-Ab/DKK1-Ab, or the bispecific antibody. Increases in callus volume and strength were seen above vehicle or monotherapy.

Notably, within my data bone formation was similarly increased with Scl-Ab treatment across genotypes by the 12 week end-point, with no additive effect within *Dkk1* KO mice. A hypothesis is that any augmented bone formation response due to DKK1 deficiency alongside Scl-Ab treatment may be transient and not measurable at the end-point assessed. Recently, a comparable murine study of weekly Scl-Ab dosing has shown that serum P1NP, a bone formation marker, is diminished by the third dose compared to aged-matched mice treated for the first time (29). Further, *Col1a1* mRNA expression within bone was also significantly reduced by 6 weeks of dosing. Regardless, within a clinical setting combining multiple Wnt antagonists still may provide a more favourable osteogenic response than mono-therapy.

2.4. Relating pre-clinical murine loading to human activity

The strain produced within all loading studies (1200 με) is intended to be comparable to an increase in higher-magnitude daily activity. A mechanical usage window has been previously proposed, describing the approximate strain on bone within windows of "disuse", "physiological", "overuse" and "pathological overload" (30). The strain of 1200 με sits within the proposed "physiological" or "homeostasis" window, below "overuse" and above "disuse." In contrast, strenuous loading has been measured in a number of vertebrates including human, horse, goose and sheep and found that such strain on bone is in a range of 2000-3500 με (31).

The frequency and cycle number (4 Hz, 1200 cycles) of load events within all loading studies of this thesis are likely the equivalent to an additional short burst of the higher-magnitude activity. Normal homeostatic daily functional activities have been suggested to be comprised of daily strain of <10 με being frequent in occurrence, i.e. within the thousands, whist higher-magnitude daily strain >1000με only occur a few times per day, as quantified in dogs, sheep and turkeys (32). Daily stress dynamics in turkeys and humans have also been investigated and corroborated by others (33, 34). It is therefore not outside the scope of daily activity to increase the number of higher-

magnitude activity events. Further, by doing so my data may indirectly suggest that increasing the higher-magnitude strain activities within normal daily life, by even a small number, may elicit an anabolic bone response.

Importantly, it has been previously shown that an anabolic bone response to increased load can occur with both high-frequency low-magnitude strain (unit of deformation) occurrences (35) and also with low-frequency high-magnitude strain occurrences (36). However, Rubin and Lanyon, through their studies, have proposed that the preference for osteogenic mechanical stimulus be through a few load cycles of high-magnitude and high-frequency (36-38).

Some published exercise studies have adopted high-magnitude, high-frequency loading. The most convincing and enduring outcomes have been seen in children. Even the incorporation of a small number of scheduled jumping exercises into the school week found significant increases in lumbar spine and femoral neck bone mineral content (39-41), showing that osteogenic improvements could be made through practical, sustainable high-magnitude daily activity.

Studies looking at the effect of exercise on the adult bone has been limited by the common use of DXA to gain outcome measures (42). DXA outcome measures do not measure the geometric changes that are likely the most beneficial effect if increased loading-based exercise. Nevertheless, a head-to-head study of high-load low-repetition exercise versus endurance-based low-load high-repetition exercise in postmenopausal women showed increased bone mass following the high-load low-repetition training but not with endurance regimen (43). Another study within postmenopausal women showed that high-intensity training prevented the significant femoral neck and lumbar spine bone loss that occurred within control individuals (44), and high-impact exercise within premenopausal sedentary women resulted in a significant increase in femoral neck bone mineral density (45).

2.5. Mechanisms underlying the augmented anabolic response to load

2.5.1. Initial hypothesis

The synergy between sclerostin deficiency and load was unexpected, and the focus of multiple mechanistic experiments. My primary hypothesis following these results was that other Wnt antagonists may show compensatory up-regulation (Chapters 2 and 3). Wnt factors, including

DKK1, Fzd, LRP6, Axin2, Naked, and Rspo are modulated by β-catenin dependent TCF/LEF transcription (46-49), and so negative feedback to Wnt/β-catenin activation is feasible. Further, elevated DKK1 expression is witnessed with sclerostin deficiency (24-26).

In the case of sclerostin deficiency, up-regulation of fellow Wnt antagonists could potentially down-regulate following bone loading to cause the augmented anabolic response. Previously, DKK1 expression has been shown to decrease following bone loading, within a rat ulnae loading model (50). This theory has been further supported by a recent *in vivo* mechanical loading study within the same *Sost* KO mice as used within this thesis (21). Elevated DKK1 expression seen within the *Sost* KO mice was significantly down-regulated 8 hours after a single tibial loading session. Similarly, in the case of complete knockout of DKK1 other Wnt antagonists, such as sclerostin, may have increased expression. This increased expression could in turn be more profoundly down-regulated following mechanical bone loading to result in an augmented anabolic response.

2.5.2. Limitations of gene profiling and mechanotransduction

Dkk1 expression was not found to be decreased 48 hrs after loading commencement, but rather was increased (Chapter 5). The discrepancy between these findings versus those of Robling *et al.* and Pflanz *et al*. (21, 50) may be attributable to differences in the time-points at which RNA was extracted. I assessed gene expression 24 hours after two loading sessions (48 hours after the first load session). In contrast, the rat ulnae loading study assessed *Dkk1* expression 24 hours after a single loading session (50).

The study by Pflanz *et al*. adds further confusion. The gene expression of a selected number of genes was assessed following a single loading session in 10 week old mice, showing a significant decrease in *Dkk1* expression 8 hours after loading in *Sost* KO mice, but no change within wild type mice at this same time-point (21). Further, *Dkk1* (and *Sost*) expression was not significantly altered at 3 or 24 hours post-loading at the 10-week age, nor at no time-point at 26 weeks age. *Sost* expression was down-regulated within the rat ulnae study at the 24 hour time-point (50). These data suggest that gene expression analyses will vary depending on the time-point assessed. This concept has been confirmed within a study investigating the temporal changes of gene expression

with loading in rodent ulnae; time-dependent patterns of gene expression was seen by microarray across a period of 4 hrs to 32 days post-commencement of daily loading (51).

Gene expression is likely to be dependent on spatial as well as temporal factors. Both were seen a recent murine tibial loading study that presented the transcriptional profile by RNAseq of cortical and cancellous bone at 3 and 24 hours post-mechanical loading (52). Cortical and cancellous bone had distinct gene expression, and the transcription profiles were markedly different at time-points 3 and 24 hours following loading. In addition to the time-point assessed and the type of bone assessed, other conditions of model and study design including age, loading regimen, animal type, animal strain, bone type, and strain-related regions of a bone must all be considered when assessing and consolidating gene expression data. There is ample evidence within the literature for these factors effecting gene expression (21, 50, 53-55).

2.5.3. Profiling of Wnt-responsive candidate bone genes

The hypothesis of compensation by fellow Wnt antagonists following deficiency of DKK1 or sclerostin was investigated within several of my pre-clinical studies.

Investigations into the changes in sclerostin expression were undertaken within the studies involving the *Dkk1* KO mouse. I undertook evaluation of the expression of the *Sost* gene following two days of compressive axial loading of tibiae within *Dkk1* KO and wild type mice, with RNA extracted 24 hours after the last loading cycle (Chapter 3). Notably, sclerostin levels were unaltered within *Dkk1* KO mice, suggesting that DKK1 deficiency may not result in a compensatory feed-back increase in sclerostin. This data represents the *Sost* expression within the cortical mid-diaphysis only, however sclerostin expression was also not seen to alter by immunohistochemistry within cancellous or cortical bone of *Dkk1* KO mice (Chapter 4).

Furthermore, sclerostin expression was significantly down-regulated with loading (Chapter 3), as has previously been observed (50, 56). However, the down-regulation of sclerostin following loading was similar between wild type and *Dkk1* KO mice, suggesting that regulation of sclerostin is not likely be the mechanism behind the augmented response to loading with DKK1 deficiency. These data agree with a previous study of DKK1-Ab administration to OVX rats, whereby authors

state that sclerostin expression was not altered with DKK1 deficiency (however data was not provided) (28).

Cortical bone from the mid-diaphysis of loaded and non-loaded C57Bl/6 tibiae were assessed by RNASeq to investigate any notable genetic expression changes with mechanical loading, Scl-Ab treatment and with loading/Scl-Ab combination (Chapter 5). Events causing the augmented anabolic bone response with loading in Scl-Ab treated mice was of particular interest, with the initial hypothesis involving consequent down-regulation following bone loading of possibly up-regulated fellow Wnt antagonists, such as DKK1.

Notably, DKK1 expression was increased following loading, regardless of drug treatment (Chapter 5). My work represents the transcriptional profile of cells from the murine tibial mid-diaphysis within a comparatively later snapshot of time post-loading. However, it remains that the augmented load response following blockade of the Wnt antagonist, sclerostin, is not likely to be solely a result of compensation from DKK1, or other Wnt antagonists. Although this may be a mechanism by which the anabolic response to mechanical loading is augmented, it is not likely to be the only or even primary mechanism. Other genes, including the Wnt factor *Wisp1* and known mechanotransduction factors, *Ptgs2*, *Tnfrsf11b*, and *Ptn* were significantly altered with combination Scl-Ab and loading above monotherapy. These may be keen areas for future investigation.

Particularly, the RNAseq data following loading and Scl-Ab treatment illustrates the complexity involved with the response to biomechanical loading and the possible intersection of many signalling pathways with the Wnt/β-catenin pathway downstream of Wnt-LRP5/6 signalling. This is a topic that has been expanding in recent years. Some of the cross-talk with the Wnt/β-catenin pathway following mechanical stimulation has been mentioned within Chapter 1, including focal-adhesion and cell-cell adhesion connections, nitric oxide, prostaglandins, and also estrogen receptor and PTH signalling (57-67).

An example within my data that contributes to the cross-talk theory is that COX-2 (encoded by *Ptgs2*) was shown to be significantly up-regulated with combination Scl-Ab and loading therapy, above either therapy alone. It is already known that mechanical loading induced bone formation is dependent on COX-2 formation of prostaglandins (68, 69). A recent publication suggests that prostaglandins are significant early responders to mechanical stimulation within bone and their

availability is likely mediated by COX-2 (64). Notably, β-catenin signalling, independent of LRP5/6, was activated in an *in vivo* mouse model as early as 1 hour post-mechanical loading (64). And this β-catenin signalling, and downstream down-regulation of sclerostin and DKK1, was inhibited when COX-2 was blocked by the COX inhibitor carprofen. This proposes that a COX-2 dependent, LRP5/6 independent, early response releases prostaglandin, activates β-catenin signalling and sclerostin and DKK1 down-regulation. Consequently, the regulation of the Wnt antagonists, sclerostin and DKK1, by these early responses may provide a mechanism for additional Wnt/β-catenin modulation.

Notably, within my RNAseq data, the Rho GTPase signalling pathway was significantly altered within tibiae of mice treated with a combination of Scl-Ab and mechanical loading, compared to tibiae of mice treated with only one of the therapies. GTPases are enzymes that bind and hydrolyse guanine nucleotide (GTP), behaving as a switch in the activity of a variety of physiological processes. Ras homologous small GTPases are activated during mechanical input (70), and the subgroup Rho GTPases have mechanotransduction roles within aortic and vascular smooth muscle cells, cardiac myocytes (71-73), and notably within osteoblasts (74-76). Additionally, one of the Rho GTPases, RhoA, mediates lineage commitment of MSCs *in vitro* in response to cell shape; MSCs adhered to a substrate underwent osteogenesis whilst rounded MSCs became adipocytes (77). Intriguingly, RhoA regulates stress fibre formation, which play an important role in cell adhesion, in response to mechanical strain (78). Within my data RhoA expression was not significantly altered within the combination Scl-Ab and mechanical loading group, above either monotherapy. However, *Ngef* (Ephexin-1) and *Srgap1* (srGAP1) were significantly increased, and amongst other roles, Ephexin-1 and srGAP1 are known to activate RhoA (79, 80).

2.6. A model for Wnt/β-catenin signalling and mechanotransduction

I currently hypothesise that following mechanical loading there is a requirement for the Wnt/β-catenin pathway to be "switched-on" to allow for mechanotransduction signal cascades. Although Wnt-LRP5/6 signalling undoubtedly plays a major role in the signalling transduction following mechanical stimulus, it is unlikely to be the sole mechanism involved and may not even be the earliest responder. An intact Wnt/β-catenin pathway is likely required to allow for β-catenin

mediated TCF/LEF transcription, which can be modulated by pathways that intersect the Wnt/β-catenin pathway independent of LRP5/6.

Two key studies have explored the importance of β-catenin in bone mechanotransduction. Javaheri *et al*. reported that deletion of a single copy of β-catenin within osteocytes ablates the anabolic response to loading (81). This suggests a minimum threshold of β-catenin expression, and thus an intact Wnt/β-catenin pathway, is critical for an anabolic response to mechanical loading. In contrast, Kang *et al*. more recently found that an anabolic bone response to loading can occur at the periosteal surface, even when β-catenin levels within DMP-1 expressing cells are significantly reduced (82). This raises the possibility that Wnt/LRP5 signalling may utilise other downstream factors independent of β-catenin to transduce a mechanosensory response.

Some study design differences are apparent that could explain for the dissimilar outcomes between the Javaheri *et al*. and Kang *et al*. studies. These two studies are mostly comparable in experimental design: mice of similar age and mixed C57Bl/6x129 background, both utilising ulna loading and similar strain engendered (2800 με versus 2500 με). However the single allele deletion of β-catenin within the Javaheri *et al*. study was from conception whilst Kang *et al*. induced adult-onset deletion of β-catenin within DMP-1 expressing cells. Kang *et al*. describe an 80% decrease in β-catenin expression, however this cannot be directly compared to Javaheri *et al*. to determine a critical threshold as levels were not described. Notably, the *Dmp1* promoter is not expressed in all osteocytes and is more active within early osteocytes (83) and so an inducible cre-recombinant deletion, as undertaken by Kang *et al*. may miss a number of the more mature osteocytes which could continue to respond to mechanical loading through β-catenin mediated mechanisms. Further to this, there is some evidence to an increased anabolic response to mechanical load with tamoxifen, though this effect is mainly seen within trabecular bone (84). Furthermore, tamoxifen is an estrogen receptor (ER) modulator, and ERα is crucial for bone to respond to mechanical load (85-87). Tamoxifen was utilised by Kang *et al*. to induce the cre-recombinant deletion of β-catenin, and it potentially may augment the response to mechanical loading.

Despite the number of limitations within the Kang *et al*. study, β-catenin independent mechanosensory pathways capable of transducing a signal response to mechanical load may not yet be definitively discounted. If β-catenin is dispensable for periosteal bone formation to occur in

response to mechanical stimulation than studies will need to look wider than pathway interactions with the Wnt/β-catenin pathway to include those that are independent of β-catenin stabilisation.

3. Future directions

3.1. Enhancing Scl-Ab therapy outcomes with exercise programs

The data supporting using exercise to augment Scl-Ab therapy, particularly in cases of low bone mass, remains one of the most profound and exciting findings. The limitations of directly translating this pre-clinical work into clinical studies have been discussed. However, the potential of applying a brief program of high-magnitude and high-frequency stimulation (36-38) makes it a practical adjunctive therapy.

Reviews on the subject of observational effects of exercise on bone suggests that walking- and jogging-based exercise have little impact in preventing osteoporosis, with resistance and weight-bearing exercise having more potential (42, 88, 89). Such future clinical investigations into exercise plans alongside Scl-Ab treatment could ultimately potentially model some successfully implemented studies whereby bone mineral density improvements were correlated with resistance-training in older adults (44, 90-93).

3.1.1. Pre-clinical studies in aged mice

As Scl-Ab is predicted to become a mainstay therapy for age-related osteoporosis it should be established whether age affects the augmented effect seen with mechanical loading alongside Scl-Ab treatment. Experimental studies have shown that the anabolic bone response to mechanical loading is reduced with age in C57Bl/6 mice (21, 53, 94-97), and may explain in part why less marked osteogenic results have been seen in clinical adult and aged exercise studies.

It is possible that Scl-Ab therapy may restore mechanoresponsiveness that is hindered in the aged. Recently, the abrogated load-induced bone formation response seen within aged wild type mice was restored within aged *Sost* KO mice (21). As sclerostin levels are known to be increased with age in humans, (98, 99) there is accumulating evidence that sclerostin may play an important role in age-related dampening of the mechanotransduction response.

I propose a pre-clinical investigation into Scl-Ab treatment alongside mechanical loading in aged C57Bl/6 mice (26 weeks old), assessing the osteogenic response to mechanical loading. The study design would be similar to that of Chapter 5, however I recommend a longer initial Scl-Ab dose period, such as two weeks prior to loading, to improve osteogenic outcomes. The greater anabolic

effect of Scl-Ab within Chapter 5 was seen within the cancellous bone, with a less marked effect seen within the cortical bone. As the osteogenic effect of Scl-Ab is dose-dependent, (22) a longer dose period may improve cortical bone outcomes for combination Scl-Ab and mechanical loading therapy.

3.1.2. Post-release monitoring of activity levels in Scl-Ab treated patients

Within the clinical setting I recommend that investigations initially commence through post-release monitoring of the impact of existing activity of individuals undergoing Scl-Ab therapy. Romosozumab/EVENITY (Scl-Ab developed by Amgen and UCB Pharma) has undergone Phase III clinical trials within postmenopausal women (3). Promising results of improved bone mass and reduced vertebral fractures means the drug may be set for achieving market approval soon. This however will depend on the US Food and Drug Administration's (FDA) approval following recent disclosure of a safety concern of increased cardiovascular events occurring within romosozumab-treated subjects (100). If romosozumab/EVENITY is released on to the market, a post-release trial could easily be implemented to assess the activity/sedentary levels of Scl-Ab treated individuals. This could be achieved through a method of a standardised survey.

Two notable quantitative history recall questionnaires have been developed specifically and used clinically to obtain information regarding the type and frequency of physical activity performed in a designated past time-period (e.g. past month, year or lifetime) (101). The Exercise Vital Sign (EVS) questionnaire, is simple in its design, with only two items asking days per week and minutes per event of moderate-intensity physical activity (102). The Physical Activity Vital Sign (PAVS) questionnaire, is designed to obtain past and typical week moderate to vigorous physical activity (103). Such monitoring could assess activity and bone density correlations for those on Scl-Ab therapy and provide some valuable evidence regarding the level of activity and type of exercise that may improve osteogenic outcomes of Scl-Ab therapy.

3.2. Pre-clinical studies combining Wnt-pathway antagonists and exercise

It remains unclear whether combination therapy with dual Scl-Ab and DKK1-Ab alongside high-magnitude exercise would further augment the osteogenic response, or whether there is some

redundancy with the three-tiered therapy. My data show within mice that bone anabolism is synergistically improved with combination DKK1 and sclerostin deficiency, and also separately with long-term sclerostin deficiency and mechanical loading. It is hypothesised that the anabolic response of bone to load will be further heightened by combined Scl-Ab/DKK1-Ab treatment.

I recommend a murine study combining weekly DKK1-Ab and Scl-Ab treatment in C57Bl/6 mice with tibial mechanical loading. Based on the study by Pflanz *et al*. study showing restored load-induced bone formation with sclerostin deficiency in aged mice (21), such a study would be optimally performed in performed in both adult and aged mice (10 weeks and 26 weeks). Bone volume, bone mineral density, cortical thickness, bone formation parameters would be important outcome measures to assess by microCT after 2 weeks of a 5 days/week loading regimen. Mechanical strength testing would also be a valuable end-point outcome to determine any physical improvements in the strength of the bone. A cyclic axial compression protocol of 1200 με, 1200 cycles, 4 Hz would allow for direct comparison to prior studies. In addition, gene expression could be measured at early response stages of 3, 8, and 24 hours post first loading cycle, and also the later response stage of 48 hours post the first loading cycle. Heightened Wnt/β-catenin signalling is expected, although the Rho GTPase signalling pathway would also be a candidate for specific interrogation. Other novel interactions could emerge from RNASeq data.

3.3. The role of the Rho GTPase pathway in bone homeostasis and mechanotransduction

The RNASeq analysis performed within my thesis provide some novel and notable findings. As mentioned, the Rho GTPase signalling pathway was altered with the combination Scl-Ab and mechanical loading therapy, above either monotherapy. Further investigations are required into the potential role that Rho GTPases may have in bone mechanotransduction.

I recommend *in vitro* biomechanical loading studies to be undertaken on established murine cell lines for osteocytes (MLO-Y4), osteoblasts (MC3T3-E1) and MSCs (C3H10T1/2), and later upon murine primary osteocyte and osteoblast cells. Rho GTPases have been implicated in mechanotransduction within aortic and vascular smooth muscle cells and cardiac myocytes (71-73), and also osteoblasts (74, 75). *In vitro* mechanical loading studies encompass a range of models including vibration, fluid flow and substrate strain, and these have been reviewed extensively for

both use in bone-derived and other cells (104-106). These studies could also include sclerostin inhibition (through Scl-Ab administration) as well as the exogenous addition of sclerostin.

These studies should involve the biochemical inhibition and activation of RhoA to investigate the role of RhoA in bone mechanotransduction. RhoA is activated by Ephexin-1 and srGAP1, both of which were significantly increased with combination Scl-Ab and loading therapy in mice, and is a prime candidate within this research. RhoA abrogation can be achieved through the addition of C3 exoenzyme (72). RhoA overexpression can be achieved through transfection of cells with constructs containing the genes encoding for constitutively activated RhoA (107, 108).

Importantly, the gene and protein expression profiling should be undertaken for these experiments. Known mechanoresponders within osteocytes, including Cox-2 and β-catenin, could be assessed, along with osteogenic factors, such as Runx2, alkaline phosphatase and osteocalcin, within osteoblasts. As RhoA has been previously shown to mediate lineage commitment of MSCs *in vitro* in response to cell shape, likely through regulation of stress fibre formation and cell adhesion (77, 78), chondrogenic, and adipogenic differentiation factors should be assessed alongside osteogenic factors, for example Sox9 and PPARγ. This could glean some information regarding MSC cell fate following mechanical stimulation and RhoA/sclerostin activation/inhibition.

Importantly, the transcription profile of the Rho GTPase pathway factors would be valuable for all these *in vitro* studies, allowing the response assessment of other family members in addition to RhoA. In some cases it may be the activity of a factor, rather than the transcription levels that should be assessed. Rac1, in particular, is a candidate of interest whereby activity has a known effect of β-catenin/TCF mediated transcription, rather than expression level (109).

3.4. Interaction between Rho GTPase and Wnt/β-catenin pathways

Rho family proteins have been previously reported to interact with the Wnt/β-catenin pathway. These are limited to cancer cells, developing embryos, and embryonic cells (109-112), however it is likely that such similar interactions could occur within bone cells. A pertinent example of this interaction was seen in a colon cancer cell line. β-catenin/TCF transcription was enhanced with activated Rac, a Rho GTPase family member, and β-catenin/TCF transcription was inhibited by dominant-negative Rac (109). The theory is that Rac enhances β-catenin accumulation and that

Rac1 facilitates the transfer of β-catenin into the nucleus (109, 110). Rho GTPase interactions may be a primary mechanism for the enhanced anabolism seen with combination Scl-Ab and mechanical loading therapy, though investigation is required to confirm this. Rac was not significantly altered with combination Scl-Ab and loading therapy, however Ephexin-1 and srGAP1 (which had increased expression) are known to activate Rac (79, 80). Importantly, it has previously been shown that it is the activation of Rac1, not the expression levels that impact β-catenin/TCF-mediated transcription (109).

Rho GTPases also have a defined central role within the (non-canonical Wnt) PCP pathway (113). Amongst other processes Wnt-PCP activation is known to regulate osteoblastogenesis and osteoclastogenesis (114). The PCP pathway organises the actin cytoskeleton through the regulation of cell polarity and convergent extension movements during axis formation (112, 115, 116). These are achieved through two divergent pathways involving the small GTPases Rac and Rho, both activated by Fzd/Dvl. Rac activation stimulates c-Jun N-terminal Kinase (JNK) and nemo-like kinase (NLK) signalling cascades (117, 118). Notably, NLK has a known ability to dissolve the binding of β-catenin to transcriptional factors and thus antagonising the Wnt/β-catenin pathway (119, 120). The alteration of the Rho GTPase signalling seen with combination Scl-Ab and loading therapy may also be a result of heightened non-canonical signalling, with downstream effects of osteoblastogenesis and osteoclastogenesis, and also potential interaction with the Wnt/β-catenin pathway. These theories are yet to be investigated.

With Rho GTPase signalling altered with combination Scl-Ab and loading, above either monotherapy (Chapter 5), this remains an important focus for future studies. Similar to studies undertaken within colon cells (109, 110), *in vitro* investigations could be undertaken to assess whether β-catenin/TCF transcription can be modulated by Rac within bone-derived cells, specifically exploring whether Rac enhances β-catenin accumulation and Rac1 facilitates β-catenin nuclear transfer.

A series of *in vitro* investigations is recommended. Rac1 activation status could be first determined within a panel of *in vitro* cell lines (MLO-Y4, MC3T3-E1 and C3H10T1/2) and primary osteocyte and osteoblast cells. Rac1-GTP (activity) levels can be determined using a Rac activity Assay kit (Upstate Biotechnology Inc, NY, USA). Next, β-catenin/TCF transcription could be assessed within a chosen *in vitro* cell line following blockade or constitutive activation of Rac1. Such Rac1

blockade/activation has previously been achieved through transfection of mutated Rac1, and β-catenin/TCF transcription levels assessed via luciferase activity following transfection with TOPFLASH to a TCF-responsive promoter (109). Following these baseline studies, Rac1 and β-catenin/TCF transcription activities could then be assessed following the addition of exogenous sclerostin and the inhibition of sclerostin (Scl-Ab). These studies would provide some valuable insight into the interaction of Rac1 and the Wnt/β-catenin pathway and downstream β-catenin/TCF-mediated transcription responses.

4. Conclusion

For bone mechanotransduction, the mechanisms, mechanosensors, and signal transducers are numerous, complex, and far from elucidated. Wnt/β-catenin signalling is nevertheless critical for this process and modulating this pathway produces profound effects on bone formation, bone resorption, and ultimately bone mass.

In this thesis, the crosstalk between the Wnt/β-catenin pathway and biomechanical loading was examined. Increased Wnt/β-catenin signalling was found to augment the response of bone to increased mechanical loading. This crucially confirms that exercise is not redundant with therapies that activate the Wnt/β-catenin pathway, such as Scl-Ab, rejecting the first hypothesis of this thesis. Indeed these therapies may enhance the response to exercise. While this may be partly due to compensation by DKK1 or other Wnt antagonists, our data suggests this is unlikely to be the sole cause. This rejects the third hypothesis of this thesis. Still, assessing the effects of dual DKK1 and sclerostin deficiency on bone anabolism suggests that combining Wnt/β-catenin activating therapies can yield synergistic effects on bone anabolism, confirming the second hypothesis of this thesis. A great deal more work is required within this area of research due to gene transcription being temporally sensitive, as well as affected by differences in model and study design.

This thesis has significant translational impact in terms of predicting the utility of neutralising antibodies to sclerostin in the context of loading and exercise. These data support the future clinical use of such antibodies within osteoporosis treatment and other conditions of bone-loss, whereby load/resistance based exercise can increase the efficacy of therapy. Furthermore, new genetic circuits (such as Wnt/β-catenin cross-talk with the Rho GTPase signalling pathway) represent targets for future pre-clinical studies. These investigations may identify new drug targets for treating osteoporosis and other bone fragility disorders.

References:

1. McClung MR, Grauer A, Boonen S, Bolognese MA, Brown JP, Diez-Perez A, et al. Romosozumab in Postmenopausal Women with Low Bone Mineral Density. The New England journal of medicine. 2014;370(5):412-20.

2. Recker RR, Benson CT, Matsumoto T, Bolognese MA, Robins DA, Alam J, et al. A randomized, double-blind phase 2 clinical trial of blosozumab, a sclerostin antibody, in postmenopausal women with low bone mineral density. J Bone Miner Res. 2015;30(2):216-24.

3. Cosman F, Crittenden DB, Adachi JD, Binkley N, Czerwinski E, Ferrari S, et al. Romosozumab Treatment in Postmenopausal Women with Osteoporosis. The New England journal of medicine. 2016;375(16):1532-43.

4. Lin C, Jiang X, Dai Z, Guo X, Weng T, Wang J, et al. Sclerostin mediates bone response to mechanical unloading through antagonizing Wnt/beta-catenin signaling. J Bone Miner Res. 2009;24(10):1651-61.

5. Spatz JM, Ellman R, Cloutier AM, Louis L, van Vliet M, Suva LJ, et al. Sclerostin antibody inhibits skeletal deterioration due to reduced mechanical loading. J Bone Miner Res. 2013;28(4):865-74.

6. Robling AG, Kang KS, Bullock WA, Foster WH, Murugesh D, Loots GG, et al. Sost, independent of the non-coding enhancer ECR5, is required for bone mechanoadaptation. Bone. 2016;92:180-8.

7. Kale PP, Addepalli V, Ghadawale SR. Impact of pre-exposure of tail suspension on behavioural parameters like locomotion, exploration, and anxiety in mice. Indian journal of experimental biology. 2013;51(9):732-8.

8. Hamrick MW. A Role for Myokines in Muscle-Bone Interactions. Exercise and sport sciences reviews. 2011;39(1):43-7.

9. Collet P, Uebelhart D, Vico L, Moro L, Hartmann D, Roth M, et al. Effects of 1- and 6-month spaceflight on bone mass and biochemistry in two humans. Bone. 1997;20(6):547-51.

10. Minaire P, Berard E, Meunier PJ, Edouard C, Goedert G, Pilonchery G. Effects of disodium dichloromethylene diphosphonate on bone loss in paraplegic patients. The Journal of clinical investigation. 1981;68(4):1086-92.

11. Chappard D, Minaire P, Privat C, Berard E, Mendoza-Sarmiento J, Tournebise H, et al. Effects of tiludronate on bone loss in paraplegic patients. J Bone Miner Res. 1995;10(1):112-8.

12. Pearson EG, Nance PW, Leslie WD, Ludwig S. Cyclical etidronate: its effect on bone density in patients with acute spinal cord injury. Archives of physical medicine and rehabilitation. 1997;78(3):269-72.

13. Roberts D, Lee W, Cuneo RC, Wittmann J, Ward G, Flatman R, et al. Longitudinal study of bone turnover after acute spinal cord injury. J Clin Endocrinol Metab. 1998;83(2):415-22.

14. Nance PW, Schryvers O, Leslie W, Ludwig S, Krahn J, Uebelhart D. Intravenous pamidronate attenuates bone density loss after acute spinal cord injury. Archives of physical medicine and rehabilitation. 1999;80(3):243-51.

15. Caillot-Augusseau A, Lafage-Proust MH, Soler C, Pernod J, Dubois F, Alexandre C. Bone formation and resorption biological markers in cosmonauts during and after a 180-day space flight (Euromir 95). Clinical chemistry. 1998;44(3):578-85.

16. Sniger W, Garshick E. Alendronate increases bone density in chronic spinal cord injury: a case report. Archives of physical medicine and rehabilitation. 2002;83(1):139-40.

17. Vanderoost J, van Lenthe GH. From histology to micro-CT: Measuring and modeling resorption cavities and their relation to bone competence. World journal of radiology. 2014;6(9):643-56.

18. Saxon LK, Jackson BF, Sugiyama T, Lanyon LE, Price JS. Analysis of multiple bone responses to graded strains above functional levels, and to disuse, in mice in vivo show that the human Lrp5 G171V High Bone Mass mutation increases the osteogenic response to loading but that lack of Lrp5 activity reduces it. Bone. 2011;49(2):184-93.

19. Robinson JA, Chatterjee-Kishore M, Yaworsky PJ, Cullen DM, Zhao W, Li C, et al. Wnt/beta-catenin signaling is a normal physiological response to mechanical loading in bone. J Biol Chem. 2006;281(42):31720-8.

20. Niziolek PJ, Warman ML, Robling AG. Mechanotransduction in bone tissue: The A214V and G171V mutations in Lrp5 enhance load-induced osteogenesis in a surface-selective manner. Bone. 2012;51(3):459-65.

21. Pflanz D, Birkhold AI, Albiol L, Thiele T, Julien C, Seliger A, et al. Sost deficiency led to a greater cortical bone formation response to mechanical loading and altered gene expression. Scientific reports. 2017;7(1):9435.

22. Padhi D, Jang G, Stouch B, Fang L, Posvar E. Single-dose, placebo-controlled, randomized study of AMG 785, a sclerostin monoclonal antibody. J Bone Miner Res. 2011;26(1):19-26.

23. McColm J, Hu L, Womack T, Tang CC, Chiang AY. Single- and multiple-dose randomized studies of blosozumab, a monoclonal antibody against sclerostin, in healthy postmenopausal women. J Bone Miner Res. 2014;29(4):935-43.

24. van Lierop A, Moester M, Hamdy N, Papapoulos S. Serum Dickkopf 1 Levels in Sclerostin Deficiency. J Clin Endocrinol Metab. 2014;99(2):E252-6.

25. Chang MK, Kramer I, Keller H, Gooi JH, Collett C, Jenkins D, et al. Reversing LRP5-dependent osteoporosis and SOST-deficiency induced sclerosing bone disorders by altering WNT signaling activity. J Bone Miner Res. 2014;29(1):29-42.

26. Florio M, Gunasekaran K, Stolina M, Li X, Liu L, Tipton B, et al. A bispecific antibody targeting sclerostin and DKK-1 promotes bone mass accrual and fracture repair. Nature communications. 2016;7:11505.

27. McDonald MM, Morse A, Schindeler A, Mikulec K, Peacock L, Cheng T, et al. Homozygous Dkk1 Knockout Mice Exhibit High Bone Mass Phenotype Due to Increased Bone Formation. Calcif Tissue Int. 2017.

28. Li X, Grisanti M, Fan W, Asuncion FJ, Tan HL, Dwyer D, et al. Dickkopf-1 regulates bone formation in young growing rodents and upon traumatic injury. J Bone Miner Res. 2011;26(11):2610-21.

29. Holdsworth G, Greenslade K, Jose J, Stencel Z, Kirby H, Moore A, et al. Dampening of the bone formation response following repeat dosing with sclerostin antibody in mice is associated with up-regulation of Wnt antagonists. Bone. 2017;107:93-103.

30. Duncan RL, Turner CH. Mechanotransduction and the functional response of bone to mechanical strain. Calcif Tissue Int. 1995;57(5):344-58.

31. Rubin CT, Lanyon LE. Dynamic strain similarity in vertebrates; an alternative to allometric limb bone scaling. Journal of theoretical biology. 1984;107(2):321-7.

32. Fritton SP, McLeod KJ, Rubin CT. Quantifying the strain history of bone: spatial uniformity and self-similarity of low-magnitude strains. Journal of biomechanics. 2000;33(3):317-25.

33. Adams DJ, Spirt AA, Brown TD, Fritton SP, Rubin CT, Brand RA. Testing the daily stress stimulus theory of bone adaptation with natural and experimentally controlled strain histories. Journal of biomechanics. 1997;30(7):671-8.

34. Huang RP, Rubin CT, McLeod KJ. Changes in postural muscle dynamics as a function of age. The journals of gerontology Series A, Biological sciences and medical sciences. 1999;54(8):B352-7.

35. Qin YX, Rubin CT, McLeod KJ. Nonlinear dependence of loading intensity and cycle number in the maintenance of bone mass and morphology. J Orthop Res. 1998;16(4):482-9.

36. Rubin CT, Lanyon LE. Regulation of bone mass by mechanical strain magnitude. Calcif Tissue Int. 1985;37(4):411-7.

37. Rubin CT, Lanyon LE. Regulation of bone formation by applied dynamic loads. J Bone Joint Surg Am. 1984;66(3):397-402.

38. Lanyon LE, Rubin CT. Static vs dynamic loads as an influence on bone remodelling. Journal of biomechanics. 1984;17(12):897-905.

39. Fuchs RK, Bauer JJ, Snow CM. Jumping improves hip and lumbar spine bone mass in prepubescent children: a randomized controlled trial. J Bone Miner Res. 2001;16(1):148-56.

40. McKay HA, Macdonald HM, Nettlefold L, Masse LC, Day M, Naylor PJ. Action Schools! BC implementation: from efficacy to effectiveness to scale-up. British journal of sports medicine. 2015;49(4):210-8.

41. Macdonald H, Manske S, Reed K, Khan K, McKay H. 270 Action Schools! BC: Daily physical activity increases bone strength in prepubertal boys. Journal of Science and Medicine in Sport. 2005;8:153.

42. Russo CR. The effects of exercise on bone. Basic concepts and implications for the prevention of fractures. Clinical Cases in Mineral and Bone Metabolism. 2009;6(3):223-8.

43. Kerr D, Morton A, Dick I, Prince R. Exercise effects on bone mass in postmenopausal women are site-specific and load-dependent. J Bone Miner Res. 1996;11(2):218-25.

44. Nelson ME, Fiatarone MA, Morganti CM, Trice I, Greenberg RA, Evans WJ. Effects of high-intensity strength training on multiple risk factors for osteoporotic fractures. A randomized controlled trial. Jama. 1994;272(24):1909-14.

45. Heinonen A, Kannus P, Sievanen H, Oja P, Pasanen M, Rinne M, et al. Randomised controlled trial of effect of high-impact exercise on selected risk factors for osteoporotic fractures. Lancet (London, England). 1996;348(9038):1343-7.

46. Khan Z, Vijayakumar S, de la Torre TV, Rotolo S, Bafico A. Analysis of endogenous LRP6 function reveals a novel feedback mechanism by which Wnt negatively regulates its receptor. Molecular and cellular biology. 2007;27(20):7291-301.

47. Chamorro MN, Schwartz DR, Vonica A, Brivanlou AH, Cho KR, Varmus HE. FGF-20 and DKK1 are transcriptional targets of beta-catenin and FGF-20 is implicated in cancer and development. The EMBO journal. 2005;24(1):73-84.

48. Kazanskaya O, Glinka A, del Barco Barrantes I, Stannek P, Niehrs C, Wu W. R-Spondin2 is a secreted activator of Wnt/beta-catenin signaling and is required for Xenopus myogenesis. Dev Cell. 2004;7(4):525-34.

49. Logan CY, Nusse R. The Wnt signaling pathway in development and disease. Annu Rev Cell Dev Biol. 2004;20:781-810.

50. Robling AG, Niziolek PJ, Baldridge LA, Condon KW, Allen MR, Alam I, et al. Mechanical stimulation of bone in vivo reduces osteocyte expression of Sost/sclerostin. J Biol Chem. 2008;283(9):5866-75.

51. Mantila Roosa SM, Turner CH, Liu Y. Regulatory Mechanisms in Bone Following Mechanical Loading. Gene Regulation and Systems Biology. 2012;6:43-53.

52. Kelly NH, Schimenti JC, Ross FP, van der Meulen MC. Transcriptional profiling of cortical versus cancellous bone from mechanically-loaded murine tibiae reveals differential gene expression. Bone. 2016;86:22-9.

53. Holguin N, Brodt MD, Silva MJ. Activation of Wnt Signaling by Mechanical Loading Is Impaired in the Bone of Old Mice. J Bone Miner Res. 2016;31(12):2215-26.

54. Silva MJ, Brodt MD, Lynch MA, Stephens AL, Wood DJ, Civitelli R. Tibial Loading Increases Osteogenic Gene Expression and Cortical Bone Volume in Mature and Middle-Aged Mice. PLoS ONE. 2012;7(4):e34980.

55. Holguin N, Brodt MD, Sanchez ME, Kotiya AA, Silva MJ. Adaptation of tibial structure and strength to axial compression depends on loading history in both C57BL/6 and BALB/c mice. Calcif Tissue Int. 2013;93(3):211-21.

56. Moustafa A, Sugiyama T, Prasad J, Zaman G, Gross T, Lanyon L, et al. Mechanical loading-related changes in osteocyte sclerostin expression in mice are more closely associated with the subsequent osteogenic response than the peak strains engendered. Osteoporosis International. 2011:1-10.

57. Sen B, Styner M, Xie Z, Case N, Rubin CT, Rubin J. Mechanical loading regulates NFATc1 and beta-catenin signaling through a GSK3beta control node. J Biol Chem. 2009;284(50):34607-17.

58. Case N, Thomas J, Sen B, Styner M, Xie Z, Galior K, et al. Mechanical regulation of glycogen synthase kinase 3beta (GSK3beta) in mesenchymal stem cells is dependent on Akt protein serine 473 phosphorylation via mTORC2 protein. J Biol Chem. 2011;286(45):39450-6.

59. Santos A, Bakker AD, Zandieh-Doulabi B, de Blieck-Hogervorst JM, Klein-Nulend J. Early activation of the beta-catenin pathway in osteocytes is mediated by nitric oxide, phosphatidyl inositol-3 kinase/Akt, and focal adhesion kinase. Biochem Biophys Res Commun. 2010;391(1):364-9.

60. Fang D, Hawke D, Zheng Y, Xia Y, Meisenhelder J, Nika H, et al. Phosphorylation of beta-catenin by AKT promotes beta-catenin transcriptional activity. J Biol Chem. 2007;282(15):11221-9.

61. Ponce DP, Maturana JL, Cabello P, Yefi R, Niechi I, Silva E, et al. Phosphorylation of AKT/PKB by CK2 is necessary for the AKT-dependent up-regulation of beta-catenin transcriptional activity. J Cell Physiol. 2011;226(7):1953-9.

62. Sunters A, Armstrong VJ, Zaman G, Kypta RM, Kawano Y, Lanyon LE, et al. Mechano-transduction in osteoblastic cells involves strain-regulated estrogen receptor alpha-mediated control of insulin-like growth factor (IGF) I receptor sensitivity to Ambient IGF, leading to phosphatidylinositol 3-kinase/AKT-dependent Wnt/LRP5 receptor-independent activation of beta-catenin signaling. J Biol Chem. 2010;285(12):8743-58.

63. Norvell SM, Alvarez M, Bidwell JP, Pavalko FM. Fluid shear stress induces beta-catenin signaling in osteoblasts. Calcif Tissue Int. 2004;75(5):396-404.

64. Lara-Castillo N, Kim-Weroha NA, Kamel MA, Javaheri B, Ellies DL, Krumlauf RE, et al. In vivo mechanical loading rapidly activates beta-catenin signaling in osteocytes through a prostaglandin mediated mechanism. Bone. 2015;76:58-66.

65. Sawakami K, Robling AG, Ai M, Pitner ND, Liu D, Warden SJ, et al. The Wnt co-receptor LRP5 is essential for skeletal mechanotransduction but not for the anabolic bone response to parathyroid hormone treatment. J Biol Chem. 2006;281(33):23698-711.

66. Guo J, Liu M, Yang D, Bouxsein ML, Saito H, Galvin RJ, et al. Suppression of Wnt signaling by Dkk1 attenuates PTH-mediated stromal cell response and new bone formation. Cell Metab. 2010;11(2):161-71.

67. Wan M, Yang C, Li J, Wu X, Yuan H, Ma H, et al. Parathyroid hormone signaling through low-density lipoprotein-related protein 6. Genes Dev. 2008;22(21):2968-79.

68. Li J, Burr DB, Turner CH. Suppression of prostaglandin synthesis with NS-398 has different effects on endocortical and periosteal bone formation induced by mechanical loading. Calcif Tissue Int. 2002;70(4):320-9.

69. Kunnel JG, Igarashi K, Gilbert JL, Stern PH. Bone anabolic responses to mechanical load in vitro involve COX-2 and constitutive NOS. Connective tissue research. 2004;45(1):40-9.

70. Thompson WR, Rubin CT, Rubin J. Mechanical regulation of signaling pathways in bone. Gene. 2012;503(2):179-93.

71. Putnam AJ, Cunningham JJ, Pillemer BB, Mooney DJ. External mechanical strain regulates membrane targeting of Rho GTPases by controlling microtubule assembly. American journal of physiology Cell physiology. 2003;284(3):C627-39.

72. Aikawa R, Komuro I, Yamazaki T, Zou Y, Kudoh S, Zhu W, et al. Rho family small G proteins play critical roles in mechanical stress-induced hypertrophic responses in cardiac myocytes. Circ Res. 1999;84(4):458-66.

73. Katsumi A, Milanini J, Kiosses WB, del Pozo MA, Kaunas R, Chien S, et al. Effects of cell tension on the small GTPase Rac. The Journal of cell biology. 2002;158(1):153-64.

74. Arnsdorf EJ, Tummala P, Kwon RY, Jacobs CR. Mechanically induced osteogenic differentiation--the role of RhoA, ROCKII and cytoskeletal dynamics. Journal of cell science. 2009;122(Pt 4):546-53.

75. Hamamura K, Swarnkar G, Tanjung N, Cho E, Li J, Na S, et al. RhoA-mediated signaling in mechanotransduction of osteoblasts. Connective tissue research. 2012;53(5):398-406.

76. Pavalko FM, Chen NX, Turner CH, Burr DB, Atkinson S, Hsieh YF, et al. Fluid shear-induced mechanical signaling in MC3T3-E1 osteoblasts requires cytoskeleton-integrin interactions. The American journal of physiology. 1998;275(6 Pt 1):C1591-601.

77. Bhadriraju K, Yang M, Alom Ruiz S, Pirone D, Tan J, Chen CS. Activation of ROCK by RhoA is regulated by cell adhesion, shape, and cytoskeletal tension. Experimental cell research. 2007;313(16):3616-23.

78. Chrzanowska-Wodnicka M, Burridge K. Rho-stimulated contractility drives the formation of stress fibers and focal adhesions. The Journal of cell biology. 1996;133(6):1403-15.

79. Tolias KF, Duman JG, Um K. Control of synapse development and plasticity by Rho GTPase regulatory proteins. Progress in neurobiology. 2011;94(2):133-48.

80. Yamazaki D, Itoh T, Miki H, Takenawa T. srGAP1 regulates lamellipodial dynamics and cell migratory behavior by modulating Rac1 activity. Molecular Biology of the Cell. 2013;24(21):3393-405.

81. Javaheri B, Stern AR, Lara N, Dallas M, Zhao H, Liu Y, et al. Deletion of a single beta-catenin allele in osteocytes abolishes the bone anabolic response to loading. J Bone Miner Res. 2014;29(3):705-15.

82. Kang KS, Hong JM, Robling AG. Postnatal beta-catenin deletion from Dmp1-expressing osteocytes/osteoblasts reduces structural adaptation to loading, but not periosteal load-induced bone formation. Bone. 2016;88:138-45.

83. Toyosawa S, Oya K, Sato S, Ishida K. [Osteocyte and DMP1]. Clinical calcium. 2012;22(5):713-20.

84. Sugiyama T, Galea GL, Lanyon LE, Price JS. Mechanical Loading-Related Bone Gain Is Enhanced by Tamoxifen but Unaffected by Fulvestrant in Female Mice. Endocrinology. 2010;151(12):5582-90.

85. Windahl SH, Saxon L, Börjesson AE, Lagerquist MK, Frenkel B, Henning P, et al. Estrogen receptor-α is required for the osteogenic response to mechanical loading in a ligand-independent manner involving its activation function 1 but not 2. Journal of Bone and Mineral Research. 2013;28(2):291-301.

86. Lee K, Jessop H, Suswillo R, Zaman G, Lanyon L. Endocrinology: bone adaptation requires oestrogen receptor-alpha. Nature. 2003;424(6947):389.

87. Lee KC, Jessop H, Suswillo R, Zaman G, Lanyon LE. The adaptive response of bone to mechanical loading in female transgenic mice is deficient in the absence of oestrogen receptor-alpha and -beta. The Journal of endocrinology. 2004;182(2):193-201.

88. Guadalupe-Grau A, Fuentes T, Guerra B, Calbet JA. Exercise and bone mass in adults. Sports medicine (Auckland, NZ). 2009;39(6):439-68.

89. Nikander R, Sievänen H, Heinonen A, Daly RM, Uusi-Rasi K, Kannus P. Targeted exercise against osteoporosis: A systematic review and meta-analysis for optimising bone strength throughout life. BMC Medicine. 2010;8:47.

90. Kukuljan S, Nowson CA, Bass SL, Sanders K, Nicholson GC, Seibel MJ, et al. Effects of a multi-component exercise program and calcium-vitamin-D3-fortified milk on bone mineral density in older men: a randomised controlled trial. Osteoporosis international : a journal established as result of cooperation between the European Foundation for Osteoporosis and the National Osteoporosis Foundation of the USA. 2009;20(7):1241-51.

91. Maddalozzo GF, Snow CM. High intensity resistance training: effects on bone in older men and women. Calcif Tissue Int. 2000;66(6):399-404.

92. Menkes A, Mazel S, Redmond RA, Koffler K, Libanati CR, Gundberg CM, et al. Strength training increases regional bone mineral density and bone remodeling in middle-aged and older men. Journal of applied physiology (Bethesda, Md : 1985). 1993;74(5):2478-84.

93. Pruitt LA, Taaffe DR, Marcus R. Effects of a one-year high-intensity versus low-intensity resistance training program on bone mineral density in older women. J Bone Miner Res. 1995;10(11):1788-95.

94. Birkhold AI, Razi H, Duda GN, Weinkamer R, Checa S, Willie BM. The influence of age on adaptive bone formation and bone resorption. Biomaterials. 2014;35(34):9290-301.

95. Birkhold AI, Razi H, Duda GN, Weinkamer R, Checa S, Willie BM. Mineralizing surface is the main target of mechanical stimulation independent of age: 3D dynamic in vivo morphometry. Bone. 2014;66:15-25.

96. Lynch ME, Main RP, Xu Q, Schmicker TL, Schaffler MB, Wright TM, et al. Tibial compression is anabolic in the adult mouse skeleton despite reduced responsiveness with aging. Bone. 2011;49(3):439-46.

97. Razi H, Birkhold AI, Weinkamer R, Duda GN, Willie BM, Checa S. Aging Leads to a Dysregulation in Mechanically Driven Bone Formation and Resorption. J Bone Miner Res. 2015;30(10):1864-73.

98. Bhattoa HP, Wamwaki J, Kalina E, Foldesi R, Balogh A, Antal-Szalmas P. Serum sclerostin levels in healthy men over 50 years of age. Journal of bone and mineral metabolism. 2013;31(5):579-84.

99. Modder UI, Hoey KA, Amin S, McCready LK, Achenbach SJ, Riggs BL, et al. Relation of age, gender, and bone mass to circulating sclerostin levels in women and men. J Bone Miner Res. 2011;26(2):373-9.

100. Amgen And UCB Announce Top-Line Phase 3 Data From Active-Comparator Study Of EVENITY™ (Romosozumab) In Postmenopausal Women With Osteoporosis [press release]. 21 May 2017.

101. Ainsworth B, Buchholz SW. How to Assess Physical Activity in Clinical Practice and for Scholarly Work. The Journal for Nurse Practitioners. 2017;13(1):14-20.e2.

102. Young DR, Coleman KJ, Ngor E, Reynolds K, Sidell M, Sallis RE. Associations Between Physical Activity and Cardiometabolic Risk Factors Assessed in a Southern California Health Care System, 2010-2012. Preventing Chronic Disease. 2014;11:E219.

103. Greenwood JL, Joy EA, Stanford JB. The Physical Activity Vital Sign: a primary care tool to guide counseling for obesity. Journal of physical activity & health. 2010;7(5):571-6.

104. Michael Delaine-Smith R, Javaheri B, Helen Edwards J, Vazquez M, Rumney RMH. Preclinical models for in vitro mechanical loading of bone-derived cells. BoneKEy reports. 2015;4:728.

105. Huesa C, Bakker AD. Mechanical stimulation of bone cells using fluid flow. Methods in molecular biology (Clifton, NJ). 2012;816:573-92.

106. Davis CA, Zambrano S, Anumolu P, Allen AC, Sonoqui L, Moreno MR. Device-based in vitro techniques for mechanical stimulation of vascular cells: a review. Journal of biomechanical engineering. 2015;137(4):040801.

107. Oishi A, Makita N, Sato J, Iiri T. Regulation of RhoA Signaling by the cAMP-dependent Phosphorylation of RhoGDIα. The Journal of Biological Chemistry. 2012;287(46):38705-15.

108. Ghosh PM, Ghosh-Choudhury N, Moyer ML, Mott GE, Thomas CA, Foster BA, et al. Role of RhoA activation in the growth and morphology of a murine prostate tumor cell line. Oncogene. 1999;18(28):4120-30.

109. Esufali S, Bapat B. Cross-talk between Rac1 GTPase and dysregulated Wnt signaling pathway leads to cellular redistribution of beta-catenin and TCF/LEF-mediated transcriptional activation. Oncogene. 2004;23(50):8260-71.

110. Jones WM, Bejsovec A. RacGap50C negatively regulates wingless pathway activity during Drosophila embryonic development. Genetics. 2005;169(4):2075-86.

111. Wu X, Tu X, Joeng KS, Hilton MJ, Williams DA, Long F. Rac1 activation controls nuclear localization of beta-catenin during canonical Wnt signaling. Cell. 2008;133(2):340-53.

112. Habas R, Dawid IB, He X. Coactivation of Rac and Rho by Wnt/Frizzled signaling is required for vertebrate gastrulation. Genes Dev. 2003;17(2):295-309.

113. Schlessinger K, Hall A, Tolwinski N. Wnt signaling pathways meet Rho GTPases. Genes Dev. 2009;23(3):265-77.

114. Wang Y, Li Y-P, Paulson C, Shao J-Z, Zhang X, Wu M, et al. Wnt and the Wnt signaling pathway in bone development and disease. Frontiers in bioscience (Landmark edition). 2014;19:379-407.

115. Tanegashima K, Zhao H, Dawid IB. WGEF activates Rho in the Wnt–PCP pathway and controls convergent extension in Xenopus gastrulation. The EMBO journal. 2008;27(4):606-17.

116. Chen Y, Alman BA. Wnt pathway, an essential role in bone regeneration. J Cell Biochem. 2009;106(3):353-62.

117. Habas R, Dawid IB. Dishevelled and Wnt signaling: is the nucleus the final frontier? Journal of biology. 2005;4(1):2.

118. Huelsken J, Behrens J. The Wnt signalling pathway. Journal of cell science. 2002;115(Pt 21):3977-8.

119. Ishitani T, Kishida S, Hyodo-Miura J, Ueno N, Yasuda J, Waterman M, et al. The TAK1-NLK mitogen-activated protein kinase cascade functions in the Wnt-5a/Ca(2+) pathway to antagonize Wnt/beta-catenin signaling. Molecular and cellular biology. 2003;23(1):131-9.

120. Ishitani T, Ninomiya-Tsuji J, Nagai S, Nishita M, Meneghini M, Barker N, et al. The TAK1-NLK-MAPK-related pathway antagonizes signalling between beta-catenin and transcription factor TCF. Nature. 1999;399(6738):798-802.